Transactions

of the

ASME

Investigation of Turbulent Flow and Heat Transfer in Smooth Tubes, Including the Effects of Variable Fluid Properties . . . . . *R. G. Deissler* 101

New Technique for Obtaining Heat-Transfer Parameters of the Wall and Combustion Gas in a Rocket Motor . . . . . *M. E. Ellion* 109

Photographic Study of Surface-Boiling Heat Transfer to Water With Forced Convection . . . . . *F. C. Gunther* 115

Chemical Removal of Copper From Boilers . . . . . *R. G. Call and W. L. Webb* 125

Phosphoric-Acid-Cleaning of Boilers . . . . . *T. E. Purcell and S. F. Whirl* 135

Accurate Spring Counterbalancing . . . . . *W. S. Rouverol* 141

Displacement Versus Time Characteristics of Hydraulic Actuators . . . . . *L. Sigfred Linderoth, Jr.* 147

The Design of Nonlinear Leaf Springs . . . . . *S. P. Clurman* 155

On the Design of Rotor-Coil Support Rings . . . . . *J. J. Ryan* 163

Development and Testing of Brakes for High-Speed Railroad Equipment . . . . . *C. E. Tack* 167

Comparative Strengths of Some Adhesive-Adherend Systems . . . . . *N. J. DeLollis, Nancy Rucker, and J. E. Wier* 183

Dynamic Shear Properties of Rubberlike Polymers . . . . . *I. L. Hopkins* 195

Metals for High-Pressure Hydrogenation Plants . . . . . *G. A. Nelson* 205

Cyclone-Fired Pressurized Steam Generator . . . . . *Merle Newkirk* 215

FEBRUARY, 1951

VOL. 73, NO. 2

Transactions

of The American Society of Mechanical Engineers

Published on the tenth of every month, except March, June, September, and December

---

Published monthly by The American Society of Mechanical Engineers. Publication office at 20th and Northampton Streets, Easton, Pa. The editorial department is located at the headquarters of the Society, 29 West Thirty-Ninth Street, New York 18, N. Y. Cable address, "Dynamic," New York. Price $1.50 a copy, $12.00 a year for Transactions and the *Journal of Applied Mechanics;* to members and affiliates, $1.00 a copy, $6.00 a year. Changes of address must be received at Society headquarters three weeks before they are to be effective on the mailing list. Please send old as well as new address. . . . By-Laws: The Society shall not be responsible for statements or opinions advanced in papers or . . . printed in its publications (B13, Par. 4). . . . Entered as second-class matter March 2, 1928, at the Post Office at Easton, Pa., under the Act of August 24, 1912. . . .

Investigation of Turbulent Flow and Heat Transfer in Smooth Tubes, Including the Effects of Variable Fluid Properties

By R. G. DEISSLER,[1] CLEVELAND, OHIO

Equations are derived for the prediction of radial velocity distributions for fully developed turbulent flow in smooth tubes both with and without heat transfer. The analysis results in an equation which represents both the conventional buffer layer and the laminar layer. In order to check the analysis and determine values for the constants appearing in the equations, tests were conducted to determine fully developed velocity distributions for air flowing without heat transfer in a smooth tube. The results are correlated by using conventional velocity and distance parameters, and agree closely with those of Nikuradse and other investigators. The analysis is extended to include flow with heat transfer, and equations for this case are obtained for Prandtl number of 1 in which the effects of the variation of fluid properties due to temperature variation across the tube were considered. By use of the equations for velocity and temperature distributions, relations are also obtained among Nusselt number, Reynolds number, and friction factor for a fluid with a Prandtl number of 1 for the case where the variation of fluid properties across the tube is large. The trends predicted analytically were found to be similar to those determined experimentally by measurement of average surface heat-transfer coefficients and friction factors of air flowing in tubes.

Nomenclature

The following nomenclature is used in the paper:

c_p = specific heat of fluid at constant pressure, (Btu/lb-deg F)

C, C_1 = constants of integration

d = exponent the value for which depends on the variation of the viscosity of the fluid with temperature

D = inside diameter of tube, ft

e = base of natural logarithms

g = acceleration due to gravity (32.2 ft/sec^2)

h = heat-transfer coefficient (Btu/sec-ft^2-deg F)

k = thermal conductivity of fluid (Btu-ft/sec-ft^2-deg F)

$k_{0.4}$, $k_{0.5}$, $k_{0.6}$ = thermal conductivity of fluid evaluated at $t_{0.4}$, $t_{0.5}$, $t_{0.6}$, respectively (Btu-ft/sec-ft^2-deg F)

k_b = thermal conductivity of fluid evaluated at t_b (Btu-ft/sec-ft^2-deg F)

K = von Kármán constant

n = constant

q = total rate of heat transfer toward tube center per unit area, Btu/(sec-ft^2)

q_0 = total rate of heat transfer at wall toward tube center per unit area, Btu/(sec-ft^2)

r = radius, distance from tube axis, ft

r_0 = inside tube radius, ft

t = absolute static temperature, deg R

t_b = bulk or average static temperature of fluid at cross section of tube, deg R

$t_{0.4} = 0.4\,(t_0 - t_b) + t_b$, film temperature, deg R

$t_{0.5} = 0.5\,(t_0 - t_b) + t_b$, film temperature, deg R

$t_{0.6} = 0.6\,(t_0 - t_b) + t_b$, film temperature, deg R

t_0 = absolute wall temperature, deg R

u = velocity parallel to axis of tube, fpc

u_b = bulk or average velocity at cross section of tube, fps

y = distance from tube wall, ft

ϵ = coefficient of eddy diffusivity for momentum, sq ft/sec

ϵ_h = coefficient of eddy diffusivity for heat, sq ft/sec

ρ = mass density (lb-sec^2/ft^4)

ρ_0 = mass density of fluid at wall (lb-sec^2/ft^4)

ρ_b = bulk or average density at cross section of tube, (lb-sec^2/ft^4)

$\rho_{0.4}$, $\rho_{0.5}$, $\rho_{0.6}$ = density of fluid evaluated at $t_{0.4}$, $t_{0.5}$, $t_{0.6}$, respectively, (lb-sec^2/ft^4)

μ = absolute viscosity of fluid, (lb-sec/sq ft)

μ_b = absolute viscosity of fluid evaluated at t_b, (lb-sec/sq ft)

μ_0 = absolute viscosity of fluid at wall, (lb-sec/sq ft)

$\mu_{0.4}$, $\mu_{0.5}$, $\mu_{0.6}$ = absolute viscosity of fluid evaluated at $t_{0.4}$, $t_{0.5}$, $t_{0.6}$, respectively, (lb-sec/sq ft)

τ = shear stress in fluid, psf

τ_0 = shear stress in the fluid at the wall, psf

Dimensionless groups:

$$\beta \equiv \frac{q_0\sqrt{\tau_0/\rho_0}}{c_p g\,\tau_0\,t_0} = \text{heat-transfer parameter}$$

$$f \equiv \frac{2\tau_0}{\rho u_b^2} = -\frac{D\,\frac{dp}{dx_{fr}}}{2\rho u_b^2} = \text{friction factor}$$

$$f_b \equiv \frac{2\tau_0}{\rho_b u_b^2} = \text{friction factor with density evaluated at } t_b$$

$f_{0.4}$, $f_{0.5}$, $f_{0.6}$ = friction factor with density evaluated at $t_{0.4}$, $t_{0.5}$, $t_{0.6}$, respectively

$Nu \equiv hD/k$ = Nusselt number

$Nu_b \equiv hD/k_b$ = Nusselt number with thermal conductivity evaluated at t_b

Nu_0 = Nusselt number with thermal conductivity evaluated at t_0

$Nu_{0.4}$, $Nu_{0.5}$, $Nu_{0.6}$ = Nusselt number with thermal conductivity evaluated at $t_{0.4}$, $t_{0.5}$, $t_{0.6}$, respectively

$Pr \equiv c_p\mu g/k$ = Prandtl number

$Re \equiv \rho u_b D/\mu$ = Reynolds number

---

[1] Research Engineer, National Advisory Committee for Aeronautics, Lewis Flight Propulsion Laboratory. Jun. ASME.

Contributed by the Heat Transfer Division and presented at the Heat Transfer and Mechanics Institute Meeting, Los Angeles, Calif., June 28–30, 1950, of The American Society of Mechanical Engineers.

Note: Statements and opinions advanced in papers are to be understood as individual expressions of their authors and not those of the Society. Manuscript received at ASME Headquarters, August 14, 1950.

$Re_b \equiv \rho_b u_b D/\mu_b$ = Reynolds number with density and viscosity evaluated at t_b

Re_0 = Reynolds number with density and viscosity evaluated at t_0

$Re_{0.4}$, $Re_{0.5}$, $Re_{0.6}$ = Reynolds number with density and viscosity evaluated at $t_{0.4}$, $t_{0.5}$, $t_{0.6}$, respectively

$$r_0^* \equiv \frac{\sqrt{\tau_0/\rho_0}}{\mu_0/\rho_0} r_0 = \text{tube radius parameter}$$

$$t^* \equiv \frac{(t_0 - t)c_p g \tau_0}{q_0 \sqrt{\tau_0/\rho_0}} = \frac{1 - t/t_0}{\beta} = \text{static temperature parameter}$$

$$t_b^* \equiv \frac{1}{\beta}\left(1 - \frac{t_b}{t_0}\right) = \text{static bulk temperature parameter}$$

$$u^* \equiv \frac{u}{\sqrt{\tau_0/\rho_0}} = \text{velocity parameter}$$

$$u_b^* \equiv \frac{u_b}{\sqrt{\tau_0/\rho_0}} = \text{bulk velocity parameter}$$

$$y^* \equiv \frac{\sqrt{\tau_0/\rho_0}}{\mu_0/\rho_0} y = \text{wall distance parameter}$$

Introduction

For some time work has been in progress at the NACA Lewis Flight Propulsion Laboratory for investigating heat transfer and associated pressure-drop phenomena for fluid flow through tubes. Most of the work to date has been of an experimental nature and has been directed toward obtaining average heat-transfer coefficients and friction factors in tubes. In order to obtain a somewhat more fundamental knowledge of fluid flow and heat transfer in smooth tubes, the present analytical and experimental investigation from the standpoint of velocity and temperature distributions was undertaken. In the present paper some of the results of this investigation are presented.

The portion of the velocity distribution at a distance from the tube wall for fully developed turbulent flow without heat transfer has previously been represented satisfactorily by equations derived from the similarity theory of von Kármán (1).[2] In the present investigation, a new equation which represents the region close to the wall, that is, the laminar layer and the so-called buffer layer, is obtained by making certain reasonable assumptions as to the nature of the mechanism for the turbulent transfer in the vicinity of the wall. For the region far from the wall, the von Kármán-Prandtl development is used. This development, as well as the development for flow close to a wall, is extended to include flow with high rates of heat transfer for a fluid with a Prandtl number of 1.

General Theory

For obtaining the velocities and temperatures in the tube as functions of the distance from the wall, the differential equations for shear stress and heat transfer are often written in the following form

$$\tau = \mu\, du/dy + \rho\epsilon\, du/dy \quad [1]$$

$$q = -k\, dt/dy - \rho c_p\, g\epsilon_h\, dt/dy \quad [2]$$

where ϵ and ϵ_h are known as the coefficients of eddy diffusivity for momentum and heat transfer, the values for which are dependent upon the amount and kind of turbulent mixing at a point.

In order to make practical use of Equation [1], it is necessary to evaluate the eddy diffusivity ϵ, for each portion of the flow. For the region at a distance from the wall, von Kármán has shown (1) that the shear stress is given by

$$\tau = \rho K^2 \frac{(du/dy)^4}{(d^2u/dy^2)^2} \quad [3]$$

where K^2 is a constant of proportionality determined experimentally. Comparison of this equation with Equation [1] and neglecting the viscous shear stress, because it is small except in the region close to the wall, gives for the eddy diffusivity at a distance from the wall

$$\epsilon = K^2 \frac{(du/dy)^3}{(d^2u/dy^2)^2} \quad [4]$$

This equation indicates that ϵ, or the mechanism for the turbulent transfer of momentum at a point away from the wall, can be considered to be dependent only on the derivatives of the velocity with respect to distance from the wall, that is, on the velocities in the vicinity of the point relative to the velocity at the point, and to be unaffected by the velocity relative to the wall or the distance from the wall.

Although the effects of the velocity relative to the wall and the distance from the wall on the turbulence mechanism can be neglected for the region at a distance from the wall, it appears that they should be considered for the region close to the wall. It is, therefore, desirable to obtain an expression for ϵ close to the wall which contains these factors, as well as the velocity derivatives. The experimental data available indicate that the turbulent transfer of momentum, and thus the turbulent shear stress $\rho\epsilon\, du/dy$, become very small in the region close to the wall, so that close to the wall the shear stress is practically all produced by viscous action, and the velocity u is very nearly a linear function of y. Therefore it can be assumed that the second and possibly higher-order derivatives approach the constant value zero in the vicinity of the wall, and that the first derivative approaches a constant which is defined when u and y are given. As a first approximation ϵ is therefore written as a function only of u and y. The range of values of y for which this approximation is sufficient will be determined experimentally. From dimensional analysis

$$\epsilon = n^2 uy \quad [5]$$

where n^2 is a constant of proportionality to be determined experimentally. Equation [5] gives the expression for ϵ to be substituted into Equation [1] for flow close to the wall.

Velocity-Distribution Equations for Incompressible Flow Without Heat Transfer

In order to obtain equations which are in dimensionless form, the conventional dimensionless quantities u^* and y^* are used. (These quantities are defined in the nomenclature. The subscripts 0 refer to values at the wall.)

The differential equation for the velocity distribution close to a wall is obtained by substituting the expression for ϵ from Equation [5] into Equation [1]

$$\tau = \mu\, du/dy + n^2\rho uy\, du/dy \quad [6]$$

In this equation τ can be replaced by τ_0 because the shear stress does not vary appreciably in the region close to the wall, and μ and ρ can be replaced by μ_0 and ρ_0 respectively, because they are constant across the tube for incompressible flow without heat transfer. On making these replacements and introducing u^* and y^*, Equation [6] becomes, in dimensionless form

$$dy^*/du^* - n^2 u^* y^* = 1 \quad [7]$$

[2] Numbers in parentheses refer to the Bibliography at the end of the paper.

Solution of this equation yields, with the condition that $u^* = 0$ when $y^* = 0$

$$y^* = \frac{1}{n} \frac{\frac{1}{\sqrt{2\pi}} \int_0^{nu^*} e^{\frac{-(nu^*)^2}{2}} d(nu^*)}{\frac{1}{\sqrt{2\pi}} e^{\frac{-(nu^*)^2}{2}}} \quad \ldots\ldots\ldots [8]$$

where the expression in the denominator is the normal error function of nu^*, and the expression in the numerator is the integral of the normal error function, both of which are tabulated in mathematical tables. Equation [8] is the desired relationship between u^* and y^* for incompressible flow close to a wall without heat transfer.

The relationship between u^* and y^* for incompressible flow without heat transfer for the region at a distance from the wall can be obtained by integration of Equation [3]. This integration has been carried out by von Kármán for the region close to a wall (effect of viscosity neglected) by assuming constant shear stress (1), and applied by Prandtl to the region far from the wall. Integration of Equation [3] yields the well-known logarithmic equation

$$u^* = (1/K) \ln y^* + C \ldots\ldots\ldots\ldots [9]$$

where C is a constant of integration, the value for which is known when the ranges of applicability of equations for flow close to a wall and at a distance from a wall are known.

Experimental Verification of Velocity-Distribution Equations

In order to obtain values for the constants n and K in the equations and to determine the range of values of y^* for which each of the equations applies, experiments were conducted at the Lewis laboratory to determine velocity distributions for air flowing without heat transfer in a smooth tube having an inside diameter of 0.87 in. and a length of 87 in. In order to insure fully developed flow, the tests were made near the exit of the tube at approximately 100 tube diam from the entrance. The velocity distributions were obtained by measuring total pressure distributions across the tube with a very small total head probe.

Fig. 1, where u^* is plotted against y^* on semilogarithmic coordinates, shows the velocity-distribution data which were obtained, together with the equations which were derived. The data agree closely with those of Nikuradse (2), and of other investigators, the maximum deviation being about 5 per cent. The Reynolds number in the tests varied between 10,000 and 200,000 and the Mach number varied from a small value to 0.5.

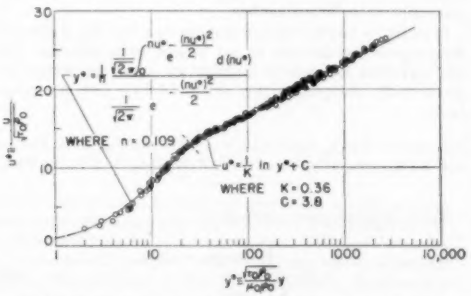

Fig. 1 Generalized Velocity Distribution for Fully Developed Adiabatic Turbulent Flow in Smooth Tubes
(Reynolds-number range for data, 10,000 to 200,000.)

The curve corresponding to the equation for incompressible flow close to a wall (Equation [8]) is plotted in the figure and is seen to be in good agreement with the experimental results for values of y^* from zero to 26. The value of the constant n in the equation is 0.109 as determined from the experimental data. An important property of this equation is that for small values of y^*, u^* and y^* are approximately equal, or in other words, the flow predicted by the equation is very nearly laminar. The equation thus obviates the necessity of assuming the existence of a separate layer near the wall which is purely laminar (but does not eliminate the possibility of its existence), as has generally been done in previous investigations. Therefore a single equation has been obtained which adequately represents the two regions which are commonly called the "laminar layer" and "buffer layer."

The curve corresponding to the equation for flow at a distance from the wall (Equation [9]), which was obtained by von Kármán, is also shown in the figure and is seen to be in good agreement with the data for values of y^* greater than 26. The constant K was determined experimentally to be 0.36, and C was found from the equation for flow close to the wall, when evaluated at y^* equals 26, to be 3.8.

The slopes of the curves representing the equations for flow close to the wall and at a distance from the wall are not quite equal at their intersection at y^* equals 26; this would, however, be expected because the two equations were derived by assuming that different factors affect the turbulent transfer of momentum in the two regions, and hence an abrupt change in turbulence mechanism at the intersection is implied in the equations. Actually, there is probably a gradual change, which could not be investigated by the simplified methods used here. Inasmuch as the actual error in values of u^* in the vicinity of the intersection is insignificant, the present treatment is considered adequate.

Equations for Velocity Distributions for Flow With Heat Transfer With Variable Fluid Properties for a Prandtl Number of One

The equations derived in this section are intended to approximate the effects of heat transfer on the velocity distributions of gases flowing in smooth tubes. The Prandtl number is assumed not to vary with temperature and to be equal to 1. The effects of compressibility as caused by high subsonic velocities and of variation of shear stress across the tube are neglected, inasmuch as the effects of these factors on velocity distributions were shown (4) to be small. The equations derived are for fully developed velocity and temperature distributions.

When heat transfer takes place in a gas flowing through a tube, a temperature gradient exists across the tube, and the gas properties vary from point to point. The gas properties which vary with temperature and are important in the present investigation are the density ρ, the viscosity μ, the thermal conductivity k, and the specific heat at constant pressure c_p. Of these, the variation with temperature of the specific heat is of a lower order of magnitude than the variation with temperature of the other properties, so that, in the present analysis, the specific heat is considered to be constant with temperature.

The equation for heat transfer (Equation [2]) can be rewritten as

$$q/(c_p g) = (\mu/Pr + \rho\epsilon_h) \frac{dt}{dy} \ldots\ldots\ldots\ldots [10]$$

The following assumptions are made in the use of this equation and Equation [1] for the developments for flow with heat transfer:

1 The eddy diffusivities for momentum and heat transfer (ϵ and ϵ_h) are equal. Previous analysis for flow in tubes based upon this assumption yielded heat-transfer coefficients and friction factors which agree with experiment (3).

2 The expressions for eddy diffusivity (Equations [4] and [5]), which were found to apply to flow without heat transfer, apply also to flow with heat transfer with variable fluid properties.

3 The shear stress τ and heat transfer q, can be considered uniform across the tube. It is shown elsewhere (4) that the shear stress can be considered with good approximation to be uniform across the tube for turbulent flow. Because the temperature and velocity profiles for a Prandtl number of 1 are known to have the same general shape, the heat transfer is also considered to be uniform across the tube and to be equal to the heat transfer at the wall.

4 The static pressure can be considered constant across the tube.

Dividing Equation [10] by Equation [1] and integrating between the wall and a point in the fluid gives, for a Prandtl number of 1

$$\frac{q_0 u}{c_p g\ \tau_0} = t_0 - t \quad \ldots\ldots [11]$$

or

where

$$t/t_0 = 1 - \beta u^* \quad \ldots\ldots [12]$$

$$\beta \equiv \frac{q_0 \sqrt{\tau_0/\rho_0}}{c_p g \tau_0 t_0}$$

From the perfect gas law, the density at any point across the tube is, with the assumption of constant static pressure across the tube

$$\rho = \rho_0/(1 - \beta u^*) \quad \ldots\ldots [13]$$

The variation of the viscosity of a gas with temperature can be written as

$$\mu/\mu_0 = (t/t_0)^d \quad \ldots\ldots [14]$$

or

$$\mu = \mu_0 (1 - \beta u^*)^d \quad \ldots\ldots [15]$$

For obtaining the equation for flow close to a smooth wall, these expressions for ρ and μ are substituted into Equation [6] (assumption 2), which, on the substitution of τ_0 for τ, becomes in dimensionless form

$$dy^*/du^* = n^2 u^* y^*/(1 - \beta u^*) = (1 - \beta u^*)^d$$

integrating

$$y^* = e^{-\frac{n^2}{\beta} u^*} (1 - \beta u^*)^{-\frac{n^2}{\beta^2}} \int_0^{u^*} e^{\frac{n^2 u^*}{\beta}} (1 - \beta u^*)^{\frac{n^2}{\beta^2} + d} du^* \quad \ldots\ldots [16]$$

Equation [16] gives, for flow close to a wall with heat transfer, the relation between u^* and y^* for various values of the heat-transfer parameter β.

For obtaining the equation for flow at a distance from a wall, the expression for ρ from Equation [13] is substituted into Equation [3]. Integrating twice and using the condition that $dy^*/du^* = 0$ when $y^* = 0$, since the velocity gradient near the wall is very large compared with that at a distance from the wall gives

$$y^* = \frac{C_1 \beta}{2K^2} e^{-\frac{2K}{\beta} \sqrt{1 - \beta u^*}} \left(\frac{2K}{\beta} \sqrt{1 - \beta u^*} + 1 \right) \quad \ldots\ldots [17]$$

where C_1 is a constant of integration, the value for which is known when the ranges of applicability of the equations for the two regions are known. Equation [17] gives the relation between u^* and y^* for various values of β for flow at a distance from a wall with heat transfer.

Equations [16] and [17] are plotted in Fig. 2. The values for the constants ($n = 0.109$ and $K = 0.36$), which were found from the experimental data for flow without heat transfer, are used for plotting the equations. The same limits of applicability for the equations for flow close to a wall and at a distance from a wall are used as were used for the equations for flow without heat transfer, that is, Equation [16] is taken to apply for $0 < y^* < 26$ and Equation [17] for $y^* > 26$. The exponent d was found from viscosity data to be approximately 0.68 for air and most common gases.

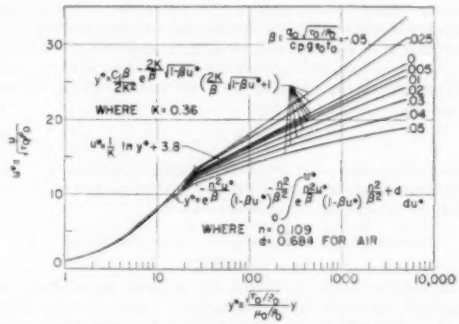

FIG. 2 GENERALIZED VELOCITY DISTRIBUTION FOR FLOW OF GASES WITH HEAT TRANSFER
(Prandtl number = 1.)

The plots of the equations in Fig. 2 indicate a flattening of the velocity profile in the central portion of the tube for heat addition (positive values of β) and a peaking of the profile at the center of the tube for heat extraction (negative values of β). These trends are opposite to those for laminar flow of a gas, the explanation being that for turbulent flow, the turbulent shear stress, which is governed by the density, is more important in the central portion of the tube than is the viscous shear stress. The variation with temperature of the density is opposite to that of viscosity, so that the changes in profile shape in the center of the tube for turbulent flow, caused by heat addition or extraction, are opposite to those for laminar flow.

It should be mentioned here that the curves in Fig. 2 also give temperature distributions, as can be seen from Equation [12]. The equations for velocity distributions should be verified experimentally inasmuch as they are based upon certain assumptions.

NUSSELT NUMBER, REYNOLDS NUMBER, AND FRICTION FACTOR FOR A PRANDTL NUMBER OF ONE, WITH VARIABLE FLUID PROPERTIES

The bulk temperature is defined as

$$t_b \equiv \frac{\int_0^{r_0} t \rho u (r_0 - y)\, dy}{\int_0^{r_0} \rho u (r_0 - y)\, dy} \quad \ldots\ldots [18]$$

In dimensionless form this becomes

$$t_b^* = \frac{\int_0^{r_0^*} t^*(\rho/\rho_0)u^*\,(r_0^* - y^*)\,dy^*}{\int_0^{r_0^*} (\rho/\rho_0)u^*\,(r_0^* - y^*)\,dy^*} \quad \ldots\ldots [19]$$

where r_0^*, t^*, and t_b^* are defined in the nomenclature. Equation [12], together with the definition of t^*, indicates that t^* and u^* are equal for a Prandtl number of 1. Use of the perfect gas law (constant pressure) and substitution of the value of t/t_b from Equation [12] into Equation [19] gives

$$t_b^* = \frac{\int_0^{r_0^*} \frac{u^{*2}\,(r_0^* - y^*)}{1 - \beta u^*}\,dy^*}{\int_0^{r_0^*} \frac{u^*\,(r_0^* - y^*)}{1 - \beta u^*}\,dy^*} \quad \ldots\ldots [20]$$

Using the definitions of Nu_0, h, Pr, r_0^*, β, and t_b^*, the expression for the Nusselt number with the thermal conductivity based upon the wall temperature may be written as

$$Nu_0 = 2\,r_0^*\,Pr/t_b^* \quad \ldots\ldots [21]$$

It is desired to obtain Nusselt numbers with the conductivity evaluated at temperatures other than the wall temperature, say, the bulk temperature. For doing this, the ratio of bulk-to-wall static temperature can be obtained in dimensionless form from Equations [18] and [13] as

$$\frac{t_b}{t_0} = \frac{\int_0^{r_0^*} u^*\,(r_0^* - y^*)\,dy^*}{\int_0^{r_0^*} \frac{u^*\,(r_0^* - y^*)\,dy^*}{1 - \beta u^*}} \quad \ldots\ldots [22]$$

With the assumptions of constant Prandtl number and constant specific heat, the law for the variation with temperature of the conductivity must be the same as the law for variation with temperature of the viscosity. Therefore the viscosity ratio may be replaced by the conductivity ratio in Equation [14]. The Nusselt number with the conductivity evaluated at any temperature between the wall and bulk temperatures can then be found from the definition of Nusselt number and Equations [21], [22], and [14] with viscosities replaced by conductivities in the last equation. The quantity t_b^* is obtained from Equation [20], and the relationship between u^* and y^* is obtained from the curves in Fig. 2.

Similarly, equations for Reynolds number and friction factor with properties based on the wall temperature are found to be

$$Re_0 = 2u_b^*\,r_0^* \quad \ldots\ldots [23]$$

and

$$f_0 = \frac{2}{u_b^{*2}} \quad \ldots\ldots [24]$$

where

$$u_b^* = \frac{2}{r_0^{*2}} \int_0^{r_0^*} u^*(r_0^* - y^*)\,dy^* \quad \ldots\ldots [25]$$

Reynolds numbers and friction factors with the density and viscosity in their definitions based on some other temperature may be obtained readily by use of Equations [22], [14], and the perfect gas law (constant pressure). For calculating values of Nusselt number, Reynolds number, and friction factor, r_0^* is allowed to vary arbitrarily.

Figs. 3, 4, and 5 show predicted Nusselt numbers plotted against Reynolds numbers for a Prandtl number of 1 for various

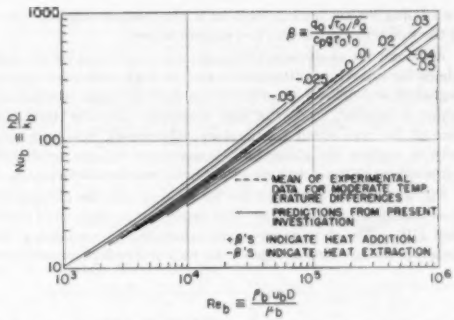

FIG. 3 NUSSELT NUMBER VERSUS REYNOLDS NUMBER FOR FLOW OF GASES WITH GAS PROPERTIES EVALUATED AT STATIC BULK TEMPERATURE
(Prandtl number = 1.)

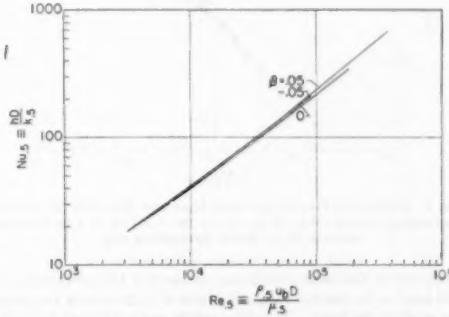

FIG. 4 NUSSELT NUMBER VERSUS REYNOLDS NUMBER FOR FLOW OF GASES WITH HEAT ADDITION AND EXTRACTION WITH GAS PROPERTIES EVALUATED AT AVERAGE OF WALL AND BULK TEMPERATURES
(Prandtl number = 1.)

values of the heat-transfer parameter β. In Fig. 3 the physical properties in the Nusselt number and Reynolds number are evaluated at the bulk temperature. It is seen that increasing positive values of the heat-transfer parameter β cause a decrease in Nusselt number. Increasing values of β correspond, in general, to increasing values of the ratio of wall-to-bulk temperature t_0/t_b; the curves shown correspond to a range of ratios of wall-to-bulk temperature of from 1 to about 7 for heating, and from 1 to about 0.4 for cooling. The same trends for heating have been observed experimentally in tests to determine average heat-transfer coefficients in tubes with a range of ratios of wall-to-bulk temperature of from 1 to about 3½ (6, 7, 9, and 10). The dotted line in the figure represents the mean of experimental data for moderate and low temperature differences (11) and agrees, in general, with the predicted line for $\beta = 0$ for Reynolds numbers greater than 10,000.

In Fig. 4 the Nusselt numbers and Reynolds numbers are plotted with the gas properties in both parameters evaluated at the average of the wall and bulk temperatures, $t_{0.5}$. By use of this temperature for evaluating the fluid properties, the maximum separation of the curves for both heating and cooling is reduced to about 9 per cent. The separation of the curves can be eliminated for heating by evaluating the properties at a temperature slightly closer to the bulk temperature designated by $t_{0.4}$ and

for cooling by evaluating them at a temperature slightly closer to the wall temperature, $t_{0.6}$ (see nomenclature).

Although the analysis in this paper was carried out for the case where the compressibility effects due to high velocities can be neglected, it is shown in reference (5) that the same correlations apply, in general, to flow at high velocities. For the latter case (except for very small temperature differences), it is necessary only to replace the static bulk temperature by the total bulk temperature in the definition of the heat-transfer coefficient h.

Fig. 5 shows the predicted line for heating with the gas properties evaluated at $t_{0.4}$ together with experimental data from reference (10). The data points were calculated by evaluating the gas properties at the average of the wall and bulk temperatures;

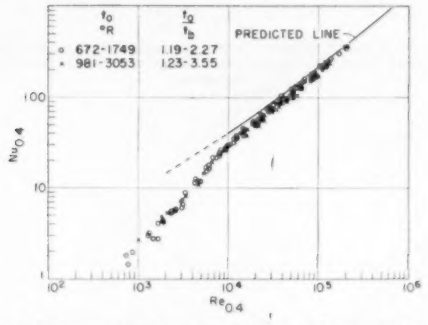

FIG. 5 PREDICTED HEAT-TRANSFER LINE FOR HEATING WITH GAS PROPERTIES EVALUATED AT $t_{0.4} = t_{0.4}\,(t_0 - t_b) + t_b$ AND EXPERIMENTAL DATA FROM REFERENCE (10)

substantially the same results are obtained if the properties are evaluated at $t_{0.4}$ for the range of ratios of wall-to-bulk temperature used in the tests. The data, which were obtained for heating air, were corrected to a Prandtl number of 1 by dividing the Nusselt numbers by $Pr^{0.4}$. The data are seen to agree substantially with the predicted line for heating for Reynolds number above 10,000. The deviation of the data from the predicted line at low Reynolds numbers is probably caused by transitional effects in the fluid flow which were not considered in the analysis.

In the experimental work described in references (6, 7, 8, 9, 10), it was found that the effects of ratio of wall-to-bulk temperature on the Nusselt numbers were practically eliminated when the gas properties were evaluated at either the wall or the average of the wall and bulk temperatures. In the present analysis, however, where the maximum ratio of wall-to-bulk temperature is about twice that in the experimental work, separation of the curves was found when the properties were evaluated at the wall temperature. It should be mentioned that the analytical and experimental results are not strictly comparable because the analytical results are for local heat-transfer coefficients at a cross section in the tube, whereas the experimental results give average heat-transfer coefficients for a whole tube.

Figs. 6 and 7 show predicted friction factors plotted against Reynolds numbers for various values of the heat-transfer parameter β. The same trends and correlation are seen to hold for friction factors as held for Nusselt numbers. These trends have also been observed experimentally (7). The dotted line in Fig. 6 represents the mean of experimental data for isothermal flow and is seen to agree substantially with the predicted line for $\beta = 0$ for Reynolds numbers greater than 10,000. As in the case of

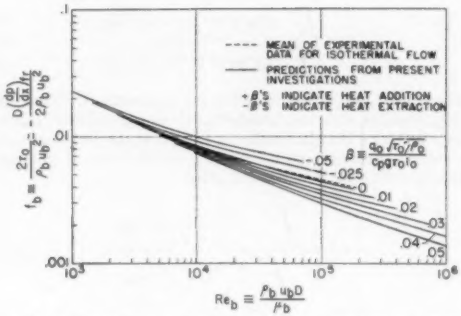

FIG. 6 FRICTION FACTOR VERSUS REYNOLDS NUMBER FOR FLOW OF GASES WITH GAS PROPERTIES EVALUATED AT STATIC BULK TEMPERATURE
(Prandtl number = 1.)

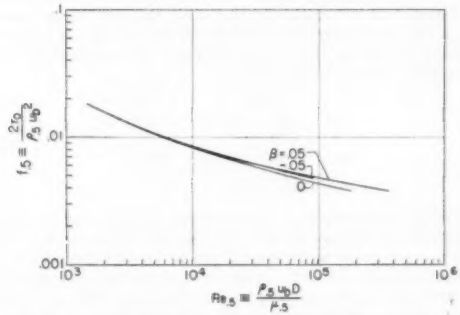

FIG. 7 FRICTION FACTOR VERSUS REYNOLDS NUMBER FOR FLOW OF GASES WITH GAS PROPERTIES EVALUATED AT AVERAGE OF WALL AND BULK TEMPERATURES

Nusselt numbers, the separation of the curves can be eliminated for heating by evaluating the gas properties in the friction factor and Reynolds number at $t_{0.4}$ and for cooling by evaluating them at $t_{0.6}$.

SUMMARY OF RESULTS

In the present investigation of turbulent flow and heat transfer in smooth tubes, a new equation for the velocity distribution close to a smooth wall was obtained which represents both the laminar layer and the so-called buffer layer.

The development for flow close to the wall, as well as the von Kármán development for flow at a distance from the wall were extended to include flow with heat transfer for a fluid with a Prandtl number of 1 for the case where the variation of fluid properties due to temperature variation across the tube is appreciable. Nusselt numbers, Reynolds numbers, and friction factors were obtained and it was found that the effect of variable fluid properties on the Nusselt number and friction-factor correlations for both heating and cooling can be eliminated by evaluating the fluid properties in the Nusselt numbers, Reynolds numbers, and friction factors at a temperature close to the average of the wall and bulk temperatures. The predicted results for heating agree with experimental results for heat transfer to air.

BIBLIOGRAPHY

1 "Turbulence and Skin Friction," by Th. von Kármán, *Journal of Aeronautical Sciences*, vol. 1, January, 1934, pp. 1–20.

2 "Fluid Mechanics for Hydraulic Engineers," by Hunter Rouse, McGraw-Hill Book Company, Inc., New York, N. Y., first edition, 1938, p. 242.

3 "The Analogy Between Fluid Friction and Heat Transfer," by Th. von Kármán, Trans. ASME, vol. 61, 1939, pp. 705–710.

4 "Analytical and Experimental Investigation of Adiabatic Turbulent Flow in Smooth Tubes," by R. G. Deissler, NACA TN, 2138.

5 "Analytical Investigation of Turbulent Flow in Smooth Tubes With Heat Transfer With Variable-Fluid Properties for a Prandtl Number of One," by R. G. Deissler, NACA TN, 2242.

6 "Heat Transfer From High-Temperature Surfaces to Fluids. I—Preliminary Investigation With Air in Inconel Tube With Rounded Entrance, Inside Diameter of 0.4 Inch and Length of 24 Inches," by L. V. Humble, W. H. Lowdermilk, and M. D. Grele, NACA Report RM E7L31, 1948.

7 "Heat Transfer From High-Temperature Surfaces to Fluids. II—Correlation of Heat-Transfer and Friction Data for Air Flowing in Inconel Tube With Rounded Entrance," by W. H. Lowdermilk and M. D. Grele, NACA Report RM E8L03, 1949.

8 "Heat Transfer From High-Temperature Surfaces to Fluids. III—Correlation of Heat-Transfer Data for Air Flowing in Silicon Carbide Tube With Rounded Entrance, Inside Diameter of 3/4 Inch, and Effective Length of 12 Inches," by E. W. Sams and L. G. Desmon, NACA Report RM E9D12, 1949.

9 "Influence of Tube-Entrance Configuration on Average Heat-Transfer Coefficients and Friction Factors for Air Flowing in an Inconel Tube," by M. D. Grele and W. H. Lowdermilk, NACA RM E50 E23.

10 "Correlation of Forced Convection Heat-Transfer Data for Air Flowing in Smooth Platinum Tube With Long Approach Entrance at High Surface and Inlet Air Temperature," by L. G. Desmon and E. W. Sams, NACA RM E50 H23.

11 "Heat Transfer," by W. H. McAdams, McGraw-Hill Book Company, Inc., New York, N. Y., second edition, 1942, p. 168.

New Technique for Obtaining Heat-Transfer Parameters of the Wall and Combustion Gas in a Rocket Motor

By M. E. ELLION,[1] PASADENA, CALIF.

The design of regeneratively cooled rocket motors has been hindered seriously by the lack of available data for the physical properties of both the propellants and alloys used in rocket-motor construction. Bell Aircraft has initiated a program to extend the accuracy and range of available data together with an attempt to broaden the fundamental basis for generalizing the heat-transfer analysis. The program includes a laboratory-test study of the heat transfer through liquid-coolant film, combustion-gas film, and rocket-motor wall. This paper is primarily concerned with the heat transfer through the rocket wall. A test method is discussed for obtaining gas side wall temperatures in a rocket motor in order to evaluate the suitability of various alloys for rocket-motor construction. Eight alloys have been studied by employing a thick-walled water-cooled nozzle into which cylindrical specimens could be inserted for tests. The heat flows and wall temperatures have been determined by employing the nozzle as a heat meter and by using a new calculation method that accounts for variable thermal properties with temperature. The thermal conductivities of all alloys tested have been determined accurately by the Institute of Research, Lehigh University. A modification of this technique is suggested for measuring the combustion-gas film coefficient in a rocket motor.

Nomenclature

The following nomenclature is used in the paper:

a = area perpendicular to heat flow, sq ft
C = a const
h = film heat-transfer coefficient (Btu/ft²-hr-deg F)
K = thermal conductivity (Btu/ft²-sec-deg F/in.)
n = dimension in direction of heat flow
Nu = Nusselt number
Pr = Prandtl number
q = heat flow per unit time (Btu per sec)
r = radius, in.
Re = Reynolds number
T = temperature, deg F
x = dimension in direction of heat flow, in.
α = a constant
β = a constant
Δ = finite increment
λ = fuel-oxidizer ratio
Σ = finite summation
φ = function of what follows

Subscripts

g = gas
i = surface through which heat enters system, i.e., for specimen it indicates gas interface, and for copper nozzle it indicates specimen-copper interface.
o = surface through which heat leaves system

Introduction

One of the more complex calculations involved in liquid-propellant rocket-motor design is the analysis of the cooling requirements. Regenerative cooling is the most direct design approach, but the analysis remains mainly empirical because of the lack of complete data for the physical properties of both the propellants and the alloys used in motor construction. Combustion pressures of 20 atm and temperatures of the order of 5000 F are required for good performance; heat fluxes up to 7.0 (Btu/in²-sec) are required for cooling; and gas velocities of sonic and above occur at the throat and divergent sections of the motor. As a consequence, the heat-transfer coefficients for the liquid coolant, metal wall, and combustion gas may be of the same order of magnitude. The four parameters which define these three types of heat transfer; h_L (liquid film), K, and allowable T_i (metal wall), and h_g (gas film), must be determined before the analysis may be reduced to an analytical solution.

In view of the lack of basic information, a test program has been initiated at Bell Aircraft to extend the accuracy and range of available data, together with an attempt to broaden the fundamental basis for generalizing the cooling design.

This paper will present an insight into this test program along with a detailed description of the heat transfer through the metal wall.

Test Program

Liquid Film Coefficient (h_L). Since little is known of the physical properties of rocket propellants, it is seldom possible to employ the conventional equation, $\text{Nu} = C(\text{Re})^{\alpha}(\text{Pr})^{\beta}$, to obtain the liquid film coefficient. Furthermore, the extremely high velocities needed to cool the rocket throat section by forced convection alone would cause prohibitively high pressure drops and manufacturing difficulties. The required liquid velocity may be reduced appreciably by taking advantage of the high heat flux obtainable with surface or nucleate boiling. At present there is no general equation that correlates nucleate-boiling heat transfer successfully.

Fig. 1 shows an apparatus suitable for determining the liquid film coefficient up through the nucleate-boiling region (1).[2] The test fluid is passed through an annulus formed by an electrically heated stainless-steel tube and a stainless-steel case. The direct-current power supplied to the tube, the flow rate, fluid

[1] Jet Propulsion Laboratory, California Institute of Technology, formerly Bell Aircraft Corporation, Buffalo, N. Y.

Contributed by the Heat Transfer Division and presented at the Heat Transfer and Fluid Mechanics Institute Meeting, Los Angeles, Calif., June 28–30, 1950, of The American Society of Mechanical Engineers.

Note: Statements and opinions advanced in papers are to be understood as individual expressions of their authors and not those of the Society. Manuscript received at ASME Headquarters on August 14, 1950.

[2] Numbers in parentheses refer to the Bibliography at the end of the paper.

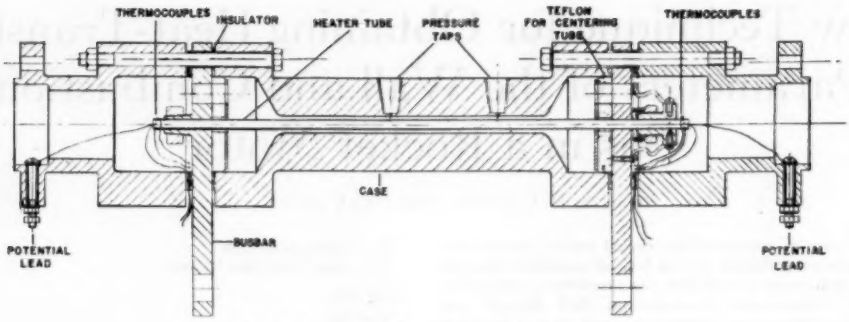

FIG. 1 LIQUID FILM-COEFFICIENT TEST APPARATUS

pressure, and temperatures of the fluid and tube are measured. The liquid-film coefficient may be calculated from these values. The effects of varying fluid pressure, temperature, and velocity along with tube temperature may be studied. Heat fluxes to white fuming nitric acid up to 5.5 (Btu/in.^{2} sec) have been measured with this unit at Bell Aircraft.

Thermal Conductivity, K (2). The heat flow by conduction through the rocket-motor wall may be obtained easily if accurate values of thermal conductivity are available. Since the temperature difference through the wall often exceeds 1000 deg F, it also becomes necessary to consider the variation of thermal conductivity with temperature.

Bell Aircraft has subcontracted to the Institute of Research, Lehigh University, for the measuring of thermal conductivities, employing a modification of the Forbes bar method adapted to high temperatures. Table 1 shows the results obtained to date.

TABLE 1 THERMAL CONDUCTIVITY, CAL/CM-SEC DEG C

Temp, deg C	Type 310	Type 316	Type 347	SAE 1010	A Nickel	Inconel X
0	0.031	0.0620	0.0459	—	—	—
100	0.034	0.0670	0.0489	0.163	0.157	0.038
200	0.039	0.0714	0.0526	0.153	0.139	0.043
300	0.044	0.0754	0.0564	0.144	0.122	0.048
400	0.048	0.0792	0.0607	0.136	0.114	0.054
500	0.054	0.0831	0.0656	0.130	0.121	0.060
600	0.060	0.0865	0.0700	0.123	0.129	0.065
700	0.066	0.0908	0.0753	0.117	0.136	0.073
800	0.072	0.0948	0.0808	0.111	0.143	0.081
900	0.078	0.0995	0.0868	—	0.151	0.089
1000	0.084	—	—	—	0.158	—

Allowable Wall Temperature (T_i). It is necessary to know the temperature at which an alloy exposed to the combustion gases will break down due to melting, plastic flow, or oxidation. The oxidation, plastic flow, or erosion temperatures will be a function not only of alloy properties, but also of the composition and velocity of the combustion gases. It is clear that such an answer will not yield to a purely analytical solution. As a result, a test program was initiated in January, 1949, to test, under actual rocket conditions, the suitability of alloys for rocket-nozzle construction. The determination of maximum safe wall temperature had been impossible heretofore because of the difficulty of measuring the wall temperature next to the combustion gases, but a logical solution to the problem presented itself with the availability of accurate thermal-conductivity data.

HEAT TRANSFER IN ROCKET WALL

Method of Determining Heat Flow and Temperature (4). The Fourier law of heat conduction would readily yield a solution for steady-state unidirectional heat flow were it not for the variation of thermal conductivity with temperature. While it is always possible to express the conductivity-temperature relation with the series

$$K = \sum_0^m C_n T^n$$

and solve the Fourier equation analytically,[5] it was believed that the solution would be obtained more readily by graphical methods. It will be seen that this is the case, since only one curve is needed to represent the Fourier equation for any alloy regardless of heat flow, temperature, or geometry of the system.

The general equation for steady-state unidirectional heat flow may be written as

$$\frac{dq}{da}\,dn = -KdT \qquad [1]$$

or, since $(dq)/(da_i)$ is a constant for any given system

$$\frac{dq}{da_i}\int \frac{da_i}{da}\,dn = -\int KdT \qquad [2]$$

where n is the dimension in the direction of heat flow, and a_i is the area of the surface through which heat enters the system.

Equation [2] suggests a family of curves of temperature versus $(dq)/(da_i)\int (da_i)/(da)\,dn$. However, we may note upon differentiating Equation [2]

$$\frac{dT}{\dfrac{dq}{da_i}\,d\displaystyle\int \frac{da_i}{da}\,dn} = -\frac{1}{K} = \varphi(T) \qquad [3]$$

that the slopes of the curves are a function of temperature alone, that is, all curves may be represented by one, if the abscissa scale is shifted to fulfill boundary conditions.

It is now clear that a curve of temperature versus $(dq)/(da_i)\int (da_i)/(da)\,dn$ is independent of the geometry, temperature, or heat flow of the system and, consequently, becomes a general curve for the given alloy.

Either Equation [2] or [3] may be used for construction.

Fig. 4 shows such a curve for Armco iron. The maximum temperature of interest with this metal is 1650 F, so this was chosen as the ordinate intercept. Points on the curve were obtained by measuring the area under the K versus T curve from $T_i = 1650$ to T. The value of the abscissa at any point on the general curve is this area and the ordinate value is T. An

[5] Reference (5) illustrates an analytical solution for a linear variation of conductivity with temperature.

equivalent effect of sliding the abscissa is obtained by treating it only as a difference scale.

The abscissa for standard shapes becomes

Slab

$a = a_i$ and independent of n

$n \equiv x$

$$\frac{dq}{da_i}\int_{n_i}^{n}\frac{da_i}{da}\,dn = \frac{q}{a_i}(x - x_i)$$

Cylinder

$$a = 2\pi rL$$
$$a_i = 2\pi r_i L$$
$$n \equiv r$$

$$\frac{dq}{da_i}\int_{n_i}^{n}\frac{da_i}{da}\,dn = \frac{q}{a_i}\,r_i \log_e \frac{r}{r_i}$$

Sphere

$$a = 4\pi r^2$$
$$a_i = 4\pi r_i^2$$
$$n \equiv r$$

$$\frac{dq}{da_i}\int_{n_i}^{n}\frac{da_i}{da}\,dn = \frac{q}{a_i}\,r_i^2\left(\frac{1}{r_i} - \frac{1}{r}\right)$$

The curve may be plotted at about 45 deg slope for convenience. This is easily accomplished by choosing the abscissa scale factor (Btu-in/ft²-sec per unit) equal to an average K times the ordinate scale factor (deg F per unit).

It is noted that the validity and simplicity of this method hold for any conductivity variation with temperature. The accuracy of the curve is the same as that of the conductivity data.

Description of Apparatus: Six-Pass Motor (6). Fig. 2 illustrates the six-pass rocket, which was the first attempt made at Bell Aircraft to measure both heat flows and wall temperatures.

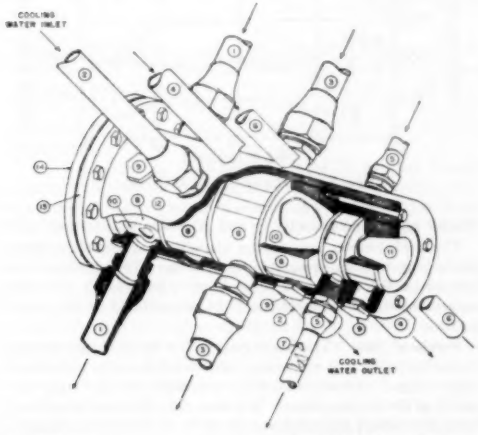

1 First pass
2 Second pass
3 Third pass
4 Fourth pass
5 Fifth pass
6 Sixth pass
7 Mixing baffles
8 Shroud-block halves (in place)
9 Thermocouple-outlet plug
10 Combustion chamber
11 Nozzle
12 Cooling jacket
13 Head-mounting flange
14 Injector head

FIG. 2 SIX-PASS ROCKET MOTOR

The coolant was divided into six passages perpendicular to the motor axis so that the enthalpy increase at each station could be recorded. Thermocouples were copperplated to the wall next to the coolant to allow gas side wall temperatures to be calculated.

This apparatus was built (at considerable expense) and tested, but the inaccuracies experienced were sufficient to discourage detail testing.

Material Test Motor (7). With the availability of reliable thermal-conductivity data and the temperature versus $[q/a_i \int (da_i)/(da)\,dn]$ curves, a different approach to the problem was possible.

Fig. 3 shows a cross section of a thick-walled water-cooled copper nozzle into which cylindrical specimens can be inserted for test. This arrangement allows both heat flows and gas side wall temperatures to be determined.

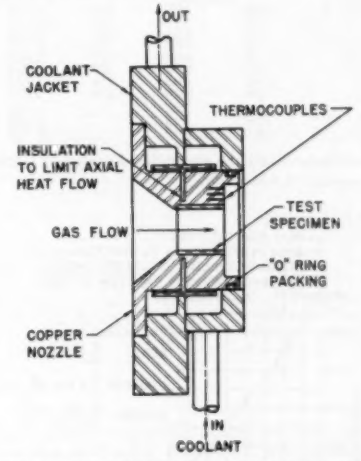

FIG. 3 ROCKET-MOTOR NOZZLE FOR MATERIAL TEST

The copper nozzle is used as a heat meter. Nine thermocouples arranged in three radial groups were inserted into the copper parallel to the nozzle axis, and the outputs continuously recorded on nine Leeds and Northrup Speedomax recorders. Any two thermocouples along a radius are sufficient to establish heat flow and thus temperature at any point along the radius.

As an illustration that two thermocouples are sufficient to establish heat flux and thus temperature at any radius, consider Fig. 4 for an Armco-iron cylinder. For the example, let the two thermocouples located at $r_1 = 1.000$ in. and $r_2 = 1.081$ in. indicate 1300 F and 800 F, respectively. The value of $(q/a_i)r_i \log_e(r_2/r_1)$ is read from the curve as 59—20 = 39 and thus

$$\frac{q}{a_i} = \frac{39}{r_i \log_e \frac{r_2}{r_1}} = 1000 \text{ Btu/ft}^2\text{-sec}$$

with $r_i = 1/2$ in. The temperature at any other point, e.g., $r_3 = 1.203$, may be obtained at an abscissa value of

$$\frac{q}{a_i}\,r_i \log_e \frac{r_3}{r_2} = 53.5$$

from T_3, giving $T_3 = 300$ F. It is seen that the solution using

TABLE 2 TEST SPECIMENS

Alloy	q/α Btu/ft² sec	T_i deg F	Thrust, lb	Fuel/oxidiser ratio, A	Chamber pressure, psi	Time, sec	Wall thickness, in.	Remarks	Recommended maximum allowable temperature, deg F
Armco iron	700	1260	176	0.849	250	60	0.10	Heavy oxidation	
	740	1320	191	0.880	295	60	0.10	Heavy oxidation	1350
	760	1390	175	0.614	246	50	0.10	Some loss of metal	
Type 1010	720	1110	178	0.949	268	40	0.10	Light oxidation	
	900	1400	217	0.854	321	30	0.10	Heavy oxidation	1570
	930	1460	235	0.865	347	30	0.10	Heavy oxidation	
	1063	1570	194	0.805	290	30	0.10	Little erosion	
Type 347	875	1900	230	0.673	330	60	0.10	Light oxidation	
	758	2400	244	0.960	330	30	0.20	Heavy localised erosion and loss of metal	2200
Type 446	561	1560	171	0.90	330	44	0.15	Light oxidation	
	545	1450	171	0.90	330	44	0.15	Light oxidation	1900
	717	1875	200	0.825	375	50	0.15	Very close to failure	
Type 310	557	1792	160	...	308	26	0.15	Light oxidation	1900
	685	2000	177	...	330	40	0.15	Heavy erosion	
Aluminum Type 61S-T	995	770	202	0.934	278	40	0.10	Little effect	
	860	800	174	0.894	246	30	0.10	Little effect	
	928	838	190	0.904	267	30	0.10	Little effect	850
	958	867	202	0.934	278	35	0.10	Some erosion	
	1100	1000	200	0.704	280	60	0.10	Heavy loss of metal	
Nickel Type "A"	1010	1560	214	0.793	290	75	0.10	No effect	
	1150	1720	204	0.753	280	75	0.10	Light oxidation	Test to be
	1110	2110	255	0.823	375	91	0.20	Light oxidation	completed
	1150	2200	250	0.940	370	82	0.20	Light oxidation	(Above 2200)
Inconel "X"	570	1470	197	0.905	278	60	0.10	Light oxidation	
	640	1580	207	0.925	295	40	0.10	Light oxidation	1700
	680	1640	216	1.010	307	40	0.10	Heavy oxidation	
	780	1800	229	1.010	328	40	0.10	Moderate erosion	
Copper	1300	920		0.534	283	45		Motor not designed for this material to fail	
	1380	970		0.483	280	80			
	1470	1040		0.916	337	64			

the curve follows closely the conventional analytical method employing constant conductivity.

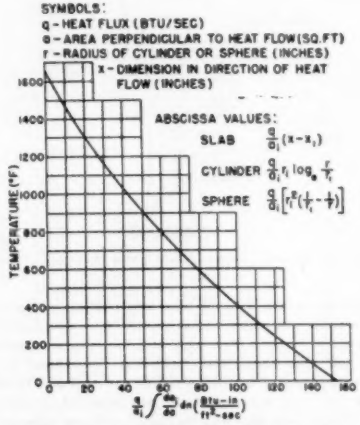

FIG. 4 TEMPERATURE DISTRIBUTION CURVE THROUGH A FLAT SLAB, CYLINDER OR SPHERE WITH THERMAL CONDUCTIVITY A FUNCTION OF TEMPERATURE
(Material-Armco ingot iron.)

In order to pick up any heat-flux variation around the circumference of the copper nozzle, three groups of thermocouples were inserted with an additional thermocouple in each group as a check.

The thermocouples were 0.008-in. Advance wire with the copper nozzle acting as the other junction metal. It is apparent that the diameter of the thermocouple was of importance, since a radial temperature gradient of over 1000 deg F per in. existed in the copper. The Advance wire was insulated from the nozzle except for a $^1/_{16}$-in. junction, so that the temperature gradient along the axis had little effect.

The gas side wall temperature of the specimen was varied by changing combustion-gas pressure and temperature. Since the combustion-gas pressure was limited to about 350 psia, the specimens were made of different thicknesses to allow failure, Table 2. The thickness required to cause any alloy to fail, of course depended upon the conductivity and allowable wall temperature.

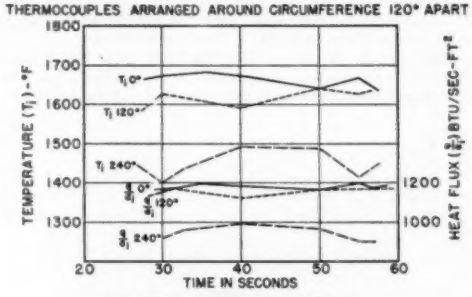

FIG. 5 MATERIAL TEST "A" NICKEL

The rocket-motor combustion chamber was made conservatively long to insure complete combustion. The specimen was located at the throat and thus it was subjected to the most severe heat-transfer conditions to be encountered in the rocket motor.

Results of Tests. The initial runs with a liquid oxygen-alcohol motor indicated that some care was needed to insure reliable results. Fig. 5 presents values for a preliminary test with "A" nickel as the test specimen. It is seen that the temperature and heat flow varied appreciably both with time and with circumferential position.

The nickel specimen was slipped into the copper nozzle, depending on thermal expansion for good thermal contact. Micrographic inspection of the nickel after testing indicated temperatures appreciably higher than the calculated values. The error was attributed in part to the large unknown value of thermal resistance at the interface between the specimen and the copper

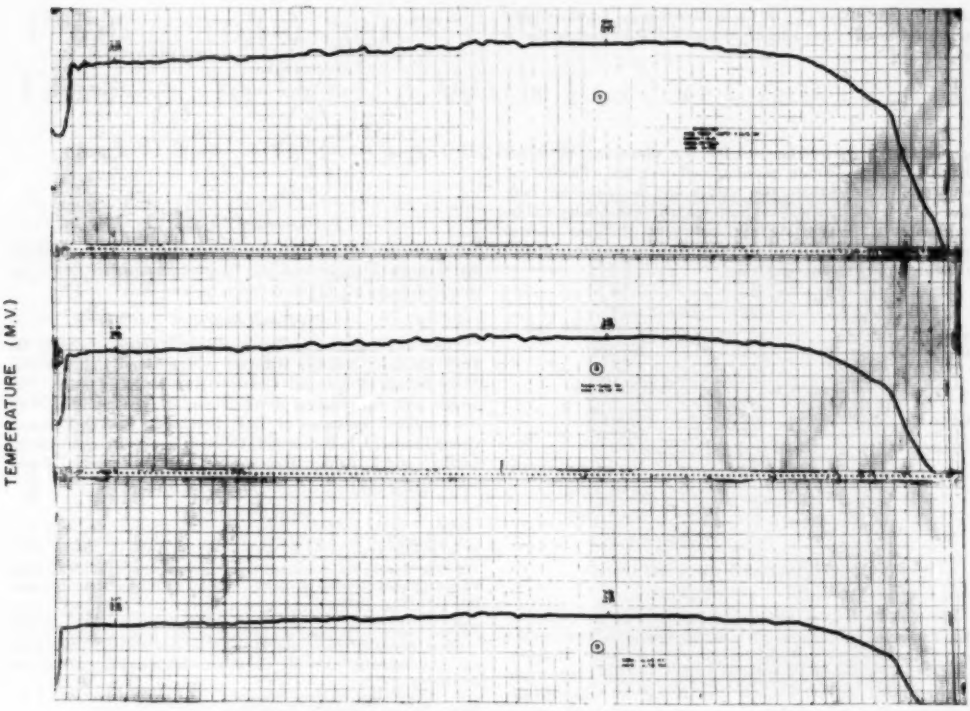

FIG. 6 TEMPERATURE-TIME TRACES

nozzle. This difficulty was corrected by silver-soldering the specimens into the copper. Variations in circumferential gas conditions were improved by increasing the length of the combustion chamber, and temperature fluctuations with time were decreased by insulating the thermocouple reference junctions from the effects of combustion-gas exhaust.

Fig. 6 shows temperature-time traces for three radial thermocouples with a copper specimen after the foregoing modifications were made. The variation in temperature during the run is less than 2 per cent, confirming the validity of employing a steady-state analysis.

Table 2 lists the results obtained for seven alloys tested. The heat flux (q/a_i) and wall temperature (T_i) at the combustion-gas specimen interface were calculated from the nine thermocouple readings and curves similar to Fig. 4. From this it was possible to pick a recommended allowable wall temperature above which loss of metal from the test specimen occurred due to melting, erosion, or plastic flow. Heat flux and wall temperatures are probably within 3 per cent of the true values. The choice of the most suitable alloy for rocket-motor construction depends on several factors in addition to the allowable inside wall temperatures. The strength, density, and thermal conductivity of the alloy along with the corrosiveness and physical properties of the coolant are equally important. It is beyond the scope of this paper to discuss these factors in more than a general manner (3).

It should suffice to point out that a superficial comparison of the alloys would probably indicate that the most suitable was the one having the highest allowable wall temperature and, consequently, the lowest required heat flux. However, the high-temperature alloys, in general, have the lowest thermal conductivity. Thus, for the high-temperature low-conductivity alloys, the temperature drop through the wall may cause the coolant wall temperature to be too low for proper cooling even for the low heat flux. This is especially true of motors that require thick walls for structural stability, and thus conductivity for these motors may be of greater importance than high allowable wall temperatures.

In this case it may be advantageous to employ a high-conductivity alloy clad with a high-temperature alloy, chromized low-carbon steel, or other methods of combining high allowable temperature with high conductivity. An alternative is to decrease wall thickness and employ the strength of the coolant jacket to obtain structural stability.

GAS FILM COEFFICIENT (h_g)

The heat-meter method may be extended to measure effective gas temperature and over-all gas-film coefficient. Fig. 7 shows a compact device which is inserted through the wall of the rocket motor to measure these quantities. The hot combustion gas flows across the uninsulated tips of the two alloys A and B. Consequently, heat is drawn from the gas along the alloys into the coolant chamber of the probe. Two thermocouples located at known distances along each of the alloys allow heat flux (q/a_i)

and tip temperatures (T_i) at the combustion-gas interface to be calculated from curves similar to Fig. 4. The Newton law of cooling

$$\frac{q}{a} = h_g(T_g - T_i)$$

applied at the gas interface for the two alloys may be solved simultaneously to obtain gas-film coefficient and effective gas temperature, since these two values are the same for both alloys. The heat flux and tip temperature for each alloy will be appreciably different if alloys of sufficiently different thermal conductivity are chosen. The design may be modified by constructing two radiation shields.

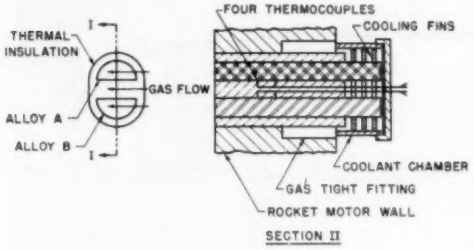

FIG. 7 TEMPERATURE-MEASUREMENT PROBE

This unit has not yet been tested; however, the technique has been demonstrated successfully from measurements made on the copper nozzle of the material test motor described. Measurements of heat flux (q/a_i) and inside wall temperature were made for Armco iron and 347 stainless steel during two runs with the motor operating at as close to the same values of chamber pressure and fuel/oxidizer ratio as was possible. With the heat flux and T_i obtained, the simultaneous solution of equation, $q/a_i = h_g(T_g - T_i)$, for the two tests gave

$$h_g = \frac{\left(\frac{q}{a_i}\right)_{347} - \left(\frac{q}{a_i}\right)_{Fe}}{(T_i)_{Fe} - (T_i)_{347}} = 1000 \text{ Btu/ft}^2\text{-hr-deg F}$$

and

$$T_g = \frac{(T_i)_{347}\left(\frac{q}{a_i}\right)_{Fe} - (T_i)_{Fe}\left(\frac{q}{a_i}\right)_{347}}{\left(\frac{q}{a_i}\right)_{Fe} - \left(\frac{q}{a_i}\right)_{347}} = 3800 \text{ F}$$

T_g (theoretical) = 4300 F

The discrepancy between calculated effective gas temperature and theoretical temperature may be attributed to variation in the combustion-gas conditions between the two runs.

ACKNOWLEDGMENTS

These investigations are sponsored by the United States Air Force Contract Number W33-038 ac-14169 and United States Navy Bureau of Ordnance Contract Number NOrd 9876. The design and experimental development was accomplished with the combined assistance of T. F. Reinhardt, Rocket Research Group Leader; J. L. B. Selwood, Assistant Rocket Research Group Leader; and E. Ashley, Development Test Engineer; Bell Aircraft Corporation.

BIBLIOGRAPHY

1 "Liquid Film Coefficient Tests," by T. F. Reinhardt and R. B. Foster, Meteor Report BAC-1, May, 1947.

2 "A Survey of Existing Data and Methods of Measuring Thermal Conductivities of Metals," by M. E. Ellion, Meteor Report BAC-18, May, 1948.

3 "Requirements for Metals for Regeneratively Cooled Rocket Motors," by J. L. B. Selwood, Meteor Report BAC-13, July, 1947.

4 "A Study of Heat Flow Through Metals With Variable Thermal Conductivity," by M. E. Ellion, Meteor Report BAC-21, November, 1948.

5 "Conduction of Heat in Solids," by H. S. Carslow and J. C. Jaeger, Oxford University Press, New York, N. Y., 1947.

6 "Six Pass Rocket Motor," by T. F. Reinhardt, M. E. Ellion, and R. Albert, Meteor Report BAC, April, 1950.

7 "A New Technique for Evaluating Rocket Nozzle Materials," by M. E. Ellion, BAC Report, April, 1950.

Photographic Study of Surface-Boiling Heat Transfer to Water With Forced Convection[1]

By F. C. GUNTHER,[2] PASADENA, CALIF.

To investigate the effect of forced convection on the mechanism of heat transfer with surface boiling, a high-speed, high-resolution photographic study was made. The test section was a transparent channel of rectangular cross section $^3/_{16} \times ^1/_2 \times 6$ in., with an electrically heated metal strip $^1/_8$ in. wide suspended lengthwise to divide the channel into two flow passages. To facilitate photography of boiling on the metal strip near burnout conditions, the burnout limits for this section were determined experimentally. An empirical equation was fitted to the points.

Introduction

TO investigate the effect of forced convection on the mechanism of heat transfer with surface boiling, a high-speed high-resolution photographic study is being made. The test section used was a transparent channel of rectangular cross section $^3/_{16} \times ^1/_2 \times 6$ in., with an electrically heated metal strip, $^1/_8$ in. wide, suspended lengthwise to divide the channel into two flow passages. To facilitate photography of boiling on the metal strip near burnout conditions, the burnout limits for this section were determined experimentally. The empirical equation which was devised to fit the results of 38 determinations of burnout heat-transfer rate is

$$(q/A)_{\text{burnout}} = 0.0135V^{0.6}\,\Delta T_{\text{sub}}$$

where q/A = burnout heat flux (Btu/sq in. sec); V = fluid velocity, fps; and ΔT_{sub} = subcooling = $T_{\text{saturation}} - T_{\text{liquid}}$, deg F; T_{liquid} = mixed outlet temperature.

The photographic results indicate that the coolant velocity does not detach vapor bubbles from the heating surface at large subcooling. The attached bubbles slide downstream during growth and collapse, producing turbulence in the sublayer from the translational motion of the bubbles in addition to that resulting from their growth and collapse action. The effect of an increase in stream velocity or subcooling is to reduce bubble size and life span. An increase of heat-transfer rate causes bubble population to increase up to a limit where bubbles coalesce to vapor clumps, Fig. 1. Bubble coalescence signifies incipient film boiling and burnout, as indicated by the fact that Fig. 1 was photographed within 10 per cent of the maximum burnout heat flux. Quantitative data relating bubble size, population, and frequency to the heat-transfer conditions are presented.

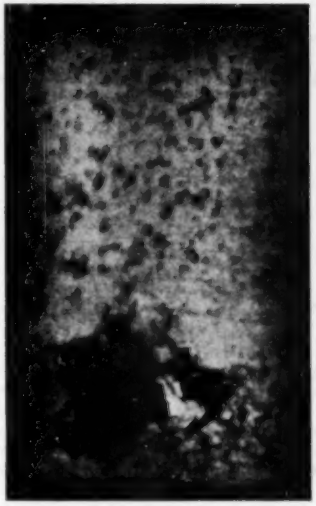

Fig. 1 Plan View of Boiling on Metal Strip in Stream of Water Flowing 25 Fps, Subcooled 190 F, at a Heat-Transfer Rate of 13 Btu/Sq In. Sec

Apparatus and Experimental Method

Heat-Transfer Apparatus. The burnout test section consisted of a channel of rectangular cross section $^3/_{16}$ in. wide and $^1/_2$ in. high. An electrically heated metal strip $^1/_8$ in. wide and 0.004 in. thick was suspended axially in the channel mid-plane dividing the channel into two equal flow passages. The upper and lower passages were not separated completely, since $^1/_{32}$-in. clearance at each edge of the heating strip was necessary to prevent damage to the glass channel walls by thermal shock during burnouts, Fig. 2(*a*). Therefore, in both the upper and the lower flow passages, the objective of two-dimensional flow between parallel plane walls, one cold and one heated, was only approximated. The use of a wider metal strip in a wide channel, to improve the approximation of two-dimensional flow, would have restricted maximum flow velocity and heat-transfer rates because of limitations in the available pumping system and supply of current for direct-current heating. It is believed that the very small-scale boiling phenomenon was not modified appreciably by exchange flow around the strip edges or by side-wall boundary layer. A second apparatus, with a transparent flow channel $^1/_4$ in. square in cross section, divided by a heating strip $^3/_{16}$ in. wide, Fig. 2(*b*), was used for photographic tests.

Distilled water was circulated through the test section from the stainless-steel flow system sketched in Fig. 3. Prior to each test, the system was degassed by aspirating the degassing tank to a pressure of 3 in. of mercury, absolute, while water was cir-

---

[1] This paper presents the results of one phase of research carried out at the Jet Propulsion Laboratory, California Institute of Technology, under U. S. Army Ordnance Department Contract No. W-04-200-ORD-455.

[2] Jet Propulsion Laboratory, California Institute of Technology.

Contributed by the Heat Transfer Division and presented at the Heat Transfer and Fluid Mechanics Institute Meeting, Los Angeles, Calif., June 28–30, 1950, of The American Society of Mechanical Engineers.

Note: Statements and opinions advanced in papers are to be understood as individual expressions of their authors and not those of the Society. Manuscript received at ASME Headquarters, August 14, 1950.

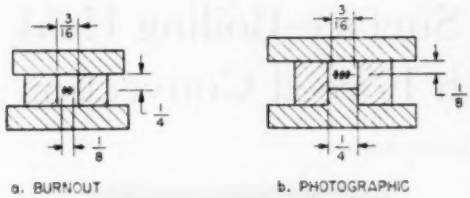

FIG. 2 CROSS SECTIONS OF FLOW CHANNELS USED IN BURNOUT AND PHOTOGRAPHIC TESTS

(a, Burnout: Hydraulic diameter = 1/2 in.; length = 6 in.; heated length = 3 in. b, Photographic: Hydraulic diameter = 1/4 in.; length = 6 in.; heated length = 2 1/2 in.)

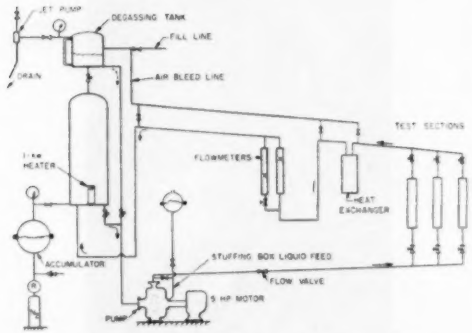

FIG. 3 FLOW CIRCUIT USED FOR PHOTOGRAPHIC STUDY

culated for about 1/2 hr with heat addition to boil off a portion of the water. Next, the system was isolated from the degassing tank, and compressed nitrogen was applied to the accumulator diaphragm to establish the desired pressure level for the test. This procedure reduced the concentration of dissolved air to about 0.3 cc per liter, as determined by the chemistry section of this laboratory. Since air-bubble release at the heating surface was absent in photographs taken with less rigorous degassing, it was found sufficient to degas until visible bubbles in the low-pressure wake of the rotameter float disappeared. No effect of dissolved-air content on the burnout limit has been detected.

To test for burnout limits, the flow velocity and static pressure level in the test section were fixed. Since burnout occurred consistently near the outlet end of the heating strip, where subcooling was minimum, outlet mixed bulk temperature was taken as the pertinent liquid temperature T_L. The heating-current input was increased carefully by compressing a carbon-pile resistor in series with the field of a 12-kw d-c generator. Current was read visually by two operators on a 1/4 per cent millivoltmeter paralleled with a shunt of 1/2 per cent accuracy. From the known (by calibration) resistivity of the heating strip as a function of temperature, burnout heat-transfer rate was computed from the maximum current reading by the equation

$$q/A = \frac{I^2\rho l}{1055 A_{\text{current flow}} A_{\text{heat transfer}}}$$

where I = current (amp), ρ = electrical resistivity (ohm in.), l = length (in.), and A = area for current flow (sq in.); $A_{\text{heat transfer}}$ included the wetted edges as well as top and bottom surfaces of the heating strip.

As a check on this measurement of heat-transfer rate, voltage-tap needles were inserted through the flowing stream to contact the heating strip at a fixed spacing. Wattage input measured by volt-amperes was in close agreement with that computed from I^2 and resistivity in check tests up to a heat flux of 7 Btu/sq in. sec.

Heating-surface temperature was not measured, since additional or more precise information on surface temperature during surface boiling[3,4] was considered of importance secondary to securing photographic data and information on burnout limits.

Photography. As in the photographic study of surface boiling in a pool,[5] the Kerr-cell, electro-optical shutter was used in conjunction with the General Radio 35-mm shutterless camera. Since a large improvement in photographic resolution was necessary in order to study the much smaller bubbles encountered in forced convective surface boiling, a considerable amount of trial-and-error work was performed. The end result was the arrangement shown in Fig. 4. About 60 rolls of 35-mm film, in 100-ft lengths, were used for preliminary and data-taking tests in this study.

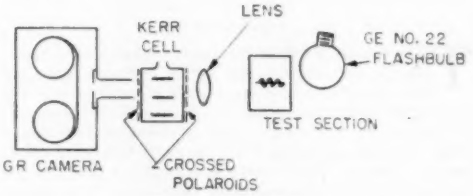

FIG. 4 CAMERA SETUP

To obtain a photograph, the desired boiling condition was established in the channel. By depressing a hand switch, relays applied 220 volts to the camera drive and initiated an electronic timer. After a 1.2-sec interval for camera acceleration, the timer triggered two parallel relays which fired the photoflash bulb and the power supply feeding 14,000-volt pulses to the Kerr cell at a preset pulse length and frequency. The power supply was able to sustain Kerr-cell pulses for about 0.05 sec. As a result, only 5 ft of exposed film was obtained after an 85-ft film acceleration. By reversing the film in the camera, an additional photograph was obtained on the other end of each film. With the image magnified 5 diam on the negative, flashbulb illumination was sufficient for exposures of 2 microsec. To prevent image overlap at the shuttering rate of 20,000 frames per sec, it was necessary to mask the image with a focal plane slit of 0.072 in. The field of view at magnification ×5 measured 0.014 × 0.100 in.

Photographs with the camera axis normal to the heating surface were necessary in determining bubble population and size. Because sufficient lighting could not be obtained to illuminate bubbles by reflection from the vapor-liquid interfaces, it was necessary to incline the lens axis 20 deg from perpendicular and photograph the direct reflection of flashbulb light from the pol-

[3] "Heat Transfer to Water at High Flux Densities With and Without Surface Boiling," by Frank Kreith and M. Summerfield, Trans. ASME, vol. 71, 1949, pp. 805–816.

[4] "Heat Transfer at High Rates to Water With Surface Boiling," by W. M. McAdams, et al., *Industrial and Engineering Chemistry*, vol. 41, 1949, pp. 1945–1953.

[5] "Photographic Study of Bubble Formation in Heat Transfer to Subcooled Water," by F. C. Gunther and Frank Kreith, Heat Transfer and Fluid Mechanics Institute, Berkeley, Calif., published by THE AMERICAN SOCIETY OF MECHANICAL ENGINEERS, New York, N. Y., May, 1949, pp. 113–126.

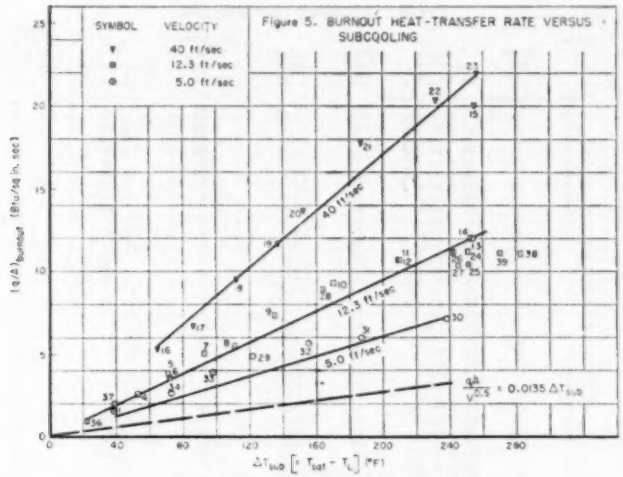

FIG. 5 BURNOUT HEAT-TRANSFER RATE VERSUS SUBCOOLING

ished heating surface. Bubbles were thus outlined by their interruption of reflection from the metal surface, as shown in Fig. 1, giving resolution of bubbles as small as 0.002 in. in radius.

EXPERIMENTAL RESULTS

Burnout Limits. The 38 determinations of burnout limit in the photographic test section were first plotted with the two burnout correlations which McAdams[4] devised to fit data from nine burnout tests, ranging in heat transfer from 1 to 3.9 Btu/sq in. sec, and made in an annulus. Since the author's data at higher heat flux ranged up to 100 per cent above the extrapolated McAdams predictions and deviated in systematic velocity groups, the 38 points were replotted as $(q/A)_{burnout}$ versus ΔT_{sub} on linear paper, Fig. 5. The most satisfactory fit which could be expressed as a simple equation was obtained by drawing straight lines of constant velocity radiating from zero. Division by $V^{0.5}$ caused the best superposition of all data, expressible by the equation

$$(q/A)_{burnout} = 0.0135 V^{0.5} \Delta T_{sub} \quad \ldots\ldots\ldots\ldots [1]$$

In Fig. 6 the experimental points from Table 1 are plotted for comparison with Equation [1]. When the effect on burnout limit of flow-duct configuration, liquid properties, and other variables is clarified by future experiment, an effort can be made to generalize Equation [1] to dimensionless form.

Photographic Results. Profile photographs of surface boiling at large subcooling show that bubbles roughly hemispherical in shape grow and collapse while remaining attached to the heating surface, simultaneously sliding downstream under the influence of coolant velocity. Fig. 7, a typical print from a sequence of 20,000 frames per sec, demonstrates this lack of bubble detachment. For profile photographs the camera axis, although normal to the channel axis, was raised 10 deg from tangency with the heating surface; the bright zone in each frame is thus the upper surface of the heating strip near the far edge. Each bubble casts a shadow toward the observer. Deformation of bubbles from hemispherical to teardrop shape is visible at this stream velocity of 20 fps. The sliding velocity of bubbles was approximately $^{9}/_{10}$ of stream velocity, increasing slightly with bubble size.

Kerr-cell photographs from the plan view (camera axis 20 deg from normal to the heating surface) were taken at high repetition rate at each heat-transfer condition in order to permit measurement of the following bubble parameters:

R_{max} = radius at full growth of the "average" bubble at the heat-transfer condition. The radius-versus-time relation was measured for several bubbles, from 100-diam projection of the negatives, and plotted as in Figs. 8 to 10, inclusive. By reference to these plots and visual examination of the entire sequence on the negative, an average R_{max} was estimated. The restricted field of view and length of each photographic sequence made statistical determinations of average R_{max} impossible.

θ = lifetime of an average bubble associated with the heat-transfer condition. As in the case of R_{max}, θ was also estimated from radius-versus-time curves in conjunction with examination of the negative.

N = number of new bubbles of average size appearing on unit area per unit time. N was obtained by counting bubble starts in the field of view during 300 frames (0.015 sec), counting each bubble as more or less than unity in accord with the ratio of its area to that of the selected average bubble.

F = percentage of heating surface covered by bubbles, averaged over time. F was calculated by the expression

$$F = 100\, N\theta \left\{ \frac{1}{\theta} \int_0^{\theta} \pi\, [R(t)]^2\, dt \right\} \text{ per cent} \ldots\ldots [2]$$

where t = time in seconds, and the bracketed term represents the area covered by one bubble averaged over its lifetime. By integrating area-versus-time curves graphically for a number of bubbles, it was found that the bracketed term is approximated closely by a simplified expression

$$\left\{ \frac{1}{\theta} \int_0^{\theta} \pi\, [R(t)]^2\, dt \right\} = 0.57\, \pi R^2_{max}$$

Substituting in Equation [2]

$$F = 100\, N \left(\frac{\text{bubbles}}{\text{sq in. sec}} \right) (0.57\, \pi\, R^2_{max}\, \theta) \left(\frac{\text{sq in. sec}}{\text{bubble}} \right) \text{per cent}$$

TABLE 1 BURNOUT TEST RESULTS

Test no.	Velocity, fps	Symbol	Pressure, absolute	T_{liquid}, deg F	ΔT_{sub}, deg F	$(q/A)_{exp}$, Btu/sq in. sec	q/A by Equation [1]	Ratio of $(q/A)_{exp}$ to q/A by Equation [1
1	5	⊙	28.8 in. Hg	172	38	1.45	1.15	1.26
2	Failed to observe power at burnout							
3								
4	12.3	⊡	31.8 in. Hg	162	53	2.55	2.50	1.02
5	12.3	⊡	29.3 in. Hg	140	71	3.85	3.35	1.15
6	12.3	⊡	29.8 in. Hg	140	72	3.55	3.41	1.04
7	12.3	⊡	30 in. Hg	119	93	5.05	4.39	1.15
8	12.3	⊡	29.8 in. Hg	101	111	5.5	5.23	1.05
9	12.3	⊡	29.8 in. Hg	77	135	7.35	6.37	1.15
10	12.3	⊡	29.4 psia	80	170	9.3	8.05	1.16
11	12.3	⊡	60 psia	82	210	10.7	9.90	1.08
12	12.3	⊡	60 psia	83	210	10.7	9.90	1.08
13	12.3	⊡	114 psia	84	254	12.0	12.0	1.00
14	12.3	⊡	113 psia	86	252	12.0	11.9	1.01
15	40	△	114 psia	82	255	20.0	21.7	0.92
16	40	△	62.8 in. Hg	187	65	5.3	5.54	0.96
17	40	△	58.2 in. Hg	162	86	6.7	7.28	0.92
18	40	△	57.2 in. Hg	135	112	9.5	9.60	0.99
19	40	△	57.3 in. Hg	111	136	11.7	11.6	1.01
20	40	△	57.3 in. Hg	96	152	13.7	12.9	1.06
21	40	△	39 psia	79	187	17.8	15.9	1.12
22	40	△	81 psia	81	232	20.4	19.8	1.03
23	40	△	114 psia	81	256	22.0	21.8	1.01
24	12.3	⊡	114 psia	86	251	11.2	11.8	0.95
25	12.3	⊡	114 psia	87	250	10.4	11.9	0.87
26	12.3	⊡	113 psia	94	242	11.2	11.4	0.98
27	12.3	⊡	114 psia	92	245	10.4	11.6	0.90
28	12.3	⊡	29 psia	85	164	8.9	7.73	1.15
29	5.0	⊙	29.8 in. Hg	89	122	4.87	3.61	1.34
30	5.0	⊙	114 psia	99	248	7.1	7.34	0.97
31	5.0	⊙	56 psia	92	197	5.95	5.83	1.02
32	4.8	⊙	57.4 in. Hg	92	155	5.6	4.58	1.22
33	5.0	⊙	30.8 in. Hg	115	98	3.85	2.90	1.33
34	5.0	⊙	29.6 in. Hg	138	73	2.6	2.16	1.20
35	12.3	⊡	31.8 in. Hg	Failed to obtain outlet temperature				
36	12.3	⊡	29.6 in. Hg	190	22	0.81	1.04	0.78
37	12.3	⊡	29.8 in. Hg	173	39	2.0	1.85	1.08
38	12.3	⊡	164 psia	84	282	11.1	13.3	0.83

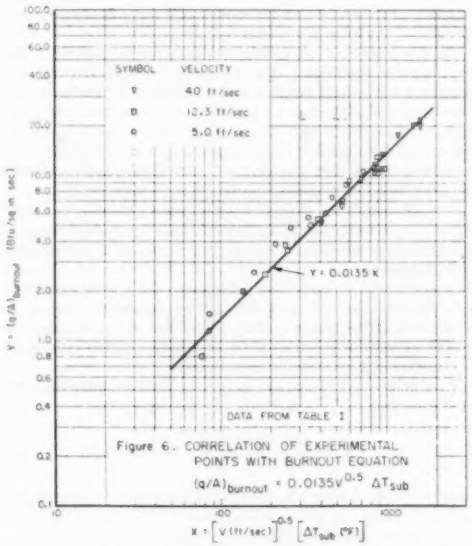

FIG. 6 CORRELATION OF EXPERIMENTAL POINTS WITH BURNOUT EQUATION

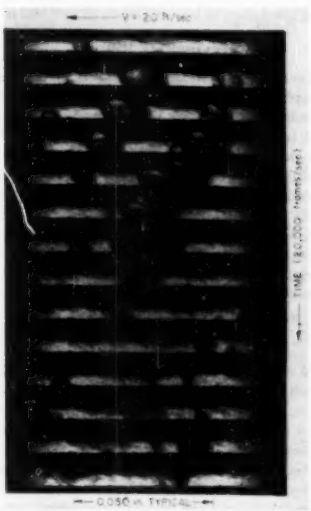

FIG. 7 OBLIQUE VIEWS OF HEATING SURFACE WITH ATTACHED HEMISPHERICAL BUBBLES SLIDING DOWNSTREAM (q/A = 3.75 Btu/sq in. sec; ΔT_{sub} = 150.)

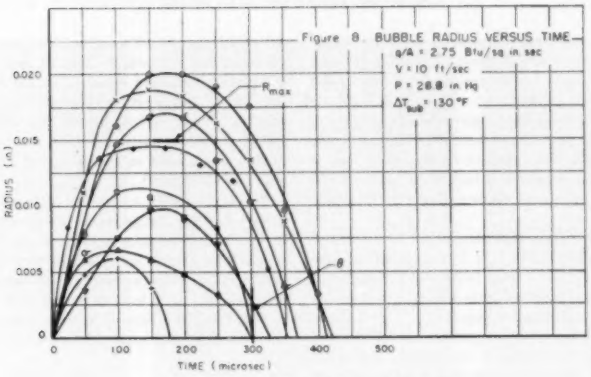

FIG. 8 BUBBLE RADIUS VERSUS TIME

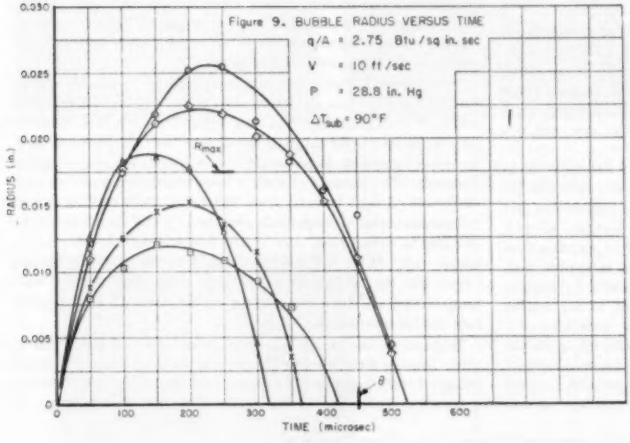

FIG. 9 (*left*) BUBBLE RADIUS VERSUS TIME

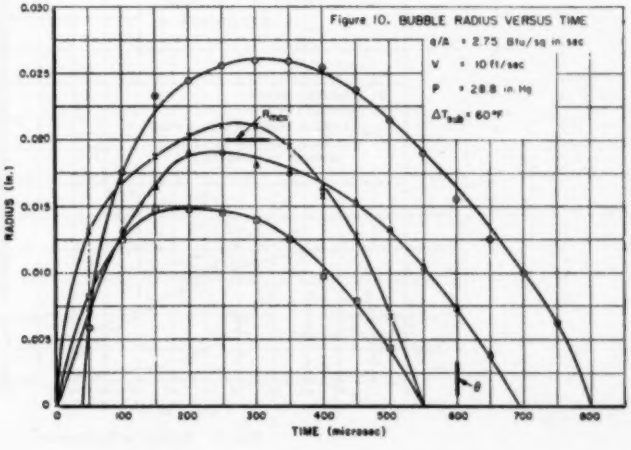

FIG. 10 (*right*) BUBBLE RADIUS VERSUS TIME

In these measurements of bubble parameters from the Kerr-cell photographs, the human element must be considered as a source of possible error. Every effort was made to obtain the best counts and measurements consistent with a reasonable expenditure of time. The employment of rigorous statistical counting and measuring methods would have been extremely difficult, as well as unprofitable, since the objective of the study was to determine the basic trends of bubble behavior for guidance in future experimental and theoretical studies of nucleate surface boiling.

In Fig. 11 the four bubble parameters are plotted for a series of tests at 2.75 Btu/sq in. sec and velocity of 10 fps, in which subcooling was reduced systematically from 200 to 62 F, approaching burnout. In the lower range of subcooling, reduction of ΔT_{sub} causes bubble size R_{max}, lifetime θ, population N, and vapor coverage F, to increase as burnout is approached. The same trends can be observed in the series of high-speed plan-view photographs from which the data were taken, Fig. 12(*a*), (*b*), and (*c*). At incipient burnout several large, closely packed bubbles coalesce to a local vapor film, as shown in broad plan view in Fig. 13.

Fig. 14 is a graphical summary of the results of three photographic tests made at coolant velocities from 5 to 20 fps, with other heat-transfer conditions held constant. It is apparent that decrease of coolant velocity toward burnout causes bubble size, population, lifetime, and coverage to increase until bubble coalescence and burnout occur, as was the case with decrease of subcooling.

In Fig. 15 data are presented from a series of five tests made with flow conditions held constant as heat-transfer rate was increased from 1.4 to 6.5 Btu/sq in. sec. Whereas bubble size and lifetime decrease about 40 per cent with the increase of q/A over this range, bubble population increases sharply, causing a resultant increase in bubble coverage as burnout is approached. The intensity of boundary-layer turbulence caused by surface boiling is appreciated by noting from Fig. 15 that, at 6.5 Btu/sq in. sec, more than 16,000,000 bubbles per sec were generated on 1 sq in. of heating surface. Since increase of subcooling in the range of 200 F decreases bubble size with compensating increase in population, Fig. 11, it is apparent that extrapolation to very high subcooling at high heat-transfer rates would yield astronomical population densities of bubbles too small and short-lived for photographic resolution. Fig. 16 shows minute surface boiling, not photographically resolved, at 200 F subcooling, 25 fps velocity, and 13 Btu/sq in. sec heat-transfer rate. Fig. 1 was photographed at similar conditions but with subcooling reduced to 190 F, producing larger bubbles, and breakdown of the nucleate boiling mechanism to a local vapor film (visible at the bottom center of the figure).

To illustrate the excitation of boundary-layer turbulence by surface boiling, a shadowgraph sequence is presented as Fig. 17, in which heat-transfer rate from the metal strip to a laminar stream of water is increased in three steps. A heated laminar boundary layer first appears at the metal surfaces. In Fig. 17(*c*) first boiling causes local disturbance of the laminar stream; and in Fig. 17(*d*) the boundary layer is seen to be torn by fully developed turbulence excited by vigorous boiling.

Discussion

Turbulent mixing adjacent to the heating surface, excited by boundary-layer boiling, makes possible the high heat-transfer rates observed experimentally. The sliding of bubbles observed on the heating surface should add to the turbulence caused by the action of bubble growth and collapse.

The burnout limit, or breakdown of the nucleate surface-boiling process, merits some discussion. Since clumping of nucleate boiling bubbles into local vapor films has been observed only in photographs taken at conditions near the burnout limit, bubble coalescence is associated with instability and incipient burnout. The passage of such a local vapor film must momentarily retard heat transfer from the metal wall, causing a local temperature rise of magnitude governed by the time interval for the film to sweep past, and by the heat-storage capacity of the metal wall. With sufficient local temperature rise, the moving vapor film can stabilize and enlarge, producing further wall-temperature rise to burnout even though over-all heat-transfer rate has been constant.

Because of the small heat-storage capacity of the 0.004-in-thick heating strip used in the present tests, the burnout limits obtained with the apparatus should be conservative, representing a sensitive indication of the onset of partial film boiling. In

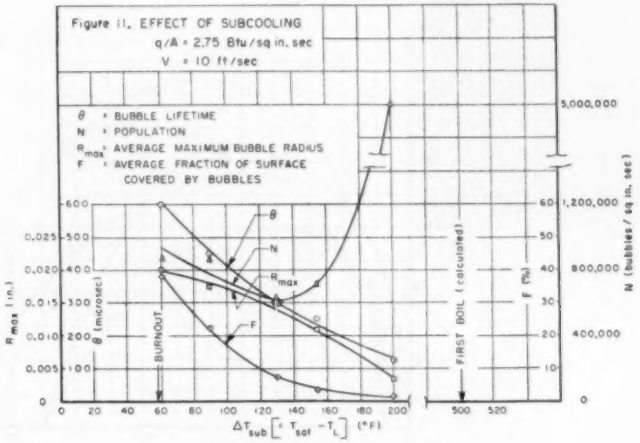

Fig. 11 Effect of Subcooling

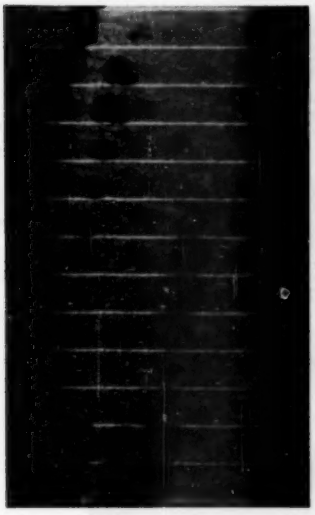

FIG. 12(a) BOILING AT HEAT-TRANSFER RATE 2.75 BTU/SQ IN. SEC, VELOCITY 10 FPS, AND SUBCOOLING 130 F

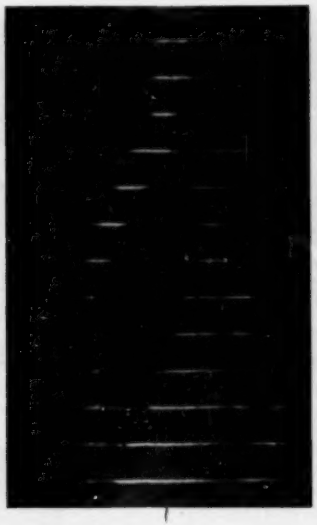

FIG. 12(b) BOILING AT HEAT-TRANSFER RATE 2.75 BTU/SQ IN. SEC, VELOCITY 10 FPS, AND SUBCOOLING 90 F

FIG. 12(c) BOILING AT HEAT-TRANSFER RATE 2.75 BTU/SQ IN. SEC, VELOCITY 10 FPS, AND SUBCOOLING 60 F

FIG. 13 BROAD PLAN VIEW OF BOILING AT SUBCOOLING 60 F

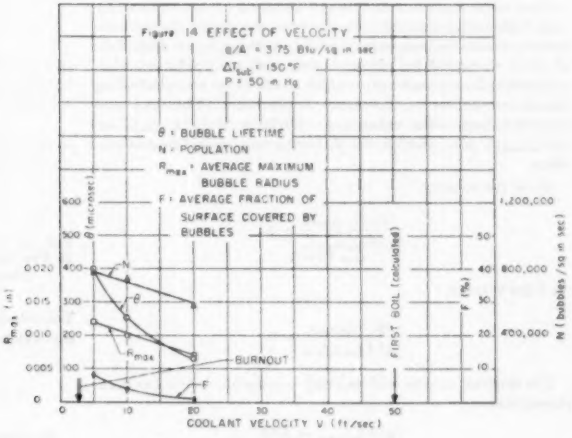

FIG. 14 EFFECT OF VELOCITY

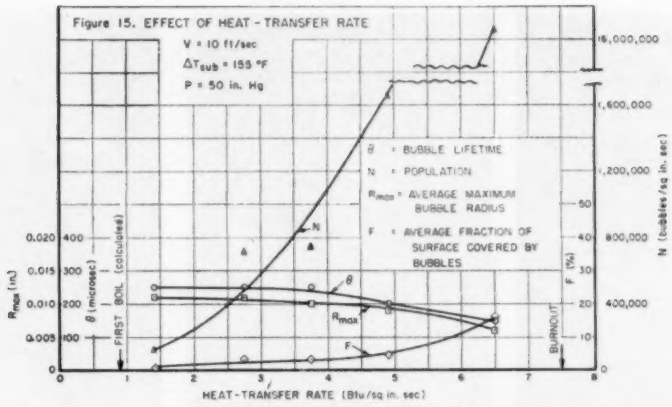

FIG. 15 EFFECT OF HEAT-TRANSFER RATE

McKenney's[6] burnout tests, made with thick-walled (0.012-in.) tubular heaters of $^1/_8$ in. diam at the axis of an annular flow passage carrying distilled water, burnout limits were obtained falling well above heat-transfer rates predicted by Equation [1]. However, with a thin-walled heating tube (0.005 in.) in the same apparatus, very consistent burnout results were obtained which fell within 12 per cent of correlation Equation [1], based upon burnout test results obtained with the thin-strip heater.

The tendency for burnout points to fall below the straight-line correlation at subcooling larger than 200 F, Fig. 5, occurred in McKenney's data as well. Whether the trend is real or is caused by slight imperfections in the thin-walled heating elements which become significant as bubble size decreases with subcooling is a question for future investigation.

Over-all temperature differences between heater surface T_W and bulk liquid temperature T_L were calculated for surface-boiling conditions near burnout at 5 and 40 fps, based upon data of other workers[4,6] for surface-boiling wall temperatures. Corresponding heat-transfer rates which would occur with nonboiling forced convection at the same temperature differences and velocities were then calculated. Division of $(q/A)_{burnout}$ by $(q/A)_{nonboil}$ then yielded the following rule-of-thumb relationships.

At 40 fps velocity,

$$\frac{(q/A)_{burnout}}{(q/A)_{convective,\ same\ T_W - T_L}} = 3$$

At 5 fps velocity,

$$\frac{(q/A)_{burnout}}{(q/A)_{convective}} = 6$$

The decrease in ratio with velocity is rational, since it has been shown that

$$(q/A)_{burnout} \approx V^{0.8}$$

and

$$(q/A)_{convective} \approx V^{0.2}$$

[6] Unpublished data of Jack McKenney of Jet Propulsion Laboratory, Pasadena, Calif.

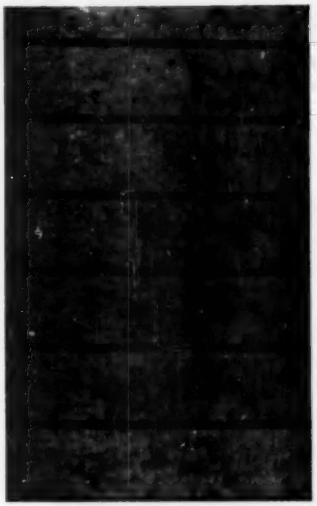

FIG. 16 PLAN VIEW OF BOILING ACTIVITY AT STREAM VELOCITY 25 FPS, HEAT TRANSFER 13 BTU/SQ IN. SEC, SUBCOOLING 220 F
(Photographic resolution inadequate for small scale of boiling.)

The velocity dependence can then be introduced to generalize the expression as follows

$$\frac{(q/A)_{burnout}}{(q/A)_{convective,\ same\ T_W - T_L}} = \frac{10}{V^{0.8}}$$

An insensitive dependency on subcooling also exists but has been neglected as an unwarranted refinement.

CONCLUSIONS

Maximum heat-transfer rate in 38 burnout tests for the $^1/_8$-in-wide metal heating strip dividing a rectangular channel $^3/_{16}$ in. wide and $^1/_2$ in. high, having a hydraulic diameter of $^1/_2$ in.

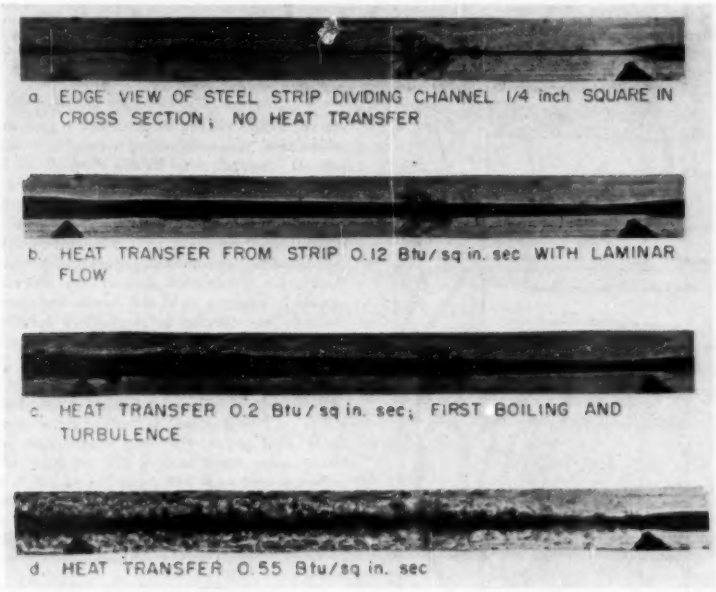

FIG. 17 EXCITATION OF BOUNDARY-LAYER TURBULENCE BY SURFACE-BOILING SHOWN IN SHADOWGRAPHS
(Pyramid markers indicate 2-in. heated length; blemishes are on glass windows; $V = 0.5$ fps; $T_L = 80$ F; $R_x = 1050$.)

and a ratio of heated length to hydraulic diameter of 6, was correlated by the equation

$$(q/A)_{burnout} = 0.0135\ V^{0.5}\ \Delta T_{sub}$$

The ratio of burnout heat flux to heat flux by nonboiling convection at the same velocity and temperature difference ranges from an approximate value of 6 at a velocity of 5 fps to about 3 at 40 fps.

At subcooling greater than 100 F, surface-boiling bubbles do not detach from the heating surface, but grow and collapse as approximate hemispheres while being swept along the heating surface by coolant velocity.

Bubble size, lifetime, population, and coverage of heating surface increase as burnout is approached by decreasing velocity.

Bubble size, lifetime, population, and coverage also increase as burnout is approached by decreasing the subcooling.

In the third approach to burnout, by increasing heat-transfer rate while holding velocity and subcooling constant, bubble size and lifetime decrease moderately, whereas bubble population and coverage of heating surface are strongly increasing functions of q/A.

Chemical Removal of Copper From Boilers

By R. G. CALL[1] and W. L. WEBB,[1] NEW YORK, N. Y.

When acid-cleaning a 1,000,000-lb per hr boiler for removal of deposits which were predominantly iron oxide, the boiler metal was heavily plated with copper. During subsequent operation this copper became detached in large sheets such as to affect circulation adversely, making copper removal mandatory. Because laboratory tests on previously used copper solvents gave poor performance, a solvent was developed containing ammonium persulphate, ammonium hydroxide, and caustic soda which, when used on this boiler, removed about 300 lb of copper. Laboratory conclusions and field-cleaning procedures, results, and costs are indicated.

THE boiler from which copper was chemically removed is designated as boiler A located in the Appalachian Electric Power Company's Logan Plant at Logan, West Va. It is a 6-drum, bent-tube, tangentially fired, dry-bottom unit, rated 1,000,000 lb per hr, 1350 psi, 925 F total steam temperature. An elevation view of this boiler, which first went into operation in November, 1937, is indicated in Fig. 1. Boiler A has been acid-cleaned three times, namely, in January, 1948, March, 1949, and January, 1950, the latter cleaning including the subsequent use of a solvent for removing copper.

Evidence of Need for Copper Removal

Immediately after the acid-cleaning of boiler A in March, 1949, with 5 per cent inhibited hydrochloric acid, followed by a conditioning boil, employing a 0.25 per cent sodium-chromate solution, selected wall tubes were turbined, removed deposits were weighed, and three samples analyzed. Results are shown in the left-hand portion of Table 1. These indicated an average copper content of about 52 per cent, and an average deposit weight of 125 grams for a pair of tubes forming a bifurcated tube 37 ft long. In general, the after-deposits appeared to be more extensive than in any previous case, partly because of all surfaces being plated with copper, much of which had become partially detached.

It was noted that the plated copper was not only heavier in the lower part of the boiler, but the maximum thickness of plating (about 12 mils) occurred on highly stressed metal such as rolled ends of tubes and tube flares.

Twelve hours after the boiler was returned to service, a floor screen tube failed in the form of a 6-in. longitudinal split on the bottom of the tube about 5 ft from the lower waterwall header. This failure was believed to have resulted from repeated cold-working of the tube in straightening bends caused by heavy pieces of falling slag. During this outage, drums and lower headers were found to contain much dislodged sheet copper. In so far as possible this copper was removed mechanically, the quantity being estimated as 75 to 150 lb.

During an outage in October–November, 1949, representative tubes were turbined and deposits collected and analyzed as before. These data are indicated in the right-hand portion of Table 1.

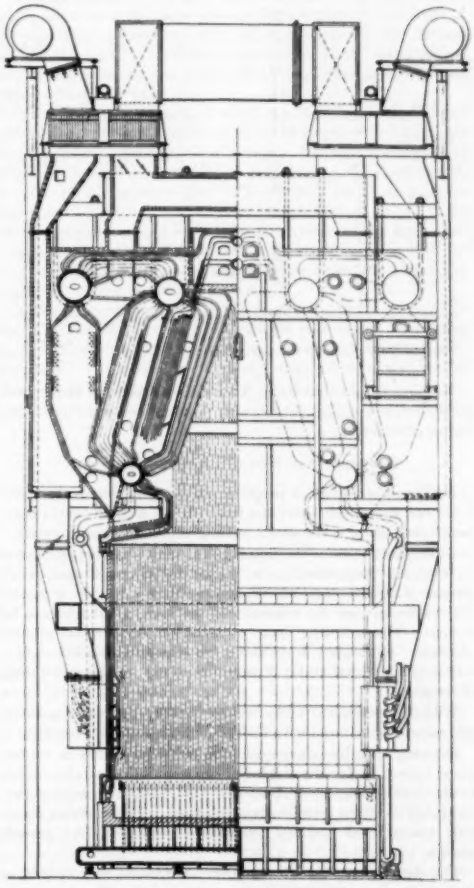

Fig. 1 Elevation View of Logan Boiler A Rated 1,000,000 Lb Per Hr, 1350 Psi, 925 F Total Temperature

A comparison of the weights and analyses of the deposits in Table 1 shows the following:

(*a*) Weights of deposits from tubes previously turbined following the March, 1949, cleaning were relatively low, ranging from 7 to 33 grams.

(*b*) The average weight of deposit from tubes not previously turbined was almost double that following the March, 1949, cleaning, and, although the percentage was less, the total quantity of copper had increased by almost one third.

[1] Mechanical Engineering Division, American Gas and Electric Service Corporation.

Contributed by the Joint Research Committee on Boiler Feedwater Studies and Power Division and presented at the Semi-Annual Meeting, St. Louis, Mo., June 19–23, 1950, of The American Society of Mechanical Engineers.

Note: Statements and opinions advanced in papers are to be understood as individual expressions of their authors and not those of the Society. Manuscript received at ASME Headquarters on May 10, 1950. Paper No. 50—SA-34.

TABLE 1 WEIGHTS AND ANALYSES OF BOILER A WALL-TUBE DEPOSITS FOLLOWING THE MARCH, 1949, CLEANING, AND PRECEDING THE JANUARY, 1950, CLEANING

Bifurcated tube designation		Following March, 1949, cleaning: Weight, grams	Analysis (%): Ign. loss	Fe_3O_4[a]	Cu	Before January, 1950, cleaning: Weight, grams	Analysis (%): Ign. loss	Fe_3O_4[a]	Cu	Zn	SiO_2
North wall											
East	18	76	..	..	..						
	20	..	..	..	..	238	..	..	..	..	..
West	15	67	..	..	..	..	..	..	..	..	..
	16	80	..	..	..	..	..	..	..	..	..
	30	..	..	..	..	360	5.5	57.6	27.8	6.4	0.8
	32	214	7.5	33.1	57.8	10	7.1	52.3	37.8	..	..
South wall											
East	5	48	..	..	..	..	..	..	..	..	..
	13	..	..	..	..	280	5.8	47.6	39.3	..	..
	25	136	..	..	..	..	..	..	..	..	..
West	3	..	..	..	..	170	..	..	..	..	..
	33	115	..	..	..	..	..	..	..	..	..
	35	99	..	..	..	10	..	..	..	..	..
East wall											
North	3	..	..	..	..	220	..	..	..	..	..
	8	124	11.1	38.3	51.4	33	8.0	39.6	48.4	..	..
	9	161	..	..	..	..	..	..	..	..	..
	16	158	..	..	..	..	..	..	..	..	..
South	3	..	..	..	..	238	..	..	..	..	..
	14	129	..	..	..	..	..	..	..	..	..
	20	..	..	..	..	200	22.3	73.6	3.5	..	0.9
West wall											
North	7	102	..	..	..	..	..	..	..	..	..
	18	224	10.7	42.0	47.7	7	9.4	46.1	45.3	..	..
	22	196	..	..	..	..	..	..	..	..	..
South	2	65	..	..	..	..	..	..	..	..	..
	15	..	..	..	..	224	..	..	..	..	..
	18	..	..	..	..	285	6.8	52.2	34.0	..	..
Average excluding tubes turbined following March, 1949, cleaning						246					
Average		125									

[a] Present predominantly as magnetic oxide.

It was apparent that boiler A should be cleaned at the earliest possible date and that the cleaning procedure should remove the copper effectively.

Experimental Work on Copper Removal

In November, 1949, a proposal covering the removal of iron oxide and copper deposits from boiler A was secured from a company specializing in chemical cleaning of industrial equipment.

Subsequent tests of the initially recommended copper solvent by both the American Gas and Electric Service Corporation's general laboratory and the chemical-cleaning service organization indicated that the efficiency of the solvent left much to be desired. The oxidizing agent used in this solvent was sodium chlorate. Laboratory tests under the stipulated conditions of a 6-hr soaking period at 170 F resulted in only partial dissolution of the copper.

With the scheduled boiler outage rapidly approaching, both laboratories were faced with the development of a new formula.

Drawing upon its experiences with oxidizing agents in ammonium hydroxide for the etching of copper prior to metallographic examination, the general laboratory of the authors' company concentrated its efforts on solvents of this type. The oxidizing materials investigated included perborates, peroxides, and persulphates.

The data obtained indicated that ammonium persulphate in the presence of sufficient ammonium hydroxide offered promising possibilities as a solvent for copper.

Although it is not the purpose of this paper to describe in detail the preliminary work on the various oxidizing materials tested, the data obtained with a number of persulphate solutions indicated the following:

1 A solvent of this type acts extremely rapidly at room temperature in removing copper from iron surfaces.

2 The reactions involved are of a complex nature and are not stoichiometric with respect to persulphate concentration.

3 It may be that the dissolution of copper by solvents of this type is due not only to the oxidizing reagent and ammonia, but also to atmospheric oxygen and cell-action currents.

4 The addition of a small amount of sodium hydroxide to the solutions tested appeared to increase the initial attack of the copper.

5 The persulphate type of solvent is considerably more expensive than the basic chlorate type.

Economic consideration of the various formulas investigated indicated that the use of one containing 0.75 per cent ammonium persulphate, 1.4 per cent NH_3, and 40 ppm of sodium hydroxide might be justified on the basis of certainty of removal of copper from boiler A.

As all of the foregoing data were obtained in the usual laboratory manner using copper tubes, and iron and copper strips immersed in beakers of solutions, it was evident that more practical tests should be undertaken. Furthermore, it should be established whether or not copper removal should precede or follow acid-cleaning.

Small sections of a boiler tube removed from boiler A with deposits intact were treated with the solvent. Examination of the remaining deposit showed the absence of copper. The specimens were then acid-cleaned and, after removal of the iron oxide, copper was found plated on the tube.

It is believed that the copper present was in the form of plating which occurred during the first acid-cleaning of the boiler, and that a layer of iron oxide and copper had been deposited over it during subsequent operation. From this observation it was concluded that the removal of copper from boiler A should follow acid-cleaning. Further tests were conducted using a test apparatus that was designed for studying chemical-cleaning procedures for boilers. This apparatus, shown in Fig. 2, consists of a 30-in. section of $2^1/_4$-in-ID high-pressure boiler tube supported on a ring stand. The internal area of the tube at operating level is 1.445 sq ft, and the effective volume 1900 ml. A hinged removable insulating jacket containing heating elements in each half surrounds the tube. The heating units are rated 700 watts each, and temperature is controlled by varying the applied voltage. The rubber stopper in the bottom of the boiler-tube section is fitted with filling and draining connections.

A number of tests made with the apparatus, when the total copper plated on the boiler tube varied from 2 to 3 grams, showed that the persulphate solvent entirely removed the copper in 2 hr at room temperature, and that corrosion was negligible.

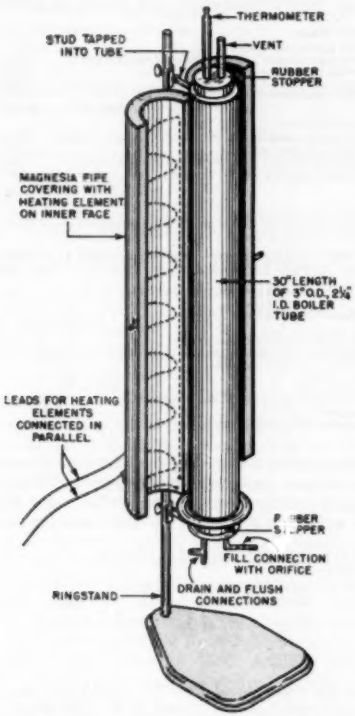

FIG. 2 TEST APPARATUS FOR STUDYING CHEMICAL-CLEANING PROCEDURES FOR BOILERS

The procedure used for plating the tube consisted of adding cupric oxide which had been dissolved in concentrated hydrochloric acid, to a 5 per cent solution of inhibited hydrochloric acid. The section of boiler tube containing this solution was maintained at 150–160 F for 2 hr. The reduction in the quantity of copper in the inhibited-acid solution was assumed to be equal to the copper plated.

In order to study the effect of the copper solvent upon corrosion of unplated surfaces, and to detect possible replating of copper from the copper solvent, these characteristics having been reported by the chemical-cleaning service organization which also was studying this formula, tests were made in which only one half of the boiler-tube section was plated. In a typical test where the weight of copper initially plated on the tube was 9.6 grams, the unagitated solvent maintained at 98–101 F in the tube for 6 hr contained 1.65 grams of copper. Following draining of this solvent from the tube section, a fresh charge of solvent was added. At the end of 2 hr, this fresh solvent had taken 2.87 grams of copper into solution. Another fresh charge of solvent at the end of 2 hr contained 2.73 grams of copper. From these data it was evident that replating of the copper had occurred and examination of the tube showed that the replating was confined to a narrow band at the bottom of the tube section.

As the copper solvent is strongly alkaline at all times, it is believed that the redeposition of copper is due to the higher-density copper-ammonium complex settling to the bottom of the tube as the copper dissolves, thereby setting up a cell action between two metals and two solutions of different composition.

In another test, in which the copper solvent was occasionally agitated, replating was reduced considerably as shown by the presence of 3.4 grams of copper in the solution at the end of 6 hr.

Recognizing that the conditions under which replating occurred might not exist if the tests were conducted more on the order of the conditions encountered when cleaning the boiler, the bottom inlet to the boiler-tube section was equipped with an orifice so that filling would require 2 to 3 hr, a period comparable to that required for filling boiler A.

In another group of tests of which the following is typical the tube section was first plated over its entire length with 3.34 grams per ft or a total of 8.6 grams of copper. The copper solvent was admitted through the orifice at an average rate of 630 ml per hr, the time for filling being 3 hr. The temperature of the solution was held at 98–101 F. The solution was allowed to remain in contact with the copper surface for 1 hr and was then drained at a rate of about 960 ml per hr, the draining time being 2¼ hr. The tube was then filled with rinse water twice and allowed to soak each time for 1 hr before draining.

In order to remove the copper remaining in the tube, two additional treatments with copper solvent were made, employing rapid filling and draining, and limiting the contact time to 2 hr in each case. The following data were obtained from analysis of the three copper solvents:

	Grams of copper
Solvent No. 1	3.22
Solvent No. 2	4.62
Solvent No. 3	0.128
Unaccounted for	0.252

The corrosion of the tube after removing solvent No. 1 was somewhat greater than previously observed, and during draining the surfaces dried leaving a blue film of the copper complex that was insoluble in the rinse water. This film may have increased the copper content of solvent No. 2, which contained more copper than was usually found.

From the data secured, the solubility of copper in the persulphate solvent was estimated to be 1700 ppm or 0.17 per cent under the test conditions of filling, soaking, and draining as previously described, these conditions being comparable to those under which boiler A would be cleaned.

FIELD TRIAL OF COPPER SOLVENT

An estimate of the total quantity of copper in boiler A based on deposits turbined from tubes, indicated about 150 lb was present. The volume of the boiler is about 33,000 gal. This quantity of copper solvent, consisting of 0.75 per cent ammonium persulphate, 1.4 per cent NH_3, and 40 ppm of sodium hydroxide, was believed to be capable of dissolving 0.17 per cent or 470 lb of copper which was considered ample for an extreme condition. Furthermore, the rapidity of attack of this solvent on copper was expected to speedily put into solution or to disintegrate and slough off the heavy films of sheet copper previously observed to have a maximum thickness of 12 mils.

Arrangements were made with the chemical-cleaning service organization to furnish the inhibited hydrochloric acid, the ammonium hydroxide, and the facilities and personnel for proportioning and heating the solvents and for pumping them to the boiler. The Appalachian Electric Power Company furnished the ammonium persulphate, nitrogen, heating steam, and temporary piping, and handled adjustment of boiler temperature.

The boiler was first acid-cleaned with 7.5 per cent inhibited hydrochloric acid, the soaking period being 6 hr with initial and

final metal temperatures of 145–165 F and 135–155 F, respectively. The acid was then displaced with nitrogen as were the two subsequent water rinses. During these rinses the boiler temperature was adjusted to 100 F maximum. The copper solvent was then pumped in over a period of about 4 hr at about 85 F and allowed to soak for 30 min, during which time it was recirculated out of the top and into the bottom of the boiler. The draining time was 2.5 hr. The copper solvent and the two subsequent rinses were displaced with compressed air. Filtered water was used for rinsing in all cases.

Samples of the copper solvent taken from the boiler during the filling showed a range of copper concentration of 0.06 to 0.25 per cent with an average of 0.16 per cent. Analyses of the acid and the copper solvents as drained from the boiler are indicated in Table 2.

Copper in solution in the drained solvent was 300 lb, corresponding to the 0.113 per cent concentration. This does not include that sloughed off and found mixed with iron oxide in the bottom of drums and lower headers. This mixture, which had a copper content of about 60 per cent, was estimated to contain about 80 lb of copper.

TABLE 2 ANALYSES OF ACID AND COPPER SOLVENTS AS DRAINED FROM BOILER A FOLLOWING JANUARY, 1950, CLEANING

Acid solvent	Per cent	Copper solvent	Per cent
Hydrochloric acid (HCl)	6.09	Ammonium persulphate ($(NH_4)_2S_2O_8$)	0.013
Copper (Cu)	Trace	Ammonia (NH_3)	0.970
Iron oxide (Fe_2O_3)	1.0	Copper (Cu)	0.113
Phosphate (PO_4)	0.04	Iron oxide (Fe_2O_3)	0.011
Calcium (Ca)	0.0014		
Magnesium (Mg)	0.0014		

TABLE 3 WEIGHTS AND ANALYSES OF BOILER A WALL TUBE DEPOSITS FOLLOWING JANUARY, 1950, CLEANING

Bifurcated tube designation	Weight, grams	Analysis, per cent			
		Ign. loss	Fe_2O_3	Cu	SiO_2
East wall, South 19	89	7.5	87.1	4.2	1.7
North wall, West 31	93	6.3	76.7	13.2	4.5
West wall, South 17	3	...	...	...	...
South wall, West 31	20	...	...	...	...

An inspection of visible internal surfaces of the boiler revealed no signs of plated copper. However, all surfaces were coated with a brown-red deposit which presumably resulted from oxidation of the boiler metal by persulphate. This deposit when wet could be removed with the finger and when dry was readily removed by wire-brushing, exposing no etching or pitting from acid or persulphate attack.

The weights and analyses of deposits turbined from selected tubes following the cleaning operation are indicated in Table 3. From these data it is evident that the iron oxide produced by the persulphate was undesirably high, but based on before and after conditions, the bulk of the copper was removed.

Cost of Copper Removal

An itemization of the costs of the boiler A cleaning operation totaling $10,258 are indicated in Table 4. Minor costs such as those for steam and gas for solvent and boiler heating, rinse water, compressed air, and caustic soda are not indicated.

As shown by Table 4, in which the costs are allocated to show the additional expense for copper removal over and above that for acid-cleaning only, the copper removal cost was $3295, or about $11 per lb of copper taken into solution by the solvent.

On the basis that the temporary piping costs, and the general expenses are shared equally by the acid-solvent and copper-solvent stages, the respective total costs would be $6283 and $3975, equivalent to $13.25 per lb of copper taken into solution by the copper solvent.

It is possible that further laboratory work on solvents of the type used in boiler A may show that the chemical cost can be reduced without impairing copper-removal efficiency. This possibility is indicated by data obtained after the cleaning of boiler A and shown in Table 5. In these tests the persulphate concentration was reduced from 0.75 to 0.5 per cent, and the temperatures held between 75 and 80 F. The filling time was increased, and the soaking and draining periods decreased. Under the conditions indicated, the solubilities of copper in the solvent were 0.193 and 0.223 per cent. These values are higher than those obtained from solutions in which over-all contact time was greater and temperatures higher.

TABLE 4 COST ITEMIZATION FOR BOILER A CLEANING OF JANUARY, 1950

Acid-solvent stage:		
Inhibited hydrochloric acid	$3417	
Cleaning organization's service and mileage charges	1478[a]	
Unsalvable temporary piping	230	
Nitrogen	383	
Local labor and supervision	1455	
Total	$3963	
Copper-solvent stage:		
Ammonium persulfate	598	
Ammonium hydroxide	990	
Cleaning organization's service and mileage charges	1382[a]	
Local labor and supervision	325	
Total		3295
Grand total		$10258

[a] Allocated from total charge on the basis of proportionate time required.

TABLE 5 LABORATORY COPPER-REMOVAL TESTS CONDUCTED AFTER JANUARY, 1950, CLEANING OF BOILER A

Solvent: 0.5 per cent ammonium persulphate
1.4 per cent NH_3
Temperature: 75 to 80 F

	Test no. 1	Test no. 2
Weight of copper plated on tube, grams	5.34	7.11
Weight of copper per lineal ft, grams	2.26	2.90
Time to fill from bottom, hr-min	4–20	3–45
Soaking time, min	30	30
Draining time, min	55	45
Total time, start of fill to end of drain, hr-min	5–45	5
Copper removed, grams	4.24	3.67
Copper concentration in solvent, per cent	0.223	0.193

Although sufficient tests have not yet been made to show the exact effect of higher temperatures, indications are that above 100 F, corrosion of iron by the persulphate is accelerated, and the net amount of copper placed in solution is reduced, presumably due to rapid decomposition of the persulphate.

Need for Further Research

In presenting the foregoing method for removal of copper from boilers, the authors do not wish to imply that the concentrations of the constituents of the solvent are particularly critical or that the solvent used is the most economical one. It is one that was developed within a limited time to meet a cleaning deadline.

Other solvents were available, but time did not permit a full investigation of their merits.

It is hoped that this presentation will stimulate interest and research not only on the most effective and economical means of removing copper from boilers, but also to show the following:

(*a*) Why in the presence of large amounts of copper, serious plating accompanies acid-cleaning in some instances and is hardly detectable in others.

(*b*) Whether conditions influencing solution of copper during acid-cleaning can be controlled so that plating is substantially prevented and at least the major portion of the copper detached by

sloughing off, making it removable by flushing of drums, headers, and near horizontal sections of tubes.

Conclusions

The following conclusions have been drawn from the study of chemical removal of copper from boilers:

1 Although copper in boiler deposits which are predominantly iron oxide may be no more hazardous to operation than the iron oxide itself, an instance is cited in which copper could quite seriously affect boiler availability.

2 Although the process used on the one boiler cleaned was costly, and left much to be desired with respect to boiler cleanliness, it is feasible to remove copper by the use of the persulphate solution described.

3 Further research is needed both on copper solvents along the lines of formulating and controlling solvents used for iron-oxide removal so to prevent plating of copper, and to cause copper in the initial deposits to slough off and be removable by flushing.

Discussion

F. N. Alquist.[3] The project described in the paper is the type of research that R. C. Corey had in mind in an earlier one.[3] In a discussion of Mr. Corey's paper, the writer submitted data showing x-ray diffraction analysis of 15 deposits obtained over a 10-year period from boilers containing copper in which the copper varied from 5 to 25 per cent.

In the present paper the authors state the following problem: "Why in the presence of large amounts of copper, serious plating accompanies acid-cleaning in some instances and is hardly detectable in others?" Most of the copper in boilers before acidizing is in the form of metallic copper, which is insoluble in hydrochloric acid alone; but in the presence of ferric oxide, which acts as an oxidizing agent, copper dissolves during acidizing. The redeposition of copper during acidizing is not yet explained. The Hall Laboratories, in a study of how copper was taken into solution in acid-cleaning and then plated out, indicated the oxidizing agent to be ferric ion.

All cases of redeposition of copper during an acid cleaning should be reported to the Joint Research Committee on Boiler Feedwater Studies. From the writer's knowledge, this redeposition occurs in less than 5 cases in 100 acid cleanings. The data obtained could be made available to operators or used for research on methods of preventing copper redeposition.

The present paper indicates that solvents for copper redeposited in acidizing are ammoniacal oxidizing agents such as aqueous solutions of ammonia with chlorates, perborates, or persulphates. We have found that to remove copper from scaled boilers the boiler must first be acidized before the ammoniacal copper solvent is used.[4] We have found that aqueous solutions of chlorates, persulphates and perborates with ammonia are useful solvents. The writer has not studied the effect of the addition of caustic.

A solution of a chlorate with ammonia was used twice to remove copper from the Montaup No. 6 boiler after acidizing. Eight pounds of copper were removed from this boiler the first time and 66 lb on the second treatment.

R. F. Andres.[5] In recent years with the development of water treatment which furnishes practically pure condensate for feedwater to high-pressure boilers, sludge deposits are principally composed of iron oxides, copper, and copper oxides. The increased use of acid-cleaning as a means for removing iron-oxide deposits, in our case, has resulted in a rather serious problem with regard to the copper in the deposits which replates from the acid solvent. This plated copper may or may not be adherent, and, under the influence of heat and rapid circulation, as the boiler is returned to service, may be loosened from the tubes and headers and moved to areas where the circulation is less rapid. This results in excessively heavy sludge deposits in localized areas which may impair circulation or cause overheating with ultimate tube failure. It has been necessary to clean our boilers mechanically following acid treatment to eliminate this potential operating hazard. This procedure is time-consuming, and the copper plated out in inaccessible locations remains in the boiler to prove troublesome at a later date. Chemical solution of the plated copper seems a logical answer to this problem.

A wide variety of ammonia-base oxidizing solvents are available which dissolve metallic copper under varying temperature conditions and periods of time. The ammonium persulphate solution used by the authors is rapidly reactive with copper in the cold state and is perhaps the easiest solvent to use. The somewhat less rapid oxidizing agents such as potassium bromate, sodium chlorate, sodium perborate, etc., used at elevated temperatures and for longer intervals of contact time seem to have comparable copper-dissolving capabilities.

Numerous solvents of the latter type tried in our laboratory reacted with copper relatively rapidly until the concentration of copper in the solvent approached 0.15 to 0.20 per cent. As the solvent spent itself, the rate of copper solution decreased materially, and the tendency of the solvent to replate copper increased. If the ammonia content of the solvent reaches extremely low values, or if the oxidizing salt is depleted, all of the solutions tested tended to lose their copper already in solution. A stage treatment involving the removal of the spent solvent and the addition of fresh solvent would tend to reduce the replating characteristics of the solution by reducing the dissolved copper content and stabilizing the oxidizing salt and free ammonia concentrations but would be rather costly. The ammonium persulphate solvent, because of its extremely reactive nature, must be handled carefully during the contact period with copper, in order to prevent redeposition of copper while the less reactive solvents are not so critical. It is obvious from the replating characteristics of these solvents that uniformity of chemical concentrations throughout the solvent must be maintained at all times.

Recirculation as used in the Logan boiler is one solution to this problem, although the results lack a degree of certainty since the volume of solution recirculated is small compared to the total solvent volume and may move through a limited number of tubes in the boiler. In the case of the solvents used in the heated state, positive chemical circulation may be induced by intermittent firing of the boiler. This method has several disadvantages: namely, (1) localized areas of the boiler may be overheated, causing increased rate of attack of tube metal by the oxidizing agents present in the solvent, (2) the ammonia may be depleted momentarily in these areas, causing the copper to replate and, as this plating occurs, equivalent amounts of iron are taken into solution reverting in the alkaline solvent to insoluble iron oxide, and (3) although ammonia does not follow true gas laws, some ammonia may be driven into the air space in the boiler drums which renders the over-all solvent less concentrated and, therefore, less effective.

These adverse reactions were apparent during the chemical copper cleaning of one of our boilers. The chlorate-bromate-ammonia solvent was introduced into the boiler at a temperature of 120 F to 160 F. Samples of the solvent taken prior to the

[3] Organic Research Laboratory, The Dow Chemical Company, Midland, Mich.

[3] "Corrosion of High-Pressure Steam Generators: Status of Our Knowledge of the Effect of Copper and Iron Oxide Deposits in Steam Generating Tubes," by R. C. Corey, Proceedings of the ASTM, vol. 48, 1948, pp. 907–941.

[4] Process Patent pending.

[5] Chief Chemical Engineer, The Dayton Light & Power Company, Dayton, Ohio.

firing were relatively free of iron oxide and contained from 0.07 to 0.13 per cent of dissolved copper and 0.15 per cent available ammonia for reaction. After firing the boiler for 5-min intervals on three occasions to bring solvent temperature up to 180 F, the solvent decreased both in ammonia and dissolved-copper content. After a 7-hr contact period, the drain samples from the boiler had an ammonia content of only 0.09 to 0.16 per cent, the dissolved copper content had dropped to 0.05 per cent, and the iron-oxide content had risen to 0.20 per cent. From these data it is readily apparent that some of the mentioned reactions occurred which were not anticipated, and the treatment was not too successful.

It is noted that the authors did not use the conventional soda-ash boil following the acid stage of their cleaning treatment. In the chemical cleaning of our boiler we also relied on the ammonia solvent to neutralize any residual acid. This may have been wishful thinking on our part. The boiler was regasketed completely after the chemical and subsequent mechanical cleaning. After the hydrostatic test on the boiler and during the setting and testing of safety valves with attendant application of heat and pressure, numerous gasket leaks developed and acid odors were noted. On inspection the soft-steel gaskets were found to be coated with a soft black deposit. This is the first time that a neutralizing boil was not used after acid treatment and, coincidentally, it is the first time a gasket problem has developed.

Some of the peculiarities of copper cleaning solvents and procedures have been briefly discussed. Future copper cleaning of boilers in our plants will be based upon the following concepts drawn from this paper and discussion:

1 Accessible sludge deposits will be removed prior to and following the acid stage of the treatment, reducing the sludge pile-ups of copper which are difficult to dissolve chemically.

2 A soda-ash neutralizing boil will be used between the acid- and copper-removal stages of the treatment.

3 The copper solvent will be of the bromate-chlorate type with an increased content of bromate and ammonia. Soda ash will be used in the solvent, since this alkalinity seems to reduce attack on the tube metal by the oxidizing agents.

4 The boiler will be heated before the ammonia solvent is introduced, and the solvent will be put in warm. The solvent will not be heated by firing the boiler.

5 Recirculation of the solvent seems desirable and may be used in an effort to maintain uniform temperature and concentration conditions.

6 Frequent tests will be made to determine the concentrations of the various constituents present in the solvent during the ammonia treatment to determine the proper time to drain the solvent.

7 The boiler will be inspected and cleaned if necessary before being returned to service.

The copper cleaning of the Logan boiler was apparently about 80 per cent effective in removing the copper present in solution. Further development of solvents and cleaning procedures should make the complete chemical solution of copper a reality and eliminate this troublesome deposit from boilers. This paper, concerning the authors' attempts to remove copper chemically, represents a long stride forward in the constant effort to obtain and maintain clean internal boiler surfaces.

P. H. CARDWELL.[6] This paper is valuable in that it covers the actual treatment of a boiler for the removal of copper, and gives a considerable amount of laboratory data on copper solvents. We became interested in the problem of copper removal about 7 years ago. The starting point of our laboratory work at that time was reference in a book by Clyde Baker[7] to a formula for a copper solvent. This formula consisted of an aqueous solution of ammonia, ammonium persulphate, and ammonium carbonate. The disadvantage of the persulphate solvent is threefold; its cost, which is rather great, its temperature limitation of about 100 F, which may or may not be a disadvantage depending upon the particular treatment, and the formation of iron-oxide rust upon the steel surface.

These disadvantages led to additional work which included trying various oxidizing agents as a replacement of ammonium persulphate. As a result of this work, a solvent was developed using as its base, sodium chlorate. The chlorate solvent with the necessary auxiliary chemicals overcomes two of the disadvantages of the persulphate solvent, namely, it is only one half as costly as the persulphate solvent, and, if used correctly, does not cause rusting of steel surfaces. The solvent does have one somewhat minor objection in that it has to be used at a temperature of 150 F or higher.

The first treatment using the chlorate solvent was made December 27, 1948. To our knowledge, this was the first treatment in which copper was chemically removed from a boiler. The boiler was a forced-circulation 650,000-lb-per-hr steam generator. The chemical procedure used on this boiler was first a stage of inhibited hydrochloric acid to remove the iron oxide deposit. Following this, the boiler was washed twice with water and then filled with the copper solvent. The copper solvent was left in the boiler for a period of 7 hr, after which it was drained. The boiler was rinsed once with water then given a 2-hr after-boil treatment using soda ash and trisodium phosphate. The treatment was called successful in that a series of tubes was turbined, and the examination showed the absence of copper in all of the material removed.

The problem, as pointed out in the paper, as to whether or not the copper-removal treatment should precede or follow the acid-cleaning is one upon which we have done a considerable amount of work. We had an opportunity in September, 1949, during an outage period of a high-pressure 375,000-lb-per-hr boiler to carry out an experiment using two tubes "in place" in the boiler. The test was to determine whether it would be advisable to remove the copper prior to the acid-washing or to leave the copper-removal treatment until after the acid-washing. The results of our tests in this case indicated that it would be advisable to perform the acid-washing of the boiler first and then to perform the copper-removal treatment. We also have found boiler deposits where it was advisable to remove the copper prior to the acid-washing stage. These deposits were those in which the copper seemed to have been formed over the iron oxide. Thus the problem of which treatment to perform first depends upon the chemical make-up of the deposit.

The authors mentioned the need for further research on the problem of preventing the deposition of copper during the acid-washing of boilers. It is hoped that within the near future it will be possible to add to the acid a specific chemical to combine with the copper to prevent its plating onto the boiler metal during the acid-washing treatment. This may take a more or less "tailor-made" chemical, but it will insure prevention of copper deposits and will make the total cost of the treatment considerably less than the present-day two-stage treatment.

The authors are to be complimented on this paper in that they have brought to the attention of the power industry that it is possible to remove copper from boilers chemically. The laboratory tests and apparatus used are of considerable interest, and

[6] Chief Chemist, Dowell Incorporated, Tulsa, Okla., Mem. ASME.

[7] "Modern Gun Smithing," by Clyde Baker, second edition, Small Arms Technical Publishing Company, Marines Onslow County, N. C., 1933, p. 528.

valuable information is reported on the persulphate copper-removal solvent.

R. C. Corey.[8] The initiative of the authors in tackling another of the many problems related to the maintenance of clean steaming surfaces in boilers conceivably may lead to a new approach to internal cleaning.

The writer recalls finding large amounts of paper-thin deposits of metallic copper in sectional headers following cleaning with inhibited acid. At the time, it seemed a hopeless task to remove all of this copper, so the boiler was closed and returned to service. Although no subsequent damage to the tubes could be attributed definitely to the presence of the copper, the element of doubt existed—and remains so today.

The authors' careful observations, attending the use of persulphate-ammonia wash in the test unit and in the Logan boiler, raise a few questions which they may care to comment upon:

1 Did the persulphate-ammonia wash appear to have any solvent action on the deposits and scale from the Logan boiler? It may be possible that such a solution may be used as a one-stage wash, that is, without primary treatment with inhibited acid.

2 It is reported by the authors that, following the persulphate-ammonia wash, the internal surfaces of the boiler were coated with a brown-red deposit. They believe it to be iron oxide resulting from oxidation of the steel by the persulphate ion, but the writer would suggest confirmatory tests to identify the constitution of the deposit; preferably by means of an x-ray diffraction analysis.

3 A number of case histories dealing with copper in boilers report that small copper balls, consisting essentially of copper-plated globules of magnetite, were found in various parts of high-pressure boilers. This suggests the possibility of incorporating finely divided metallic iron into the inhibited-acid wash, to serve as possible nuclei on which copper would plate preferentially, rather than upon the boiler surfaces. The fact that copperplated more extensively upon stressed areas, such as rolled tube ends, confirms the fact that such areas are anodic to adjacent, unstressed areas. Finely divided metallic iron may act similarly.

4 Did the authors have an opportunity to observe if copper within pits in the tube metal was dissolved by the persulphate-ammonia wash?

The authors' observation that no pitting of the tube metal was found after the copper was removed is an important one, since it indicates that the plating takes place uniformly rather than selectively.

The authors raised two cogent questions in their outline for further research, and the writer urges strongly that the appropriate subcommittee of the ASME Joint Research Committee on Boiler Feedwater Studies be assigned the problem of finding the answers.

I. B. Dick.[9] The writer has no first-hand experience with copperplating following acid-cleaning of boilers, although the company with which he is connected has extensive background in acid-cleaning. However, there are indications of increasing percentages of copper in residual deposits after chemical cleaning, so that this paper strikes a sympathetic chord.

Review of the chemistry of copper removal indicates, as the authors state, that there is a large field for future work, and the writer would urge the chemical-cleaning service organization mentioned in the paper to take the initiative in this work.

From reports, oral and published, it would seem that copper deposits in high-pressure boilers are not uncommon, and in some cases are becoming a matter of concern. This, then, seems an appropriate time to reopen the subject of the pickup of copper by boiler feedwater and its deposition in boilers. Granted the necessity of removing copper from boilers when its accumulation jeopardizes operation, basically the problem goes back to the copper-bearing alloys in the feedwater cycle. One of the difficulties in the way of such work is the very small quantities involved. The authors mention some 380 lb of metallic copper removed from their boiler. Presumably this represents an accretion of years. Compared with the total evaporation over that period of time, the amount of deposited copper, expressed in terms of the volume of feedwater, must have been in parts per billion, not parts per million; and one part per billion is one ten-millionth of one per cent. So the chemistry involved is very difficult.

E. B. Powell.[10] The deposit of copper on the heating surfaces of high-pressure steam boilers has become a subject pressing for correction. The full nature and scope of action to be attributed to such deposits are much questioned topics, but evidence of the damaging effect in numerous instances of tube overheating is quite definite. The present paper, accordingly, makes a very important contribution to high-pressure steam-boiler maintenance.

The authors bring out clearly the real need, at the present stage of experience, for preliminary trials of chemical-cleaning procedures, with practical evaluation of chemical combinations and methods by application to appropriately selected tube specimens from the specific boiler to be cleaned. One of the by-products cited, the recognition of the importance of turbulence in a particular copper-solvent solution, gained from noting copper redeposited from the unagitated solution in the chemical-cleaning test apparatus, compared with relative absence of copper redeposition when that apparatus was rapidly filled and drained, presents an example of benefit to be derived from thorough analysis of these preliminary trials. The data secured on the effects of temperature on the activities of the persulphate solution are very constructive.

For all the thorough detail from the preliminary tests and the observations made on the chemical-cleaning process, we are very grateful to the authors. It is of tremendous importance to learn also how and why the copper was deposited in the boiler-furnace tubes. This design and operating aspect of the problem is emphasized in the present discussion, recognizing that it calls for further information which may well be considered beyond the paper's scope, but with the hope that the authors may still take up these other items. The chemical nature of the copper and iron in the deposit as initially formed is probably one of the less difficult of the items not covered in the paper. The relative influence, in determining the distribution of the copper deposit, exerted by temperature and other factors in the state of the metal surface, such as cold-work mentioned by the authors, in comparison with the simple physical factor of sequence in proximity to the rising stream of fluid is a more difficult item but would seem to warrant special study for assistance toward understanding the conditions under which the deposit formed. Further light on the origin of the deposit would be had from items such as the following:

The extent and nature of copper and copper-alloy surfaces and their respective typical temperature ranges in contact with condensing steam and feedwater reaching boiler A, and approximate dates when any of these surfaces was renewed.

The composition, including dissolved gas content and pH, of

[8] Supervising Engineer, Combustion Research Section, Bureau of Mines, Pittsburgh, Pa. Mem. ASME.

[9] Division Engineer, Chemical Engineering Bureau, Mechanical Engineering Department, Consolidated Edison Company of New York, Inc., New York, N. Y.

[10] Consulting Engineer, Stone & Webster Engineering Corporation, Boston, Mass. Mem. ASME.

the condensate and drips, with their relative proportions, and of feedwater.

Presumably boiler A had been cleaned mechanically prior to January, 1948, and the copper accumulation found after the acid-cleaning in March, 1949, had been a product of conditions obtaining subsequent to some time in early 1947.

S. T. Powell[11] and J. K. Rummel.[12] The efficient cleaning of boilers of accumulated deposits at reasonable cost, with minimum damage to the boiler metal and least loss of time, has long been an operating problem in the modern steam-power station. Considering the capital investment in a large high-pressure boiler, and the lack of outage time which is normally available, it is generally agreed that it is not economical to have unscheduled or scheduled outages which would interfere with production. For these reasons the judicious use of acid and other suitable solvents for cleaning the boilers has been looked upon with general favor, and the contributions which the authors have made to our knowledge of solvent-cleaning has been of considerable value and general interest.

Apparently, the difficulty in removing copper from boilers will depend to an appreciable extent on the physical condition of the copper and how it may be intermixed with other deposits which are present. No doubt there are other factors which contributed to condition and arrangement of the copper noted by the authors, following acid-cleaning. Therefore it appears that a further study of the acid-cleaning operation may lead to some means of removing both the copper and other deposits from the boiler during the same soaking operation. It has been our observation that large residues of copper in boilers after acid-cleaning and boiling out with soda are not common. However, closer examination, as in the case of the Logan boiler, may show that more copper remains behind than may be expected.

With reference to the plating-out of copper in sheets or long strings, it is possible that this may take place over an underlying film or layer of iron oxide. This may happen in much the same manner as the copper collects on iron-oxide particles and can be observed in many boiler deposits. In this event it seems likely that sheets of copper may at any time become dislodged and may accumulate in parts of the boiler where water flow can become restricted. While this is not the usual case, we have observed that on some occasions it was necessary to use mechanical means for removing copper left after acid-cleaning, and it is of interest to know that solvents such as used by the authors are available for dissolving the copper. Further development of such solvents should be profitable.

Regarding the order of applying dual solvents such as has been reported, it appears that since the iron oxide may not be found in heavy layers over the copper it may be advantageous first to apply the copper solvent and remove the iron oxide with the acid treatment. This should avoid any heavy plating-out of copper from residues which may remain with the iron oxide. It would be of interest if some additional data on the problem of the best order of applying solvents could be furnished, as by treating individual boiler tubes and noting the results.

Regarding the cost of treatment, many high-capacity boilers hold considerably less volume of liquid per pound of steam produced than the Logan boiler, and the chemical cost may be reduced by at least one third. For example, a 1,000,000-lb-per-hr boiler may hold as little as 20,000 gal instead of 33,000 gal as in the Logan boiler.

[11] Consulting Chemical Engineer, Baltimore, Md. Fellow ASME.
[12] Associated with Sheppard T. Powell, Baltimore, Md., Mem. ASME.

E. S. Roberts.[13] From the data presented in the paper, we conclude that the boiler surfaces become copperplated during the acid-cleaning, and that the copper deposited, together with iron oxides and other material during boiler operation, is metallic copper and not copper oxide. During the acid-cleaning with inhibited hydrochloric acid, some metallic copper is dissolved by the action of HCl and ferric iron, and subsequently is plated out by cementation with iron.

A pickling solution of sulphuric acid of approximately 5 per cent may be preferable since practically no copper will be dissolved by sulphuric acid. However, the action of the ferric iron, which is dissolved by the acid solution, will still cause some of the copper to dissolve. This action can be prevented by adding a suitable reducing agent to the pickle liquor. The proper choice of reducing agent will depend upon preliminary laboratory or pilot-plant tests. Formaldehyde, in small quantities, may fulfill the requirements.

Instead of trying to prevent the dissolution of copper, it may be better to precipitate the dissolved copper as sulphide. Cheap iron sulphide or iron-sulphide-bearing ore or concentrate may be added to the cleaning acid solution. The copper sulphide precipitates may adhere to the metal surfaces of the boiler. The character and nature of such precipitates should be investigated in the laboratory using conditions similar to those found in the boiler surfaces. In any event, if copperplating during acid-cleaning cannot be prevented, attempts should be made to find a cheaper copper cleaning solution than the one presently in use (ammonia-ammonium persulphate). We suggest that a warm ammoniacal solution of cupric acetate (approximately 10 grams Cu and 20 grams NH_3 per liter) followed by a wash with dilute ammonia solution should be tried. Such ammoniacal solutions of cupric salts dissolve metallic copper by forming cuprous copper, which can easily be regenerated into cupric copper by aeration.

Authors' Closure

The many discussions of this paper are most gratifying to the authors as they emphasize that copper removal from power boilers is a subject of quite general interest.

Power engineers likely will subscribe to Dr. Alquist's suggestion that there be a clearinghouse to which to report cases of copperplating during acid cleaning of boilers. The Joint Research Committee on Boiler Feedwater Studies might well perform that function. Depending upon the prevalence of this problem in the near future, that Committee might wish to sponsor research both on the reduction of copper carried to boilers, and upon its removal. It would seem, however, as pointed out by Mr. Dick, that the chemical-cleaning service organizations should take the initiative on studies of copper-removal procedures.

Mr. Andres' experiments indicating that as the copper content of the solvent increases and as the ammonia concentration is reduced, the tendency for the solvent to plate copper is increased, confirms the authors' findings. It appears necessary by thermal or forced circulation to limit the concentration of the heavy copper complex in the lower portions of the boiler if replating is to be avoided.

In the event a boiler is fired to maintain copper solvent temperature, it would seem wise to keep vents closed and to increase the ammonia excess so that the partial pressure of ammonia in the steam space above the solvent would be such to prevent depletion of the ammonia concentration.

Mr. Andres' experience with gasket leakage following copper removal where this stage was not preceded by the conventional alkaline conditioning boil, may, as he indicates, be due to unac-

[13] Vice-President and Chief Engineer, Chemical Construction Corporation, New York, N. Y.

ceptable acid neutralization. In the Logan instance, the handhole caps and header seats were refaced before the boiler was returned to service. No gasket leakage was subsequently experienced.

Mr. Andres' desire to have all copper taken into solution by the solvent seems rather an idealistic viewpoint, just as it would be to expect an acid solvent to take all iron oxide into solution. The authors would expect some portions of these materials to slough off and accumulate on horizontal and near-horizontal surfaces to such a thickness that their complete solution would be impractical without agitation. All such cleaning operations should be followed by a thorough flushing of such surfaces for removal of accumulated solids.

The authors agree with Dr. Cardwell that the ammonia persulfate solvents have objectionable characteristics. The prime object in presenting the paper was to give the details of one instance in which many pounds of copper were quickly and successfully removed from a boiler, in the hope that others facing this problem would be inspired to carry the investigations to a point where effective solvents having a minimum of objectionable qualities would be developed. As indicated in the paper, tests on chlorate solvents were interpreted to indicate that a more effective type of solvent was required for the Logan boiler.

The power industry impatiently awaits the completion of Dr. Cardwell's work on an additive which will hold copper in solution and thereby prevent plating during acid cleaning. With plant capacity as critical as it now is and with the expectation that there will be difficulty in installing new capacity rapidly enough to meet the needs, definite assurance of no copperplating and consequently no necessity for prolonging a boiler outage would be a most welcome contribution.

Dr. Corey's questions will be answered in so far as the authors' knowledge and opinions permit in the order in which they were asked.

1 Tests on tube specimens from the Logan boiler indicated a series of laminar depositions of copper and iron oxide. A single copper-solvent stage would remove the exposed copper but leave undissolved copper below the iron-oxide layer.

2 A chemical analysis of the deposit left in the Logan boiler after copper removal, showed substantially 99 per cent iron oxide. No x-ray diffraction analyses were made.

3 Copper balls similar to those described, containing as high as 70 per cent copper found in the Windsor boilers after extended periods of operation, lend weight to Dr. Corey's opinion that finely divided metallic iron in inhibited acid may serve as nuclei on which copper may be preferentially plated. Laboratory tests should demonstrate the feasibility of such a plan and shed light on the problems of maintaining the iron in suspension and subsequently removing it from the vessel being cleaned.

4 There were no pits in the tube specimens used by the authors in their laboratory copper-removal experiments. It would be expected that where pits contain alternate layers of copper and iron oxide, the two-stage treatment employed would not necessarily clean the pits.

Concerning Mr. Dick's thought that 380 lb of copper removed from the Logan boiler represents the accumulation of many years, the authors believe that the total copper carried to the boiler actually was much greater than this. Undoubtedly much was removed in sloughed-off material during the several acid cleanings, and in the turbining of wall tubes on several occasions. However, a problem requiring serious consideration is the reduction of copper carried to the boiler. Powell[14] has reported the influence of some of the factors which affect copper pickup in the cycle.

Mr. E. B. Powell outlines many aspects of the picture that must receive study to permit an understanding of what controls the quantity of copper carried to the boiler and its deposition on internal surfaces. The authors plan to contribute to such investigations and hope that others will do likewise.

Messrs. S. T. Powell and Rummel quite logically point out that the cost of the copper-removal operation might be influenced to a considerable degree by the ratio of the volume of the boiler to its rating. This same relationship might well be considered also in limiting the concentration of copper taken into solution by the copper solvent from the standpoint of possible replating. The cost reduction from a lower volume-rating ratio might at least be partially counterbalanced by a need for higher concentrations of solvent chemicals.

The authors' conclusions concerning the mechanism by which copper is plated during acid cleaning conform to those expressed by Mr. Roberts. His suggested use of sulphuric instead of hydrochloric acid warrants consideration even though it is somewhat hazardous to handle and would complicate temperature control during dilution. The many reducing agents tested by the authors for retarding the action of ferric iron in causing copper to dissolve, proved to be comparatively ineffective. Formaldehyde, however, was not studied.

A single-stage solvent made by adding iron sulphide to the acid cleaning solvent for taking copper into solution and precipitating it as a sulphide, as suggested by Mr. Roberts, deserves study both as to its effectiveness and to establish the ease with which the copper sulphide can be mechanically removed from the boiler. His indication of the need for a cheaper solvent than ammonia-ammonium persulphate for removing plated copper, if plating cannot be prevented, is most pertinent. Preliminary experiments with ammoniacal solution of cupric acetate suggested by Mr. Roberts look promising.

The authors wish to express their appreciation to the discussers for their many contributions toward helping to solve the problem of removal of copper in power boilers. It is hoped they and others will be inspired to continue this research and to report their findings.

[14] "Causes and Prevention of Iron Oxide in Boilers," by S. T. Powell, L. G. Von Loesberg, and J. K. Rummel. Proceedings of Midwest Power Conference, vol. 12, April 5, 6, 7, 1950.

Phosphoric-Acid-Cleaning of Boilers

By T. E. PURCELL[1] and S. F. WHIRL,[2] PITTSBURGH, PA.

The demand for clean surfaces, the ability to reach otherwise inaccessible areas, and the speed of the process have been largely responsible for the acceptance of acid-cleaning of high-pressure, high-heat-input boilers. It provides a convenient method with a minimum of labor for removing rust and mill scale from new boilers and water-formed insoluble deposits from old ones. Despite its recognized undesirable features, inhibited hydrochloric acid is generally used for this purpose. Because of the limitations and adverse effects of hydrochloric acid, which were quite evident during the authors' experience in the cleaning of two boilers, the possibility of using phosphoric acid for boiler cleaning was investigated in the laboratory. These experiments demonstrated that inhibited phosphoric acid is a good solvent without the unfavorable properties and characteristics of inhibited hydrochloric acid. Guided by the results of this study, inhibited phosphoric acid was used successfully for removing rust and mill scale from a new boiler.

Hydrochloric Acid Versus Phosphoric Acid

THE comparative properties of phosphoric and hydrochloric acids, of importance in boiler cleaning, are summarized in Table 1. The principal advantage of phosphoric over hydrochloric acid is that it can be boiled in the unit by direct firing of the boiler with negligible attack on the metal. This is possible because the inhibitor is effective at these temperatures. In addition to the beneficial washing action, the resulting natural circulation promotes distribution and provides a sufficiency of acid at the desirable locations at all times. Furthermore, the boiling operation sends solutions into certain regions at the top of the boiler which otherwise could not be reached except by recirculation with an elaborate system of internal baffling. By contrast, inhibited hydrochloric acid can be used only at temperatures below 150–165 F. Above this temperature, the effectiveness of the inhibitor decreases with progressively more severe attack of the boiler metal. With hydrochloric acid, the acid-cleaning process must consist either of "soaking" or recirculation with external heating. External heating by steam jets or heat exchangers increases the complexity and the cost of the cleaning operation, while attempts to utilize the sensible heat of the furnace and boiler without recirculation would introduce hazards of imperfect mixing, acid excess or deficiency, corrosion due to hot spots, and the possibility of inadequate cleaning.

Stability. Hydrochloric acid is the gas, hydrogen chloride, dissolved in water. Even at room temperature, hydrochloric-acid vapors leave the solution and as the temperature is increased to that encountered in boiler cleaning, the rate of decomposition becomes appreciable. Since the inhibitor remains in the solution, its benefits do not extend to the vapor; thus the metal surfaces of drum, safety valves, boiler and superheater tubes above the level of the cleaning solution are exposed to corrosive uninhibited hydrochloric acid. While the valves may be protected by their removal and superheaters by isolation or filling with condensate, there are always some regions that are beyond protection.

TABLE 1 COMPARISON OF HYDROCHLORIC AND PHOSPHORIC ACIDS AS BOILER-CLEANING SOLUTIONS

Hydrochloric acid	Versus	Phosphoric acid
Strong acid		Weak acid
HCl, a gas dissolved in water		H_3PO_4, a solid dissolved in water
Unstable, gives off corrosive HCl vapor which attacks metal above solution		Stable, gives off no acid vapors
Inhibitor not effective above 150–165 F		Inhibitor effective at 212 to 220 F
Excessive attack of metal when used above 150–165 F		Negligible attack of metal when used at 212 to 220 F
Process limited to "soaking" or mechanical recirculation		Can be boiled; permits direct firing, utilizing natural circulation
Promotes after-rusting		Prevents after-rusting
Corrosive acid fumes pervade plant atmosphere, requires ventilation		Nonfuming

During the cleaning operation with hydrochloric acid, invariably, HCl vapors pervade the plant atmosphere. These fumes are not only corrosive to power-plant equipment, meters, and exposed metalwork, but also are toxic to plant personnel. In warm weather, ventilation may not be a serious problem, but in subfreezing temperatures, as during the authors' first acid-cleaning experience, the adverse effects of the fumes were noticed throughout the plant.

Phosphoric acid, by contrast, is a solid dissolved in water. It is extremely stable even at temperatures well above the boiling point of the solution used and therefore presents no corrosive or noxious-fumes problem.

After-Rusting. After-rusting of metal surfaces is a most undesirable characteristic of hydrochloric-acid cleaning. The freshly cleaned metal surfaces react rapidly with the atmosphere to form rust, especially in a moist condition. Even in the laboratory, a metal specimen which is rinsed rapidly with distilled water following acid-cleaning, then dipped in alcohol and dried, will subsequently rust. Hydrochloric acid possesses no passivating or film-forming properties. Call[3] experimented with chromate solutions and a 0.5 per cent phosphoric acid after boil-out to prevent the after-rusting. The authors tried these and other methods, including chelating agents and inert atmospheres for acid displacement, with reduction but not elimination of the rusting conditions. The more extensive work of Cardwell[4] essentially has confirmed these findings.

It was the early work of Call,[3] the general passivating characteristics of phosphoric acid, and the experiences of the German Navy with cold 35 per cent phosphoric acid which prompted the authors' study of phosphoric acid for the cleaning process. It was found that a 5 per cent inhibited phosphoric-acid solution boiling at atmospheric pressure gave good deposit removal, negligible attack of metal and a surface resistant to rusting.

---

[1] General Superintendent of Power Stations, Power Stations Department, Duquesne Light Company. Fellow ASME.

[2] Chemical Operating Engineer, Power Stations Department, Duquesne Light Company.

Contributed by the Joint Research Committee on Boiler Feedwater Studies and Power Division and presented at the Semi-Annual Meeting, St. Louis, Mo., June 19–23, 1950, of The American Society of Mechanical Engineers.

Note: Statements and opinions advanced in papers are to be understood as individual expressions of their authors and not those of the Society. Manuscript received at ASME Headquarters on June 5, 1950. Paper No. 50—SA-44.

[3] Private communication and also reported to Power Station Chemistry Subcommittee, Prime Movers Committee, Edison Electric Institute.

[4] "Prevention of Black Iron Oxide Deposits Following Chemical Cleaning," by P. H. Cardwell, Proceedings of the Midwest Power Conference, vol. 12, 1950, p. 147.

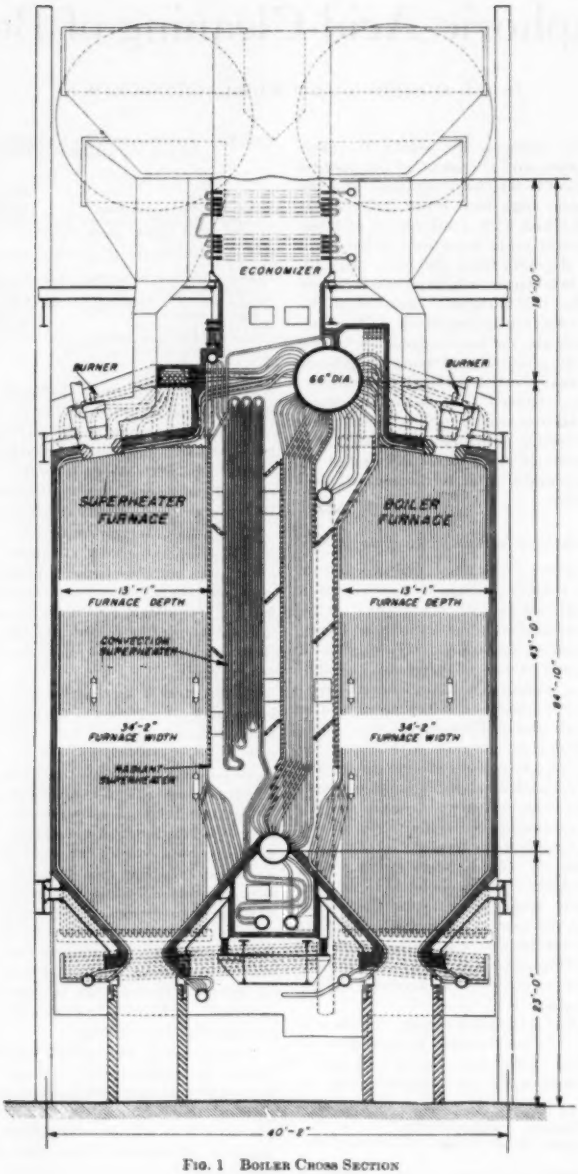

FIG. 1 BOILER CROSS SECTION

Cleaning of a New Boiler Unit

Description. The No. 3 boiler unit at the Frank R. Phillips Power Station is a Foster Wheeler twin-furnace-type steam generator, equipped with water-cooled furnace walls, radiant and convection superheaters, economizer, and air preheaters. A cross section of the boiler is shown in Fig. 1. The boiler is fired by pulverized fuel using two Hardinge ball-type pulverizers and twelve vertical intervane-type burners.

The boiler is rated at a normal steaming capacity of 600,000 lb per hr. It is designed for a maximum output of 700,000 lb per hr and a maximum working pressure of 1100 psi. The normal operating steam pressure and temperature are 900 psi and 900 F, respectively, at the convection-superheater outlet.

The total saturated heating surface in the boiler unit is 23,286 sq ft of which 10,996 sq ft is boiler heating surface and 12,290 sq ft is in the water-cooled furnace walls. The other heating surfaces are: Radiant superheater, 2160 sq ft; convection superheater, 15,600 sq ft; economizer, 13,800 sq ft; and Ljungström air preheater, 161,600 sq ft. The total effective furnace volume is 35,000 cu ft. The water required to fill No. 3 boiler to the normal operating level which is 6 in. below the center line of the drum is 158,000 lb.

Since it was anticipated that this boiler would be acid-cleaned at some time, sufficient drains were provided to empty the boiler completely from normal level in less than 1 hr. After the acid boil-out, during which both the economizer and the steam space of the drum were filled, it required just over 60 min to drain the boiler.

The chemical-cleaning procedure consisted of the following steps:

(*a*) Alkaline boil-out at an average pressure of 244 psi for a 24-hr period, using trisodium phosphate and sodium sulphite.

(*b*) Acid boil-out at atmospheric pressure for an 8-hr period, using inhibited phosphoric acid.

(*c*) Alkalizing and surface-conditioning boil-out at an average pressure of 246 psi for a 12-hr period, using tetrapotassium pyrophosphate, potassium hydroxide, and potassium sulphite.

The chemicals used and their cost appear in Table 2.

The water used for the boil-out operation was "treated water" and condensate. The treated water is Ohio River water clarified by coagulation with ferrous sulphate and caustic soda in sludge-blanket-type equipment followed by filtration through anthrafilt.

A schematic diagram showing the special drain and recirculation piping for the cleaning operation is shown in Fig. 2.

Preparation and Changes to Boiler and Piping:

(*a*) Sheet-metal baffles were installed over the radiant superheater tubes to protect them from direct radiation of the oil fires during the acid boil-out when steam was vented directly from the drum to the atmosphere.

(*b*) All safety valves were removed. The flanges on three superheater safety-valve connections and one drum safety-valve connection were blanked. A temporary safety valve set at 275 lb was installed on one of the drum safety-valve flanges and a 3-in. vent from the remaining safety-valve flange was connected through a 250-lb gate valve to the roof.

(*c*) All blowdown valves were connected to a temporary 2-in. tie line, one branch of which was connected to the suction side of the circulating pump and the other branch discharged to the ash-sluice trench. This arrangement permitted circulation of the alkaline cleaning solution through the economizer when boiler pressure was below 50 psi and continuous circulation of acid solutions during this phase of the operation. The phosphoric-acid solution was heated and circulated in the boiler by use of oil torches in the furnace. These are part of the regular equipment used in starting the boiler. The pump was necessary only for circulating the solution to the economizer. The mixing of the acid and feeding by gravity into the boiler proper could have been done just as easily by locating the tank at the economizer level.

(*d*) During the acid boil-out only, to protect the superheater from acid solutions and overheating, condensate was admitted to the radiant-superheater intermediate header to fill both the radiant and convection superheaters. Sufficient flow was maintained through the radiant superheater to provide continuous overflow from the convection-superheater outlet-header drain as long as fuel was being burned in the superheater furnace.

Strong Alkaline Boil-Out. The method of introducing chemicals was the same for all operations. Treated water drained by gravity into the mixing tank, where chemicals were added, and

TABLE 2 QUANTITY AND COST OF CHEMICALS USED FOR CHEMICALLY CLEANING NEW BOILER

Chemical	Formula	Pounds used	Cost, dollars	Phase of cleaning in which used
Trisodium phosphate	$Na_3PO_4.12H_2O$	500	22.50	Strong alkaline boil-out
Sodium sulphite	Na_2SO_3	20	0.75	Strong alkaline boil-out
Phosphoric acid	75%, H_3PO_4	14350	1262.25	Acid boil-out
NEP No. 22 inhibitor	.....	400	132.00	Acid boil-out
Phosphoric acid	75%, H_3PO_4	375	31.88	Acid rinse
Tetrapotassium pyrophosphate	$K_4P_2O_7$	23	3.91	Surface conditioning
Potassium hydroxide	KOH	86	43.00	Surface conditioning
Potassium sulphite	K_2SO_3	14	3.47	Surface conditioning
Total cost of chemicals	.....	...	1499.76	

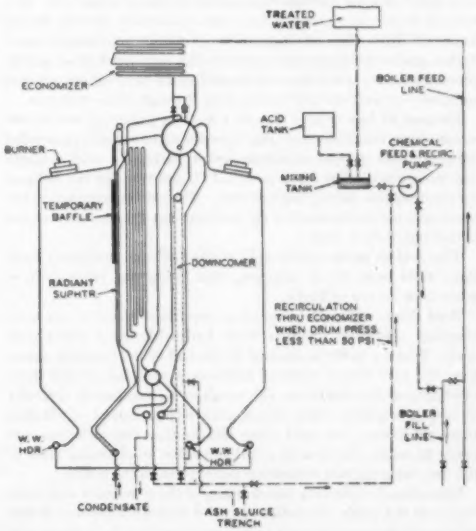

Fig. 2 Schematic Diagram of Boiler and Piping Used During Chemical Cleaning

the resulting solution was pumped through the boiler fill line, the boiler feed line, and economizer to the boiler. Condensate when used was fed through the boiler fill line; under these circumstances the solution from the mixing tank was more concentrated to allow for dilution by the condensate.

For the strong alkaline boil-out a solution of trisodium phosphate and sodium sulphite, prepared at the mixing tank with treated water, was boiled in the unit for 24 hr at 250 psi. Whenever the pressure was below 50 psi, the solution was circulated through the economizer, the 50-psi limitation being imposed by the pump available.

The trisodium phosphate was selected for the alkaline boil-out because of its proved superiority to plain caustic as a detergent and the authors' conviction that silicates and caustic have no place in the high-pressure boiler. Sodium sulphite was used to react with the dissolved oxygen in the undeaerated water and to provide reducing conditions during the boil-out. Samples of the solution taken near the end of the operation analyzed 550 ppm PO_4, 50 ppm SO_3, and pH 11.4.

The strong alkaline boil-out was followed by a rinse, wherein the boiler was filled and drained, using both treated water and condensate. The condensate was used to reduce filling time.

Phosphoric-Acid Boil-Out. The purpose of the acid cleaning was to remove rust and mill scale from the boiler surfaces. The action was prompted by the hydrostatic tests with treated water, the intervals when the moist surfaces were open to atmospheric rusting, the probability of rusting during shipment, storage, and erection, especially during cold winter months when condensation is prevalent and drying rate very slow, and the observation that mill scale and rust were noted in visible portions of the boiler. The quantity of such rust and scale may be considered by some as of no consequence; however, a simple computation shows that an iron-oxide scale 1 mil thick over the more than 40,000 sq ft of metal surface would weigh more than $^1/_2$ ton.

A solution of commercial phosphoric acid; 75 per cent H_3PO_4 and NEP No. 22 inhibitor prepared at the mixing tank with treated water was pumped into the condensate flowing in the boiler fill line. The resulting mixture of acid, inhibitor, treated water, and condensate was boiled in the unit for 8 hr at atmospheric pressure; the steam was vented to the atmosphere, and the solution was recirculated continuously through the economizer.

Because of loss of acid due to a leaking gasket at one of the steam-drum manholes, periodic blowdowns to remove suspended material, and several handhole-gasket leaks, the acid strength was somewhat below 5 per cent H_3PO_4 and was further reduced by consumption during the boil-out. The acid concentration immediately before the start of the boil-out was 4.6 per cent; at end of boil-out, 3.4 per cent.

The acid solution at the end of the boil-out contained more than 4000 ppm Fe in solution, this being the equivalent of more than $^1/_2$ ton of Fe_2O_3.

Acid Rinse. The acid rinse is an important phase of any acid-cleaning operation whether with hydrochloric or phosphoric acid. When a boiler is drained at the end of the cleaning operation, the thin film of residual solution, containing several thousand ppm of dissolved iron, can result in a considerable quantity of iron precipitate when mixed with either neutral or alkaline rinse solutions. An acid rinse dilutes this iron-rich film and tends to retain the iron in solution so that on draining most of the iron derived from deposits is removed from the boiler.

Immediately following the draining of the 5 per cent acid solution from the boiler, the boiler was filled with a 0.1 per cent H_3PO_4 solution in the same manner as was employed for the original acid and then drained.

Alkalizing and Surface Conditioning Boil-Out. The final step of the cleaning operation consisted of an alkaline treatment for the purpose of neutralizing the residual acid and conditioning of the metal surfaces. To accomplish the latter, a boiling-out process is believed essential as explained elsewhere.[5]

The boiler was blown down regularly and cyclically at all blowdown points. At the end of the boil-out, the pressure was permitted to drop normally to 20 psi when all blowdown and drain valves were opened and the boiler drained completely and as quickly as possible.

The specified conditions for this boil-out were to be 200 ppm PO_4, pH 11.0–11.2, and 10 ppm SO_3 using potassium chemicals. Due to the residual acid remaining in the boiler and, undoubtedly, some iron phosphate, the potassium-hydroxide requirement to secure the required pH of 11+ was quite high (approximately 75 lb). During this boil-out, the PO_4 concentration increased to 550 ppm without further additions of phosphate chemicals.

Potassium chemicals were used in this phase of the operation because the boiler was to operate with these chemicals when in service.

Inspection. After the final alkalizing boil-out, the visible metal surfaces of the boiler drums, tubes, and headers were clean, exhibiting the gray color of pickled steel. No rusting was seen in any location. There was no pitting evident except on the hand-hole caps where slight etching had occurred under the periphery of the seating surface for the stainless-steel gaskets. The condition was not serious but was notably more prevalent on the caps of the upper headers. This observation led to some laboratory work on gasket corrosion described later. Specimens of boiler tube which were placed in both the steam and mud drums just prior to the acid boil-out were in excellent condition and showed a negligible loss of metal with maximum calculated penetration of 0.0004 in. Several bushels of flaky mill scale and deposit, mixed with additional miscellaneous debris, were removed from the lower regions of the boiler.

It is noteworthy that when the boiler was placed in service, the boiler water was clear and free of suspended iron oxide whereas the two boilers which were cleaned with inhibited hydrochloric acid were troubled with black boiler water.

Laboratory Investigation

The laboratory work was done in glass vessels using 1-in-square × $^1/_4$-in-thick boiler-tube sections. The tests covered the use of hydrochloric as well as phosphoric acid with various concentrations, inhibitors, and other additions followed by an assortment of rinses.

The weight-loss test specimens were cleaned thoroughly in both organic solvents and acid-pickle solutions. Those used to determine efficiency of cleaning were scaled in a muffle furnace at 750 C and furnace-cooled. Those used in rusting tests were degreased but otherwise in "as-received" new tube condition.

Laboratory Tests. The after-rusting of hydrochloric-acid-cleaned specimens could not be prevented by the following, either singly or in combination:

1 Either alkaline or neutral phosphate rinses.
2 Chromate solutions as rinses or as after-soaking treatments.
3 The use of nitrogen for acid displacement and drying.
4 Weak phosphoric-acid rinses.
5 Inhibited phosphoric-hydrochloric acid mixtures as cleaning solutions.

The parallel tests using scaled specimens with boiling phosphoric-acid cleaning solutions in concentrations of 1, 2, 3, 5, and 10 per cent by weight H_3PO_4, followed by either air-drying or a 0.1 per cent phosphoric-acid rinse, then air-drying, were yielding rust-free specimens. The tests similarly indicated that the simulated

[5] Corrosion Handbook Sponsored by the Electrochemical Society, John Wiley & Sons, New York, N. Y., 1948, p. 524.

mill scale formed on specimens prior to test by heating in a muffle to 750 C, while removed completely, was not kept in solution by acid concentrations below about 2 per cent residual. From this it was evident that an initial acid strength of 4 to 5 per cent would be necessary in the boil-out operation to compensate for the errors in computed capacity of the boiler, economizer, and piping, the consumption of acid by scale dissolution, leakages, and other losses generally incidental to a boil-out operation.

Phosphoric acid had demonstrated a satisfactory cleaning ability and yielded a rust-resistant surface; however, many of the acid-cleaned specimens showed pitting and corrosion that were associated with acid attack. Weight-loss tests showed that the uninhibited acid was quite aggressive but that the attack could be controlled by an inhibitor. The results of the tests with different inhibitor and acid concentrations appear in Table 3.

TABLE 3 ATTACK OF METAL BY PHOSPHORIC-ACID PICKLE SOLUTIONS; RESULTS OF LABORATORY TESTS RUN FOR 6 HR AT ATMOSPHERIC BOILING

Concentration—H_3PO_4 wt, per cent	Inhibitor,* wt, per cent	1 × 1 × 1/4 in. specimen wt loss, per cent	Remarks
1	0.60	0.96	Precipitate formed in 1 hr, acidity restored to original hourly
2	0.00	6.94	Precipitate formed in 2 hr, acidity restored to original every 2 hr
2	0.10	0.20	No precipitate
2	0.25	0.02	No precipitate
5	0.00	13.70	Precipitate formed in 3 hr, acidity restored to original
5	0.10	0.01	No precipitate
5	0.25	0.01 (gain)	No precipitate

* Inhibitor in laboratory tests and field trial was NEP No. 22, a proprietary product of the Wm. M. Parkin Company, Pittsburgh, Pa.

An inhibitor concentration of 0.1 per cent appeared to be sufficient, but in view of the much larger ratio of metal area to solution volume in the boiler, a 0.2 per cent concentration was used for the actual boil-out to insure inhibitor sufficiency.

NEP No. 22 inhibitor used throughout our laboratory tests and field trial is a proprietary product selected on the basis of familiarity and previous experience.

Gasket Corrosion. It was observed at the final inspection of the boiler that the handhole caps on the headers were slightly pitted and etched in a band about 1/16 in. wide adjacent to the outer edge of the gasket seating surface. Beyond the etching there was a band of clean metal to the edge of the cap. The gasket was stainless steel; consequently, it was suspected that an electrochemical couple between steel and stainless steel resulted in anodic attack of the steel.

The pitting was investigated in the laboratory by a special test, wherein a section of gasket and a polished surface of hot-rolled steel were clamped together and immersed in acid cleaning solutions. The tests indicated that pitting is encountered with stainless gaskets in either hydrochloric or phosphoric-acid solutions; the pitting was more severe with 5 per cent inhibited hydrochloric-acid solutions at 140 F than with corresponding phosphoric-acid solutions at 212 F. Likewise, the amount of attack with stainless-steel gaskets was invariably much greater than with Armco-iron gaskets. The composition of the gasket appears to be more important than the acid used. The combination 5 per cent HCl, 0.1 per cent inhibitor, Armco iron, yielded less attack than 5 per cent H_3PO_4, 0.5 per cent inhibitor, stainless steel. The least attack of the base metal was obtained in tests using the combination 5 per cent H_3PO_4, 0.2 per cent inhibitor, Armco iron.

All of the foregoing tests were made using the NEP No. 22 inhibitor at 140 F for hydrochloric-acid solutions and at atmospheric boiling for phosphoric-acid solutions.

Conclusions

1 Phosphoric acid is a good solvent for acid-cleaning of boilers.

2 Inhibited phosphoric-acid solutions can be boiled at atmospheric pressure with negligible attack on the boiler metal, thus permitting the solution to be heated and circulated by normal low-level firing of the boiler.

3 Phosphoric-acid solutions are stable at atmospheric boiling and yield no corrosive vapors above the solution or noxious fumes in the plant.

4 Boiler surfaces cleaned with phosphoric acid are resistant to rusting.

5 Following the cleaning of a new boiler with inhibited phosphoric acid, the boiler water during subsequent initial operation was clear and free of black-iron-oxide suspensions.

Accurate Spring Counterbalancing

By W. S. ROUVEROL,[1] BERKELEY, CALIF.

The design of spring counterbalances for commercial purposes customarily has involved a sacrifice in accuracy for the sake of simplicity and economy. Overhead garage doors, automobile trunks, pipe hangers, and many other such products are ordinarily provided with a simple form of spring loading which produces true equilibrium at some central position but 10 to 15 per cent over or underbalancing at the extreme positions. This paper shows that this compromise with real accuracy is unnecessary and describes a method for attaining perfect full-rotation counterbalancing by the proper connection of a standard helical spring.

Introduction

IF a body is too heavy or bulky to be carried conveniently by hand, the simplest way to move it a short distance is to hinge it to a stationary frame. As a rule, a vertical axis of rotation is employed, enabling the body to be swung freely into or out of position, as in the case of a hinged door. If the axis cannot be vertical, because of the orientation of the supporting frame, the space limitations, or the shape of the body, a horizontal or tilted axis may be used; this, however, immediately introduces the problem of the tendency of the gravitational force to rotate the body downward. To offset this tendency, the weight of the body must be balanced, either by counterweights or a spring counterbalance.

Counterweights have the advantage of producing perfect static equilibrium at all angles of elevation of the load, but the great dead weight and rotational inertia have come to be considered undesirable in an increasing number of commercial items. Overhead garage doors, pipe hangers, automobile hoods and trunks, vertical drafting machines, etc., are typical examples of products now being balanced by springs rather than by counterweights, despite the fact that the prevailing method of spring loading provides only approximate balancing.

The spring balance normally employed consists merely of a standard helical extension spring attached directly between the lever arm of the load and a fixed point on the frame. The height of attachment of the fixed end of the spring, and the spring modulus, are in this case chosen so as to produce static equilibrium at some mean position of the load. As the load is moved up or down from this mean position, however, the geometry of the system causes an increasing disparity between the spring-force moment and the load moment. The use of excessive friction in the pivot to overcome this disparity is normally not satisfactory, since the presence of a frictional moment sufficient to overcome an unbalance in one direction doubles the resistance to movement in the opposite direction.

The failure of these simple spring-loading systems to provide equilibrium at all positions is due to the fact that the line of action of the load, which is usually simply the weight of the body acting downward through its center of gravity, remains parallel to itself, while its effective lever arm changes as a function of the angle of elevation. As the body is rotated, the load moment therefore must vary sinusoidally. The force exerted by a standard helical balancing spring, on the other hand, varies linearly with deflection. It is the reconciliation of this linear spring characteristic with the sinusoidal load moment which must be accomplished if accurate balancing is to be provided.

A number of different mechanisms have been devised to effect such a reconciliation, utilizing kinematic linkages, cam arrangements, or nonlinear springs. Unfortunately, however, the complexity of these devices has made their manufacture so expensive that commercially they have been unable to offer serious competition to the inexact but simpler type of direct spring loading. Even where the inaccuracies inherent in direct spring loading are as conspicuously undesirable as they are in overhead garage doors, devices affording more exact balancing have had to be bypassed for economy's sake. It is therefore evident that an improved spring counterbalance of practical value must, in addition to reconciling the linear and sinusoidal characteristics, meet a second condition of having a cost more or less comparable to that of simple spring loading.

The following analysis suggests a balancing system which appears to meet these qualifications. A standard helical spring is utilized in such a way as to produce perfect static equilibrium at all angles of elevation of the load, and the mounting of this spring is only slightly more involved than in the simplest type of direct spring loading.

Analysis

Fig. 1 shows a body pivotally connected to a supporting frame at point A, about which the body may be rotated in a vertical plane; B is the point at which a load of constant magnitude and direction is applied. The load may be external, as in a pipe hanger, or may be the weight of the body itself, in which case point B is the center of gravity.

To balance the tendency of this load to cause clockwise rotation, some form of spring device, to be referred to as "the yielding

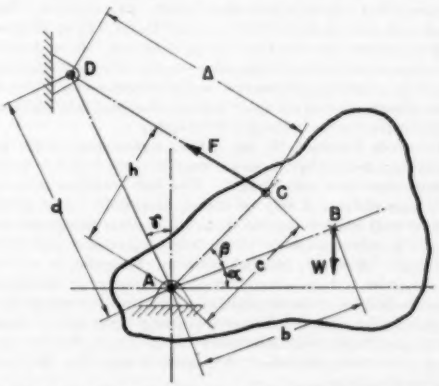

Fig. 1 Free-Body Diagram of a Counterbalanced Body in Static Equilibrium

[1] Lecturer in Engineering Design, College of Engineering, University of California.

Contributed by the Machine Design Division and presented at the Semi-Annual Meeting, St. Louis, Mo., June 19–23, 1950, of The American Society of Mechanical Engineers.

Note: Statements and opinions advanced in papers are to be understood as individual expressions of their authors and not those of the Society. Manuscript received at ASME Headquarters, November 16, 1949. Paper No. 50—SA-6.

means," will be attached to the body at point C, and to the stationary frame at point D. The exact location of these two points, as well as the load-deflection characteristic of the yielding means, are assumed for the present to be unknown. The direction of force F, which the yielding means exerts on the body at point C, is necessarily toward point D, however.

For perfect counterbalancing, the clockwise and counterclockwise moments about point A must be equal for all values of angle α; the equilibrium equation is then

$$W \cdot b \cdot \cos \alpha = F \cdot h \quad \ldots\ldots [1]$$

Of the three variables in this expression, which are the angle of elevation α, the spring force F, and its moment arm h, it is possible to eliminate one by noting the relation between α and h, as obtained by equating two expressions for the area of triangle ACD

$$\frac{h \cdot \Delta}{2} = \frac{d \cdot c \cdot \sin [\gamma + (\pi/2 - \alpha - \beta)]}{2}$$

$$h = \frac{d \cdot c \cdot \sin [\pi/2 - (\alpha + \beta - \gamma)]}{\Delta}$$

$$= \frac{d \cdot c \cdot \cos (\alpha + \beta - \gamma)}{\Delta} \quad \ldots\ldots [2]$$

The substitution of this value into Equation [1] gives

$$F = \frac{W \cdot b \cdot \Delta \cdot \cos \alpha}{c \cdot d \cdot \cos(\alpha + \beta - \gamma)} \quad \ldots\ldots [3]$$

By proper location of point D, angle γ in this equation may be made equal to angle β. The cosine terms will then cancel out, leaving an expression for the spring force F in terms of a single variable Δ

$$F = \frac{W \cdot b}{c \cdot d} \cdot \Delta \quad \ldots\ldots [4]$$

It is evident from this equation that the force F required for perfect counterbalancing is directly proportional to a linear distance Δ between the two points of attachment of the yielding means. A spring with a linear load-deflection characteristic therefore can be used, provided the force it exerts is directly proportional to the distance between its points of attachment. This requires that the distance between points C and D be at all times a direct measure of the total spring deflection. It is this requirement which makes it impossible to achieve correct balancing merely by attaching an extension spring between points C and D, for in this case part of the space between these points would have to be occupied by the free length of the spring.

To satisfy Equation [4] the yielding means must fulfill two conditions: it must have a spring constant equal to $W \cdot b/c \cdot d$, and it must have zero initial length. The first condition is easily met, since distance d may be chosen arbitrarily. Any spring may be used which is capable of storing as strain energy the difference in potential energy of the body at its upper and lower positions. Obviously, from an economy standpoint, it will be advantageous to have a minimum of strain energy in the spring when the body is at the top position. This may be accomplished by making the arbitrary distance d as nearly equal to c as dead-center and clearance considerations will permit, so that the distance Δ, and hence the force F, will approach zero when the body is at top dead center.

The other condition, that the yielding means have "zero initial length," is a more unusual specification, but one which nevertheless may be met easily. For example, if a compression spring is to be used, a tie rod of effective length equal to the free length of the spring may be passed through the center of the spring, as shown in Fig. 2. The spring is thus constrained between a plate or washer at one end of the tie rod and a collar pivotally mounted at point D. The tie rod is passed through the collar and its free end pivotally attached at C. The collar normally will have some effective thickness g, as shown, so that the length f, of the tie rod between the washers and point C, must equal the free length of the spring plus the collar dimension g. Then, if the yielding means is detached from point C, and the spring allowed to expand to its free length, the end of the tie rod previously attached at C must pull back to a point immediately adjacent to point D. This is what is meant by zero initial length.

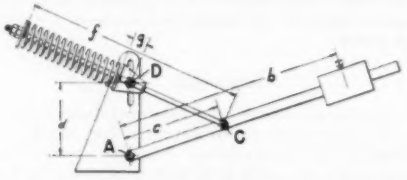

FIG. 2 MODEL OF A LOADED MEMBER COUNTERBALANCED BY A YIELDING MEANS OF ZERO INITIAL LENGTH

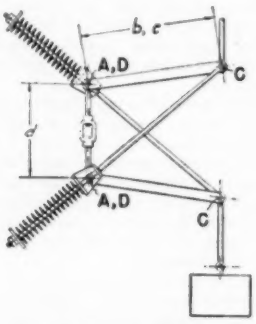

FIG. 3 MODEL OF A COUNTERBALANCING DEVICE TO GIVE STRAIGHT-LINE MOTION OF THE LOAD

It should be noted in the construction of Fig. 2 that the angles β and γ of Fig. 1 have been taken as zero; this is of course arbitrary, the only requirement being that they be equal. Fig. 2 also shows a slot at D, the function of which would be to accommodate changes in the load or in the length of its lever arm, or both. For any given load and lever arm, the pivot point D would be locked in the slot at a distance d equal to $W \cdot b/c \cdot k$, where k is the spring modulus. This adjustability slot is of course an optional feature, of value chiefly in such articles as pipe hangers, to permit a single commercial model to be easily adapted to a variety of loads. It should also be noted that such an adjustability slot could be located at point C instead of D, and that the yielding means could be reversed, with the collar mounted at C instead of D, if desired. In addition, if the dimensions c and d are chosen so as to provide clearance at top dead center, the body may be rotated through a complete revolution, or several revolutions, in either direction, exhibiting perfect balance at any point in the 360 deg of travel.

If two devices such as shown in Fig. 2 are connected in series, with the lower one inverted, the resulting mechanism provides for straight-line motion of the load. This arrangement is shown in Fig. 3. A load hung from such a mechanism will remain suspended at any desired elevation and may be moved up or down in a vertical line by application of only enough force to overcome friction and inertia. Since the device is accurate for any angle of rotation of its arms, the total permissible travel will be 4 times the length of the arm b, provided interference is eliminated by locating the members in different planes. In practice, a pipe hanger embodying this principle would need arms only 1 or 2 in. in length constructed as cranks or eccentrics.

If an extension spring is to be used, instead of a compression spring, as shown in Figs. 2 and 3, the tie rod must be replaced by a column of suitable slenderness ratio. For example, the spring may be encased in a cylindrical tube of length equal to the free length of the spring, with proper guidance provided to keep the tube colinear with the portion of the spring drawn out of the open end of the tube.

It should be noted that the types of yielding means described and shown in Figs. 2 and 3 will tend to throw a small degree of unbalance into the system because the weight of the spring itself has not been taken into consideration in the equilibrium equation. This moment due to the unbalance of the yielding means normally will be much smaller than that due to the load, but in order to attain perfect balancing it should be eliminated. One method of doing this is to employ two identical compression springs of modulus $2 \cdot W \cdot b/c \cdot d$, one at each end of the tie rod, with collars at both points C and D. The yielding means will thus be perfectly symmetrical, so that one half its weight will bear vertically at C at all times and may be balanced as part of the load. Or, if an extension spring is used, the cylinder in which it is encased may be made up of two segments, one of which is small enough in diameter to telescope into the other; a slot on each side of the larger cylinder will permit bosses on the mid-point of the inner cylinder to serve as points of attachment.

A far more desirable method of eliminating the small unbalance due to the weight of the yielding means, however, and one which will not increase the cost of the mechanism, is to take the weights and moment arms of all of the various parts of the yielding means into consideration in setting up the equilibrium equations. For example, referring to Fig. 2, the weight of the spring, tie rod, washer, bolts, and collar all tend to produce a vertical upward reaction at C contributing to the counterclockwise moment. This upward force may be expressed mathematically as a summation of the effects due to each of the parts of the yielding means. When calculated, this summation will be found to include several terms which, like the spring force, are functions of the variable distance Δ between points C and D, as well as several terms which are independent of Δ.

In order to satisfy the more elaborate equilibrium equation so obtained, it will be necessary to alter slightly the zero initial length by making the effective length of the tie rod slightly longer than the free length of the spring. That is to say, if the yielding means were to be detached from point C, the end of the tie rod would no longer pull back to a point immediately adjacent to point D, but instead to a point a short distance ahead of point D. If this distance is called r, the total spring deflection becomes $\Delta - r$, and the spring force is

$$F = k(\Delta - r) \quad [5]$$

Substituting this value for the spring force into the equilibrium equation and collecting terms, an expression in the following form may be obtained

$$(X - kd)\Delta + Yr - Z = 0 \quad [6]$$

where X, Y, and Z are all summations of several terms involving only the constants of the system such as fixed dimensions and weights. The only variable in this equation is Δ, which changes with the angle of elevation of the body; hence the equation can be true for all Δ's only if the coefficient of Δ of zero; from this fact the expression for d is obtained

$$d = \frac{X}{k} \quad [7]$$

The remainder of the equilibrium equation, $Yr - Z = 0$, determines the required initial length of the yielding means

$$r = \frac{Z}{Y} \quad [8]$$

The satisfying of these two relationships will provide perfect counterbalancing for systems employing either extension or compression springs. It perhaps should be noted, however, that if an extension spring with some initial tension I is used, Equation [5] will become

$$F = I + k(\Delta - r) \quad [9]$$

If this value for F, instead of the simpler expression of Equation [5], is substituted into the equilibrium equation, one additional term will appear in the Z-summation of Equation [6], and the value of r will be increased proportionately in accordance with Equation [8]. The presence of initial tension in the spring, therefore, will add no particular complication to the design.

When Equation [8] is written out with the full Z and Y-summations, it will be observed that the major component of the distance r is attributable to the initial tension term in the numerator, even when the initial tension is comparatively small. Therefore it might be inferred that if the initial tension could be increased sufficiently, r could be made to approach the free length of an extension spring attached directly between points C and D. Unfortunately, the relationships between free length, spring modulus, and maximum obtainable initial tension are such that this simplification is not possible.

Design Procedure

In the design of compression or extension-spring counterbalances embodying the foregoing principles, trial-and-error methods may be avoided by approaching the problem through the following procedure:

1 Select a spring which is capable of storing as strain energy the difference in potential energy of the load in its extreme upper and lower positions. If the load must be rotated to top dead center, clearance considerations will require a spring of 10 to 15 per cent excess capacity. If a compression spring is used, it must be safe against buckling. Note the weight, free length, modulus, and maximum deflection of the spring selected.

2 Design all parts of the yielding means. In a compression-spring system, the tie rod must be of sufficient stiffness to rotate the collar at D without excessive flexure. In an extension-spring system, attention must be given to the avoidance of possible binding or buckling of the cylindrical case at maximum spring deflection. When the various parts have been designed, their weights and the locations of their centers of gravity should be computed.

3 Next, assign a dimension to the distance c. The correct choice for this dimension depends on both the angle through which the body must rotate and on the allowable deflection of the spring. As a rule, a satisfactory value for c is found to equal about one half the maximum spring deflection divided by the sine of one half the maximum angle DAC, which is the angle the body turns through in passing from top dead center to its lowest position.

For example, if the body must rotate down to bottom dead center, the dimension c, should be one half the maximum spring deflection.

4 Write the equilibrium equation for the body at some angle α, including moment components due to all parts of the yielding means. Cancel out the cosine factor as in Equation [3], and substitute for the spring force F the expression of Equation [5] or [9]. Rearrange and collect terms into the form of Equation [6] to determine X, Y, and Z. Compute the distance d from Equation [7], and r from Equation [8].

5 Check the geometry of the system to insure that there is sufficient clearance when the body is in its uppermost position and that the maximum deflection of the spring is not exceeded when the body is in its lowest position. If necessary, alter the dimension c slightly and revise the computations of step 4 accordingly.

6 In the design of balancing systems for commercial products, it will normally be necessary to provide adjustment nuts at the end of the tie rod (or cylindrical case) and also a slot on the line AD, as shown in Fig. 2. The purpose of these features, other than to accommodate changes in load, is to permit small final adjustments to be made in the dimensions r and d at the time of assembly, to correct for the small variations in free length and modulus customarily encountered in commiercially manufactured springs. These adjustments, the magnitude of which will depend upon the spring tolerances specified, may be made either empirically or by correcting the computations of the distances r and d made in step 4.

Discussion

M. F. Spotts.[3] This paper should be of worth-while service to designers confronted with counterbalancing problems. By an ingenious arrangement of links, the author has shown how a pivotally mounted weight can be kept in static equilibrium regardless of the angular position of the weight. In other words, a spring with a straight-line stress-strain relationship can be made to produce a variable moment equal and opposite to that of the weight as it rotates on its pivot. Practical difficulties may arise at times in providing sufficient clearance for the spring and tie rod. These members may become rather large as compared to the size of the remainder of the mechanism.

Springs with nonlinear load-deflection characteristics are frequently needed in mechanical equipment. Volute springs and blocks of rubber can be used where a spring of stiffness increasing with deflection is required. The Belleville spring can be proportioned to give a wide variety of stress-strain curves. One of the most useful is that one where a considerable range of deflection can be obtained at a constant load. A linear leaf spring can be made to give a nonlinear curve by mounting the ends in suitably designed shackles.

Another case where a linear spring is made to give a nonlinear load-deflection curve consists of the torsion-bar spring frequently applied to vehicles. Such a spring with a Hickman type suspension is shown in Fig. 4 of this discussion. The spring runs parallel to the frame of the vehicle; the far end of the spring is fixed to the frame and the near end is carried in a bearing attached to the frame. The near end of the spring is connected by splines to the torque arm OA. Shackle AB connects the end of the torque arm to a projection of the axle extending to B. If the pin at A should be removed and the spring be completely unloaded, the torque arm would assume position OA_o at angle α with the horizontal. Point B is offset inwardly by amount a from the full radius r.

[3] Professor of Mechanical Engineering, Mechanical Engineering Department, Northwestern University, Evanston, Ill. Mem. ASME.

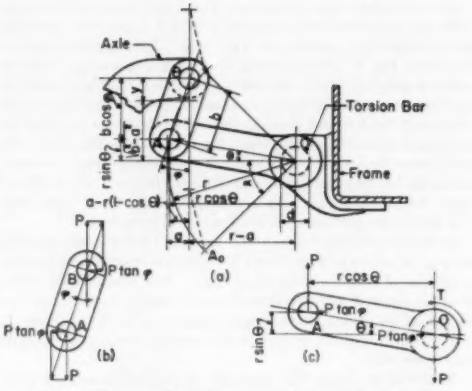

Fig. 4 Hickman Type Mount of Torsion-Bar Spring

Let P be the vertical load carried by the spring. Let angle θ represent the inclination of the torque arm with the horizontal, and angle φ represent the inclination of the shackle with the vertical. A relationship between angles θ and φ, from Fig. 1(a), is seen to be

$$\sin \varphi = \frac{a - r(1 - \cos \theta)}{b} \quad [10]$$

The shackle, as a two-force member, must have a resultant load lying along AB. It will therefore be subjected to the loads shown in Fig. 4(b). Fig. 4(c) shows these loads transferred to the end of the torque arm at A. The torque about point O is equal to

$$T = Pr \cos \theta + Pr \sin \theta \tan \varphi \quad [11]$$

The total angle of twist sustained by the spring is $\alpha + \theta$. By elementary theory for the torsion of round bars

$$T = \frac{JG(\alpha + \theta)}{l} \quad [12]$$

where J = polar moment of inertia for the cross section
G = modulus of elasticity in shear for the material
l = effective length of the spring

Equations [11] and [12] can be combined to give

$$Pr\, l\, (\cos \theta + \sin \theta \tan \varphi) = JG(\alpha + \theta) \quad [13]$$

Figure 4(a) shows that the axle travel y is equal to

$$y = r \sin \theta + b \cos \varphi - \sqrt{b^2 - a^2} \quad [14]$$

Equations [10], [13], and [14] permit the load-deflection curve of the spring to be plotted. Suitable values for θ are chosen, and the corresponding values of φ are found by Equation [10]. Load P and axle travel y are then found by Equations [13] and [14].

Fig. 5 gives the load-deflection curve for a suspension of the following values:

Spring diameter, d = 1.200 in.
Effective length, l = 120 in.
Polar moment of inertia, $J = \frac{\pi d^4}{32} = 0.2036$ in.^{4}
Torque-bar radius, r = 6 in.
Shackle length, b = 3 in.
Offset, a = 1 in.

Initial angle, $\alpha = 45$ deg
Modulus of elasticity in shear, $G = 11{,}400{,}000$ psi

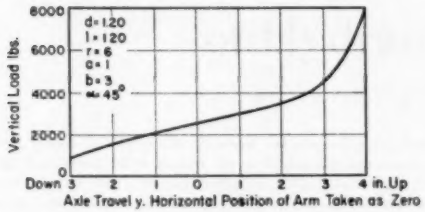

FIG. 5 LOAD-DEFLECTION CURVE FOR TORSION-BAR SPRING

The manner in which the stiffness of the suspension increases with increase of load is shown by the curve. This is a desirable property for vehicle mounts since a heavy overload will continue to be supported by the springs without bottoming of the frame. In addition, the lengths can be proportioned so that the riding qualities will remain practically unchanged. The natural frequency of vibration of a heavy load and stiff spring can be made equal to the natural frequency of the vehicle when the load is light and the spring is soft.

BIBLIOGRAPHY

"Torsion Bars for Commercial Vehicles," by N. E. Bateson, SAE Quarterly Transactions, October, 1947, vol. 1, no. 4, p. 549.

"Torsional Rod Springs and How They Are Designed," by H. E. Simi, *Product Engineering*, vol. 13, 1942, p. 710.

"Torsion-Bar Suspensions," by J. M. Colby, SAE Quarterly Transactions, April, 1948, vol. 2, no. 2, p. 195.

"Design of Torsion Rod Springs Used in M-18 Tank Destroyer," Staff Articles, *Product Engineering*, vol. 16, 1945, p. 390.

F. HIRSCH.[3] Although they will be materially aided by Mr. Rouverol's paper, design engineers concerned with counterbalancing systems might find desirable a further explanation of the following:

(*a*) The dimensional limitations of d in Fig. 3 and the proper dimensional relation of d to b and c of Fig. 3.

(*b*) Indication of the origin of the summations X, Y, and Z occurring in Equations [6], [7], and [8].

(*c*) Provisions for vertical and horizontal movement in high-temperature piping installations.

(*d*) Provisions to be made for vibration isolation in piping installations.

[3] Assistant Professor, Division of Engineering Design, College of Engineering, University of California, Berkeley, Calif. Jun. ASME.

AUTHOR'S CLOSURE

The author would like to thank Professors Spotts and Hirsch for their comments. Professor Spotts' analysis of the Hickman type suspension adds some useful material to the paper. It might be well to point out that while the balancing method outlined in my own analysis could readily be altered to give a soft-spring type of suspension, for example, by making distance d slightly larger than the value given by Equation [7], there would seem to be little if any advantage in so doing. The characteristics of a good spring balance are not necessarily similar to those of a good vehicle suspension system, as the latter requires a variation in load-deflection relations of the type indicated in Professor Spotts' Fig. 5.

Taking in order Professor Hirsch's suggestions regarding points in need of clarification:

(*a*) The only dimensional limitation on distance d of Fig. 3 is that it must satisfy Equation [7]; it corresponds to the similarly labeled dimension in Fig. 2. The dimensions b and c in Fig. 3 are shown as being equal, but need not necessarily be so. The dimension b would normally be selected so as to equal about one fourth of the required vertical travel of the load, and dimension c would be about half the safe spring deflection. The assignment of these two dimensions enables the distance d to be computed from Equation [7].

(*b*) With regard to the origin of the summations X, Y, and Z of Equation [6], they come directly from the equilibrium equation when terms containing Δ and r are grouped together, and the Δ or r, as the case may be, is factored out. Since both of these terms appear only in the first power, such collecting and factoring will always be possible.

(*c*) A device embodying the principles of Figs. 2 and 3 used as a constant-support pipe hanger would provide a constant lifting force despite vertical movement of the piping. Horizontal movement could be accommodated either by mounting the hanger so that its frame could swivel about a vertical axis, if the Fig. 2 type of mechanism is used, or, if there were adequate space above the pipe, simply by inserting a long vertical rod between the pipe and the hanger.

(*d*) Since the device is designed to provide constant lifting force regardless of vertical position of the load, no spring forces would be transmitted to the supporting frame by a vibrating load, provided the amplitude of vibration was less than the vertical travel afforded by the type of mechanism shown in Fig. 3. There would, however, be some small forces transmitted due to the inertia of the various parts of the yielding means. These could be kept relatively small by designing for lightness of the yielding means parts and by the strategic location of pivot points at or near centers of percussion.

Displacement Versus Time Characteristics of Hydraulic Actuators

By L. SIGFRED LINDEROTH, JR.,[1] AMES, IOWA

This paper develops the relation between the displacement and time of a piston in a hydraulic actuator in terms of the load, mass, pressure drop, viscosity, and special operating conditions. It is based upon the Fanning law of friction in pipes and the value of the friction factor in smooth pipes as given by Hagen-Poiseuille and Blasius. The relation developed will cover most conditions met in the design of hydraulic equipment and will suggest a means to analyze those conditions not covered. This method is valid for pressures up to 100 atm and, with modifications, to higher pressures.

IN designing complex hydraulic equipment, particularly equipment in which several hydraulic actuators must operate with definite relations to each other, it becomes necessary for the design engineer to know with reasonable certainty what the characteristics of the motion of the actuator will be. It is the purpose of this paper to develop a general method for determining the displacement-time relation of a hydraulic actuator in terms of pressure, flow, viscosity, friction, mass, and load.

Fig. 1 is a diagram illustrating the basic elements in the hydraulic system for operating the actuator. The source of fluid is an accumulator of sufficient capacity to maintain the maximum required flow at a constant pressure P_0 in the accumulator. A hydraulic line of inside diameter D_1 and equivalent length L_1 connects the accumulator through the control valve to the inlet on the actuator. A similar hydraulic line of diameter D_2 and equivalent length L_2 connects the outlet end of the actuator through a control valve to the sump or fluid reservoir, discharging the fluid at pressure P_3. P_1 is the fluid pressure acting on piston area A_1; and P_2 is the fluid pressure acting on piston area A_2. The piston rod and piston packing create friction or drag which must be overcome by the differential force on the piston. The equivalent lengths L_1 and L_2 are the lengths of straight smooth tubing which have the same resistance as the actual tubing, including bends and valves. It is assumed that the change in resistance or pressure drop of the actual tubing, fittings, and valves will be the same as the equivalent length of straight tubing. This assumption has been substantiated by other experimenters.[2]

The net force on the piston will overcome friction, balance the load, and accelerate the total mass of all the moving parts. This can be expressed by the following equation

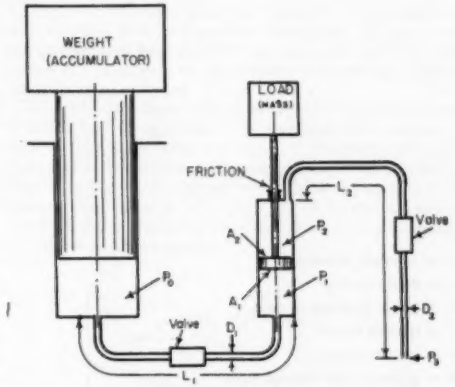

FIG. 1 DIAGRAM OF COMPONENTS IN HYDRAULIC SYSTEM

$$F = P_1A_1 - P_2A_2 = \text{friction} + \text{load} + \text{mass} \times \text{acceleration}$$

$$= Fr + Lo + M \times \frac{dV}{dt} \quad \ldots\ldots [1]$$

P_1 and P_2 can be expressed as functions of the pressure at the remote ends of the connecting tubes L_1 and L_2 and the respective pressure drops ΔP_1 and ΔP_2 in these tubes for a given piston velocity V

$$P_0 - \Delta P_1 = P_1 \quad \ldots\ldots [2]$$

and

$$P_3 + \Delta P_2 = P_2 \quad \ldots\ldots [3]$$

Substituting these values in Equation [1] and rearranging the terms results in the expression

$$\frac{dV}{dt} = \frac{[P_0 - \Delta P_1]A_1 - [P_3 + \Delta P_2]A_2 - [Fr + Lo]}{M} \quad \ldots [4]$$

It is assumed that conditions are such that P_0 and P_3 are constant, since these pressures usually can be fixed by the designer. Friction and load are also constant. Rearranging the terms of Equation [4] to place all the constants together results in

$$\frac{dV}{dt} = \frac{[P_0A_1 - P_3A_2 - Fr - Lo] - [\Delta P_1A_1 + \Delta P_2A_2]}{M} \quad \ldots [5]$$

If the piston starts at rest and, consequently, no fluid is in motion, ΔP_1 and ΔP_2 are zero and Equation [5] reduces to

$$\frac{dV}{dt} = \frac{P_0A_1 - P_3A_2 - Fr - Lo}{M} \quad \ldots\ldots [6]$$

During the initial stage of motion the flow of fluid through the tubing is relatively slow. The flow is viscous and ΔP will vary

---

[1] Professor of Mechanical Engineering, Iowa State College of Agriculture and Mechanic Arts. Mem. ASME.

[2] Crane Co., 836 S. Michigan Ave., Chicago, Ill. The reader is referred to this company for data for the calculation of equivalent lengths of tubing for various types of valves, fittings, bends, and diameter changes.

Contributed by the Machine Design Division and presented at the Semi-Annual Meeting, St. Louis, Mo., June 19–23, 1950, of THE AMERICAN SOCIETY OF MECHANICAL ENGINEERS.

NOTE: Statements and opinions advanced in papers are to be understood as individual expressions of their authors and not those of the Society. Manuscript received at ASME Headquarters, February 28, 1950. Paper No. 50—SA-5.

according to this type of flow. As the piston speed increases, the fluid velocity in the tube increases, and a point is soon reached when viscous flow will change to turbulent flow. The change in ΔP will then follow a turbulent-flow equation.

The pressure drop ΔP in a straight smooth tube can be found from Fanning's relation

$$\frac{\Delta P}{L} = f\,\rho\,\frac{v^2}{2D} \qquad [7]$$

in which

ρ = absolute density
v = fluid velocity
D = inside diameter of tube
f = friction factor
L = length of tube
ΔP = pressure drop through tube

The value of f for viscous flow (Hagen-Poiseuille) is

$$f = \frac{64}{N_R} = \frac{64\,\nu}{Dv} \qquad [8]$$

where N_R is the Reynolds number and ν is the kinematic viscosity of the fluid. D and ϑ are as in Equation [7]. By combining Equations [7] and [8] the pressure drop for viscous flow results

$$\Delta P = 32\,\frac{L\nu\rho v}{D^2} \qquad [9]$$

Likewise f for turbulent flow is

$$f = \frac{0.316}{\sqrt[4]{N_R}} = \frac{0.316\nu^{1/4}}{D^{1/4}v^{1/4}} \qquad [10]$$

which is the Blasius approximation for the resistance in smooth pipe or tubing. Substituting the value of f from Equation [10] in Equation [7] results in a final equation for turbulent flow

$$\Delta P = 0.158\,L\,\rho\,\frac{\nu^{1/4}\,v^{7/4}}{D^{5/4}} \qquad [11]$$

Since the piston velocity V is of primary interest the fluid velocity ϑ in Equations [9] and [11] is replaced by an expression relating ϑ to V. This is written

$$v = \frac{4\,VA}{\pi\,D^2} \qquad [12]$$

in which A is the piston area on which acts the fluid flowing at velocity v in the tube of D inside diameter.

Equations [9] and [11] become, respectively

$$\Delta P = 40.8\,\frac{L\rho\nu A\,V}{D^4} \qquad [13]$$

$$\Delta P = 0.241\,\frac{L\rho\nu^{1/4}A^{7/4}V^{7/4}}{D^{19/4}} \qquad [14]$$

The pressure-drop values from Equations [13] and [14] are substituted for ΔP_1 and ΔP_2 in Equation [5]. This gives the following equation for viscous flow

$$\frac{dV}{dt} = \frac{[P_aA_1 - P_bA_2 - Fr - L\sigma] - \left[40.8\rho\nu\left(\frac{L_1A_1^2V}{D_1^4} + \frac{L_2A_2^2V}{D_2^4}\right)\right]}{M} \qquad [15]$$

and for turbulent flow

$$\frac{dV}{dt} = \frac{[P_aA_1 - P_bA_2 - Fr - L\sigma] - \left[0.241\rho\nu^{1/4}\left(\frac{L_1A_1^{11/4}V^{7/4}}{D_1^{19/4}} + \frac{L_2A_2^{11/4}V^{7/4}}{D_2^{19/4}}\right)\right]}{M} \qquad [16]$$

This apparently cumbersome expression can be greatly simplified since most of the terms remain constant during an operating cycle, and if the pressure range is not over 100 atm, the viscosity ν can be considered a constant for such fluids as water and mineral oil. The absolute density ρ for this pressure range and these fluids varies less than 1 per cent and can be considered constant. This leaves V the piston velocity as the only variable, and Equations [15] and [16], therefore, can be reduced to

$$\frac{dV}{dt} = C_1 - C_2 \times V \qquad [17]$$

for viscous flow and

$$\frac{dV}{dt} = C_1 - C_3 \times V^{7/4} \qquad [18]$$

for turbulent flow. The constants are

$$C_1 = \frac{P_aA_1 - P_bA_2 - Fr - L\sigma}{M}$$

$$C_2 = \frac{40.8\rho\nu}{M}\left(\frac{L_1A_1^2}{D_1^4} + \frac{L_2A_2^2}{D_2^4}\right)$$

$$C_3 = \frac{0.241\,\rho\nu^{1/4}}{M}\left(\frac{L_1A_1^{11/4}}{D_1^{19/4}} + \frac{L_2A_2^{11/4}}{D_2^{19/4}}\right)$$

Fig. 2 illustrates a plot of the curves of Equations [17] and [18] with acceleration dV/dt as ordinates and velocity V as abscissa. It is noticed that the viscous-flow curve is a straight line and intersects the turbulent-flow curve. The flow pattern in the hydraulic lines starts as a viscous flow with an acceleration of C_1 at V = zero. Viscous flow is maintained up to the velocity of the intersection of the two curves. At this point the flow pattern changes to turbulent and the characteristics follow the turbulent-flow curve. The transition from viscous to turbulent flow occurs not at an exact point on either curve but rather as a transition of indeterminate duration. From classic flow data this transition period has been shown to occur between Reynolds numbers 2000 and 4000. From these data the approximate duration of the viscous flow can be calculated.

Fig. 3 illustrates a plot made for a specific installation. In this actuator the duration of the viscous flow was very short and the analysis could be carried out with good accuracy considering the entire flow pattern as turbulent. The actual time or duration of the viscous-flow period up to the intersection of the two curves is 0.0208 sec. The total duration of the acceleration is on the order of 2 sec. Therefore the error in displacement from assum-

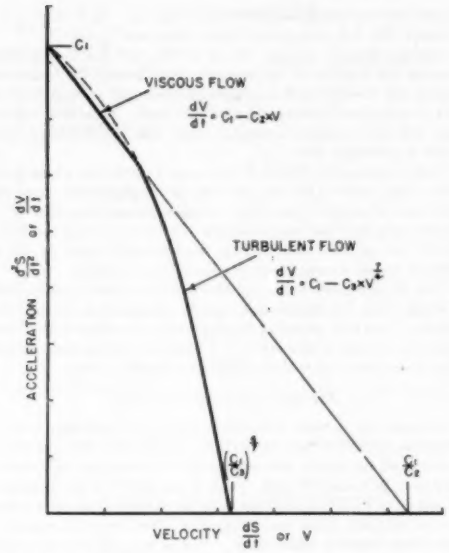

FIG. 2 ACCELERATION-VELOCITY CURVE OF PISTON

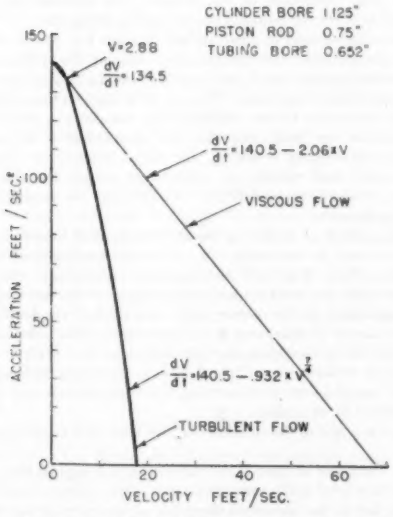

FIG. 3 ACCELERATION-VELOCITY CURVE OF PISTON IN A SPECIFIC PROJECT

ing turbulent flow throughout the entire period will be of no practical significance.

Equation [17] for viscous flow can be integrated and the values of dV/dt, V, and S are as follows

$$\frac{d^2S}{dt^2} = \frac{dV}{dt} = C_1 e^{-C_2 t} \quad \ldots\ldots [19]$$

$$\frac{dS}{dt} = V = \frac{C_1}{C_2}(1 - e^{-C_2 t}) \quad \ldots\ldots [20]$$

$$S = \frac{C_1}{C_2}\left[t - \frac{1}{C_2}(1 - e^{-C_2 t})\right] \quad \ldots\ldots [21]$$

Equation [18] with the variable V raised to a fractional power does not lend itself to analytical integration. It can be quite easily integrated by a graphical method, and the degree of accuracy is limited only by the number of parts into which the original curve is divided.

The integration of the viscous-flow equation suggests a method of attack for the integration of the turbulent-flow equation. As shown in Fig. 4, the curve $A = A_1 - CV^{7/4}$ is divided into several parts and each is replaced by a straight line. Acceleration and velocity in Fig. 4 are designated by A and V, respectively. The shorter the distances $A_1V_1 \ldots A_3V_3$, $A_2V_2 \ldots A_3V_3$, etc., are, the more nearly the series of lines will represent the curve, and the more accurate will be the integration.

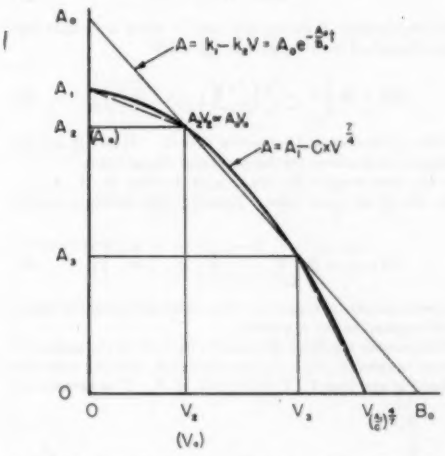

FIG. 4 DIAGRAM ILLUSTRATING METHOD OF GRAPHICAL INTEGRATION

An equation can be written for each of the straight lines and will take the general form

$$A = A_0 e^{-\frac{A_0}{B_0} t} \quad \ldots\ldots [22]$$

Each straight line will have a different value for A_0 and B_0, and these values are established by projecting the line to the coordinate axes and measuring the values at this point as shown for the line $A_2V_2 \ldots A_3V_3$.

The time t_3 at which acceleration A_3 occurs is calculated from the equation

$$A_3 = A_0 e^{-\frac{A_0}{B_0} t_3} \quad \ldots\ldots [23]$$

A_3, A_0, and B_0 for this equation are measured on the line $A_1V_1 \ldots A_3V_3$, and the values substituted in the equation which can then

be solved and the value of t_2 established. For this line the time t_1 at which A_1 occurs is zero since this is the start of the curve.

The time elapsed for the change in acceleration from A_1 to A_2 is, therefore

$$T_1 = t_2 - t_1 = t_2 \quad [24]$$

Likewise, any subsequent time T_2, T_3, . . T_n can be established. The next line from A_2V_2 to A_3V_3 would have two equations

$$A_2 = A_{02}e^{-\frac{A_2}{B_2}t_2} \quad [25]$$

$$A_3 = A_{03}e^{-\frac{A_3}{B_3}t_3} \quad [26]$$

in which A_0 and B_0 are the same but not equal to the A_0 and B_0 of Equation [23]. A_2 and A_3 are again measured from the co-ordinate axes (A_2 being the same as in Equation [23]), and the values for t_2 and t_3 calculated. It should be noted that the time t_2 in Equation [25] is not the same as t_2 in Equations [23] and [24].

Elapsed time T_2, for the acceleration to change from A_2 to A_3 is therefore

$$T_2 = t_3 - t_2 \quad [27]$$

The displacement S during any time T along a straight line can be determined from the general equation

$$\Delta S = B_0\left[T - \frac{B_0}{A_0}\left(\frac{A_a}{A_0}\right)\left(1 - e^{-\frac{A_a}{B_0}T}\right)\right] \quad [28]$$

A_a is the acceleration at the start of time T. A_0 and B_0 are the co-ordinate intersections for this particular straight line.

For the first straight line starting at A_1 (Fig. 4), A, A_a, A_1, and A_b, are all the same value. Equation [28] therefore reduces to

$$\Delta S_{A1-A2} = B_0\left[T_1 - \frac{B_0}{A_0}\left(1 - e^{-\frac{A_2}{B_0}T_1}\right)\right] \quad [29]$$

which corresponds to Equation [21]. The derivation of Equation [28] appears in the Appendix.

In this manner the displacements S_1, S_2, . . S_n of the piston for each time interval T_1, T_2, . . T_n are calculated; and the total displacement at any time T_1, $T_1 + T_2$, . . $T_1 + T_2$ . . T_n is determined by the corresponding summation S_1, $S_1 + S_2$, . . $S_1 + S_2 + \ldots S_n$. A curve, Fig. 5, is then plotted from these data.

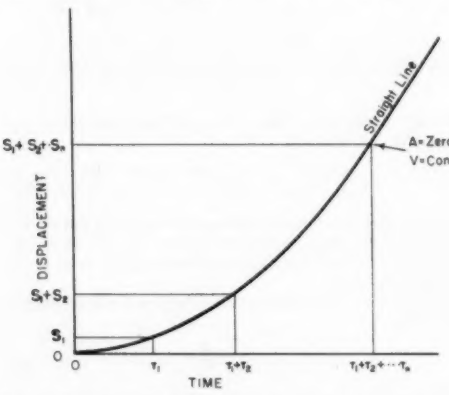

FIG. 5 DISPLACEMENT-TIME CURVE FROM GRAPHICAL INTEGRATION

At some time $T_1 + T_2 + \ldots T_n$ the acceleration has become zero because the increase in the pressure drop through the hydraulic tubing has reached such a magnitude that only enough force is left to overcome friction and balance the load. From this time on the velocity remains constant, and the displacement-time curve is a straight line.

Referring again to Fig. 2, if the design is such that a large portion of the curve is for viscous flow, the displacement curve for this part is plotted from data calculated from Equation [21], establishing the time from Equation [19] by measuring the value for dV/dt on the curve. This displacement curve is not a straight line so several values of t should be calculated.

The displacement curve for the turbulent flow is calculated starting with the acceleration at the intersection of the two curves. For this graphical integration it is assumed that the transition occurs at the point of intersection of the two curves. The error caused by this assumption is probably small.

APPLYING METHOD TO DESIGN

In using this method to evolve a design it is necessary first to establish values for the constants C_1, C_2, and C_3. Certain specifications of the design will take care of the values of such variables as L, ρ, ν, and M, but A and D are fixed by the designer. It will be necessary to estimate these for the first trial, go through the calculations, plots, and integration, then see if the resulting space-time curve is satisfactory. If it is not, changes will have to be made in the variables at the designer's disposal and a new curve established. If the time of displacement is too short, L can be lengthened by introducing a resistance in the form of a valve. If the time is too long, D must be increased or L shortened. The experience of the designer will indicate the best method to effect the required changes in the constants.

The actuator used to illustrate this analysis is a double-acting piston and cylinder with vertical axis. Placing the cylinder in a horizontal position merely removes the load Lo in Equation [1] and subsequent equations. The use of a single-acting cylinder merely eliminates all the discharge-line components, but in no way affects the basic analysis. In considering a hydraulic motor with rotating output V, the piston velocity is replaced with ω, the shaft velocity, in radians per second, and the constants are modified accordingly. In all cases the basic principles are the same.

This method of analyzing the displacement of a piston with time was used in the design of a complex hydraulically operated machine which was built and operated successfully. No extensive work was done to check the accuracy of the method, but it was adequate for the specific project for which it was developed.

As a means of indicating in a simple fashion the order of accuracy of the method, a curve of the form $A = 10 - 0.10\ V^{1/2}$ was integrated between $A = 10$ and $A = 1$, by taking successively shorter straight lines and summing the displacements and times as outlined in the paper.

Fig. 6 is a plot of the equation and the lines used in the integration.

Fig. 7 is a plot of time T and displacement S against the number of lines used in the approximation. It is evident from these curves that if the maximum deviation of the curve of the equation being integrated from the straight lines is less than 3 per cent of the length of that line, then the order of accuracy will approach plus or minus 2 per cent.

It is felt that the described method of determining the displacement time relation of an actuator gives the designer basic and necessary information of adequate accuracy with a minimum expenditure of time and effort.

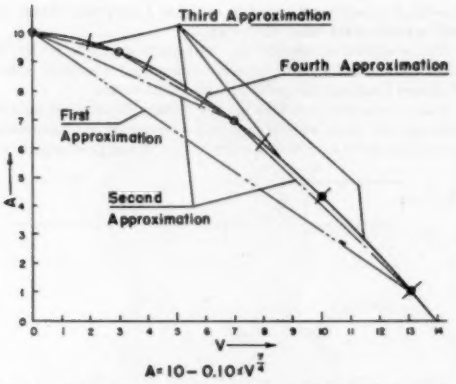

FIG. 6 ACCELERATION-VELOCITY CURVE—ACCURACY DETERMINATION

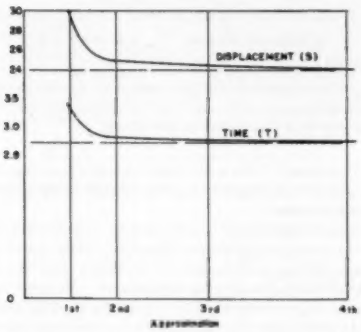

FIG. 7 DISPLACEMENT AND TIME VERSUS DEGREE OF APPROXIMATION

ACKNOWLEDGMENTS

The author is indebted to Dr. E. W. Anderson, Professor of Mathematics at Iowa State College, for assistance in the study of the differential equations.

The integration of the equation $dV/dt = C_1 - C_2 V$ is based on an unpublished analysis of similar equations by Messrs. W. H. Birnie, J. G. Hollick, H. Ross, and R. Elliot of the United Shoe Machinery Corporation of Beverly, Mass.

The derivation of Equation [28] was suggested by Mr. E. J. Crane, ASME Papers Committee.

Appendix

Referring to Fig. 4, the equation of any straight line drawn on the co-ordinate axes will be

$$A = k_1 - k_2 V$$

This line when extended will intersect the acceleration (vertical) axis at A_0 and the velocity (horizontal) axis at B_0; k_1 and k_2 are constants that must be evaluated for each straight line.

Let time measured from t_1 be

$$T = t - t_1$$

and let the velocity at time t_1 be V_a then

$$A = \frac{dV}{dT} = k_1 - k_2 V$$

and

$$\int_0^T dT = \int_{V_a}^{V} \frac{dV}{k_1 - k_2 V}$$

$$T = \left[-\frac{1}{k_2} \log_e (k_1 - k_2 V) \right]_{V_a}^{V}$$

or

$$e^{k_2 T} = \frac{k_1 - k_2 V_a}{k_1 - k_2 V}$$

from which

$$V = \frac{k_1}{k_2} - \frac{k_1 - k_2 V_a}{k_2} e^{-k_2 T}$$

Now

$$V = \frac{dS}{dt} = \frac{dS}{dT}$$

since

$$dT = d(t - t_1) = dt$$

hence

$$\int_{S_1}^{S} dS = \int_0^T \frac{k_1}{k_2} dT - \int_0^T \frac{k_1 - k_2 V_a}{k_2} e^{-k_2 T} dT$$

from which

$$\Delta S = \frac{k_1 T}{k_2} - \frac{k_1 - k_2 V_a}{k_2} \times \frac{1 - e^{-k_2 T}}{k_2}$$

Evaluating k_1 and k_2, when $V = 0$, $A = A_0$, and

$$A_0 = k_1 - k_2 \times 0 = k_1$$

and when $A = 0$, $V = B_0$, and

$$0 = A_0 - k_2 B_0$$

$$k_2 = \frac{A_0}{B_0}$$

therefore

$$\Delta S = \frac{A_0 T}{A_0/B_0} - \frac{A_0 - \frac{A_0}{B_0} V_a}{A_0/B_0} \times \frac{1 - e^{-\frac{A_0}{B_0} T}}{A_0/B_0}$$

Now, since $A_a = k_1 - k_2 V_a$ by definition of the straight line by its equation, and for a particular line

$$A_a = A_0 - \frac{A_0}{B_0} V_a$$

V_a can be determined as follows

$$A_a - A_0 = -\frac{A_0}{B_0} V_a$$

$$V_a = \frac{B_0}{A_0} (A_0 - A_a)$$

$$= B_0 - \frac{B_0 A_a}{A_0}$$

from which follows

$$\Delta S = B_0\left[T - \frac{B_0}{A_0}\frac{A_s}{A_0}\left(1 - e^{-\frac{A_0}{B_0}T}\right)\right]$$

which appears as Equation [28].

Data for Figs. 6 and 7

The following data were calculated for plotting curves in Fig. 6 and Fig. 7, using the method outlined in the paper:

$$A = 10 - 0.10 \times V^{7/4}$$

V	$V^{7/4}$	A
0	0	10.00
1	1	9.90
2	3.365	9.66
3	6.65	9.34
4	11.5	8.85
5	16.7	8.33
6	23.0	7.70
7	30.0	6.98
8	37.1	6.19
9	46.5	5.35
10	56.8	4.32
11	66.3	3.37
12	77.4	2.26
13	89.1	1.09
13.9	100.0	0.00

	S	T
Trial 1	29.70	3.34
Trial 2	24.78	2.81
Trial 3	24.49	2.77
Trial 4	23.90	2.71

Discussion

J. L. Shearer.[3] Professor Linderoth's paper very effectively illustrates the nonlinear phenomena present in many hydraulic systems. The effect of the nonlinear characteristics of fluid flow present in hydraulic systems is very pronounced when operation over wide ranges of flow is considered.

It is also significant that the analysis of the dynamic behavior of hydraulic systems is closely associated with the loads for which they are designed. In this paper a load consisting essentially of a pure mass is considered. The load on the actuator therefore varies linearly with the acceleration of the mass, and thus the problem has an element of simplicity in it. In many engineering applications the loads vary with the speed and position of the output member as well as with its acceleration. In addition the relationships between forces, displacements, velocities, and accelerations are nonlinear in many cases.

Of greatest interest are the difficulties which nonlinearities present to the designer. Graphical integration has been for some time a widely used tool in the solution of nonlinear differential equations. This method has definite limitations particularly where a wide survey of system parameters is desirable for design purposes. It is a means only of evaluating a proposed design.

The work being done in the development of electronic analog computer components should prove to be of immense value to the designer in this field. Electronic analog components which will generate nonlinear functions have been developed to make the solution of this type of problem straightforward and rapid. When the analog of a given system has been set up, system parameters can be varied by the twisting of dials. The accuracy achieved with electronic analog equipment is directly related to the care observed in calibration of the components, and, in general, it is sufficiently good to evaluate a particular design as well as perform the initial survey work.

Fig. 8 illustrates how analog components would be set up to solve electronically the nonlinear differential equation which Professor Linderoth has solved by graphical means.

Each component operates on the voltage signal or signals it receives and when all the required components are connected properly a closed loop results which will solve the given equation.

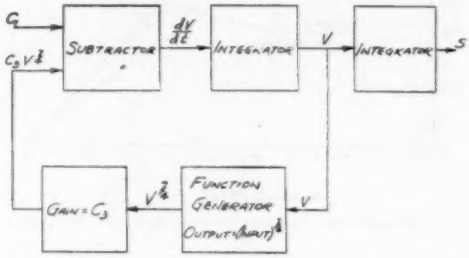

Fig. 8 Block Diagram of Setup of Analog Components

(Differential equation $\frac{dV}{dt} = c_1 - c_3 V^{7/4}$.)

The problems involved in the analysis of the performance of hydraulic systems are sufficiently interesting to provide the basis for more papers of this nature in the future.

J. D. Dietiker.[4] The author provides, in a practical manner, a method of determining the time-displacement characteristics of hydraulic actuators.

The method immediately lends itself to such obvious applications as hydraulic cylinders for actuating machine-tool mechanisms, agricultural and industrial machines and hoists, and innumerable other slow-moving applications. However, we were interested in determining whether it would have value in predicting the characteristics of a very rapidly moving hydraulic mechanism.

The application of hydraulic units in aircraft turrets is an example of a unit requiring rapid time-displacement characteristics. With military aircraft traveling at speeds in excess of 600 mph resulting in much shorter tracking time, it becomes imperative to have the turret-control response time minimized.

The method described in Professor Linderoth's paper was used to calculate the response of a typical hydraulic actuator used to position the yoke of a variable pump used as a part of an aircraft turret-control drive. A photograph of this unit is shown in Fig 9 and a schematic diagram of the actuator in Fig. 10. This is a follow valve device and we were interested in determining the time lag from the instant that the pilot valve was moved to the time that the yoke would move to any position of its travel. The source of pressure P_s is a small gear pump which also supplies the replenishing system of the hydraulic transmission. The constants indicated on the circuit diagram were used in evaluating the theoretical response of the actuator. The calculated velocity-acceleration curve is shown in Fig. 11 and the time-displacement curve in Fig. 12.

To check the validity of the theoretical response, oscillograms were taken of the actual actuator movement as a result of a step-function input to the valve controlling the actuator. This was accomplished by coupling a variable-capacitance pickup to the actuator. This capacitance formed one element of a tuned cir-

[3] Massachusetts Institute of Technology, Cambridge, Mass. Jun. ASME.

[4] Vickers, Inc., Detroit, Mich.

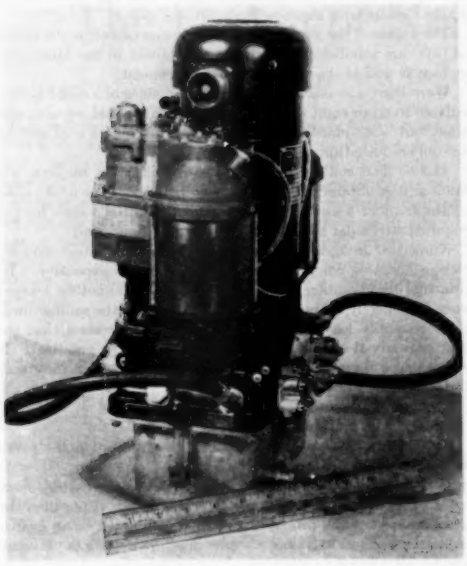

FIG. 9 TYPICAL HYDRAULIC ACTUATOR

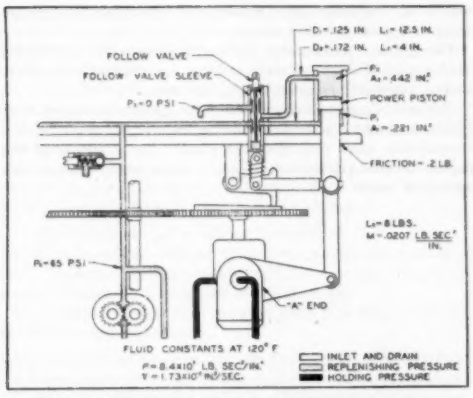

FIG. 10 SCHEMATIC DIAGRAM OF HYDRAULIC ACTUATOR

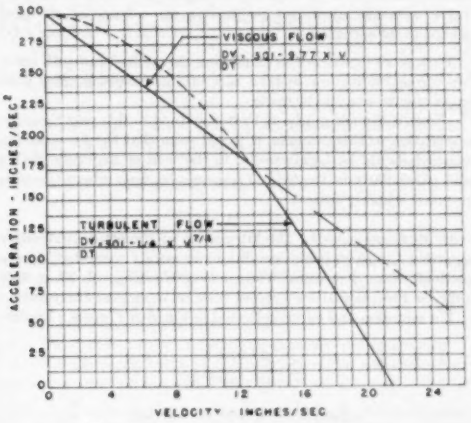

FIG. 11 VELOCITY-ACCELERATION CURVE

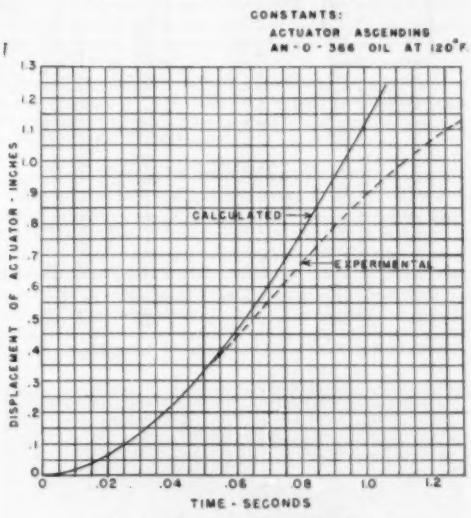

FIG. 12 TIME-DISPLACEMENT CURVE

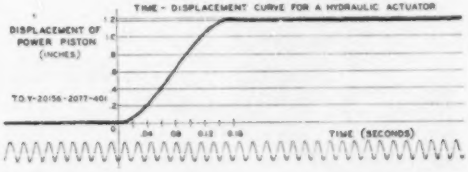

FIG. 13 RECORDED OSCILLOGRAPH OF OUTPUT VOLTAGE

cuit inductively coupled to a fixed frequency oscillator. The linear portion of the resonance curve of voltage output versus capacitance was utilized to yield an output voltage proportional to actual displacement. This voltage after being rectified and amplified was fed into a recording oscillograph to obtain a permanent record as shown in Fig. 13.

The two curves indicating the calculated and actual response are shown in Fig. 12. It will be noted that the two curves coincide during the first portion of the actual movement and then the experimental curve falls below the calculated curve. This diversion condition is probably due to the following factors:

1 The circuit components are such that the pressure from the source does not remain constant with changing actuator movement.

2 Near the end of the stroke, the follow valve, which moves in

such a manner so as to wipe out the signal impressed on the pilot valve, becomes significant in limiting the volume of oil being ported to the actuator.

With more experience in employing the method and with suitable correction factors to take care of the foregoing, very good approximations could be made.

From a limited study of Professor Linderoth's paper and its application to this example, it would seem that the formulas developed should be highly useful in the field of hydraulic design and particularly in the field of servomechanisms where the time response is highly critical.

H. R. GRUMMANN.[5] The integration of Professor Linderoth's equation for given initial conditions is readily made by Milne's method. (See *American Mathematical Monthly*, vol. 33, p. 455, 1926, or Professor Milne's recent book on numerical analysis.)

The equation and curve indicated in Fig. 6 of Professor Linderoth's paper define a particular solution which was calculated at Parks College with the results shown in Table 1:

TABLE 1

$$\ddot{s} = 10 - 0.10\,(\dot{s})^{7/4}$$

	s	$\dot{s}$	$\ddot{s}$	$(\dot{s})^{7/4}$
0.0	0.00000	0.0000	10.000	0.0
0.1	0.04987	0.9954	9.901	0.9920
0.2	0.1986	1.976	9.671	3.2935
0.3	0.4441	2.927	9.347	6.54
0.4	0.7828	3.843	8.945	10.548
0.5	1.2112	4.714	8.492	15.081
0.6	1.725	5.539	8.000	20.005
0.7	2.317	6.313	7.486	25.143
0.8	2.986	7.036	6.960	30.404
0.9	3.723	7.706	6.437	35.633
1.0	4.525	8.324	5.921	40.790
1.1	5.386	8.889	5.454	45.745
1.2	6.301	9.413	4.942	50.585
1.3	7.267	9.880	4.493	55.067
1.4	8.276	10.31	4.078	59.220
1.5	9.327	10.70	3.675	63.250
1.6	10.42	11.05	3.303	66.971
1.7	11.60	11.36	2.971	70.293
1.8	12.69	11.64	2.663	73.375
1.9	13.92	11.89	2.381	76.188
2.0	15.06	12.12	2.125	78.750
2.1	16.33	12.32	1.898	81.011
2.2	17.53	12.50	1.691	83.098
2.3	18.83	12.66	1.515	84.851
2.4	20.10	12.80	1.335	86.655
2.5	21.39	12.93	1.184	88.165
2.6	22.69	13.04	1.052	89.482
2.7	24.00	13.14	0.9314	90.686
2.8	25.32	13.22	0.8345	91.655
2.9	26.64	13.31	0.7250	92.750
3.0	27.98	13.37	0.6518	93.482

[5] Parks College, Saint Louis University, St. Louis, Mo.

Were there any occasion to do so, the values of s could be calculated to six or eight significant figures; this would require more time, but a standard-brand multiplying machine would still be the only required apparatus.

The method could also be used to calculate the response s if laminar flow obtained for the first few instants. The final values of the laminar s and $\dot{s}$ would become the initial values for the required particular solution of the Linderoth equation.

Numerical integration is more accurate than integration by electrical analog computer and is also much less expensive. Its principal disadvantage appears to be that it cannot be learned very well merely by reading a book; perusal of the sailing directions generally leaves the reader with the impression that the matter is trivial or that it is too complicated to be practical. It seems that a characteristic of numerical methods is that they have to be practiced to be appreciated.

AUTHOR'S CLOSURE

The author appreciates very much the interest in his paper shown by Messrs. Shearer, Dietiker, and Grummann. It is no doubt true that the electronic computers can do a better job of integrating equations of the type occurring in this paper than the graphic one but the probability of such equipment being available to the engineer at a time when he most needs it is as yet small and he must resort to other means for his solution. A long-range research project could be effectively scheduled for solution on an electronic computer but a short project for a particular design would not be able to wait any protracted period and the engineer must then resort to other means.

The author is particularly indebted to Vickers, Inc., for trying out his method on one of their projects, and the excellent discussion of this work presented by Mr. Dietiker.

The use of a numerical method of integration as suggested by Professor Grummann is quite valid but looks as if it might involve considerably more time than the graphic one described in the paper. It does yield a high accuracy and in some instances this may be of value.

The Design of Nonlinear Leaf Springs

By S. P. CLURMAN,[1] GREAT NECK, LONG ISLAND, N. Y.

It is occasionally desirable to incorporate into a mechanism a spring having a particular nonlinear force-deflection relationship. This need may arise in the design of computers, certain control mechanisms, and special shock-absorbing systems. A technique is developed whereby leaf springs may be designed to follow arbitrary functions having increasing first derivatives. Some experimental results are discussed. A device is described which will produce a spring characteristic having a decreasing first derivative.

Introduction

In 1678 Robert Hooke announced his now well-known observation that the distortion of an elastic body is proportional to the external forces acting on it. This is not an exact relationship, but it is a close approximation, the accuracy depending upon the elastic material involved and its geometrical attributes. The use of this approximate law has greatly facilitated the development of the entire subject of strength of materials and the theory of structures.

Most mathematical analyses of structural problems are based upon "small deflections," i.e., a deflection which does not change the geometrical configuration which in turn controls the distribution of stresses to the material. In common problems, such as those of beams and coil springs, the linear theory yields good results if the deflections involved are not excessive. In other elastic systems an appreciable change in the geometrical configuration begins immediately, and the analysis must account for the nonlinearity. A most notable example of this latter case is the Belleville disk spring. Although the degree of nonlinearity in these cases may become quite marked as a result of arbitrarily chosen parameters, the type of nonlinearity cannot be chosen freely.

Occasionally there arise problems in which it is desirable to vary the type of nonlinearity independently. These problems may be present in three fields of design as follows:

1 The general field of mechanical computers.

2 Certain specific devices which are operated by nonlinear force functions, such as, centrifugal force versus rotational speed and magnetic force versus length of air gap.

3 Special shock-absorbing systems where it is desired to have the stiffness vary with travel.

Two examples of category (2) may be quoted. A centrifugal-speed governor which has its flyweights loaded by a constant-stiffness spring will have a varying sensitivity as the governed speed range is shifted. In order to have a constant sensitivity at all speeds, a spring having an exponential function is required.

The second example is the magnetic solenoid. When the plunger is loaded by a constant-stiffness spring, it is an unstable mechanism, i.e., it is either fully in or fully out, depending upon whether the applied voltage is above or below a critical value. If it is desired that the plunger take some intermediate position and vary this position as a function of the coil voltage, a nonlinear spring is required. The exact function can be obtained empirically from the solenoid characteristics.

Object of Study

The object of this paper is to provide a design procedure for springs having an arbitrary nonlinear characteristic. Certain restrictions, however, must be made concerning the nonlinear function:

1 The function must be continuous.

2 The first derivative must be continuous and increasing.

3 The minimum value of the first derivative cannot be less than a practical initial stiffness of the leaf will allow.

Although restriction (2) requires that the basic spring element have a stiffness increasing with load, a design will be proposed later for a compound spring which exhibits a decreasing stiffness.

The theoretical derivations to be presented here are approximate ones based upon certain assumptions which become less accurate for large deflections. The solutions are intended only as close approximations which may be obtained without recourse to experimentation. They also may be used as a starting point for a cut-and-try test routine for cases where extreme accuracy is required in the finished design.

Theory of Free-Tip Cantilever

A simple nonlinear leaf spring is shown in Fig. 1. This consists of a uniform cantilever leaf mounted over a curved base. The nonlinear action occurs when, as the leaf is deflected, a certain portion comes into solid contact with the curved base, and the stiffness is increased accordingly. It is apparent that the manner in which the stiffness increases will depend upon the type of base contour under the leaf. The problem, then, is to find a particular base curve which will provide the desired variation of spring stiffness.

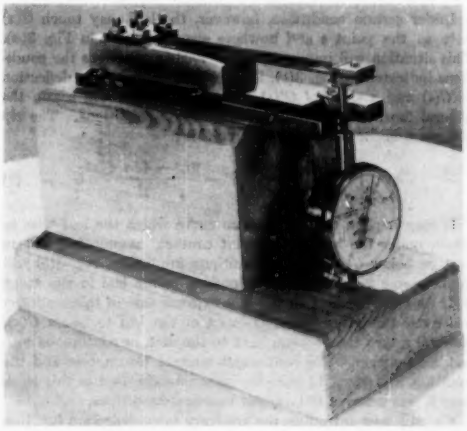

Fig. 1 Spring Designed to Follow the Function $F = 20\,\delta^2$

[1] Project Engineer, Sperry Gyroscope Company.

Contributed by the Machine Design Division and presented at the Fall Meeting, Worcester, Mass., September 19–21, 1950, of The American Society of Mechanical Engineers.

Note: Statements and opinions advanced in papers are to be understood as individual expressions of their authors and not those of the Society. Manuscript received at ASME Headquarters, June 15, 1950. Paper No. 50—F-5.

In Fig. 2(*a*) a cantilever leaf of length L and constant section stiffness EI is shown placed over a foundation whose contour is described by the function $G(x)$ and is tangent to the unloaded leaf at $x = 0$. In Fig. 2(*b*) the leaf is shown loaded by a force F and achieving a deflection h. Now, certain simplifying assumptions must be made about the nature of the contact between the leaf and the foundation curve. As shown in Fig. 2(*b*), the leaf is in continuous contact with $G(x)$ in the range

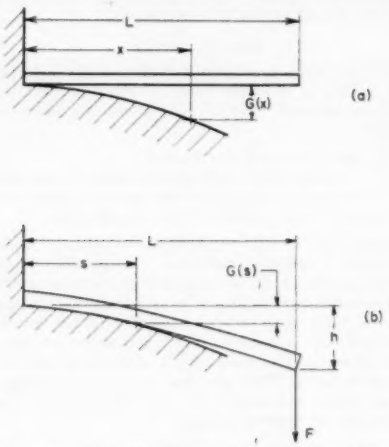

FIG. 2 ASSUMED FLEXURAL ACTION OF A SIMPLE NONLINEAR CANTILEVER LEAF

$0 < x < s$. Beyond the point s the leaf ceases further contact with $G(x)$. Under this assumption, the flexural curve of the leaf attains, of course, the ordinates and first and second derivatives of $G(x)$, and the application of flexture theory produces the relation.

$$h = \frac{1}{3}(L-s)^2G'' + (L-s)G' + G \quad \ldots\ldots [1]$$

Under certain conditions, however, the leaf may touch $G(x)$ only at the point s and nowhere else, as shown in Fig. 3(*a*). This situation will impose upon the flexure equations the conditions indicated in Fig. 3(*b*), i.e., the leaf must have a deflection of $G(s)$ and a slope of $G'(s)$ at position s, and will attain the natural flexure curve resulting from these conditions. The tip deflection under the action of force F is now

$$h = \frac{(4L-s)(L-s)}{3s}G' - \frac{2L^2-4Ls+s^2}{s^2}G \quad \ldots\ldots [2]$$

It may happen that the flexure curve which the leaf tries to attain under the second, or point contact, assumption will in part lie below $G(x)$. The conditions implied in Fig. 3(*b*) will then become invalid and some portion of the leaf in the range $0 < x < s$ must lie along $G(x)$. The extreme case of this tendency will cause the entire range $0 < x < s$ of the leaf to lie on $G(x)$, and will return the problem back to the first, or continuous contact, assumption. The continuous contact assumption and the resulting Equation [1] were the ones actually used in this work since it was believed to be closer to actual conditions.

We will now introduce the arbitrary force-deflection function

$$F = \theta[\delta] \quad \ldots\ldots [3]$$

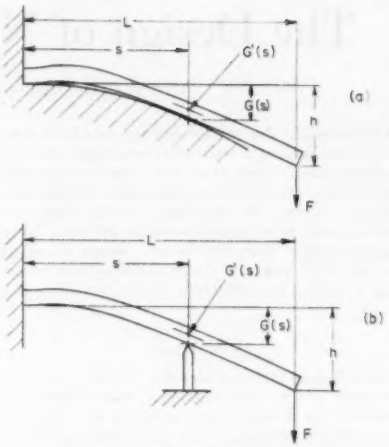

FIG. 3 ALTERNATIVE ASSUMPTION OF FLEXURAL ACTION OF NONLINEAR CANTILEVER LEAF

where

δ = deflection of ideal spring

$\theta[\delta]$ = desired functional relationship between F and δ

$$\frac{dF}{d\delta} = \theta'[\delta] \quad \ldots\ldots [4]$$

Equation [4] is now rearranged so as to describe δ explicitly.

$$\delta = \psi\left[\frac{dF}{d\delta}\right] \quad \ldots\ldots [5]$$

For a cantilever leaf of constant cross section the stiffness K is inversely proportional to the cube of its length. The least stiffness of our spring K_0, occurs when the full length of the leaf is effective

$$K(s) = \frac{L^3}{(L-s)^3}K_0 \quad \ldots\ldots [6a]$$

where

$$K_0 = \frac{3EI}{L^3}$$

For the sake of completeness, the stiffness function $K(s)$ for the point contact condition in Fig. 3(*b*) is given

$$K(s) = \frac{4L^3}{(4L-s)(L-s)^2}K_0 \quad \ldots\ldots [6b]$$

$$\frac{dF}{d\delta} = K(s) \quad \ldots\ldots [7]$$

and

$$\delta = \psi[K(s)] \quad \ldots\ldots [8]$$

or

$$\delta = \psi\left[\frac{L^3}{(L-s)^3}K_0\right] \quad \ldots\ldots [9]$$

Since the minimum stiffness of our spring is K_0, it cannot be-

have according to the function (3) below the values of (δ_0, F_0), defined by

$$\left.\begin{aligned} \theta'[\delta_0] &= K_0 \\ F_0 &= \theta[\delta_0] \end{aligned}\right\} \quad \ldots\ldots\ldots\ldots\ldots\ldots [10]$$

It is evident that under forces less than F_0 the leaf will leave contact with $G(x)$, except at $x = 0$, and will behave as a linear cantilever of stiffness K_0. A curve of the function $\theta[\delta]$ is shown in Fig. 4. A discontinuity in the second derivative of the actual spring characteristic will exist at F_0, below which the curve follows the straight line, shown dotted. From Fig. 4 we see that

$$h = \delta - \delta_0 + h_0 \ldots\ldots\ldots\ldots\ldots\ldots [11]$$

where

$$h_0 = \frac{F_0}{K_0}$$

Using Equation [9] we obtain

$$h = \psi\left[\frac{L^3}{(L-s)^3}K_0\right] - (\delta_0 - h_0) \ldots\ldots\ldots [12]$$

Finally, combining Equations [1] and [12]

$$\frac{1}{3}(L-s)G'' + (L-s)G' + G = \psi\left[\frac{L^3}{(L-s)^3}K_0\right] - (\delta_0 - h_0) \ldots [13]$$

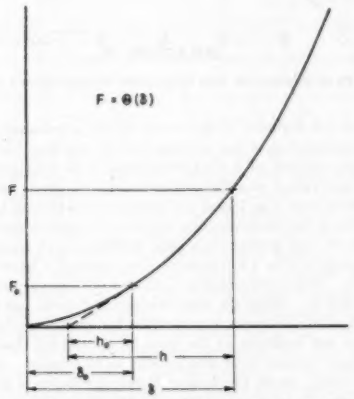

FIG. 4 FORCE-DEFLECTION RELATIONSHIP OF A SIMPLE NONLINEAR LEAF SPRING

The solution of Equation [13] will yield a spring design that will follow many types of functions. However, the three restrictions described previously must be placed on the function in Equation [3].

The requirement for a minumum force, F_0, below which the spring does not behave according to Equation [3] may be obviated by means of the device in Fig. 5. A second leaf is mounted as a simple cantilever so that the two leaves preload each other by the force F_0. This will cause the lower leaf to have an initial deflection h_0 with no external load. The characteristics of the two component leaves are shown in Fig. 6. It will be seen that the stiffness of the nonlinear component must now be less than that in Equation [7], if the combined stiffness is the one to be used.

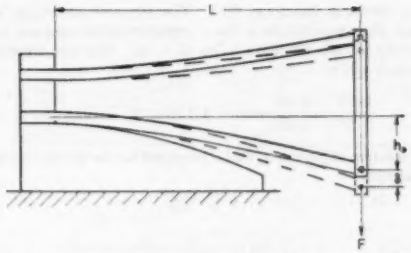

FIG. 5 A COMPOUND SPRING IN WHICH THE NONLINEARITY BEGINS IMMEDIATELY AFTER ZERO DEFLECTION

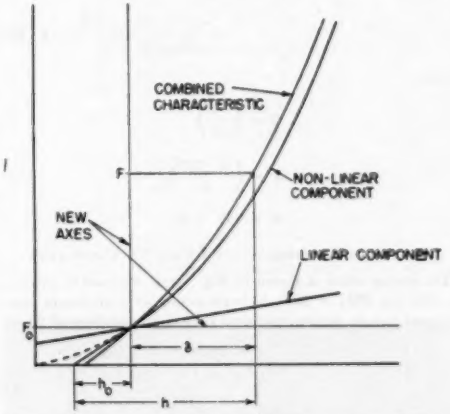

FIG. 6 FORCE-DEFLECTION RELATIONSHIP OF THE COMPOUND SPRING IN FIG. 5

Let us call the stiffness of the linear leaf k. Then its contribution to the resultant spring function will be

$$F_k = k\delta \ldots\ldots\ldots\ldots\ldots\ldots [14]$$

Therefore the base curve must be designed for the function

$$F = \theta[\delta] - k\delta \ldots\ldots\ldots\ldots\ldots\ldots [15]$$

and

$$K = \theta'[\delta] - k \ldots\ldots\ldots\ldots\ldots\ldots [16]$$

$$\delta = \psi[K + k] \ldots\ldots\ldots\ldots\ldots\ldots [17]$$

$$\delta = \psi\left[\frac{L^3}{(L-s)^3}K_0 + k\right] \ldots\ldots\ldots [18]$$

From Fig. 6 it is seen that

$$h = \delta + h_0 \ldots\ldots\ldots\ldots\ldots\ldots [19]$$

The differential equation for $G(x)$ is now

$$\frac{1}{3}(L-s)^2G'' + (L-s)G' + G = \psi\left[\frac{L^3}{(L-s)^3}K_0 + k\right] + h_0 \ldots [20]$$

The solution of Equation [13] may be obtained exactly for

many common functions $\theta[\delta]$. The simplest technique is to reduce Equation [13] to a linear equation with constant coefficients by the substitution $z = \log (L - s)$. The new differential equation will be

$$\frac{1}{3}\frac{d^2G}{dZ^2} - \frac{4}{3}\frac{dG}{dZ} + G = \psi[L^3K_0e^{-3z}] - (\delta_0 - h_0) \ldots [21]$$

A solution of Equation [13] is provided for the general category of functions

$$F = A\delta^n \ldots [22]$$

as

$$G = \left[\frac{(n-1)}{2n}Q^{\frac{1}{n-1}} - \frac{1}{2}\epsilon\right]X^3 - \left[\frac{3(n-1)}{2(n+2)}Q^{\frac{1}{n+1}} - \frac{3}{2}\epsilon\right]X + \frac{(n-1)^2}{n(n+2)}QX^{\frac{-3}{n-1}} - \epsilon \ldots [23]$$

where

$$Q = \left(\frac{K_0}{nA}\right)$$

$$X = \left(\frac{L - s}{L}\right)$$

$$\epsilon = (\delta_0 - h_0)$$

Design and Performance of a Free-Tip Cantilever

The spring which is shown in Fig. 1 was designed to produce the function $\theta[\delta] = 20\delta^2$, to begin acting at a minimum force, F_0, equal to 1 lb, and to extend up to a maximum force of 20 lb.

$$\left.\begin{aligned} F &= 20\,\delta^2 \\ K &= 40\,\delta \\ \psi(K) &= \frac{1}{40}K \end{aligned}\right\} \ldots [24]$$

The deflection at which the action becomes nonlinear, δ_0, is

$$\delta_0 = \sqrt{\frac{1}{20}} = 0.224 \text{ in.}$$

$$K_0 = 40 \times 0.224 = 8.96 \text{ lb per in.}$$

The leaf was 5 in. long, made of 0.050-in-thick spring steel, and had an (EI) value of 373 lb-in.[2] The solution of Equation [3] for these parameters is

$$G = 0.0168\,(5 - s) + \frac{3.5}{(5 - s)^2} - 0.112 \ldots [25]$$

Analysis of Results. The measured characteristic of the model built to this design is shown in Fig. 7. Drawn on the same figure is the ideal curve which is of course the parabola described in Equation [24]. The actual curve deviates from the ideal curve somewhat. To evaluate the possible error due to the leaf-contact action being other than fully continuous, a third curve was drawn. This represents calculated values of h and F for a leaf having the point contact action of Fig. 3(*b*), and the same base contour $G(x)$, obtained from the continuous-contact solution. It will be seen that this curve is virtually coincident with the ideal curve at lower values of deflection and has very little deviation at the higher values. A leaf having an error due only to some intermediate type of contact would have its characteristic curve lie somewhere between these two theoretical curves.

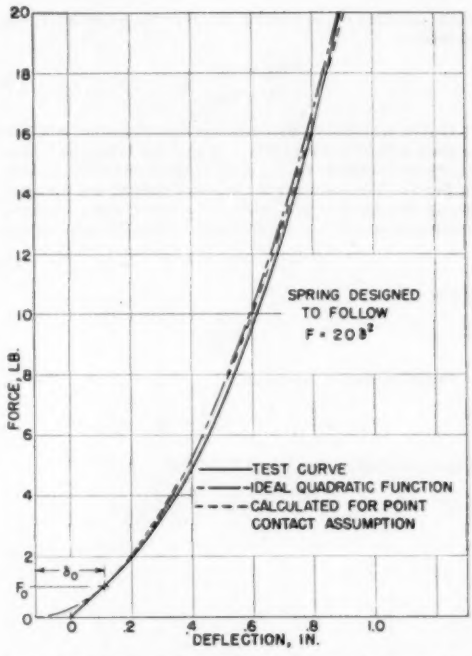

Fig. 7 Test Results of the Quadratic Spring Shown in Fig. 1

Some of the deviation of the actual curve is attributed to errors in the reproduction of the contour $G(x)$ in the base block. An important criterion of a nonlinear spring is to have certain instantaneous values of stiffness associated with given forces. It will be seen from Fig. 7 that the actual curve exhibits less than ideal stiffness for corresponding forces in the approximate range of 1 to 5 lb, and greater than ideal stiffness above about 14 lb. In the range of 0 to 5 lb the theoretical value of s varies from 0 to 1.27 in. The corresponding ordinates of $G(x)$ vary from 0 to about 0.002 in. Since the base contour had been handworked into a block of aluminum, and facilities for very accurate inspection were not available at the time, it is believed that a relatively large contour error was present in this range. In the 5 to 14 lb range, where the force-stiffness correlation is good, the theoretical value of s varied from about 1.27 to 1.95 in. In this range the ordinates increased from about 0.002 to 0.063 in., and the contour accuracy of the base block is believed to have been quite good.

The greater than ideal stiffness above 14 lb is attributed to the approximate nature of Equation [1]. This relation is based upon simple flexure theory, which neglects the first derivative of the flexure curve, an accurate assumption for small deflections. Barten[2] and Wahl[3] give the true deflection of a simple cantilever leaf as a function of the tip slope calculated by linear theory. An estimate of the error due to neglect of the first derivative may be made by comparing the leaf to a simple cantilever having the

[2] "On the Deflection of a Cantilever Beam," by H. J. Barten, *Quarterly of Applied Mathematics*, vol. 2, 1944, pp. 168–171.

[3] "Mechanical Springs," by A. M. Wahl. Penton Publishing Corporation, Cleveland, Ohio, 1944.

same tip slope. At the maximum load of 20 lb, the calculated slope of the leaf tip is 0.35. The error in the deflection of a simple cantilever calculated by linear theory is about 5 per cent for this tip slope and adequately explains the greater stiffness of the upper part of the curve.

Compound Spring With Decreasing Stiffness

Among the three restrictions on the function given in Equation [3] was the requirement that the stiffness increase with load. This is necessary for the basic leaf-spring design. However, a compound spring is shown in Fig. 8 which can be made to produce a stiffness that decreases with load. This spring is similar to the one in Fig. 5, the difference being that the nonlinear leaf is now placed above the linear leaf and is preloaded to a greater degree than that in Fig. 5. The application of an external force F will decrease the deflection of the nonlinear leaf and increase the deflection of the linear leaf. The resultant stiffness of this device K_R will be the sum of the instantaneous stiffness K of the nonlinear leaf and the constant stiffness k of the linear leaf. Since K will decrease as the nonlinear leaf is unloaded by an external force, it is obvious that K_R will also decrease with F.

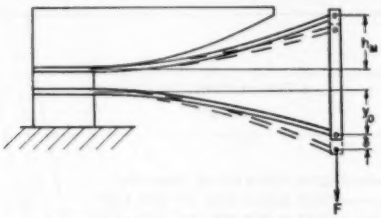

Fig. 8 A Compound Spring in Which the Stiffness Decreases With an Increasing Force

A preliminary problem is now presented: We must find an increasing stiffness function $f(h)$, which, when unloaded in the manner just described, will produce the desired function $\theta[\delta]$. In Fig. 9(*a*) are shown the characteristic curves of the two component leaves with the preload force f_M indicated on each. When an external force F on the compound spring causes a deflection δ, the new point on the linear characteristic will be δ units to the right of y_0, and that on the nonlinear characteristic will be δ units to the left of h_M. In Fig. 9(*b*), the linear characteristic is superimposed upon the nonlinear curve and intersects it at f_M. The curve of the resultant force is shown as obtained by a graphical summation of the two effects. The deflection δ is now a variable moving positively to the left of the equilibrium point h_M, and the force F will move positively below f_M. We may now choose two new axes to represent these variables and replot them with the new axes turned upright. This is done in Fig. 9(*c*), and the resultant characteristic curve is seen to have a decreasing slope, our original objective. The following functional relations hold, and, when substituted into Equation [13], will produce the required $G(x)$

$$h = h_M - \delta \quad [26]$$

$$\theta[\delta] = f_M - f[h] + k\delta \quad [27]$$

and the functions to be imposed on the component nonlinear leaf design are

$$f[h] = (f_M + kh_M) - kh - \theta[h_M - h] \quad [28]$$

$$K = \theta'[h_M - h] - k \quad [29]$$

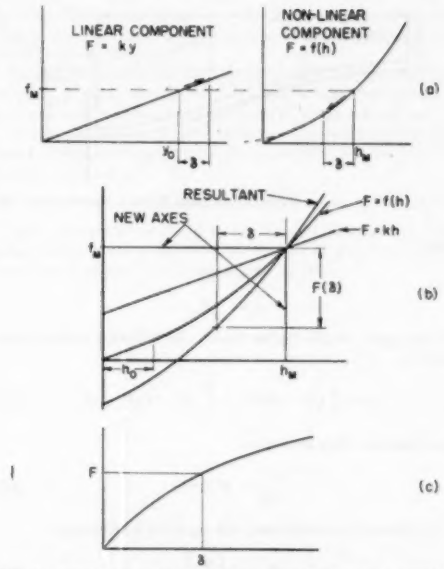

Fig. 9 Explanation of the Decreasing Stiffness of the Compound Spring in Fig. 8

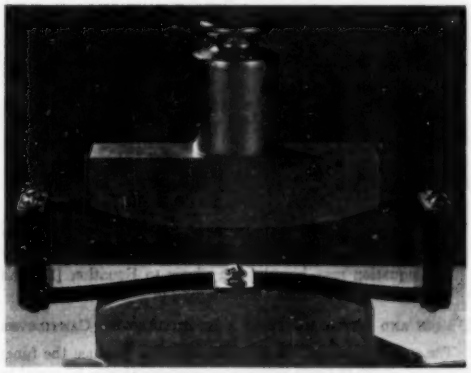

Fig. 10 Spring Designed to Follow the Function $F = e^{\delta\delta}$

Theory of Restrained-Tip Cantilever

In Fig. 10 there is shown a second type of configuration for a nonlinear leaf spring. This spring is analyzed as though it consisted of four equal cantilevers mounted over four identical base contours. A single such cantilever is shown in Fig. 11. In order to produce the over-all characteristic given by Equation [3], each of the four leaves must then carry one half of the applied load and move through one half of the required deflection. The individual leaf must then reproduce the function

$$f = \frac{1}{2}\theta[2\beta] \quad [30]$$

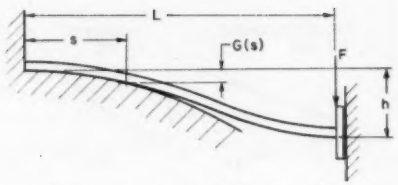

FIG. 11 A NONLINEAR CANTILEVER LEAF WITH A RESTRAINED TIP

where

$$f = {}^1/_2F$$

$$\beta = {}^1/_2\delta$$

Using, again, simple flexure theory, the following relation may be shown

$$h = \frac{1}{6}(L-s)^3G'' + \frac{2}{3}(L-s)G' + G \quad \ldots\ldots [31]$$

From Equation [30] we obtain

$$\frac{df}{d\beta} = \theta'[2\beta] \quad \ldots\ldots [32]$$

As in the previous solutions, this equation is rearranged

$$\beta = \psi\left[\frac{df}{d\beta}\right] \quad \ldots\ldots [33]$$

$$\frac{df}{d\beta} = K \quad \ldots\ldots [34]$$

$$K = \frac{L^3}{(L-s)^3}K_0 \quad \ldots\ldots [35]$$

$$K_0 = \frac{12EI}{L^3} \quad \ldots\ldots [36]$$

$$\frac{1}{6}(L-s)^3G'' + \frac{2}{3}(L-s)G' + G = \psi\left[\frac{L^3}{(L-s)^3}K_0\right] - \left(\frac{\delta_0}{2} - h_0\right) \quad \ldots [37]$$

This equation may be solved similarly to Equation [13] and will yield the base contour for the spring in Fig. 10.

DESIGN AND PERFORMANCE OF A RESTRAINED-TIP CANTILEVER

The spring shown in Fig. 10 was designed to produce the function $\theta[\delta] = e^{3\delta}$, to begin acting at a minimum force, F_0, equal to 1 lb, and to extend up to a maximum force of 20 lb

$$F = e^{3\delta} \quad \ldots\ldots [38]$$

$$\left.\begin{aligned} f &= \frac{1}{2}e^{6\beta} \\ K &= 3e^{6\beta} \\ \psi[K] &= \frac{1}{6}\log_e\frac{K}{3} \end{aligned}\right\} \quad \ldots\ldots [39]$$

The ideal action has a force of F_0 acting at zero deflection

$$\delta_0 = 0$$

$$K_0 = 3 \times 1 = 3 \text{ lb per in.}$$

Each of the four leaves was 3 in. long, made of 0.015-in-thick spring steel, and had an (EI) value of 6.75 lb-in.^{2} The solution of Equation [37] when these parameters are utilized is

$$G = \frac{1}{36}(3-s)^3 - \frac{1}{2}\log_e(3-s) + 0.2993 \quad \ldots\ldots [40]$$

Analysis of Results. In Fig. 12 there are drawn two test curves, as well as the ideal curve. The test curve for the 0.80-in-wide leaf was made first. This spring was too stiff at all points, including those within the linear range of 0–1 lb. The 0.80-in. leaf was the one with the calculated value of (EI) equal to 6.75 lb-in.^{2} The use of (EI) as a measure of section rigidity in flexure problems is based upon the assumption of a state of

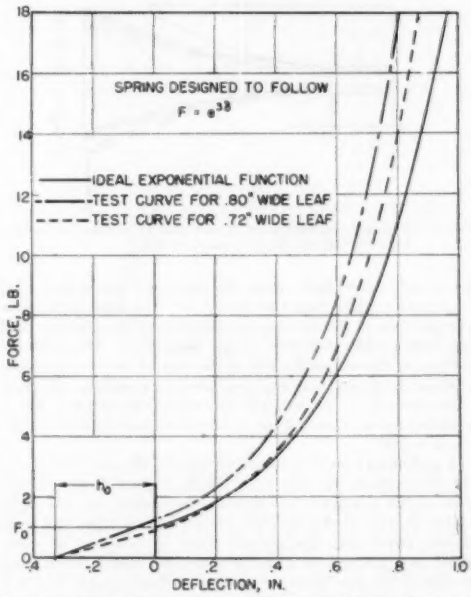

FIG. 12 TEST RESULTS OF THE EXPONENTIAL SPRING SHOWN IN FIG. 10

two-dimensional stress in the member. When the width of a flexural member becomes sufficiently wide compared to its depth, a state of three-dimensional stress will exist, and, in the limiting case of an infinitely wide member, will approach a state of two-dimensional strain. In this latter case the effective rigidity of the section is about 10 per cent greater than that implied by the value of (EI). With this in mind, the leaf width was reduced to 0.72 in. The test curve of this second leaf shows that the section rigidity is now somewhat low. For an accurate determination of suitable leaf width a cut-and-try process is indicated. Both test curves show a marked increase in stiffness above that of the ideal curve at higher loads.

In the case of this second model, the base contours were machined sufficiently accurately so as to exonerate them of any blame for the discrepancy. The excessive increase in stiffness is attributed entirely to the use of simple flexure theory. The maximum slope of the flexure curve for this leaf is greater than that for the previous case. The actual deflection of a comparable linear leaf is nearly 7 per cent less than calculations by

simple theory show. No accurate analysis has been made of the error in the nonlinear leaf design caused by neglect of the first derivative of the flexure curve.

Conclusion

The equations developed in this paper are presented as approximate ones. The closeness of solutions obtained by them to the results required will vary, depending upon the particular functions and parameters involved. In many cases the design obtained directly from the theoretical calculations will be satisfactory. In other cases where the required accuracy is too high, the theoretical solution will serve admirably as the first approximation in a cut-and-try experimentation. The theoretical solution is a convenient first approximation since its error will always be in the direction of being too stiff. By shaving down the contour of the base block, the test results can be brought very close to the ideal characteristic.

The finished design will have the advantages for manufacturing purposes, in most cases, of requiring only a close dimensional inspection, rather than a point-by-point checking calibration.

It is hoped that in the development of apparatus where nonlinear springs may improve the design outlook, this work will be of some practical aid.

Acknowledgment

Acknowledgment is made to the Stevens Institute of Technology where much of this work was originally done as a requirement for a master of science degree in 1945.

On the Design of Rotor-Coil Support Rings

By J. J. RYAN,[1] MINNEAPOLIS, MINN.

The construction of large-capacity turbogenerators has placed greater importance upon the evenness of the distribution of the field coils under the rotor-coil support rings. This paper discusses the increase in stresses in the ring due to uneven distribution of the coils, describes a photoelastic investigation for the purpose of checking the theoretical analysis, and suggests that uniform distribution of the coils would reduce the stresses in the rotor-coil support ring.

Introduction

IT has been observed that on excessive overspeed of turbogenerators, the rotor-coil support rings become elliptical in shape, with the greatest permanent elongation at the middle of the ring. This elliptical distortion indicates that failure of turbogenerator rotor-coil support rings is caused by bending moments as a result of the partially distributed coil loading.

In the ordinary design of the coils for the rotors of two-pole turbogenerators, Fig. 1, the circumferential spacing of the coils in the slots is greater than the axial spacing of the coil ends. Therefore the centrifugal forces of the coils applied to the rotor-coil support ring are distributed approximately as shown in Fig. 2.

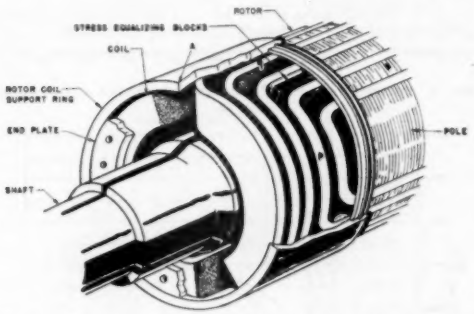

FIG. 1 TURBOGENERATOR ROTOR-COIL SUPPORT RING AND COILS

At the inner end of the ring the maximum distributed loading is between the poles, while at the outer end the maximum distributed loading is in line with the poles. Thus if the rotor-coil support ring were not supported at each end by an internal disk, it would assume an elliptical shape with major axes at right angles to each other at the ends. These distortions of the rotor-coil support ring are also shown in Fig. 2.

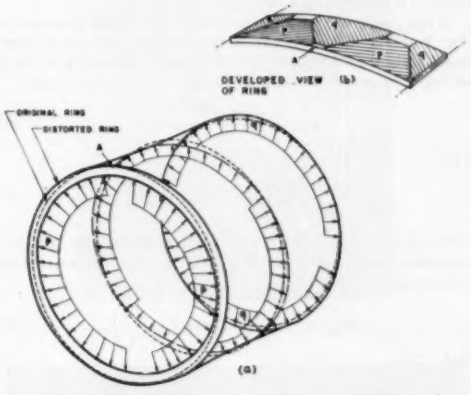

FIG. 2 DISTORTIONS OF ROTOR-COIL SUPPORT RING

The problem has been approached with a two-dimensional analysis for simplicity, although it is three-dimensional in character, for which the solution of the stresses[2] would be rather long and complicated. The theoretical investigation was checked by photoelastic tests. This analysis suggests that as great a degree of even distribution of loading as possible should be maintained for the safe design of turbogenerator rotor-coil support rings. For this purpose, it may be advisable to add additional material between the rotor coils to obtain the completely uniformly distributed loading.

Theoretical Investigation

When a ring is submitted to the action of uniformly distributed internal pressure all around the inner surface, the stresses and deformations at any point of the ring are easily calculated. If it is a thin ring, the hoop tension in the ring is

$$S_t = \frac{w\,(b + a)}{2t\,(b - a)} \qquad [1]$$

and the increase in mean diameter is

$$\Delta = \frac{w\,(b + a)^2}{2Et\,(b - a)} \qquad [2]$$

where w is the load per unit length of the center line of the ring, t the width of the ring, a the inner radius, b the outer radius, and r any arbitrary radius. If it is a thick ring, the thick-cylinder formulas may be applied. The radial and tangential stresses are found from the equations

$$S_r = \frac{a^2 w_i}{t(b^2 - a^2)}\left(1 - \frac{b^2}{r^2}\right) \qquad [3]$$

and

$$S_t = \frac{a^2 w_i}{t\,(b^2 - a^2)}\left(1 + \frac{b^2}{r^2}\right) \qquad [4]$$

---

[1] Associate Professor of Mechanical Engineering, University of Minnesota. Mem. ASME.

Contributed by the Machine Design Division and presented at the Fall Meeting, Worcester, Mass., September 19–21, 1950, of THE AMERICAN SOCIETY OF MECHANICAL ENGINEERS.

NOTE: Statements and opinions advanced in papers are to be understood as individual expressions of their authors and not those of the Society. Manuscript received at ASME Headquarters, June 2, 1950. Paper No. 50—F-6.

[2] "Theory of Plates and Shells," by S. Timoshenko, McGraw-Hill Book Company, Inc., New York, N. Y., 1940, p. 433.

where w_1 is the load per unit length of the inner surface of the ring. The increase in mean diameter is given by the equation

$$\Delta = \frac{1-m}{Et}\,\frac{a^3 w_1}{(b-a)} + \frac{1+m}{Et}\,\frac{4a^3b^3w_1}{(b-a)(b+a)^2} \quad [5]$$

where m is Poisson's ratio.

If the pressure is partially uniformly distributed, as shown in Fig. 3 or Fig. 4, the stresses in the ring are statically indeterminate and the Castigliano theorem is used. Referring to Fig. 3 or Fig. 4, the tensile forces at the cross sections mn and op are

$$P_{mn} = \frac{w(a+b)}{2t}\sin B \quad [6]$$

and

$$P_{op} = \frac{w(a+b)}{2t}(1-\cos B) \quad [7]$$

where B (shown as θ) is $^1/_2$ the angle subtending the partially uniformly distributed load. The moments at the cross sections mn and op are

$$M_{mn} = \frac{w(a+b)^2}{4t}\left(\sin B - \frac{2B}{\pi}\right) \quad [8]$$

and

$$M_{op} = \frac{w(a+b)^2}{4t}\left(1-\cos B - \frac{2B}{\pi}\right) \quad [9]$$

respectively.

The moments at any section of the ring for $\theta \leq B$ and $\theta \geq B$ are

$$M_1 = \frac{w(a+b)^2}{4t}\left[1 - \frac{2B}{\pi} + \sin B \sin\theta - \cos(B-\theta)\right] \quad [10]$$

and

$$M_2 = \frac{w(a+b)^2}{4t}\left(\sin B \sin\theta - \frac{2B}{\pi}\right) \quad [11]$$

respectively. It can be seen that as the angle B varies, the maximum moment occurs at either the cross section mn or the cross section op. Considering the ring as a curved beam subjected to bending and tension, the stresses in the ring can be calculated from the foregoing equations.

It is interesting to note that the maximum stress in a ring, which is subjected to a certain partially uniformly distributed load, is much larger than that in the ring which is subjected to a uniformly distributed load of the same intensity all around the inner edge.

When a ring is subjected to a partially uniformly distributed load, as shown in Fig. 3 or Fig. 4, the ring will deform into a shape somewhat like an ellipse. Assuming the thickness is small in comparison with the radius so that the effect of tensile and shearing forces may be neglected (considering moments only), the decrease in the diameter along the cross sections mn was found to be

$$\Delta_{mn} = \frac{3w(a+b)^4}{2Et(b-a)^3}\left[\frac{2B}{\pi} + \frac{B}{2}\cos B - \sin B\right] \quad [12]$$

and the increase in the diameter along the section op to be

$$\Delta_{op} = \frac{3w(a+b)^4}{2Et(b-a)^3}\left[\left(\frac{\pi}{4} - \frac{B}{2}\right)\sin B - \cos B + 1 - \frac{2B}{\pi}\right] \quad [13]$$

by the Castigliano theorem. This increase or decrease in diameter is also many times larger than that of a ring which is submitted

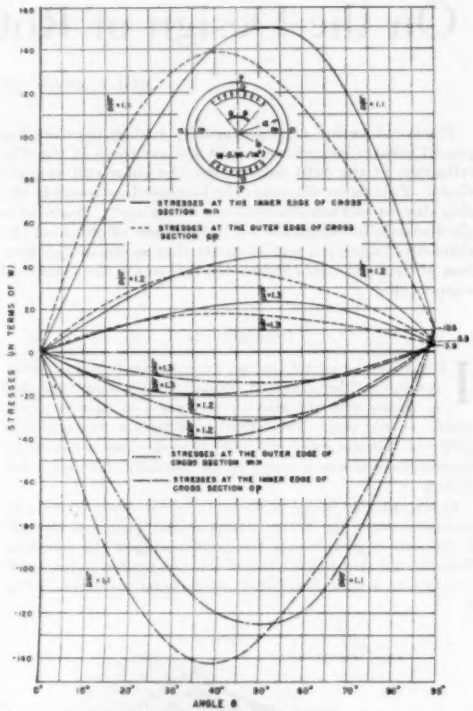

FIG. 3 STRESS CHART FOR PARTIALLY DISTRIBUTED LOADING ON RINGS

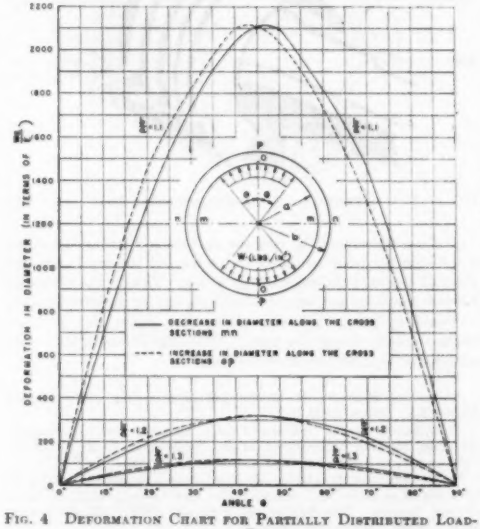

FIG. 4 DEFORMATION CHART FOR PARTIALLY DISTRIBUTED LOADING ON RINGS

to the action of a uniformly distributed load all around the inner surface.

The stresses at the inner and outer surfaces of the cross sections mn and op for $b/a = 1.1$, 1.2, and 1.3, and for $0 \leq B < \pi/2$ were calculated by use of Equations [6], [7], [8], and [9], and plotted in Fig. 3; for $B = \pi/2$ Equation [1] was used. It is seen that the maximum stress for $b/a = 1.1$ and $B = 50$ deg is 14.3 times the maximum stress of the same ring when it is subjected to the uniformly distributed load of the same intensity. The decrease in diameter along the cross section mn, and the increase in diameter along the cross section op for $b/a = 1.1$, 1.2, and 1.3, and for $0 \leq B < \pi/2$ were calculated by use of Equations [12] and [13], respectively, and plotted in Fig. 4; for $B = \pi/2$ Equation [2] was used. It is important to note that the increase in diameter for $b/a = 1.1$ and $B = 30$ deg is almost 100 times the increase in diameter of the same ring when it is subjected to the uniformly distributed load of the same intensity all around the inner surface. Also it can be seen that as the thickness of the ring increases, both the stresses and deformations decrease very rapidly.

If a rotor-coil support ring is considered to be a series of narrow rings, each ring would be a rotating ring subjected to a completely uniformly distributed load and a partially uniformly distributed load. The partially uniformly distributed load would set up large stresses and deformations in the ring, as mentioned before. Since the ends of the ring usually are supported, and the loading conditions are most serious at the middle of the ring, the middle of the rotor-coil support ring is subjected to the maximum stress and deformation.

Photoelastic Investigation

To confirm the formulas developed in the foregoing, a photoelastic model was tested. The model, a bakelite ring, shown in Fig. 5, was loaded by the centrifugal force of a number of clips and small pins in a hub which rotated at a speed of 1800 rpm.

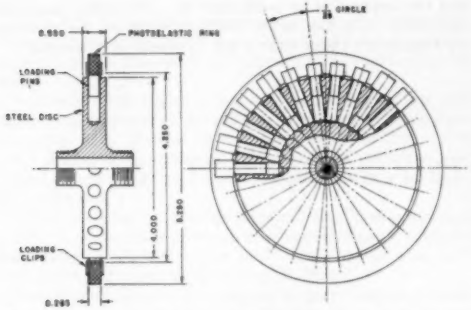

Fig. 5 Centrifugal Loading Method Used on Photoelastic Model

This centrifugal force sets up a loading on the inner surface of the model which resembles the loading that the centrifugal forces of the coils apply to a narrow portion of the rotor-coil support ring. The usual frozen-stress technique was used to freeze the resultant stresses in the model. A view of the photoelastic model after test is shown in Fig. 6. A view of the isochromatic stress pattern is shown in Fig. 7. The model fringe value was found to be 1[illegible] psi in tension at annealing temperature by use of a calibration bar. The curve of differences in principal stresses, $(S_t - S_r)$, obtained by photoelasticity along the cross section mn, where the stresses are largest, is shown in Fig. 8.

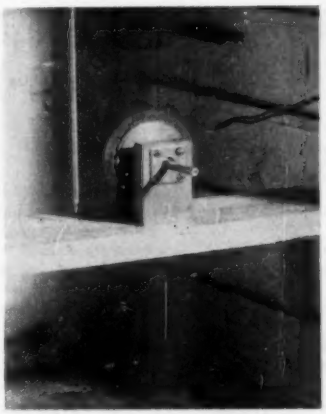

Fig. 6 Photoelastic Model After Test

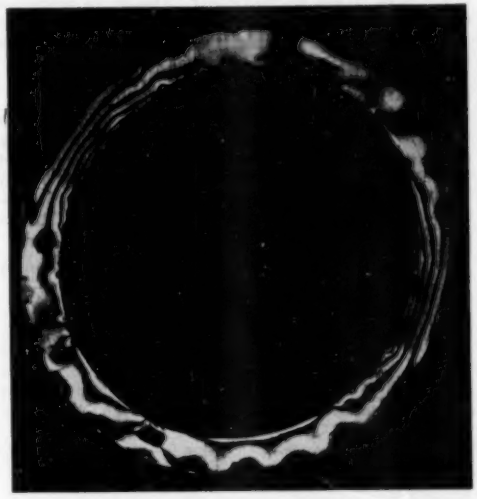

Fig. 7 Photoelastic Stresses in a Ring

The values of $(S_t - S_r)$ along mn were also calculated. The large load p was found to be 1.122 lb per in. of the inner surface, the small load q to be 0.806 lb per in. of the inner surface, and the angle B to be 62.3 deg. The common rotating-disk formulas

$$S_r = \frac{\gamma v^2}{g} \frac{3+m}{8} \left(1 + \frac{a^2}{b^2} - \frac{r^2}{b^2} - \frac{a^2}{r^2}\right) \ldots\ldots [14]$$

and

$$S_t = \frac{\gamma v^2}{g} \frac{3+m}{8} \left(1 + \frac{a^2}{b^2} - \frac{1+3m}{3+m} \frac{r^2}{b^2} + \frac{a^2}{r^2}\right) \ldots [15]$$

where m is Poisson's ratio, γ the density of the ring, and v the circumferential velocity were used to calculate the stresses due to rotation. Equations [3] and [4] were used to calculate the

stresses due to uniformly distributed load of 0.806 lb per in. of the inner surface. The following formulas,[3] with log,

$$S_r = -\frac{4M}{N}\left(\frac{a^2b^2}{r^2}\log\frac{b}{a} + b^2\log\frac{r}{b} + a^2\log\frac{a}{r}\right) \quad [16]$$

and

$$S_t = \frac{P}{(b-a)} - \frac{4M}{N}\left(-\frac{a^2b^2}{r^2}\log\frac{b}{a} + b^2\log\frac{r}{b} + a^2\log\frac{a}{r} + b^2 - a^2\right) \quad [17]$$

where

$$N = (b^2 - a^2)^2 - 4a^2b^2\left(\log\frac{b}{a}\right)^2$$

were used to calculate the stresses due to partially uniformly distributed load of

$$\frac{2.125\,(1.122 - 0.806)}{2.375} = 0.283 \text{ lb per in.}$$

of the center line of the ring where P and M were found by use of Equations [6] and [8], respectively. Finally, the summation of the differences of the principal stresses, $(S_t - S_r)$, obtained by calculation was plotted in Fig. 8. It can be seen that the curve by calculation checks quite well with that by photoelasticity.

Conclusions

From the considerations outlined, it is suggested that to obtain the lowest possible stresses in the rotor-coil support ring, evenness of the coil distribution is necessary. This could be accomplished by increasing the length of the support ring an adequate amount to allow the axial spacing of the end turns to equal the circumferential spacing of the slots. However, this solution is impractical because of the increase in length of the rotor.

[3] "Theory of Elasticity," by S. Timoshenko, McGraw-Hill Book Company, Inc., New York, N. Y., 1934, p. 58.

It may be necessary to add additional stress-equalizing blocks of an insulating nature, such as transite, between the coils in the axial direction parallel to the slots, as shown in Fig. 1. The weight of the material required per unit area to obtain evenness

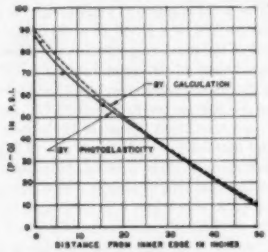

Fig. 8 Difference of Principal Stresses by Photoelastic Test and Calculation

of loading can be estimated and the size of the equalizing blocks determined.

In case it is impossible to balance the loading on the rotor-coil support ring, an increase in the thickness of the ring is an effective means to reduce the stresses and deformations.

Acknowledgment

The author wishes to express his gratitude to Dr. S. H. Mortensen, Chief Electrical Engineer, Allis-Chalmers Manufacturing Company, Milwaukee, Wis., for suggesting the subject, to Prof. W. H. Easton, Oklahoma A & M College, Stillwater, for aid in conducting the photoelastic tests, and to Mr. Chang-Kaing Tsai for his modifications of the manuscript. The experimental work was made possible by grants-in-aid from the Graduate School, and the preparation for publication by a Fellowship presented by General Mills, Inc., to the Graduate School and the Mechanical Engineering Department of the University of Minnesota.

Development and Testing of Brakes for High-Speed Railroad Equipment

By C. E. TACK,[1] CHICAGO, ILL.

The advent of the high-speed, lightweight train made it necessary to practically double braking capacity. Laboratory and road-test methods and facilities developed to meet these demands are described and discussed. Factors of brake performance are discussed with typical examples of test results which have been used as a guide to brake design.

Introduction

THE author's company has been designing, producing, and developing foundation brake gear for railroad equipment for more than one third of a century. That period has witnessed a continued search for improved brakes, and, coupled with that search, has been the acquisition of facilities to permit adequate testing and development.

In the early 1930's several of the largest railroads of the country started a program to purchase and operate streamlined trains capable of scheduled speeds up to 100 mph, which could average 60 mph and more, over distances varying from 1000 to 2400 miles. Immediately it was recognized that further and more intensive brake development was in order. Increasing the speed of a train from 70 mph to 100 mph doubles the kinetic energy which must be dissipated by the brake. In the interest of lightweight, four-wheel trucks became standard on new passenger cars, reducing the number of wheels per car from 12 to 8; thus wheel loads increased, further increasing the demand on the individual brake.

Steps were taken by the company to acquire an inertia-type brake-testing machine which would have the increased capacity necessary to test high-speed passenger-car and Diesel-locomotive brakes.

Both safety and economy demand that the utmost care and engineering judgment in brake design be coupled with adequate laboratory tests, followed by road tests, before offering a new brake design to the railroads. New ideas and untried experimental designs should not be service-tested in trains which operate at 100 mph.

Design work was initiated on improved clasp brakes and several forms of off-the-tread brakes such as drum brakes, multiple-disk brakes, a single-disk-type brake which we call the ASF rotor brake, and combinations of some of these.

Trained test engineers were assigned to observe and record with proper instruments the operating conditions encountered on several large railroads in the East and in the West. The information thus obtained was used as a guide in determining laboratory and road-test procedure. It was also used to enable the designer to determine other requirements.

Studies were made to determine the effect of weather—particularly icing conditions—on brake performance. Also studied were railroad-maintenance techniques which were found to vary widely. Operating techniques were found to differ greatly from one territory to another.

It further became apparent that the railroad-brake problem must be studied as a whole. The air-brake control apparatus, the foundation brake gear, and the friction shoe must be tested in such a manner that the proper relationship of these three is maintained. Since no laboratory facilities existed for the simultaneous testing of the completely integrated brake mechanism, the author's company's brake-testing machine was designed to enable such tests to be made.

It is equipped with very complete instrumentation to measure torque, stop distance, stop time, and forces in the brake mechanism, as well as the performance of the air-brake control apparatus. It can test all designs of railroad friction brakes—clasp brakes, disk brakes, drum brakes, and combinations of the various forms of brakes which might be used on railroad equipment.

Test Machine Developed

From Fig. 1 it will be seen that the machine consists of a rotating inertia system in which the flywheel is made up of nine demountable sections. Power is supplied by the motor system at the far end of the machine. The present 75-hp motor, which is temporary, is capable of developing speeds up to 107 mph on a 36-in. wheel. It will be replaced this year by a special 350-hp motor capable of speeds in excess of 150 mph on a 36-in. wheel at all wheel loads up to a maximum capacity of the machine, which is 40,290 lb equivalent wheel load. High-speed brake testing involves very sizable amounts of energy. The rotating system of the test machine, when adjusted to the maximum wheel load of 40,290 lb, at the maximum speed of 150 mph on a 36-in. wheel, represents a total kinetic energy of 34,700,000 ft-lb. By means of the different combinations which can be made with the nine different segments in the flywheel, it is possible to obtain 96 different inertia values in the rotating system so that practically any equivalent

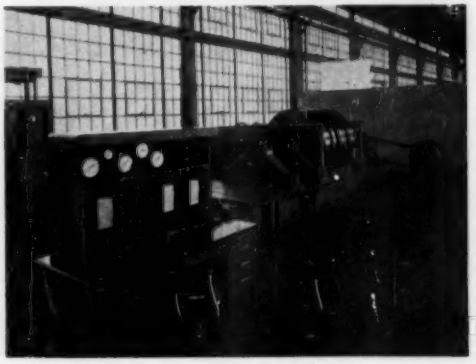

Fig. 1 General View of Test Machine

---

[1] Assistant Chief Mechanical Engineer, American Steel Foundries. Mem. ASME.

Contributed by the Rail-oad Division and presented at the Semi-Annual Meeting, St. Louis, Mo., June 19–23, 1950, of The American Society of Mechanical Engineers.

Note: Statements and opinions advanced in paper are to be understood as individual expressions of their authors and not those of the Society. Manuscript received at ASME Headquarters, March 31, 1950. Paper No. 50—S-20.

wheel load can be simulated. Test data are gathered on the indicating and recording instruments housed in the control desk in the foreground.

Fig. 2 shows a typical arrangement for test of clasp brakes. The brake mechanism to be tested is applied at the end of the machine nearest the observer, the usual setup being to mount a standard car wheel directly on the end of the rotating shaft, so that the whole of the actual brake rigging as used in service can be mounted in a suitable position for operation and observation.

The large platform at the forward end provides a base on which various types of brake mechanisms may be mounted so that they operate with the rotating wheel. This enables the entire brake mechanism to be tested as a unit and the leverage system and operating cylinders can be incorporated as they are used in actual service.

In the case of a disk brake, the car wheel is replaced by the brake disk. Fig. 3 shows how a disk-brake mechanism is mounted to be tested. The whole assembly of leverage system, cylinders, and supports is mounted so that the torque developed is applied to the hydraulic torque cell in the foreground, by which brake torque is measured and recorded. The adjustable flywheels are shown at the left.

Fig. 4 shows a disk brake being tested after freezing to temperature below —80 F. This is one of the standard test procedures followed by the company in laboratory brake tests.

Fig. 5 is a view of the control desk and instrument panel. So far as is possible, the instrumentation is arranged so that the recording of data is automatic. Recording instruments are housed in this control desk from which the operator is able to control the driving motor and the application and release of the brake. Instrument drives between control panel and machine are electrical, making use of selsyn motors and direct-current generators. The torque developed by the brake is transferred to the control panel hydraulically.

Speed, time, distance in feet and tenths, torque and brake-cylinder air pressures are all indicated on the dials at the top of the panel. Four special Esterline-Angus recording instruments make a continuous record of speed, brake-cylinder pressure, and torque. An arrangement is incorporated so that time and wheel revolutions (distance) can be marked simultaneously on the margins of all charts. The chart drives are arranged so that the length of the charts can be proportional either to time or to distance run.

In order to be able to simulate as nearly as possible actual clasp-brake performance in service, the machine is equipped with the conventional speed-governor control so that brake-

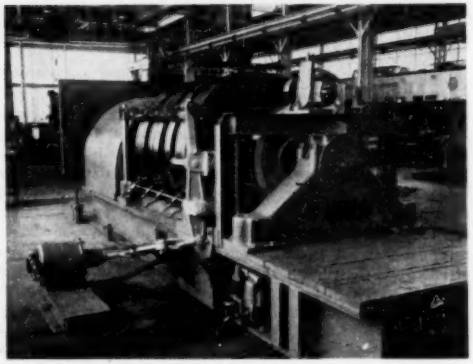

FIG. 2 CLOSE-UP OF CLASP-BRAKE SETUP

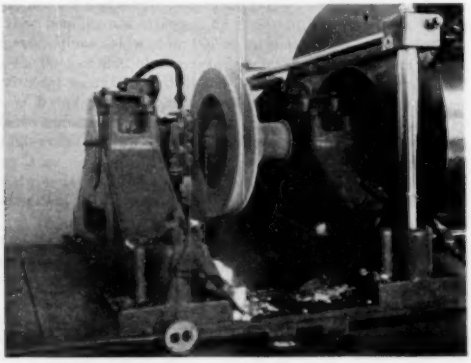

FIG. 4 DISK BRAKE BEING COLD-TESTED

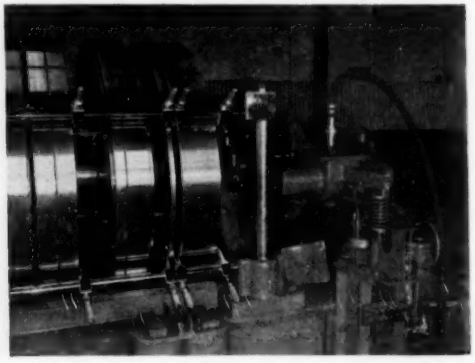

FIG. 3 CLOSE-UP OF DISK-BRAKE SETUP

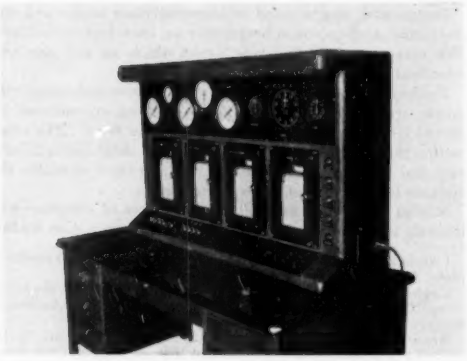

FIG. 5 INSTRUMENT PANEL—TEST MACHINE

cylinder pressures during the test can be made to follow those which are obtained in service.

While this test equipment can reproduce in the laboratory many of the factors entering into brake performance, it is obvious that laboratory tests do not reproduce several variables of great importance. These must be studied by means of road tests. For example, the highly important factor of rail adhesion is missing in the laboratory since the wheel does not roll on a rail.

A great deal of thought and effort has been expended on the problem of finding a satisfactory method of studying adhesion in the laboratory. Several years ago the company sponsored a comprehensive program in conjunction with the Armour Research Foundation, in which an attempt was made to determine the nature and values of adhesion and to design test equipment which would reproduce wheel and rail conditions accurately in the laboratory. However, results were meager. To our knowledge, no satisfactory solution to the problem of duplicating service adhesion conditions in the laboratory has yet been found.

The conditioning effect of the combination of rail and shoe on the braking surface of the wheel is also absent. Likewise, vibration, rain, ice, and snow, and other conditions present in service cannot be reproduced successfully in the laboratory.

Car Equipped for Road Testing

It was necessary, therefore, to obtain service and road experience which would enable evaluation of laboratory testing in terms of actual road performance. Accordingly, a car was acquired by the author's company and equipped with full instrumentation of the same type as incorporated in the brake-testing machine.

Fig. 6 presents an exterior view of this test car ASFX-1948. The test car was built from a standard 75-ft steel combination passenger-baggage coach on which the underframe was modified by the Pullman-Standard Car Manufacturing Company so that it would accommodate 4 and 6-wheel passenger-car trucks of all types. Weight of the car ready to run is approximately 136,000 lb. Load blocks are available to increase the running weight to 170,000 lb.

Fig. 7 shows a view of the interior of the car which was completely rebuilt to accommodate full recording instrumentation for automatic recording of necessary data. The floor of the car was fitted with large windows over the trucks at both ends to enable observation of the action of truck and brake apparatus.

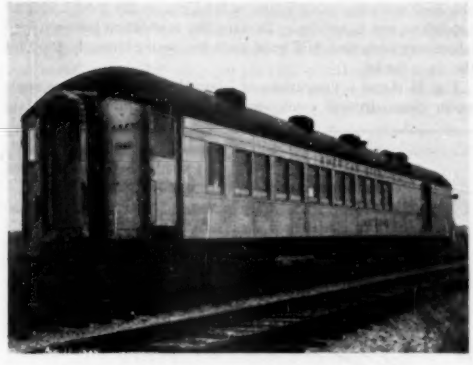

Fig. 6 Exterior of Test Car

The air-brake controls are arranged to permit the brake to be operated independently of locomotive or train. Thus the car can be used in a train to check over-all train-braking requirements, or it may be used for breakaway tests to check brake designs for performance.

Fig. 7 Interior of Test Car

Fig. 8 Instrument Panel in Test Car

Fig. 8, the front view of the instrument panel, shows the similarity to the instrumentation of the brake-testing machine.

Complete brake controls are installed along with the instrumentation so that brakes may be manipulated at will, giving the operator full information as to the brake performance and ability to manipulate the brake mechanism in any way that is desirable.

The equipment of the car also contains a complete installation of air-brake control apparatus mounted as shown in Fig. 9, on a rack located in the baggage compartment. This includes speed-governor control and automatic directional sanding ap-

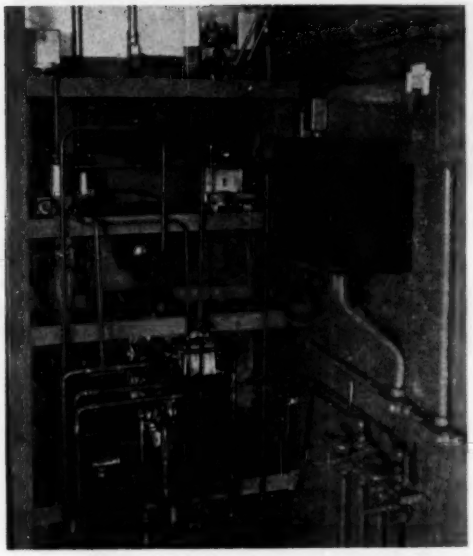

FIG. 9 AIR-BRAKE CONTROL APPARATUS IN TEST CAR

FIG. 10 EXTERIOR OF TEST TRAIN

paratus. Special manual controls are part of the installation to permit using these devices or cutting them out at will.

Water equipment to enable wetting of the rails is also built into the car.

The car is so equipped that it may be uncoupled by the crew without initiating a brake application until desired. Fig. 10 shows the exterior of the test train.

The car may be operated in a regular train or as the last unit of a special train, as shown here. It was used in this manner for breakaway tests on the Chicago, Milwaukee, St. Paul, and Pacific Railway during the summer and fall of 1949.

BREAKAWAY STOPS

In making breakaway stops with such a car, it is hauled at the rear end of a special train, pulled by a high-speed locomotive with arrangements so that the car can be uncoupled from the train while moving over a selected piece of track which is preferably straight and level. The train is brought up to a speed slightly above that at which the test is to be made and the car is uncoupled from the train so that it is rolling free, and as near as possible to the desired speed, when it reaches a selected point from which all tests are started. As the car crosses this point, the brakes are applied through the control valves in normal manner, giving proper brake-cylinder-pressure build-up time, and the distance measured across which the car rolls in coming to a stop.

When instrumentation such as is incorporated in this car is used, the test is not open to the criticism that has been directed at other methods of brake testing. When brake performance is demonstrated by actually reproducing service conditions, the evidence is conclusive.

Tests may be made over graded track as well as level, although certain stretches of track on several railroads have by long use come to be more or less standard test tracks so that results of various tests may be more accurately compared.

It is possible with our test car to wet the rail artificially to reduce adhesion and also to apply sand to restore adhesion so that these highly important factors can be studied. In applying sand during testing, it is important that sand be applied in the same manner that is used in actual railroad operation. This is usually done by initiating the application of sand automatically by means of the wheel slip-control equipment or application of the emergency brake. If sand is applied manually before and during the brake test, it is obvious that an altogether different value may be obtained, which could not be fairly compared to normal railroad operation.

So many problems of brake design lend themselves to study by the combination of laboratory and road testing that the amount of useful work scheduled by the company is limited only by the amount of time at hand.

COMPARISON OF LABORATORY AND ROAD TESTS

It is desirable to know what relation a stopping distance obtained in the laboratory may bear to the stopping distance obtained with the same brake under a car on the road under all conditions met in service. To date, the correlation between ASF laboratory tests and ASF road tests has been extremely good for the clasp brake.

Fig. 11 shows a comparison of laboratory and road stops made under clean dry-rail conditions with a disk brake designed to

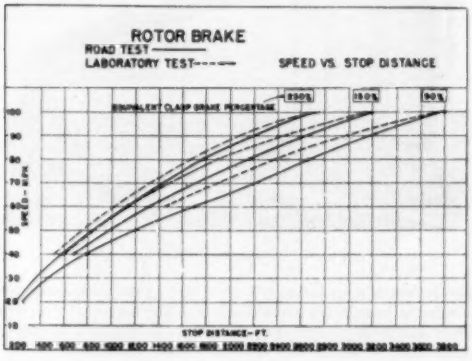

FIG. 11 COMPARISON ROAD AND LABORATORY ROTOR-BRAKE STOPS

match, as closely as possible, the performance of a clasp brake at 250 per cent braking effort with speed-governor control, using $18^1/_2$-in. carbon insert shoes.

Here, also, the results in the laboratory and the results on road tests are very well matched. It appears well established that the laboratory technique will give excellent indication of stop distances under service conditions when rail conditions are such that the effects of adhesion need not be considered.

Stopping Distance at High-Speed

Another problem examined was that of studying the practical limits to which stopping distance could be reduced at high speed and under good operating conditions as indicated by actual road tests.

Accordingly, using a disk brake, stop tests were made at several speeds with the brake-cylinder pressure adjusted to 20, 40, 60, 80, and 100 psi as the test proceeded. As shown in Fig. 12, at 80 psi brake-cylinder pressure, the brake produced stops from 100 mph in 2750 ft. Pressure was then increased to 100 psi brake-cylinder pressure, which, in the laboratory where wheel-rail adhesion is not a factor, would have resulted in a stopping distance well under 2500 ft.

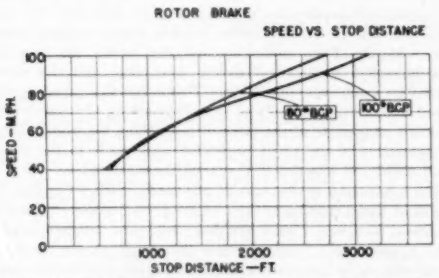

Fig. 12 Rotor-Brake Stops at Brake Cylinder Pressures 80 and 100 Psi

However, on the road test the increased pressure resulted in a torque too high to be sustained by the available effective adhesion on a good dry rail, with the result that the wheel-slip control equipment was called upon to prevent wheel sliding, and the stopping distance at high speed became longer than at 80 psi brake-cylinder pressure. This points out the fact that, even under the best rail conditions, the brake must not produce more torque than available wheel-rail adhesion can handle without the development of wheel sliding.

However, railroads operate under conditions of less than perfect rail adhesion for a large portion of the time, and it is vitally necessary to know the performance of a brake when rail adhesion is substantially less than normal. Galton's tests, made in England years ago, pointed out this fact, and later Metzken reached the same conclusion from a series of tests made in Germany. Our experience with the ASF test car also confirms this fact, as will be seen in the discussion of the test results.

Determining Adhesion Values

There are two general methods of road testing to determine adhesion values. One is to equip a car in a train with independent brake control so that the brakes may be applied while the train is moving at a constant speed over rail that is dry or wet, frosty or dirty, and observe the amount of brake pressure required to produce a break in the rail adhesion or a wheel slip.

We consider this method to be unsatisfactory. It is impossible to control the condition of the rail and next to impossible to observe from the moving train the exact condition of the rail. Moreover, conditions of the rail, track, and grade vary constantly. While speed may be determined accurately, a given test can never be repeated exactly in order to check results. It is possible, as will be shown later, that in passing over a rail joint the wheel slip can originate during a momentary reduction in wheel load; a computation of rail adhesion based on such a wheel slip would be in error. Further, the car tested is subject to varying influences from other cars in the train. Altogether, there are so many uncontrolled variables that the results obtained under such circumstances must be so recognized in study and comparisons.

An alternate of the same method is to evaluate adhesion by calculation, using the time required after release of brakes to restore a sliding wheel to rolling and using the inertia of the wheel as a measure of the forces applied. This method determines the coefficient of sliding friction, provided the exact instantaneous wheel load is known.

The method involves several assumptions which are distinctly open to question, such as the assumption that the relation between adhesion and slip velocity is the same during acceleration as it is during deceleration. Or, more dangerous still, the assumption that a change from sliding to rolling is equivalent to a change from rolling to sliding. The marked difference between the coefficient of friction in sliding and rolling has been axiomatic ever since the famous Galton tests. It would be surprising indeed if measurement of the work done by sliding as a skidding wheel resumes rotation were to give accurate indication of the force required to break the lock between wheel and rail when the wheel is rolling and not sliding. Moreover, a wheel accelerating from a state of slip does so without the same amount of weight transfer which accompanies braking action—therefore the wheel loads under the two conditions are not the same.

Consequently, we feel it is necessary to rely on breakaway tests as the only accurate method of determining how much braking torque can be applied without causing the wheel to slide, and what stopping distances can be expected.

We believe this method to be far superior, since it eliminates or controls a large number of variables and provides a test which can be repeated. Tests made with artificially wetted rails can be compared directly with tests in which the rail is dry instead of artificially wet while all other conditions remain the same.

Rails are artificially wetted under the test car by means of water in pressure tanks, carried inside the car, and applied from a fixed position by the spray heads. It has been found advisable to design and locate the spray heads so that the water will be applied uniformly and not blown away by wind and that the spray remains constant and uniformly applied.

Throughout the tests, both in the laboratory and on the road, a great deal of importance has been attached to the necessity of conducting tests so that they could be repeated again and again without any significant change in the results. In general, at least three stops have been made at each condition, and the rule has been not to make these three identical stops consecutively, but to scatter them between other stops made at other conditions, whenever this was possible. Service conditions are more closely simulated by this manner of conducting tests.

Factors Relating to Adhesion

Before analyzing the results of these tests, it is well to establish clearly the various factors so often grouped together as "adhesion" and which operate to limit the amount of braking possible.

Unfortunately, there are very few factors that tend to increase adhesion. Except for the application of sand to a rail,

there is almost no other practical method of increasing adhesion in common use today.

A study of adhesion is far beyond the scope of this paper. All that is intended here is to indicate some of the more obvious and important causes of reduction of ability to utilize brake capacity, and to indicate approximately their relative importance to the problem of producing a satisfactory brake for practical railroad use. Some of these factors are nearly always present and some of them are of a transitory nature. They may be divided roughly into two groups: (1) Those resulting from the introduction of some foreign matter, such as water, snow, dirt, or greasy substances, which reduce the normal adhesion between car wheel and rail. (2) Those which cause a reduction of the effective wheel load, and thereby reduce the capacity to utilize the available brake torque without sliding wheels. Some of these capacity-reducing factors can be calculated accurately, and some can be determined only by road tests. The effect of weight transfer due to inertia, unbalanced wheels, eccentric wheels, and track irregularities upon the force between the wheels and the rail has been computed, using the fundamental laws of mechanics. The details of this theoretical analysis, including the derivation of the basic formulas used for the calculations, are contained in the Appendix.

In calculating, the same set of conditions have been used as are present on the road test car. They will be found to approach closely the average for modern high-speed railroad equipment. These conditions are given in Table 1.

TABLE 1 STANDARD CONDITIONS OF TEST CAR ASFX-1948

Car weight (ready to run), lb	136,000
Wheel load (using 4-wheel trucks) lb per wheel	17,000
Center of gravity above rail, in.	72
Unsprung weight, lb per wheel	1,900
Center of gravity of unsprung weight, in.	17
Truck weight, lb each	20,000
Center of gravity of truck only above rail, in.	20
Bolster weight (approx), lb each	1,000
Center of gravity above rail, in.	18
Truck centers	53 ft-3 3/4 in.
Truck wheel base	8 ft-6 in.
Wheel diameter	36 in.

These conditions are common to all American Steel Foundries road tests. Details of the calculations referred to hereafter are contained in the Appendix.

Turning to the group (1) of causes of loss of wheel-rail adhesion, foreign matter between wheel and rail, the commonest cause of trouble is the damp and dirty rail. Here it has been possible to develop actual road-testing procedure, which has begun to give some data which can be used as a guide for the brake designer. One of the first projects undertaken with this new test car was an attempt to see whether or not the wet rail gave the same reduction in braking limits at low speeds as at high speeds, and whether tests could be reproduced.

In the development of the disk brake, it has been established that it may be designed to produce reasonably constant average friction at all speeds, whereas the natural characteristic of the clasp brake is a rising torque as the speed decreases.

Either type of brake can produce more torque than dry-rail adhesion can transmit. It is necessary to limit the braking torque so that it does not exceed the available traction. In order to get the best possible stop under wet-rail conditions, where only a fraction of normal adhesion can be relied upon, it is increasingly desirable that the torque curve of the brake should match closely the available adhesion, and so produce all the stopping effort possible without producing a dangerous wheel slide.

Fig. 13 shows some typical traces from the recording decelerometer used in tests made with the ASF test car, in which the torque of the disk brake at high speeds exceeds the available effective adhesion, with repeated release of brake-cylinder pressure and reduced retardation until the speed has fallen to the

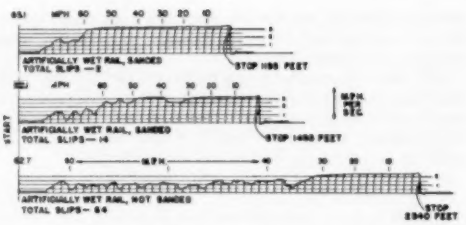

FIG. 13 TYPICAL DECELERATION CURVES

point where the effective adhesion is greater than the torque produced by the brake.

Therefore it was desirable to determine the limits to which retardation could safely be raised at various speeds when the rail was wet and whether a constant-torque brake or a brake having the increasing-torque characteristic was more desirable.

DISK-BRAKE TESTS

To this end, a series of tests were made with the disk brake, using standard break-away procedures on an artificially wet rail.

In this test the brake-cylinder pressure was controlled manually. At the first application of the brake the pressure was increased until wheel sliding developed, and the wheel controller came into operation. Thereafter the pressure was raised or lowered manually so that the braking effort was kept as nearly as possible at the point of just sliding the wheels, using the operation of the wheel controller[2] as a guide to the maximum amount of retardation that could be sustained.

The results of a typical test of this kind are shown in Fig. 14. It will be noted that higher and higher pressures are required as the speed decreases. Since the disk brake was designed to produce approximately constant average torque under changing speed, this is a clear indication that higher retardation rates are practical as the speed decreases. This is precisely what the retardation graph shows. At 50 to 60 mph, a retardation rate of $1^1/_4$ mph per sec was enough to cause wheel sliding, but at lower speeds, more than twice this rate of retardation was maintained successfully.

It is clear from repeated tests that the amount of retardation which can be sustained without wheel slip on the wet rail rises substantially as the speed decreases. Therefore the most efficient brake under wet-rail conditions is not the disk brake with constant average torque, but the clasp brake in which the rising torque curve more nearly matches the adhesion curve.

It is interesting to note that the evidence of this test is confirmed by subsequent tests in which both clasp and disk brakes were tested on artificially wet rail, using 250 per cent braking with speed governor and $18^1/_2$-in. carbon-insert shoes on the clask brake, and an equivalent braking effort on the disk brake. Fig. 15 shows this comparison.

On dry rail, both brakes made emergency stops in approximately the same distance. However, as soon as the rail is wet, the disk brake is at a very great disadvantage, since the emergency braking effort is too high at high speed and too low at low speed. The clasp brake, however, gives a considerably better stop on the wet rail (1) because the cleaning action of the brake shoe on the wheel tread results in greater available adhesion between the wheel and rail than is possible with the disk brake;

[2] The wheel control used to prevent wheel sliding during this series of tests was the W.A.B. Co. 3-AP Decelostat equipment, consisting of the P-3 Decelostat and the B-3 Decelostat valve.

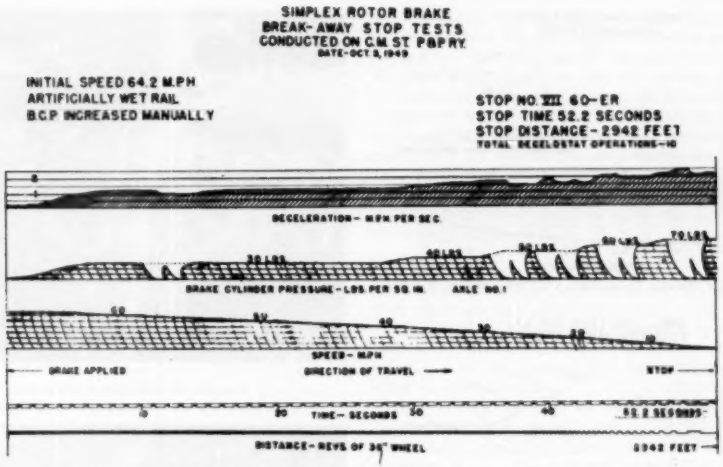

FIG. 14 DISK-BRAKE STOP WITH MANUALLY ADJUSTED BRAKE-CYLINDER PRESSURE

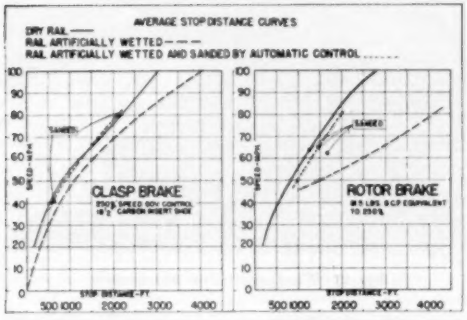

FIG. 15 WET AND DRY RAIL—CLASP VERSUS ROTOR BRAKE

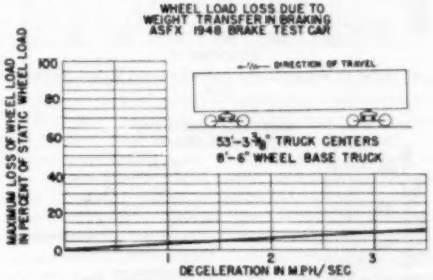

FIG. 16 LOSS OF WHEEL LOAD DUE TO WEIGHT TRANSFER

(2) the torque characteristics more nearly approach the effective torque-capacity curve existing between wheel and rail.

The second group (2) of variables, which have an effect on the ability of a brake to stop a train, are those which cause a loss of wheel load on the rail, and here it is necessary to resort to calculation to determine the range of the effects possible under several conditions known to exist in normal train operation.

Weight Transfer Due to Inertia. This loss is present whenever deceleration is present as a result of braking. It results in an increased load on the leading wheel of the truck and on the leading truck of the car, with a corresponding unloading of the trailing truck and the trailing wheels. The load on the trailing wheel on the trailing truck is, therefore, the limiting factor on the amount of braking possible in a car which must be able to run in either direction.

Fig. 16 shows the calculated loss of effective weight for the trailing wheel at various rates of deceleration. With 14 per cent adhesion, the maximum deceleration would be 3.06 mph per sec if full wheel load were present. However, due to weight transfer, the maximum obtainable deceleration is only 2.83 mph per sec (stop distance from 100 mph, 2590 ft if uniform deceleration is assumed). It is noted from the graph that an 8 per cent loss of wheel load occurs for this deceleration. While this is not a large loss, it is a loss which is always present whenever there is braking action, regardless of the type of brake or its manner of suspension. Surges resulting from slack action, it should be remembered, can produce even higher weight-transfer values, which will reduce further the values shown here which are for steady deceleration.

WHEEL-LOAD LOSSES

Unbalanced Wheels. A rotating wheel, which is out of balance dynamically, also operates to cause the load of the wheel on the rail to fluctuate, and the loss due to this cause is shown in Fig. 17. The amount of unbalance assumed is $1^1/_2$ lb at $13^1/_2$ in. from wheel center. This represents the average value found in a check of the entire complement of wheels on a typical modern high-speed train under normal operating conditions. It will be seen that at 85 mph the wheel-load loss amounts to 3 per cent.

Eccentric Wheels. Eccentric wheels are common; in fact, the perfectly concentric wheel probably does not exist.

Fig. 18 illustrates the loss in wheel load at 85 mph, when various degrees of eccentricity are encountered.

Fig. 19 shows the effect of 0.0075 in. eccentricity (0.015 in.

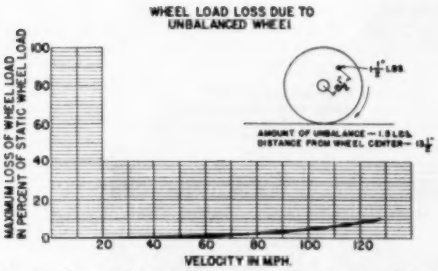

FIG. 17 LOSS OF WHEEL LOAD DUE TO UNBALANCED WHEEL

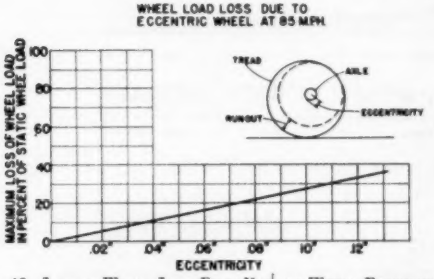

FIG. 18 LOSS OF WHEEL LOAD FROM VARIOUS WHEEL ECCENTRICITIES

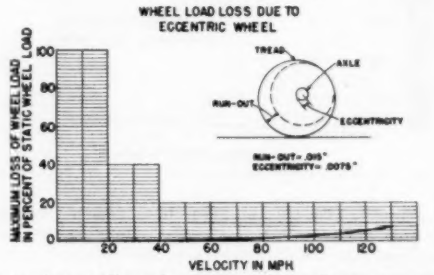

FIG. 19 LOSS OF WHEEL LOAD DUE TO WHEEL ECCENTRICITIES AT VARIOUS SPEEDS

total run-out) at various operating speeds. To obtain a better visualization of the effect on wheel loading, it might be mentioned here that eccentric wheels have been known to cause the truck equalizers to be thrown clear of the equalizer seat by a matter of $^1/_4$ to $^3/_8$ in.

Track Irregularities. This is a very common, and one of the most important, causes of loss of effective wheel load on the rail. The amount of loss resulting from a bad rail joint is seldom appreciated. In making an emergency stop from 100 mph, a pair of wheels will traverse upward of 200 rail joints, each of which is a potential cause of wheel slide.

Fig. 20 shows a rail joint on a piece of excellently maintained track, in which the mark of the sliding wheel (photographed immediately after a test stop) shows clearly the point at which the slide was initiated. Fig. 21 shows a slide which occurred just prior to the stop.

Methods of calculating the reduction of effective wheel load

FIG. 20 WHEEL SLIDE AT RAIL JOINT

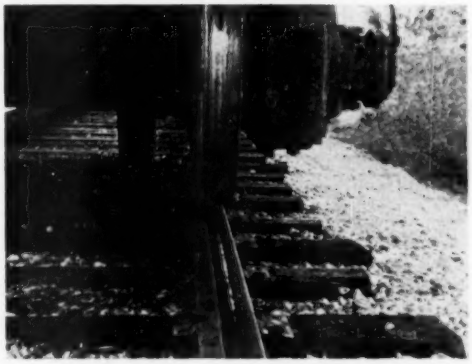

FIG. 21 WHEEL SLIDE JUST BEFORE STOP

for low spots in the rail have been developed by Timoshenko and others. Fig. 22 shows the amount of loss when the wheel passes over a rail which dips in a sine wave $^1/_2$ in. across a rail distance of 12 ft.

It will be noted how rapidly the loss reaches serious proportions as high speeds are reached, and it is possible at high speed for the wheel load to be practically zero.

It now becomes apparent that there can be a serious error in the conventional assumption that with dry-rail conditions an adhesion value of 14 per cent of the static load exists. Although it is probably true that for static conditions the 14 per cent ratio between adhesion and wheel load is correct, and even higher values may exist, the fact is that the actual dynamic wheel load is less than the assumed static load. It can be very much less.

Let us consider a case based on the normal operating conditions as they have been observed to exist. These are the conditions used in the calculations referred to previously, and it is certainly possible that they can all be present.

The conditions assumed for this example are as follows:

Speed, mph	85
Deceleration, mph per sec	$2^1/_2$
Wheel unbalance, atm, $13^1/_2$ in. from center, lb	$1^1/_2$
Eccentricity, in.	0.0075
Low spot in track	12 ft long, $^1/_2$ in. deep

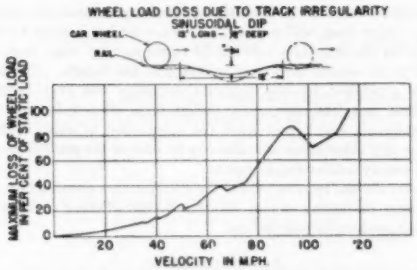

FIG. 22 LOSS OF WHEEL LOAD DUE TO TRACK IRREGULARITIES

When all of these factors occur simultaneously, the effects will add directly. The effective wheel-load loss, due to weight transfer in braking, is 7 per cent; the loss due to wheel unbalance is 3 per cent; the loss due to wheel eccentricity is 2 per cent—totaling 12 per cent—while the loss due to the track irregularity is 70 per cent. The combined effect of these factors is a wheel-load loss of 82 per cent.

These are not abnormal conditions. They are present every day in train operation. At other speeds and other combinations of conditions, the losses may differ more or less. As a matter of fact, they do vary continuously. The point is that some place and at all times, combinations of these factors are acting so that the dependable wheel load actually present and effective for use in braking is never the assumed static load. It is always less than the static load at some point in the train, and often substantially less. It is, therefore, an error to assume that the full static load is a dependable guide to the amount of braking it is possible to do without producing wheel slip.

There are still other causes of loss of effective wheel load. They are all factors which are beyond the control of those who design and those who operate railroad brakes. The only method of increasing adhesion which the brakeman has at his command—pouring sand on the rail ahead of the wheel—is a completely ineffective remedy against the forces which tend to reduce wheel load on the rail and so limit the amount of braking possible.

There remain to be examined the methods by which adhesion between the wheel and rail can be increased when foreign matter between rail and wheel reduces adhesion and limits the amount of braking it is safe to do. The most obvious solution is of course to remove the foreign matter and restore the wheel and rail to a clean condition. This, in part, is an inherent advantage of the clasp brake, since the brake shoes serve to scrub the wheel tread and, when wet, to dry it. Just how valuable this action can be is illustrated by a comparison of the stop distance on artificially wet rail with clasp brakes which scrub the wheel and disk brakes where there is no wheel cleaning. Fig. 15 shows typical stops of a clasp and a disk brake, both of the same capacity and which, on dry rail, give approximately the same performance.

Clasp-brake stops on the wet rail are only slightly longer than on the dry rail. On the disk brake, however, the stop distance begins to run out at an alarming rate as initial speed increases. At 80 mph initial speed, it is more than double the dry-rail distance, and stops were encountered in the test in which the stop distance was almost 3 times as long.

This loss of stopping ability at high speed on the wet rail with the disk brake appears to result from two causes: (1) The absence of the cleaning action on the wheel tread lowers the limit of maximum retardation. (2) The high torque characteristic of the disk brake at high speed results in wheel sliding at high speeds. The retardation curve for one of these emergency stops is shown at the bottom of Fig. 13, in which the wheel controller actually released the brake 64 times while the speed was being reduced to 30 mph. At this point the effective adhesion was great enough to handle the braking effort without further wheel sliding.

Application of sand to the wet rail, as will be seen from Fig. 15, gives a slight improvement on the clasp brake at speeds above 60 mph, where the stop may be even slightly shorter than the dry rail, due perhaps to an increase in friction on the shoe. With the disk brake, however, sanding the wet rail is imperative if wet-rail stopping distances are to be made equivalent to those of the unsanded clasp brake.

CONCLUSION

In summarizing, experience has shown that laboratory brake tests are a valuable guide, but it must be recognized that they show only laboratory conditions and are not indicative of over-all service performance. Wheel-rail adhesion and dynamic load conditions are the factors which limit the amount of braking which can be done safely.

There is much more to be learned about this all-important matter of adhesion. In studying it, we must be constantly on guard to make sure that what we determine is relative to actual conditions under an actual train, operating on actual track, and with known conditions. It appears from the road tests that the effective brake torque which can be utilized, increases as speed decreases, and follows more nearly the torque curve of the clasp brake than the flat curve of the disk brake, and that on the rail having less than ideal surface, this is a serious disadvantage for the disk type of brake.

The danger of overbraking, especially under conditions of poor adhesion, was clearly brought out in the test. Without resorting to sanding, once wheel sliding is initiated, whatever the cause, hope of a reliable short stopping distance must disappear.

Ever since the Galton tests, it has been recognized that, once started, wheel sliding tends to persist, and the stop distance is radically increased. Wheel protective devices may restore the wheel to rolling and prevent wheel damage; but, since they must do this by reducing the braking effort, the stop will, of necessity, be longer than that obtained where no wheel sliding exists. Therefore it is of prime importance that wheel sliding be avoided. There must be constant vigilance to guard against overbraking and against assuming that a given value of rail adhesion is always available or that the normal wheel load is constantly present.

Attention is called to the fact that many factors—weight transfer, wheel condition, and track irregularities—are constantly present as limits to the amount of braking it is safe to do.

To assume that a certain effective wheel load and adhesion value is constantly available is to put faith in something which has no existence in practical railroad operating conditions.

Limited to sanding as the only practical method of increasing adhesion, the main problem in brake design is to build the brake that will always be just a little below the slipping point without ever overstepping the wavering line beyond which the wheel will slide.

Present braking ratios are the result of years of experience. Long experimentation was necessary to find the practical level to which braking could be raised and still give reasonable freedom from the dangers of wheel slipping in actual day-to-day railroad service. Regardless of isolated performance and unusual laboratory results, present braking ratios are not likely to be quickly or easily changed in actual railroad operation.

There are numerous problems under investigation—a vast amount of data has been gathered and is being analyzed. As our development work continues, the results are being compared care-

fully with previous road and laboratory tests. Our search for better methods of braking and further design improvements will continue, and the results will be made available to the railroads.

As so often happens in research and development work, an investigation, which was expected to give a final and conclusive answer, succeeds also in opening up new questions which must be answered, and in uncovering new possibilities, perhaps in another related problem, which give an answer or which must be further explored.

For example, in our investigation of stopping-distance change under rapidly repeated, high-speed, high-energy stops, it was disclosed, among other things, that the wheel did not thermal check, although it was subjected to an amount of abuse in excess of that encountered in road service where thermal checks are being reported.

An investigation of the problem of stopping distance uniformity thus gave a new angle of approach to the problem of prevention of wheel damage, and made it necessary to add new investigations to those already in progress, aimed at finding the cause and cure of thermal checking. Presently a series of road tests, aimed at comparison of disk brake and clasp brake, yielded a set of wheels, submitted to highly abusive treatment, on which there is unshakable evidence of wheel punishment but no evidence of thermal checks.

The wheels shown in Fig. 23 were not a part of a project aimed directly at studying thermal checking; yet they have provided highly valuable experience in the problem of finding a cause and cure of thermal checking. It is only from the slow accumulation of evidence from many sources and from many different fields that a final and conclusive answer is to be found to this problem.

Two other factors, not strictly technical, may be touched on in conclusion. The first is safety. On no one does safety place a heavier burden than on the man responsible for the design of brakes. Brakes are the primary safety insurance. With safety, the brake designer must take no chances whatsoever. He must seek for reliability—unfailing reliability—under all weather conditions. He must aim at safe braking under the worst possible combination of circumstances the brake may be called upon to face—rain, storm, ice, snow, and rough track.

FIG. 23 TREAD OF TEST-CAR WHEELS AFTER EXCESSIVE BRAKING

Another factor which must be considered by the brake designer is that, before he can adopt a new design, it must not only be proved absolutely safe and reliable, it must not only be able to fit into the existing pattern and harmonize with the old equipment, but provision must be made for its proper handling and servicing at every point at which it may be required to operate—day or night—winter or summer.

Further, there is the problem of obsolescence and life expectance. How long will it last? Railroad brakes cannot be designed in the hope of a new model every spring; they must be built to be certain that they will outlast the bonds. No clasp brake produced by the author's company has ever become obsolete, nor has any truck design been offered for use by the railroads which prevented the application of clasp brakes. Before any other form of brake can be offered for general use, it must satisfy similar requirements.

These are the reasons behind the extreme care exercised by the company in testing design changes before offering them as a regular product for railroad use.

ACKNOWLEDGMENT

Assistance received from Mr. R. B. Cottrell, chief mechanical engineer; Mr. H. C. Keysor, mechanical engineer, and members of the staff of the Product Engineering Department of the American Steel Foundries is gratefully acknowledged.

REFERENCES

"Air Brake Tests," compiled and published by the Westinghouse Air Brake Company, Pittsburgh, Pa., 1904.

"Brake Tests," part of a report of a series of road tests of brakes on passenger equipment cars made at Absecon, N. J., by the Pennsylvania Railroad Company, 1913, No. 625.253 AOR-3P.

"Braking High-Speed Trains as an Engineering Problem," by J. C. McCune, *Mechanical Engineering*, vol. 61, August-September, 1939, pp. 583–588 and 657–660.

"Mechanical Vibrations," by J. P. Den Hartog, third edition, McGraw-Hill Book Company, Inc., New York, N. Y., 1947.

"Vibration Analysis," by Nils O. Myklestad, McGraw-Hill Book Company, Inc., New York, N. Y., 1944.

"Schwingungstechnik—Ein Handbuch für Ingenieure," by Ernst Lehr, Julius Springer, Berlin, Germany, 1930.

"Fundamentals of Vibration Study," by R. Manley, Chapman & Hall, London, England, 1942.

"Vibration of Rail and Road Vehicles," by B. S. Cain, Pitman Publishing Corporation, New York, N. Y., 1940.

"Elements of Mechanical Vibration," by C. R. Freberg and E. N. Kemler, second edition, John Wiley & Sons, Inc., New York, N. Y., 1948.

"Mechanical Vibrations—Theory and Applications," by R. K. Bernhard, Pitman Publishing Corporation, New York, N. Y., 1943.

"Vibration Problems in Engineering," by S. Timoshenko, D. Van Nostrand Company, Inc., New York, N. Y., 1928.

"Vibration and Sound," by Philip M. Morse, second edition, McGraw-Hill Book Company, Inc., New York, N. Y., 1948.

Appendix

In this section, formulas are derived for the effect of dynamic factors on braking performance, which effect it has not been possible to measure accurately in field or laboratory tests.

The factors considered here all affect braking by causing variation in the wheel-rail pressure at high speed.

They will be considered in the following order:

1 Wheel out of balance
2 Track irregularities
3 Eccentric wheel
4 Weight transfer due to brake application

1 *Wheel out of Balance.*

The pressure of an unbalanced wheel against the track will be given by the equation

$$P = W_0 + W + Q \frac{1}{1 - \left(\frac{T}{T_1}\right)^2} \cos 2\pi nt \quad \ldots\ldots [1]$$

where

W_0 = sprung weight carried by one wheel

W = unsprung weight carried by one wheel

$Q\dfrac{1}{1-\left(\dfrac{T}{T_1}\right)^2}\cos 2\pi nt$ is effect of unbalanced force. The derivation of this formula is given by S. Timoshenko and B. F. Langer.[3]

$Q = \dfrac{w}{g} r\,(2\pi n)^2$, which is the centrifugal force of the unbalanced weight.

w = unbalanced weight

r = distance from w to center of axle

n = number of revolutions per second of wheel

$\dfrac{1}{1-\left(\dfrac{T}{T_1}\right)^2}$ is the dynamic factor governed by ratio of speed of wheel to frequency of natural vibration of wheel on track.

$T_1 = 1/n$, the time for one revolution of wheel

$T = 2\pi\sqrt{\dfrac{W}{\alpha g}}$, natural period of vibration of wheel on rail, neglecting effect of comparatively soft car springs and mass of rail

α = vertical load necessary to produce a unit deflection of rail = 147,300 lb per in. for 130-lb rail on typical ballast

g = gravitational constant = 386 in./sec^2

t = time

The maximum loss of wheel-rail pressure occurs once during each revolution of the wheel, and the loss amounts to $Q\dfrac{1}{1-\left(\dfrac{T}{T_1}\right)^2}$.

2 *Track Irregularities.*

The dynamic effect of a low spot of a rail is computed from the basic equations of dynamics. The low spot is assumed to be located on a long rail which is supported on a flexible foundation (roadbed).

The solution of the problem of a vertical load on an infinitely long beam (rail) on a flexible foundation is well known. The theory is presented by S. Timoshenko.[4] The differential equation for the deflection curve is

$$EI\frac{d^4s}{dx^4} = -ks \qquad [2]$$

where

x = distance measured in direction of rail (load is located at $x = 0$)

s = static deflection of rail due to load

k = spring constant of roadbed (foundation)

EI = flexural rigidity of rail

For a single load P on a long rail, the solution is

$$s = \frac{\beta P}{2k} e^{-\beta|x|}(\cos\beta|x| + \sin\beta|x|) \qquad [3]$$

where

$$\beta = \sqrt[4]{\frac{k}{4\,EI}} \qquad [4]$$

The maximum deflection is under the load, where $x = 0$, and is

$$s_0 = \frac{\beta P}{2k} \qquad [5]$$

This equation gives us a convenient method to determine the value of k from an actual roadbed. If we assume that β and k are constant for a given roadbed, this equation shows that the deflection under the load is a linear function of the load, or that

$$P = \alpha s_0 \qquad [6]$$

where $\alpha = 2k/\beta$, which is the vertical load necessary to produce unit deflection.

The dynamic effect may now be computed from the equations of simple vibratory motion, where the term α corresponds to the constant of a simple spring. The basic theory of this analysis is contained in the paper by S. Timoshenko and B. F. Langer.[3]

Assuming that the effect of the variation of the car load on the wheel is small (which will be true for a well-riding car), and neglecting the mass of the rail, and damping, the differential equation governing the dynamic effect is

$$\frac{W}{g}\frac{d^2(y+u)}{dt^2} + \alpha y = 0 \qquad [7]$$

where

$\dfrac{W}{g}$ = unsprung mass per wheel

u = depth of low spot (given as a function of x)

$\alpha = \dfrac{2k}{\beta}$ as previously explained

y = additional deflection of rail under dynamic influence

The total deflection is thus $y + u + s_0$.

If

$$v = \text{speed of wheel}\left(\text{that is, } v = \frac{dx}{dt}\right)$$

then

$$\frac{du}{dt} = \frac{du}{dx}v \text{ and } \frac{d^2u}{dt^2} = \frac{d^2u}{dx^2}v^2 \qquad [8]$$

Substituting Equation [8] into Equation [7] and rearranging, yields

$$\frac{W}{g}\frac{d^2y}{dt^2} + \alpha y = -\frac{W}{g}v^2\frac{d^2u}{dt^2} \qquad [9]$$

We may approximate the shape of a low spot by a sine function, thus

$$u = \frac{\delta}{2}\left(1 - \cos\frac{2\pi x}{l}\right), \text{ for } 0 \leq x \leq l \qquad [10]$$

and

$$u = 0, \text{ for } x < 0, \text{ or } x > l \qquad [11]$$

where

l = length of low spot

δ = depth of low spot at middle

The solution must be obtained in two parts, the first part valid while the wheel is passing over the low spot, and the second valid after the wheel reaches level track again.

Substituting the "low-spot function," Equation [10] into Equation [9] yields

[3] "Stresses in Railroad Track," by S. Timoshenko and B. F. Langer, Trans. ASME, vol. 54, 1934, pp. 277–302.

[4] "Strength of Materials," by S. Timoshenko, part 2, second edition, D. Van Nostrand & Company, Inc., New York, N. Y., 1941, chapter 1.

$$\frac{W}{g}\frac{d^2y}{dt^2} + \alpha y = -\frac{W}{g}v^2\frac{\delta}{2}\left(\frac{2\pi}{l}\right)^2\cos\frac{2\pi x}{l} \quad \ldots\ldots [12]$$

Measuring time from the beginning of the low spot (where $x = 0$), we have $x = vt$. Substituting this into Equation [12] yields

$$\frac{W}{g}\frac{d^2y}{dt^2} + \alpha y = -\frac{W}{g}v^2\frac{\delta}{2}\left(\frac{2\pi}{l}\right)^2\cos\frac{2\pi vt}{l} \quad \ldots\ldots [13]$$

The initial conditions at time $t = 0$ are $y = 0$, $dy/dt = 0$. The solution of the differential equation, subject to the given initial conditions, is

$$y = \frac{\delta}{2}\frac{1}{1-\left(\frac{T_1}{T}\right)^2}\left(\cos\frac{2\pi t}{T_1} - \cos\frac{2\pi t}{T}\right) \quad \ldots\ldots [14]$$

where

$T_1 = \dfrac{l}{v}$, time for wheel to cross low spot

$T = 2\pi\sqrt{\dfrac{W}{\alpha g}}$, natural period of vibration of wheel on rail.

This solution is valid only while passing over the low spot. After the low spot is passed, the governing differential equation is obtained by substituting Equation [11] into Equation [9]. This yields

$$\frac{W}{g}\frac{d^2y}{dt^2} + \alpha y = 0 \quad \ldots\ldots [15]$$

The initial conditions for Equation [15] are obtained from Equation [14] by setting $t = T_1$

$$\left.\begin{aligned} y_1 &= \frac{\delta}{2}\frac{1}{1-\left(\frac{T_1}{T}\right)^2}\left(1-\cos\frac{2\pi T_1}{T}\right) \\ \left(\frac{dy}{dt}\right)_1 &= \frac{\delta}{T}\frac{\pi}{1-\left(\frac{T_1}{T}\right)^2}\sin\frac{2\pi T_1}{T} \end{aligned}\right\} \quad \ldots\ldots [16]$$

The solution of Equation [15] subject to the given initial conditions Equations [16] is

$$y = \frac{\delta\sin\frac{\pi T_1}{T}}{1-\left(\frac{T_1}{T}\right)^2}\sin\frac{\pi(2t-T_1)}{T} \quad \ldots\ldots [17]$$

This result will be correct only for the initial cycle, since the effect of damping has been neglected.

Of particular interest in wheel-adhesion problems of braking is the maximum loss of wheel-rail pressure. The change in wheel-rail pressure can be computed from the simple relation

$$\Delta P = \alpha y \quad \ldots\ldots [18]$$

and the maximum loss occurs when y is at its maximum negative value. The value of y is given by Equations [14] and [17] in terms of t, and the maximum negative value of y is obtained by choosing the appropriate value of t.

For convenience, essential nomenclature is listed below with Equations [14] and [17]

$$y = \frac{\delta}{2}\frac{1}{1-\left(\frac{T_1}{T}\right)^2}\left(\cos\frac{2\pi t}{T_1} - \cos\frac{2\pi t}{T}\right), \text{ for } 0 \le t \le T_1 \ldots [14]$$

$$y = \frac{\delta\sin\frac{\pi T_1}{T}}{1-\left(\frac{T_1}{T}\right)^2}\sin\frac{\pi(2t-T_1)}{T}, \text{ for } t > T_1 \ldots\ldots [17]$$

Nomenclature.

δ = depth of low spot
l = length of low spot
v = velocity of train
t = time from beginning of low spot
$T_1 = \dfrac{l}{v}$, time for wheel to cross low spot
$T = 2\pi\sqrt{\dfrac{W}{\alpha g}}$, natural period of vibration of wheel on rail
ΔP = change in wheel load from static load
W = unsprung weight of truck per wheel
g = gravitational constant = 386 in./sec^2
α = vertical load necessary to produce a unit deflection of rail = 147,300 lb per in., for 130-lb rail on typical ballast.

3 *Eccentric Wheel.*

The formula for the effect of an eccentric wheel can be obtained from Equation [14]. If we consider the path of the axle center, it is at once evident that the effect of an eccentric wheel is the same as the effect of a series of low spots on the rail of a depth equal to twice the eccentricity, of length equal to the circumference of the wheel, and of sinusoidal contour. However, we must now remember that the effect of damping was neglected in the derivation of Equation [14]. This was justifiable for the single low spot, but not for a long series of low spots. If damping is considered, the equation will have the form

$$y = \frac{\delta}{2}\frac{1}{1-\left(\frac{T_1}{T}\right)^2}\left(\cos\frac{2\pi t}{T_1} - e^{-\lambda t}\cos\frac{2\pi t}{T}\right) \quad \ldots [14a]$$

where

e is base of natural logarithms
λ is a constant depending upon damping of material
$e^{-\lambda t}$ is damping factor

If λ is small (which is true for a roadbed) the factor $e^{-\lambda t}$ will be approximately unity for a single low spot, and it may be omitted, as in Equation [14]. However, the effect of this factor for a long series of low spots (or an eccentric wheel) will be to reduce the second term in the parentheses to a negligible magnitude, and so Equation [14], as applied to the problem of an eccentric wheel, becomes

$$y = \frac{\delta}{2}\frac{1}{1-\left(\frac{T_1}{T}\right)^2}\cos\frac{2\pi t}{T_1} \quad \ldots\ldots [19]$$

Since an eccentric wheel causes a "steady" vibration, Equation [19] may be called the "steady-state" solution of Equation [13]. This terminology is common in vibration work.

The maximum loss of wheel-rail pressure will occur when y has a maximum negative value. The loss will amount to

$$\alpha\frac{\delta}{2}\frac{1}{1-\left(\frac{T_1}{T}\right)^2}$$

The nomenclature is the same as in the section on track irregularities.

4 *Weight Transfer Due to Brake Application.*

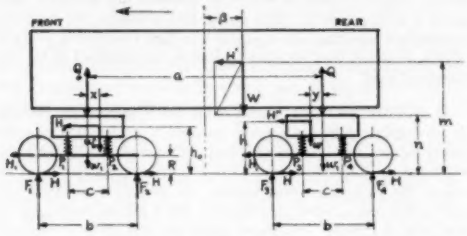

NOMENCLATURE

W = weight of car body
w_0 = weight of sprung parts, front truck
w = weight of sprung parts, rear truck
w_1 = weight of unsprung parts, either truck
α = deceleration due to braking
g = acceleration of gravity

Deceleration forces of
- car body = H'
- front truck, sprung weight = H_0
- rear truck, sprung weight = H''
- either truck, unsprung weight = H_1

$$H' = W\frac{\alpha}{g} \qquad H'' = \frac{w\alpha}{g}$$

$$H_0 = \frac{w_0\alpha}{g} \qquad H_1 = \frac{w_1\alpha}{g}$$

H = horizontal force at rail, per wheel
= retarding reaction at journal, per journal
F = vertical rail reaction, per wheel
P = spring force, per spring (or group of springs)
Q = center plate load

NOTE: β, x, and y are positive as shown in the figure; they will be negative if taken on the opposite side of car center or truck center. Include bolster with car body weight; n is height from rail to anchor rod.

The following equations have been obtained by applying the basic principles of statics, neglecting rotary inertia of wheels and axles, and assuming that the horizontal deceleration forces divide evenly between the supporting elements available to carry such forces. Thus:

$$\text{Front truck} \quad H = \frac{H'}{8} + \frac{H_0 + H_1}{4}$$

$$\text{Rear truck} \quad H = \frac{H'}{8} + \frac{H'' + H_1}{4}$$

Deceleration and static load forces only are considered, so that brake torque reactions must be handled as a separate problem.

Rail reactions (per wheel)

$$F_1 = \frac{W}{4}\left(\frac{1}{2} - \frac{\beta}{a}\right) + \frac{w_0}{2}\left(\frac{1}{2} - \frac{x}{b}\right) + \frac{w_1}{4} + \frac{\alpha}{2g}\left[\frac{W}{2}\left(\frac{m-n}{a} + \frac{n}{b}\right) + \frac{w_0h_0 + w_1R}{b}\right]$$

$$F_2 = \frac{W}{4}\left(\frac{1}{2} - \frac{\beta}{a}\right) + \frac{w_0}{2}\left(\frac{1}{2} + \frac{x}{b}\right) + \frac{w_1}{4} + \frac{\alpha}{2g}\left[\frac{W}{2}\left(\frac{m-n}{a} - \frac{n}{b}\right) - \frac{w_0h_0 + w_1R}{b}\right]$$

$$F_3 = \frac{W}{4}\left(\frac{1}{2} + \frac{\beta}{a}\right) + \frac{w}{2}\left(\frac{1}{2} + \frac{y}{b}\right) + \frac{w_1}{4} + \frac{\alpha}{2g}\left[\frac{W}{2}\left(-\frac{m-n}{a} + \frac{n}{b}\right) + \frac{wh + w_1R}{b}\right]$$

$$F_4 = \frac{W}{4}\left(\frac{1}{2} + \frac{\beta}{a}\right) + \frac{w}{2}\left(\frac{1}{2} - \frac{y}{b}\right) + \frac{w_1}{4} + \frac{\alpha}{2g}\left[\frac{W}{2}\left(-\frac{m-n}{a} - \frac{n}{b}\right) - \frac{wh + w_1R}{b}\right]$$

Spring loads (per spring, or group of springs)

$$P_1 = \frac{W}{4}\left(\frac{1}{2} - \frac{\beta}{a}\right) + \frac{w_0}{2}\left(\frac{1}{2} - \frac{x}{c}\right) + \frac{\alpha}{2g}\left[\frac{W}{2}\left(\frac{m-n}{a} + \frac{n-R}{c}\right) + \frac{w_0(h_0 - R)}{c}\right]$$

$$P_2 = \frac{W}{4}\left(\frac{1}{2} - \frac{\beta}{a}\right) + \frac{w_0}{2}\left(\frac{1}{2} + \frac{x}{c}\right) + \frac{\alpha}{2g}\left[\frac{W}{2}\left(\frac{m-n}{a} - \frac{n-R}{c}\right) - \frac{w_0(h_0 - R)}{c}\right]$$

$$P_3 = \frac{W}{4}\left(\frac{1}{2} + \frac{\beta}{a}\right) + \frac{w}{2}\left(\frac{1}{2} + \frac{y}{c}\right) + \frac{\alpha}{2g}\left[\frac{W}{2}\left(-\frac{m-n}{a} + \frac{n-R}{c}\right) + \frac{w(h - R)}{c}\right]$$

$$P_4 = \frac{W}{4}\left(\frac{1}{2} + \frac{\beta}{a}\right) + \frac{w}{2}\left(\frac{1}{2} - \frac{y}{c}\right) + \frac{\alpha}{2g}\left[\frac{W}{2}\left(-\frac{m-n}{a} - \frac{n-R}{c}\right) - \frac{w(h - R)}{c}\right]$$

Center plate loads.

$$Q_0 = W\left[\frac{1}{2} - \frac{\beta}{a} + \frac{\alpha(m-n)}{ag}\right]$$

$$Q = W\left[\frac{1}{2} + \frac{\beta}{a} - \frac{\alpha(m-n)}{ag}\right]$$

Discussion

C. D. Stewart.[5] It is doubtful if many people who have heard or will read this excellent paper of Mr. Tack's will appreciate the tremendous effort and cost incident to making available the subject matter that it contains. Mr. Tack is to be congratulated for his interesting presentation, and his company for its foresightedness in providing such fine research facilities and making the results available to all. The writer had the privilege of visiting the test car and observing the complete instrumentation and took particular note that the brake control equipment is arranged in such a way as to produce results comparable with actual service.

It may be of interest to take a moment to discuss the place occupied by the pneumatic equipment in this brake picture. The title of Mr. Tack's paper is "Development and Testing of *Brakes* for High-Speed Railroad Equipment." The term *brakes* covers groups or systems of interrelated devices, the designing and manufacturing of which are divided among numerous manufacturers. Hence the need for intercompany interest.

There are five systems, the names and functions of each being the following:

One: The running rails. The vital part they play in retarding a train can be appreciated fully by imagining the brakes being applied to the landing wheels of an airplane while it is still in flight.

Two: The brake drums—usually the car wheels which are also the convenient connecting link between the moving cars and the stationary rails.

Three: The brake shoes—which are the medium through which the kinetic energy of the car is transformed into heat.

Four: The foundation brake gear—which is the power transmitting and multiplying medium.

Five: The air brake and related electric and pneumatic devices which produce the braking forces and modulate them in response to actuating impulses.

These five groups did not always exist. With primitive man there were only two—the stationary earth and a movable sled. With the invention of the wheel a third group was added but centuries passed before man knew how properly to control the motion of the wheel. The first attempts were to convert the rolling wheels into sled runners by locking them and in spite of the fact that that has the ill effect of flattening the wheel it is surprising that such procedure is still indulged in occasionally today although it is not intentional.

To reduce the likelihood of the wheels becoming sleds one of the pneumatic accessories of the air-brake group has for its function the momentary reduction of the braking force when wheel slippage occurs. This accessory has permitted the safe use of higher braking forces without wheel sliding.

For the same end purpose another electropneumatic accessory to the air brake is the speed-governor control. This device compensates for the change in brake-shoe friction with change in train speed. As the train speed is lowered the brake-shoe friction rises and the speed-governor control modifies the braking forces proportionately.

Summing up, even when train speeds were lower and braking forces were less there were occasional incidents of slid flat wheels due to abnormal reduction in rail adhesion. With the material increase in train speeds, higher braking forces were necessary in order that stopping distance would be comparable with those from lower initial speeds. Thus, as the limit to normal rail adhesion is approached, it is necessary to employ every possible means to guard against wheels sliding. Mr. Tack has carefully explored the several causes of lowered wheel-rail adhesion and seems to have made a strong case for each cause, and although the air brake accessory means cited are dependable in their functioning, still it is highly desirable that wheel-rail adhesion be sustained at the top practical level.

H. N. Sudduth.[6] Mr. Tack's paper has been most interesting. It obviously represents a great amount of exploration into the many factors involved in retarding railway vehicles by mechanical friction. The writer would like to make a brief comment on one of the most interesting aspects, the matter of available adhesion between a wheel and the rail, which places limitations on the braking torque. The paper points out and offers an explanation for the phenomenon of decreasing available adhesion with increasing speed. Many observers noted that this effect appeared prominently during braking tests of early high-speed trains which were built for operation within the 90 to 100-mile-per-hr-zone when efforts were made to raise materially the retarding torque at the high speeds and to prevent intolerable increases in this torque at lower speeds. In several instances wheel sliding occurred at retardation rate levels that were not considered to be high when related to expected wheel and rail adhesion.

In a series of exploratory braking tests in 1937, on a single car mechanically equipped to obtain retardation rates of the nature of 4 to 5 mph per sec in the high-speed zones, it was found that even under favorable conditions of clean, dry, heavy-section rail the available adhesion proved to be considerably less than expected through theoretical consideration of coefficient of static friction between the wheel and rail and of the static wheel loading. It was suspected that values of coefficient of friction were not basically at odds with static test determinations but that the wheel loading was far from static. Mr. Tack's paper offers confirmation of this. If the continuous wheel-load variation is visualized as producing a dynamic weight envelop encompassing the high and low instantaneous values, it is the lower boundary that must be considered in determining the adhesion available to support retarding torque and this boundary apparently becomes lower with increasing speed.

Restoration of adequate adhesion values for higher retardation rates in these tests was accomplished by the use of good clean sand between the wheel and the rail. Retardation rates of the order of $4^1/_2$ mph per sec at 100 mph and well over 5 mph per sec at 60 mph were obtained without wheel sliding on a well-sanded rail. This emphasized the advantages to be gained by the proper distribution and control of good sand for maintaining adhesion between the wheel and rail and pointed to the development of an adequate and reliable car sander.

In 1940 the first successful efforts along this line resulted in a type of train-lined sanding apparatus that was controlled manually by the locomotive engineman except during emergency applications, when it automatically operated at the start of the brake application at each car. In actual train service where sanding stations were located on each car it was so effective as to be used to an extent far greater than contemplated by the sponsors, which was wasteful of sand and air.

With the later development of antiwheel slide devices, it appeared logical that the first response of such a device on a car would be the ideal indication of the need for greater adhesion to support the desired braking torque. Consequently, the development was carried farther and has resulted in a completely automatic car sander that can be combined with any known antiwheel slide device for delivering sand in a reliable manner, as and where it is needed throughout the train of cars. This type of sander

[5] Vice-President, Westinghouse Air Brake Co., Wilmerding, Pa. Fellow ASME.

[6] Director, Air Brake Engineering, The New York Air Brake Company, Watertown, N. Y. Mem. ASME.

operates promptly upon the indication of a wheel slip and provides a limited though adequate amount of sand to the point of rail and wheel contact over a timed period. It is this type of sander and sanding control to which Mr. Tack refers in his paper and which is available to the railways in suitable combinations for modern passenger cars equipped with any of the latest types of mechanical braking devices.

B. S. Cain.[7] It is shown in the paper that one of the most serious causes of loss of effective wheel load on the rail is due to track irregularities. A method of estimating this is given in the Appendix. The formula given is based on the assumption that the stiffness of the track remains constant and that the irregularity is due to a change in level, equivalent to a low spot being carved in the surface of the rail. Another common type of irregularity, not covered, is due to a variation of stiffness in the track. The track will be level until a load is placed on it and the deflection of the load will vary according to its position along the rail. In this case the calculation is not quite so easy, since the equation of motion can be solved only approximately.

The important thing is that the results may be very different. In particular, if a wheel passes over a rail joint at high speed, the oscillation may be considerably less, if the joint is more flexible than the rest of the rail, than if the flexibility is constant and the joint is low.

Rupen Eksergian.[8] In the author's analysis of weight transfer due to brake application, the author considers the more general problem of an offset center of gravity for the car body, along with unequal weights for the unsprung parts w_0 for the front truck and w for the rear truck.

The author's conclusions for the vertical rail reactions due to weight transfer cannot be sustained if the rail retarding forces H are the same for each wheel and the truck weights are unequal.

The front and rear center plate loads, i.e., the vertical component reactions between car body and trucks, are

$$Q_0 = W\left[{}^1/_2 - \beta/a + \alpha\left(\frac{m-n}{g a}\right)\right]$$

$$Q = W\left[{}^1/_2 + \beta/a - \alpha\left(\frac{m-n}{g a}\right)\right]$$

The car body horizontal components at the front and rear truck, however, do not divide equally, as assumed by the author, since the retarding wheel forces H at the rail are determined by the brake torque and therefore are sensibly the same for either rear or front truck. Using the author's nomenclature

$$H_f = 4H - H_1 - H_0 \quad \text{(front truck)}$$

$$H_R = 4H - H_1 - H'' \quad \text{(rear truck)}$$

Since $H_1 = \frac{w_1}{g}\alpha$, $H_0 = \frac{w_0}{g}\alpha$, $H'' = \frac{w\alpha}{g}$ and $H' = \frac{W}{g}\alpha$

and $8H = H' + H_0 + H'' + 2H_1$

$$H_f = {}^1/_2(H' + H'' - H_0) = {}^1/_2(W + w - w_0)\frac{\alpha}{g}$$

$$H_R = {}^1/_2(H' + H_0 - H'') = {}^1/_2(W + w_0 - w)\frac{\alpha}{g}$$

Thus an additional term $= {}^1/_4(w - w_0)\frac{\alpha}{g}\cdot\frac{n}{b}$ should be added to the expressions for rail reactions.

In addition to these reactions, assumed exerted through the center plate, there is a moment exerted at the center plate between car body and truck.

In general, the moment reaction at the center plate, which with the vertical and horizontal components are the reactions of the car body on the truck, is statically indeterminate. It depends not only on the location of the anchor rod, but also on the brake reactions and the springing of the truck. The center plate bearing should be designed to sustain the full moment of this combination to prevent upsetting during braking.

While the inertia load due to axle wheel rotation is small compared with the total inertia, it is not negligible when compared with the unsprung weights. The rotational inertia can readily be considered by augmenting w_1 by the expression,

$$(1 + K)w_1 = \left(1 + 2\frac{w_A}{w_1}\frac{\epsilon^2}{R^2}\right)w_1$$

w_A = *axle wheel assembly*, weight ϵ = radius of gyration (around $0.7R$). $\therefore K = 2\frac{w_A}{w_1}\frac{\epsilon^2}{R^2}$

When $w = w_0$, and the inertia load due to wheel rotation is neglected and the moment reaction between truck and car body at center plate equals the moment of anchor rod about center plate, the author's expression can be used as a first approximation.

If we lower the anchor-rod height above rail n to a height below the center plate, the author's formulas with *equal-weight* trucks, retain approximately their validity. If we consider the over-all truck including center plate, this implies an external moment effected by unequal bearing pressures at the center plate which resist the thrust rod moment about the center plate. But this moment can be further modified by the bolster springs. If we neglect the moment of the bolster springs about the center plate, then the anchor-rod height determines the effective moment which causes the major weight transfer. It is obvious that by lowering the anchor-rod height above rail, we can considerably reduce the weight transfer. But this also requires an ample center plate bearing for sustaining the eccentric moment of the anchor rod relative to the center plate. Another way would be to use a deep-seated spherical bowl for the center plate.

In the author's analysis of the spring loads, it is assumed that the tilting effect on the springs is due solely to the moment of the thrust-rod and spring-truck inertia force about the axle bearing at pedestal. This assumption is correct only provided the brake-torque reactions are taken *entirely* on the nonspring supported parts, i.e., on the equalizer bars. The author does not disclose how the brakes are mounted.

If, on the other hand, the brake-torque reactions are taken by the spring-supported truck frame, it is then not permissible to neglect these reactions in estimating the spring loads. Moreover the brake-torque reactions cannot be handled as a separate problem. It is the brake torque that causes the rail wheel forces H and the retardation of the trucks and car body.

In obtaining the weight transfer at the rail, it is true that the brake-torque reactions are of an internal character and therefore do not explicitly appear. When, however, the brake-torque reactions act on the truck frame, as with a nose suspension, or are suspended from the frame, as in the clasp brakes, these reactions are of an external character and must be included among the forces which determine the spring loads. For this case the spring loads would be considerably different from that given by the author.

[7] Assistant Engineer, Locomotive Engineering Division, Locomotive and Car Equipment Divisions, General Electric Company, Erie, Pa. Mem. ASME.

[8] Chief Consulting Engineer, The Budd Company, Philadelphia, Pa. Senior Staff Advisor, The Franklin Institute Laboratories, and Consulting Engineer, Lukens Steel Company, Coatesville, Pa. Fellow ASME.

With clasp brakes, the torque reaction considerably increases the spring loads over that given by the author's values.

On the other hand, when the disk-brake assembly is supported partly at the journal bearings and partly by a nose suspension, as in the *C* Frame of the Budd Disk Brake, the nose reactions on the frame practically eliminate any change in spring load during braking. In this case the truck frame does not cant in braking. Since the inclination of the car body is negligible, the bolster springs are likewise not affected in braking. This feature in the Budd Disk Brake design is important in greatly reducing augmented spring stresses during braking.

It is interesting to note that with clasp brakes and with 300 per cent braking, forward equalizer springs practically become solid.

Author's Closure

The comments by Mr. C. D. Stewart and Mr. H. N. Sudduth, amplifying the presentation, are appreciated, as are the suggestions by Mr. B. S. Cain and Mr. Rupen Eksergian.

Mr. Cain is correct in pointing out that varying track stiffness is more commonly encountered than irregularity in the surface of the track. Further, it is true that the varying stiffness will have less effect on the instantaneous wheel load on the rail, though it is another factor which does affect the amount of braking torque which can be delivered successfully by the wheel to the rail.

Mr. Eksergian is correct in stating that the horizontal forces do not divide equally when unequal truck loads are encountered. He presents a computation based upon the assumption that the retarding forces at the rail are equal for both forward and rear trucks. However, for an unsymmetrically loaded car, where the truck loads are unequal, an adjustment to proportion the braking effort is made quite simply on clasp-brake equipment by drilling the levers suitably. This adjustment is accomplished with more difficulty on disk brakes, and it is common practice to average the braking effort instead of adjusting for unequal weights on each truck. Mr. Eksergian's computation accordingly can be used only as a first approximation in a practical case. Both computations indicate the effect of weight transfer on wheel to rail load, which cannot be avoided.

The suggestion that the inertia load due to wheel and axle rotation be included in a weight-transfer calculation was considered by the author. It was decided to omit this factor, and call attention to its omission, as was done in the Appendix. To improve the accuracy, it would be desirable to use the method pointed out by Mr. Eksergian.

Mr. Eksergian's comments on the effect of anchor-rod location point out the necessity for careful design of the entire truck. If the anchor rod is lowered to reduce weight transfer in the truck, the added moment on the truck bolster must be taken into consideration, and compensation made.

In practice, the anchor rod is located to reduce the tilting moment of the truck bolster to a practical minimum. The analysis offered applies to conditions found in practically all postwar passenger cars having four-wheel equalized trucks.

The author's analysis contemplated forces due to "weight transfer" only, as these appear externally to affect instantaneous wheel load on the rail, and thus act to limit the braking which can be accomplished.

Internal reactions due to brake-torque forces cause additional spring loads, as pointed out by Mr. Eksergian—but do not appear externally and, therefore, were not included, as they have no bearing on the problem of wheel load on the rail. It should be understood clearly that the brake-torque reactions and the resulting truck-spring loads are of an internal character and, therefore, have absolutely no influence on the problem of wheel load on the rail. The question of brake torque naturally should be considered when designing a truck, and suitable allowance made in designing the springs.

Comparative Strengths of Some Adhesive-Adherend Systems

By N. J. DeLOLLIS,[1] NANCY RUCKER,[1] AND J. E. WIER,[1] WASHINGTON, D. C.

The strength properties of various adhesive-adherend combinations were determined as one phase of an investigation of the nature of adhesion. The adhesives were polyvinyl acetate, cellulose nitrate, resorcinol resin, casein, gum arabic, natural rubber, and neoprene. The adherends were stainless steel, aluminum alloy, paper-phenolic laminate, glass, birchwood, and hard rubber. The properties studied were double-lap shear, tensile, long-time loading shear, and impact strengths. The tensile-adhesion and shear-strength values for a given adhesive-adherend combination did not differ greatly except for wood and paper-phenolic laminate, which are nonisotropic. The highest values (up to 3600 psi) were obtained with polyvinyl-acetate and cellulose-nitrate adhesives. The thermosetting resorcinol resin showed no appreciable flow in supporting a load of 680 psi for 6 months, whereas the thermoplastic polyvinyl acetate failed in 45 days under a load of 200 psi. The rubber-type adhesives which were weak compared with the other adhesives in the static load tests were definitely superior in the impact tests. Better correlation of shear strengths was observed with the moduli of elasticity than with the dielectric constants of the materials used in the various adhesive-adherend combinations.

Introduction

EXPERIMENTAL work on adhesives has been concerned largely with the development and use of products for industrial purposes. The aircraft industry has employed adhesives quite extensively (1–5).[2] Current interest in sandwich construction also serves to emphasize the increasing importance of adhesives in new types of airplanes.

Study of the fundamentals of adhesion has been relatively meager (6, 7). A survey of the information available on the nature of adhesion was published recently by the National Advisory Committee for Aeronautics (8).

An investigation, under the sponsorship and with the financial assistance of the National Advisory Committee for Aeronautics, was undertaken at the National Bureau of Standards to obtain comparative data on the strengths of the bonds between various chemical types of adhesives and representative adherends. The results of these tests should give some indication of the specific attraction between these various materials and hence lead to a better understanding of the nature of adhesion.

The information will also be useful in the selection of adhesive-adherend systems for the more fundamental studies of adhesion which are in progress in this laboratory.

[1] Organic Plastics Section, National Bureau of Standards.

[2] Numbers in parentheses refer to the Bibliography at the end of the paper.

Contributed by the Rubber and Plastics Division and presented at the Fall Meeting, Worcester, Mass., September 19–21, 1950, of THE AMERICAN SOCIETY OF MECHANICAL ENGINEERS.

NOTE: Statements and opinions advanced in papers are to be understood as individual expressions of their authors and not those of the Society. Manuscript received at ASME Headquarters on June 15, 1950. Paper No. 50—F-15.

Definition of Terms

Shear Strength. Maximum load sustained by the specimen divided by the bonded area. The bonded area for a double-lap-joint specimen is twice the product of the overlap and the width.

Tensile-Adhesion Strength. Maximum load sustained by the specimen divided by the bonded area.

Statistical Terms. "Mean value" is the arithmetic mean of a set of measurements.

"Standard error of the mean" (usually called the "standard error" if no other statistic is referred to at the same time)

$$SE = \frac{r_1^2 + r_2^2 + r_3^2 + \ldots + r_i^2 + \ldots + r_n^2}{n(n-1)}$$

where

r_i = difference between ith measurement and mean value
n = number of measurements

"Coefficient of variation" (measures scattering as a percentage of the mean)

$$V = \frac{\dfrac{r_1^2 + r_2^2 + \ldots + r_i^2 + \ldots + r_n^2}{n-1}}{\text{Mean value}} 100$$

Materials

The choice of adherends and adhesives for this work was governed by the desire to study many different chemical types of bonds. The adherends used included stainless steel, aluminum alloy, paper-phenolic laminate, plate glass, birchwood, and hard rubber. The types, sources, and thicknesses of these materials are listed in Table 1.

The types of adhesives used in this investigation are as follows:

Type	Adhesive
Cellulose ester	Cellulose nitrate
Thermoplastic resin	Polyvinyl acetate
Thermosetting resin	Resorcinol-formaldehyde
Protein	Casein
Vegetable	Gum arabic
Natural rubber	Rubber (smoked sheet)
Synthetic rubber	Neoprene

Compounding agents were used with the adhesives in as small amounts as possible in order to keep the chemical nature of the bond between adhesive and adherend of the simplest possible type. Camphor was added to the cellulose nitrate in order to bring its softening or flow temperature below its decomposition temperature. Thymol was added to the gum-arabic solution as a preservative; otherwise the gum arabic became moldy. Neoprene and natural rubber were compounded with what was considered the minimum number of agents necessary to vulcanize them properly. Neither accelerators nor antioxidants were added. The types, sources, and formulation of the adhesives are shown in Table 2.

Preparation of Specimens

Surface Treatment of Adherends. The proper surface treatment

TABLE 1 DESCRIPTION OF ADHERENDS

Adherend	Type	Manufacturer	Thickness, in.
Stainless steel	18-8	Allegheny Ludlum Steel Corporation	0.10 1.87[a]
Aluminum alloy	24S-T	Aluminum Company of America	0.10 0.20 1.87[a]
Paper-phenolic laminate	Grade X	Westinghouse Electric Company	0.10 0.20 1.00
Glass	Plate glass	Pittsburgh Plate Glass Company	0.125 0.25 1.00
Wood	Yellow birch	Parkwood Corporation	0.125 0.25 1.00
Hard rubber	.....	American Hard Rubber Company	0.10 0.20 1.00

[a] Diameter of rod.

TABLE 2 DESCRIPTION OF ADHESIVES AND PROCESSING DATA

Adhesive	Type	Manufacturer	Formulation (parts by wt.)	Drying Conditions: Time (hr)	Drying Conditions: Temperature (°C)	Bonding Conditions: Time (hr)	Bonding Conditions: Temperature (°C)	Bonding Conditions: Pressure (lb/in.²)
Cellulose Nitrate	20 Sec. Viscosity	Hercules Powder Co.	a	20	25	2	120	150–200
Polyvinyl Acetate	AYAF	Carbide and Carbon Chemicals Corp.	b	2 2	60 80	2	120	3
Resorcinol Resin	Penacolite G1135-A	Pennsylvania Coal Products Co.	c	0.75	25	20	65	3
Casein	Reg. B 1	Casein Company of America	d	0.5	25	20	25	3
Gum Arabic	GU 2	Arabol Manufacturing Co.	e	0.5	25	20	25	3
Rubber	Smoked Sheet		f	1	25	7	140	150–200
Neoprene	GN	E. I. du Pont de Nemours and Co., Inc.	g	1	25	3.5	120	150–200

a. Cellulose nitrate 10, Ethyl acetate 85, Camphor 5

b. Polyvinyl acetate 20, Acetone 80

c. Resorcinol resin 5, Catalyst 1

d. Casein 100, Water 300 (Soak for 15 min), Calcium hydroxide 30, Sodium fluoride 5.8, Sodium phosphate ($12\ H_2O$) 17.4

e. Gum arabic 50, Water 50, Thymol 2.5

f. Rubber 100, Benzene 400, Zinc oxide 5, Sulfur 4

g. Neoprene 100, Ethyl acetate 200, Zinc oxide 5, Magnesium oxide 4

of the adherend was found to be of primary importance in obtaining optimum bonds. Not only was the surface cleaned, but the freshness of the surface was preserved after cleaning by immersion in a solvent until the adhesive was applied.

The metals were cleaned in a volatile organic solvent to remove oil and grease and were pickled in acids to remove any oxide film. The stainless steel was treated with 50 per cent aqua regia for approximately 5 sec and rinsed thoroughly in cold water. The aluminum alloy was treated with a 5 per cent phosphoric-acid solution for about 5 min and rinsed in cold water. The time of immersion in the respective acids was dependent on the freshness and temperature of the acids.

The paper-phenolic laminate had a glossy smooth surface to which none of the glues adhered very well. Washing with soap and water or soaking in benzene or acetone did not affect this passive surface. The surface layer had to be entirely eliminated by sanding with No. 00 sandpaper (9–11).

The glass was cleaned by heating in a sodium dichromate-sulphuric acid solution and rinsing thoroughly in water. The birchwood and hard-rubber specimens were cleaned by sanding with No. 00 sandpaper (12).

The solvent used for preserving the fresh surface depended upon the adhesive to be used, as follows:

Adhesive	Solvent used to preserve adherend surface
Cellulose nitrate	Ethyl acetate
Polyvinyl acetate	Acetone
Resorcinol-formaldehyde	Acetone
Casein	Acetone
Gum arabic	Acetone
Rubber	Benzene
Neoprene	Ethyl acetate

In the case of the resorcinol-formaldehyde, casein, and gum-arabic adhesives, which were used in aqueous solutions, the adherend surface was air-dried 15 min before applying the adhesive. Although acetone is soluble in water, it is not a solvent for casein or gum arabic and tended to precipitate them from the aqueous solutions. The wood specimens were not immersed in a solvent; the surfaces of this adherend were sanded immediately prior to application of adhesive.

Procedure for Bonding Specimens. The clamping frames used in assembling the specimens are shown in Figs. 1 and 2. It was found that, to prepare the test specimens properly, different conditions for drying the coated adherends and bonding the assemblies were required with each adhesive. The time, temperature, and pressure conditions employed are shown in Table 2.

The temperature rise during the bonding cycle with the neo-

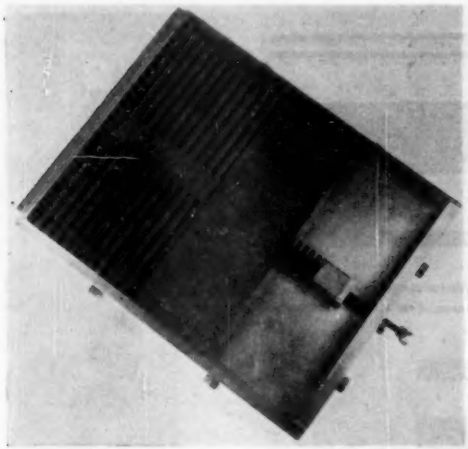

FIG. 1 CLAMPING FRAME FOR PREPARATION OF SHEAR SPECIMENS

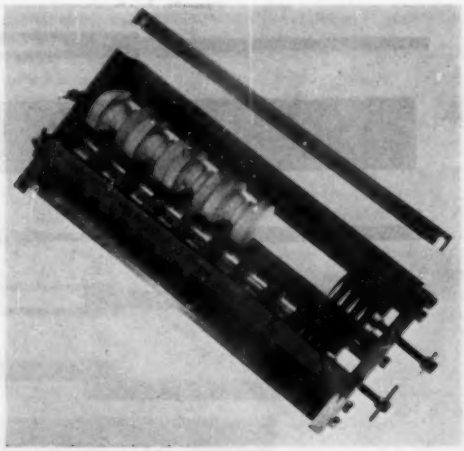

FIG. 2 CLAMPING FRAME FOR PREPARATION OF TENSILE SPECIMENS

prene adhesive was determined with a thermocouple placed in the adhesive. It was found that 2 hr was required to reach the correct temperature. The prescribed time of cure at 120 C is 2.5 hr (13). By adding 1 hr to the prescribed time to compensate for the temperature lag, a complete cure was obtained. The natural-rubber cement was cured for various lengths of time at 140 C until the curing time was found which would produce a properly vulcanized product.

For polyvinyl acetate, resorcinol-formaldehyde resin, casein, and gum arabic, all of which flow readily, a pressure of only 3 psi was required to produce full contact between the coated surfaces. For cellulose nitrate and the natural and synthetic-rubber adhesives, the resistance to flow was much greater, and pressures of 150 to 200 psi were necessary to insure close contact between the adherend surfaces in the assembly.

TEST PROCEDURES

All specimens were conditioned for a minimum period of 7 days at a temperature of 25 C and 50 per cent relative humidity and were tested under these conditions. Two Baldwin-Southwark universal hydraulic testing machines of 2400 and 60,000-lb capacities, respectively, with scale ranges of 240, 1200, 2400, 12,000, and 60,000 pounds, were used to make the shear and tensile tests.

Shear Tests. Double-lap-joint specimens were used in determining shear strengths of the adhesive-adherend combinations. The specimens were broken under a tensile load except for glass bonded with cellulose nitrate and polyvinyl acetate. These latter specimens failed repeatedly in the adherend under tensile loading; compression loading gave more satisfactory results.

Sheet material of two thicknesses, approximately $^1/_8$ and $^1/_4$ in., were used to make tensile-type shear specimens; the thicker strip was used between two of the thinner strips, as shown in Fig. 3(*a*). An exception to this was necessary in the case of the stainless steel which was available only in 0.1-in. thickness; three strips of equal thickness were used to make the shear specimens of this material. The strips were machined to 5 × 1-in. dimensions and bonded with an overlap of 1.0 in. When failure occurred in the adherend, the overlap was reduced to 0.5 or 0.3 in., as indicated in the tabulated data.

Templin-type self-aligning grips were used in the shear tests with tensile loading. The rate of loading was adjusted within the limits of 200 to 1000 lb per min so that the maximum load was applied in about 3 min. The loading rate for each system was determined by trial tests.

The compression-type shear specimens were made of strips of glass 1 in. long, 0.5 in. wide, and 0.25 in. thick, with an overlap of 0.3 in., Fig. 3(*d*). They were tested in a subpress as shown in Fig. 4. Blotting paper was placed at the bearing surfaces of the glass to prevent stress concentration and premature failure of the test specimen. The rate of loading was adjusted as described for the tests with tensile-type shear specimens.

Tensile Tests. Tensile-adhesion strengths of the adhesive-adherend combinations were determined by using specimens and self-aligning grips (14) (see Fig. 5).

The glass specimens, Fig. 6(*a*) were cast from melted 1-in-thick plate glass. The specimens were machined from $1^7/_8$-in-diam rod in the case of the two metals, Fig. 6(*b*) and from 1-in-thick sheet in the case of the phenolic laminate, birchwood, Fig. 6(*c*), and hard rubber.

The contact area for the tensile specimens was 1 sq in. except when smaller contact areas had to be used, because the specimens failed in the adherend. A contact area of 0.25 sq in. was used for the phenolic laminate bonded with cellulose nitrate, polyvinyl acetate, and casein; for glass bonded with cellulose nitrate and polyvinyl acetate; and for hard rubber bonded with cellulose nitrate, Fig. 6(*d*). A contact area of 0.5 sq in. was used for all specimens prepared with the birchwood.

The rate of loading in the tensile tests was adjusted within the limits of 200 to 1000 lb per min so that the maximum load was applied in about 3 min.

Long-Time Loading Tests. The same type of double-lap-joint specimen used in the shear tests made with tensile loading was employed in the long-time loading tests, Fig. 3(*b*). An overlap of 0.5 in. was adopted, and the strips were machined to widths selected to obtain average shear stresses of 200 to 1300 psi. The load was applied by hanging either a 50 or a 100-lb weight from the specimen, Fig. 7.

Impact Tests. Single-lap-joint specimens of aluminum alloy and wood were used to evaluate the impact strength of bonds made with the various types of adhesives. The specimens were

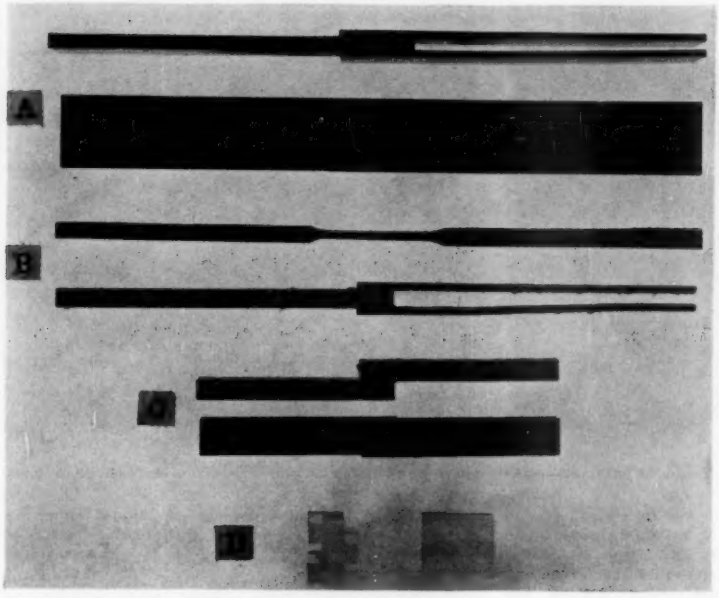

FIG. 3 SPECIMENS FOR DETERMINATION OF SHEAR AND IMPACT STRENGTHS
(A, Tensile-type shear specimen. B, Long-time loading shear specimen C, Impact specimen. D, Compression-type shear specimen.)

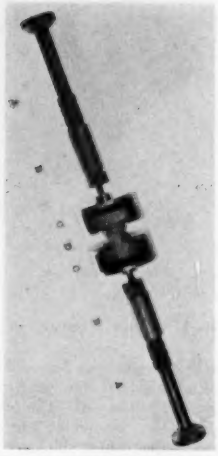

FIG. 5 SELF-ALIGNING GRIPS USED IN MAKING TENSILE-TYPE SHEAR TEST

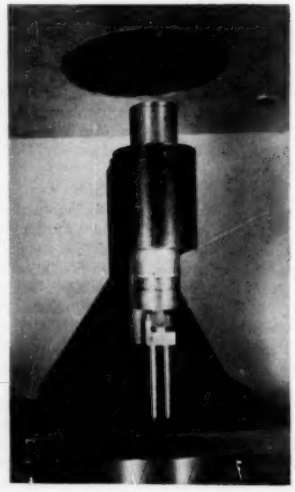

FIG. 4 SUBPRESS FOR USE IN MAKING COMPRESSION-TYPE SHEAR TEST

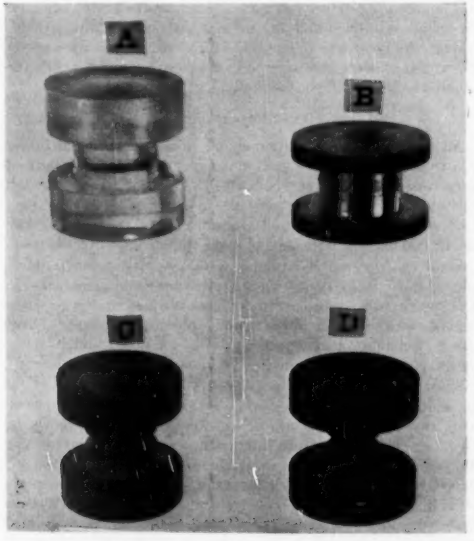

FIG. 6 SPECIMENS FOR TENSILE-TYPE SHEAR TEST
(A, Glass adherends. B, Metal adherends. C, Wood adherends. D, Hard-rubber adherends.)

FIG. 7 EQUIPMENT USED IN MAKING LONG-TIME LOADING TEST

FIG. 8 MACHINE USED IN MAKING CHARPY IMPACT TEST

made with strips 2.8 in. long and 0.5 in. wide with an overlap of 0.5 in., Fig. 3(*c*). The thickness of the strips was 0.1 in. for the aluminum alloy, and 0.25 in. for the wood. The specimens were tested both edgewise and flatwise by the Charpy impact method with a Baldwin-Southwark pendulum machine having a capacity of 2 ft-lb, Fig. 8.

RESULTS OF TESTS

Shear and Tensile-Adhesion Strength. The data obtained in the shear and tensile-adhesion strength tests are presented in Tables 3 and 4, respectively. The data are grouped according to adhesives in Fig. 9, and according to adherends in Fig. 10.

Polyvinyl-acetate adhesive gave consistently high tensile-adhesion and shear strengths with all adherends. With stainless steel and aluminum alloy the shear and tensile-adhesion strengths were 2900 to 3600 psi. In only three instances, with wood and hard rubber in tensile adhesion and with hard rubber in shear, did the polyvinyl acetate fail to give the highest values.

Cellulose nitrate plasticized with camphor ranks next to vinyl-acetate resin in giving strong bonds with all the adherends. However, it was necessary to use a large amount of the plasticizer to obtain fusible adhesive films.

The resorcinol-formaldehyde resin adhesive produced good bonds with the organic adherends and bonds of negligible strength with the inorganic substances.

Casein and gum arabic, which depend on loss of water to achieve their optimum strength, gave highest values with the absorbent materials such as wood and paper-phenolic laminate. Shear specimens of aluminum, bonded with gum arabic, showed an appreciable gain in strength when they were given a long conditioning and drying period, Table 3. They increased in strength from a value of 330 psi for the usual 7-day period to 530 psi for a 20-day drying period.

The rubber cements gave uniformly low values. Cure of the natural rubber to a hard nonrubbery texture gave higher values. For example, the tensile-adhesion value for wood, bonded with overcured natural rubber, was 530 psi, compared with 174 psi for a rubbery cure.

Good bonds were obtained with the metals and glass only with the polyvinyl-acetate and cellulose-nitrate adhesives.

Wood and paper-phenolic laminate were the only nonisotropic materials used. The load was applied in the strongest direction of these materials in the shear test and in the weakest direction in the tensile-adhesion test. The large differences between the shear and tensile-adhesion strengths of these two materials were probably due to this factor (9).

In quite a few of the tests the values were affected by the strength of the material bonded since the failures were wholly or partly in the adherends. However, the strength of the adherend is not the only determining factor in the failure of the bond. The wide spread in the strength values, obtained in tests in which a given adherend bonded with various adhesives showed cohesive failure, suggests that additional chemical or physical factors are involved. For example, with paper-phenolic laminate, adherend failure occurred with shear specimens bonded with polyvinyl acetate, cellulose nitrate, resorcinol resin, and casein adhesives at average shear stresses of 2480, 1680, 1370, and 1030 psi, respectively. The amount of adherend failure was 90 to 100 per cent for the first three adhesives and averaged 35 per cent for casein.

In a study of the effect of pH on the strength of wood veneers (10) it was shown that acids and bases definitely weaken them. The casein formulation is very alkaline; when it was used with aluminum a large amount of corrosion was observed. This chemical action may be reflected in the values obtained with other adherends. Therefore, while chemical action between the resin and adherends such as paper-phenolic laminate or wood may strengthen the bond, it may also tend to weaken the wood or phenolic laminate.

The solvents which were used as the vehicles for cellulose nitrate and polyvinyl acetate could possibly have a weakening effect on the wood because of solvent action on the ligneous fiber-bonding material. Such activity may vary with the difference in penetrating powers due to differences in viscosities of the adhesive formulation.

Another physical factor capable of explaining variable strength values when adherend failure occurs is the ductility of the adhesive. The thermoplastic adhesives, by flowing at a yield stress, can relieve stress concentrations which exist at the ends of the laps in the shear specimen (11).

Long-Time Loading Shear. The results of the long-time loading tests are presented in Table 5. Fig. 11 indicates clearly the difference in behavior of thermosetting and thermoplastic resin adhesives.

For the specimens bonded with polyvinyl acetate, the static test is an indication of the adherend strength since the speed of loading is greater than the plastic flow, and the adhesion strength is greater than the adherend strength.

On the other hand, in the long-time loading tests with specimens bonded with polyvinyl acetate, plastic flow of the adhesive is the main cause of failure. The rate of plastic flow is such that from 600 to 2500 psi the bonds fail in less than 4 hr. Below 600 psi the plastic flow decreases rapidly so that a relatively small drop in stress greatly increases the time to failure.

Three wood specimens bonded with resorcinol resin were subjected to the long-time load test. Two of them broke under loads of 1360 and 1070 psi in 65 and 219 hr, respectively. In both cases the failure was partially in the wood. The third specimen supported a load of 680 psi for 6 months, at which time the test was discontinued. Thus plastic flow of the adhesive is not a major factor in the failure of wood joints bonded with the thermosetting resin.

Impact Strength. The results of the impact tests on single-lap-joint specimens are shown in Table 6. The rubber adhesives

TABLE 3 SHEAR-STRENGTH DATA FOR VARIOUS ADHESIVE-ADHEREND COMBINATIONS[a]

	Cellulose Nitrate	Polyvinyl Acetate	Resorcinol Resin	Casein	Gum Arabic	Rubber	Neoprene
Stainless Steel							
Shear Strength (lb/in.^{2})	1580	2960	0	190	130	270	90
Standard Error (lb/in.^{2})	29	44	—	29	16	18	4.5
Coefficient of Variation (%)	6.2	5.2	—	55	30	90	17
Number of Specimens	11	12	—	12	6	9	11
Aluminum Alloy							
Shear Strength (lb/in.^{2})	1360	3560	0	120	330[f]	250	130
Standard Error (lb/in.^{2})	32	65	—	12	52[f]	15	21
Coefficient of Variation (%)	8.0	8.8	—	28	50[f]	18	53
Number of Specimens	12	23	—	8	10[f]	9	11
Paper-Phenolic Laminate							
Shear Strength (lb/in.^{2})	1680[b,d]	2480[b,c]	1370[b,c]	1030[b]	440	130	250
Standard Error (lb/in.^{2})	31	93	28	30	24	5.5	6
Coefficient of Variation (%)	6.4	12	6.8	10	18	15	8.2
Number of Specimens	12	10	11	12	11	12	12
Glass							
Shear Strength (lb/in.^{2})	1680[b,d,e]	2310[b,d,e]	0	29	210	43	100
Standard Error (lb/in.^{2})	42	110	—	6	7.1	3.5	14
Coefficient of Variation (%)	9.5	11	—	55	10	28	48
Number of Specimens	14	6	—	8	9	12	11
Birch Wood							
Shear Strength (lb/in.^{2})	1390[b]	1990[b,c]	1940[b,c]	1660[b,c]	630	160	180
Standard Error (lb/in.^{2})	39	66	46	55	24	12	4.6
Coefficient of Variation (%)	9.3	10	9.7	11	13	26	8.9
Number of Specimens	11	10	17	12	11	12	12
Hard Rubber							
Shear Strength (lb/in.^{2})	1000[b,d]	630[b,c]	590[b,c]	150	240	190	230
Standard Error (lb/in.^{2})	18	44	61	9.6	13	7	8.9
Coefficient of Variation (%)	6.3	22	23	21	18	13	13
Number of Specimens	12	10	5	12	12	12	12

a. A double-lap tensile-type specimen with an overlap of 1 inch was used unless otherwise noted.

b. Specimens failed partly in adherend.

c. Overlap 0.5 inch.

d. Overlap 0.4 inch or less.

e. Compression shear.

f. Specimens dried for 20 days instead of 7 days gave the following:

Shear Strength (lb/in.^{2})	530
Standard Error (lb/in.^{2})	68
Coefficient of Variation (%)	43
Number of Specimens	11

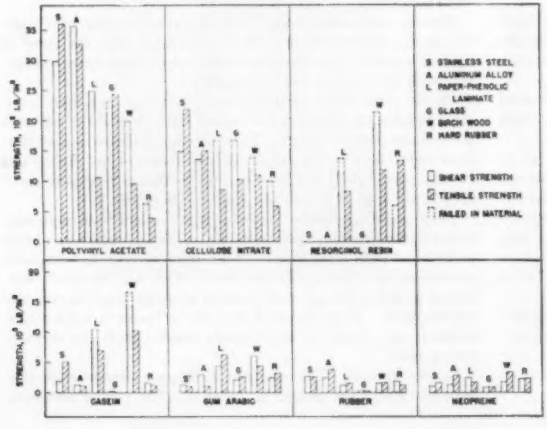

FIG. 9 COMPARATIVE BOND-STRENGTH VALUES GROUPED ACCORDING TO ADHESIVES USED

TABLE 4 TENSILE-ADHESION STRENGTH DATA FOR VARIOUS ADHESIVE-ADHEREND COMBINATIONS[a]

	Cellulose Nitrate	Polyvinyl Acetate	Resorcinol Resin	Casein	Gum Arabic	Rubber	Neoprene
Stainless Steel							
Tensile-Adhesion Strength (lb/in.^{2})	2180	3600	0	510	110	260	170
Standard Error (lb/in.^{2})	66	72	—	31	6	17	9
Coefficient of Variation (%)	10	10	—	21	19	23	16
Number of Specimens	12	25	25	12	11	12	9
Aluminum Alloy							
Tensile-Adhesion Strength (lb/in.^{2})	1500	3270	0	110	110	390	290
Standard Error (lb/in.^{2})	100	59	—	9.5	7	26	9
Coefficient of Variation (%)	23	9	—	30	18	23	10
Number of Specimens	12	25	17	12	9	12	12
Paper-Phenolic Laminate							
Tensile-Adhesion Strength (lb/in.^{2})	860[b,d]	1060[b,d]	830[b]	690[b,d]	630	160	170
Standard Error (lb/in.^{2})	110	75	62	37	42	15	9
Coefficient of Variation (%)	40	23	19	18	21	31	17
Number of Specimens	10	10	9	11	10	10	12
Glass							
Tensile-Adhesion Strength (lb/in.^{2})	1040[b,d]	2430[b,d]	0	0	260	34	90
Standard Error (lb/in.^{2})	230	170	—	--	17	5	12
Coefficient of Variation (%)	60	16	—	--	21	47	46
Number of Specimens	7	5	13	6	10	10	11
Birch Wood							
Tensile-Adhesion Strength (lb/in.^{2})	1100[b,c]	960[b,c]	1180[b,c]	1020[b,c]	400[c]	170[c]	340[c]
Standard Error (lb/in.^{2})	66	39	42	16	15	45	13
Coefficient of Variation (%)	19	14	14	5.3	12	26	12
Number of Specimens	10	12	16	8	9	9	10
Hard Rubber							
Tensile-Adhesion Strength (lb/in.^{2})	590[d]	400	1340[b]	130	320	130	240
Standard Error (lb/in.^{2})	50	26	50	4	32	18	7
Coefficient of Variation (%)	27	20	12	11	31	44	12
Number of Specimens	10	9	10	10	10	10	18

a. A specimen with a contact area of 1 square inch was used unless otherwise noted.

b. Specimens failed partly in adherend.

c. Contact area 0.5 square inch.

d. Contact area 0.25 square inch.

which were relatively weak in the static-strength tests were superior in resistance to impact. This behavior is most pronounced for the aluminum specimens. The average impact strength of the neoprene-bonded aluminum specimens for flatwise and edgewise testing was about 1 ft-lb compared with 0.17 ft-lb or less with polyvinyl-acetate cement, a factor of 6 or more in favor of the neoprene adhesive. In contrast, the tensile-adhesion and shear-strength values for the neoprene with aluminum alloy are about one tenth of the values for specimens bonded with polyvinyl acetate.

Likewise, the wood-impact specimens, bonded with natural rubber and resorcinol adhesives, had impact strengths of 0.6 and 0.4 ft-lb, respectively, in edgewise tests and 0.17 and 0.08 ft-lb, respectively, in flatwise tests. In the static tests with wood specimens, the resorcinol-resin adhesive was 2 to 10 times as strong as the rubber cement.

Theoretical Aspects

It is of interest to consider the results of these tests on the relative strengths of various adhesive-adherend combinations with respect to the nature of the interface. A knowledge of the physical and chemical nature of the surfaces involved is necessary to establish the type of bond formation which may occur (8). Several types of bonds are recognized as factors in adhesion: (*a*) Electrostatic or polar bonds which are formed in the actual transfer of electrons from one atom to another; (*b*) covalent bonds which are the type encountered in diatomic elements and most organic compounds; (*c*) co-ordinate covalent bonds which are weaker than the true covalent type and are exemplified by

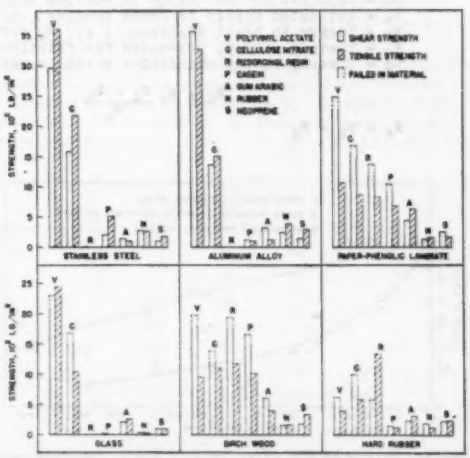

FIG. 10 COMPARATIVE BOND-STRENGTH VALUES GROUPED ACCORDING TO ADHEREND USED

TABLE 5 LONG-TIME LOADING SHEAR DATA FOR VARIOUS ADHESIVE-ADHEREND COMBINATIONS[a]

Adherend	Adhesive	Width, in.	Overlap, in.	Stress, psi	Time to failure, hr
Paper-phenolic laminate.....	Polyvinyl acetate	1.00	0.50	2480	Static test[b]
		0.075	0.51	660	2½
		0.102	0.51	480	36
		0.220	0.50	230	1080
Birchwood	Polyvinyl acetate	0.98	0.52	1990	Static test[b]
		0.069	0.52	1600	1/20
		0.102	0.52	1070	2
		0.102	0.52	1070	2½
		0.067	0.50	750	2½
		0.160	0.52	660	4
		0.106	0.51	500	168
		0.12	0.48	460	48
		0.100	0.55	450	30
		0.162	0.52	300	13
Birchwood	Resorcinol resin	0.99	0.52	1940	Static test[b]
		0.081	0.51	1360	65[b]
		0.102	0.51	1070	219[b]
		0.077	0.48	680	4320 (6 months without failure)

[a] A double-lap tensile-type specimen was used.
[b] Partial failure in adherend.

TABLE 6 IMPACT-STRENGTH DATA FOR ADHESIVE-ADHEREND COMBINATIONS[a]

Adherend	Adhesive	Energy to Break Specimens, W_b (ft-lb)	Wood Failure (%)	Tossing Energy, W_c (ft-lb)	Tossing Energy Correction, W_d (ft-lb)	Impact Strength, W_e (ft-lb)
		EDGEWISE IMPACT TESTS				
Birch Wood	Polyvinyl Acetate	0.241	0	0.040	0.034	0.207
	Resorcinol Resin	0.428	50	0.040	0.031	0.397
	Gum Arabic	0.152	0	0.044	0.040	0.112
	Rubber	0.618	80	0.042	0.028	0.590
Aluminum Alloy	Polyvinyl Acetate	0.210	0	0.041	0.036	0.174
	Neoprene	0.985	0	0.042	0.021	0.964
		FLATWISE IMPACT TESTS				
Birch Wood	Polyvinyl Acetate	0.163	3	0.041	0.037	0.126
	Resorcinol Resin	0.116	65	0.040	0.037	0.079
	Gum Arabic	0.065	0	0.044	0.042	0.023
	Rubber	0.208	45	0.042	0.037	0.171
Aluminum Alloy	Polyvinyl Acetate	0.106	0	0.043	0.040	0.066
	Neoprene	0.056	0	0.045	0.021	1.035

a. The quantities in the table are defined as follows:
W_o = Capacity of that range of machine being used.
W_a = Indicated energy to break specimen, i.e., not corrected for friction and windage losses.
W_b = Energy to break specimen, i.e., W_a corrected for friction and windage losses.
W_c = Tossing energy, corrected for friction and windage losses.
W_d = Tossing energy correction which is assumed to be as follows:

$$W_d = W_c \frac{W_o - W_a}{W_o}$$

$$W_e = W_b - W_d$$

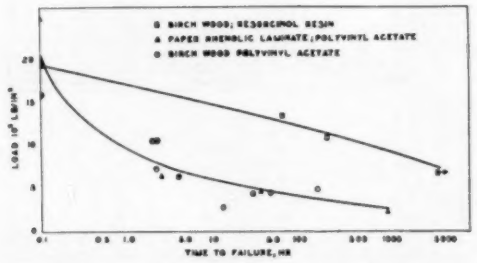

FIG. 11 EFFECT OF LONG-TIME SHEAR LOAD ON THERMOPLASTIC (POLYVINYL-ACETATE) AND THERMOSETTING (RESORCINOL-RESIN) ADHESIVES

hydrogen bridging; (*d*) Van der Waal's forces which consist of molecular attractions operating over greater distances than those involved in the formation of primary valence bonds. Specific adhesive bonds may be attributed to any of the foregoing factors or to various combinations of them.

It might be expected that when secondary forces are involved, the polarity of the materials at an interface would be a predominant factor in the strength of the bond between them. It is known that the force between molecules with high dipole moments is greater than that between molecules with low or no dipole moments. The dielectric constant can be used as a relative measure of the polarity or dipole moment. Consequently, adhesive-adherend combinations in which the sum of the dielectric constants is high should have high strength, provided that the interfacial surfaces are clean.

Measurements of the dielectric constants of specimens of the

materials used in this project were made by the Inductance and Capacitance Section of the National Bureau of Standards. The resorcinol resin had an unexpectedly high dielectric constant for which no explanation is known (rechecked with second specimen). Dielectric-constant measurements of the metals were not possible because of their conducting nature. Metal structure is relatively homogeneous and nonpolar. However, because of its freely flowing electrons, a metal has mirror-image forces induced at its surfaces which are equal and opposite to the polar forces in the adhesive used with it (15). Therefore, in so far as polar properties are concerned, an adhesive should have as great an affinity for a metal as it would have for a material of like polarity.

Since all the adhesives were applied in a liquid or solution form, the dipoles present were free to orient themselves while setting, according to the influence of any forces present in the adherends. In Table 7 the double-lap shear strengths of the various adhesive-adherend combinations are shown with the adhesives and adherends arranged according to increasing dielectric constants. The double-lap shear strength values were used because for this type of specimen the strongest grain direction was used for wood and paper-phenolic laminate. These values would then be a closer approach to the actual bond strength since cohesive failures play a smaller role in this test. This table does not show that the polar forces involved played any dominating part in the adhesive strength. The higher adhesive strengths are not concentrated in the regions where the sums of the dielectric strengths are higher. Rather, the higher shear strengths are distributed over a wide range of dielectric constants.

When the values in the columns of Table 7 are averaged horizontally and vertically, four values stand out. These are the values for polyvinyl acetate and cellulose nitrate of the adhesives, and for wood and paper-phenolic laminate of the adherends. Polyvinyl acetate has the highest value with five of the six adherends. If the bond strengths correlated with dielectric constant, the strengths of the combinations made with cellulose nitrate should be superior to those made with polyvinyl acetate. The average values for all combinations for these two adhesives are the reverse of that expected on this basis. The combinations with cellulose nitrate are second highest with four of the six adherends and first with hard rubber.

Except for the value of casein with birchwood, the values for the combinations of polyvinyl acetate and cellulose nitrate are consistently higher with all the adherends than for any of the other adhesives. The reason for this can probably be found in their thermoplastic properties. These properties allow them to form an ideal bond, one which is bubble-free and strain-free, and which retains enough flow to compensate for temperature differentials. Thus fuller use is made of the existing attractive forces since they are not modified so much by the mechanical factors involved in adhesion and testing as is the case with thermosetting adhesives.

Birchwood and paper-phenolic laminate, while not so strong as the metals, have consistently high values with a greater range of adhesives. This is illustrated in their higher over-all averages. Here again the respective polarities, as represented by the dielectric constants, do not seem to be the deciding factors. Neoprene with a fairly high dielectric constant has consistently low strength values with all the adherends. Birchwood and paper-phenolic laminate have properties which allow them to accommodate a wide range of adhesives. These two materials have a larger effective surface area and more attractive groups for the adhesives than the other adherends.

Adhesives had very poor adhesion to paper-phenolic laminate unless its surface was sanded. This sanding may tend to expose cellulose fibers similar to the wood fibers.

Since the rigidity of the materials may have a bearing on the results, the double-lap shear strengths of the various adhesive-adherend combinations are shown in Table 8, with the adhesives and adherends arranged according to the moduli of elasticity in tension. For birchwood the modulus of elasticity varies from 80,000 psi perpendicular to the grain to 2,000,000 psi parallel to the grain. The modulus of elasticity of gum arabic could not be found in the literature but was assumed to be of the order of that of casein. The value for resorcinol resin was assumed to be similar to that for unfilled phenolic resin.

The values in Table 8 seem to have a more definite correlation than those in Table 7. Where the modulus values of both adhesive and adherend are low, the strength values are low. Combinations of high-modulus materials also give low strength values. Combinations which include at least one material of medium modulus exhibit the highest strengths. Natural rubber and neoprene are soft materials and in testing assemblies containing them a concentration of stresses is produced at the bond between the soft highly elongated rubber adhesive and the hard slightly elongated adherend when low loads are applied. When both adhesive and adherend have high modulus values, neither material flows sufficiently during the final stages of the bonding process to relieve the stresses developed when the adhesive layer shrinks on cooling (16) and drying (17). Resorcinol-resin combinations with glass and the metals are good illustrations of the incompatibility of high-modulus materials.

Several metal-to-metal adhesives now available commercially make the best use of their inherent strong adhesive forces not by attempting to change the polarity but by adjusting the physical properties. These adhesives are sometimes known as mixed phenolic-elastomer type. The rigidity of the phenolic-resin base

TABLE 7 DOUBLE-LAP SHEAR-STRENGTH VALUES VERSUS DIELECTRIC CONSTANTS OF THE ADHESIVES AND ADHERENDS[a,b]

	Hard rubber 2.91, psi	Stainless steel, psi	Aluminum alloy, psi	Birch wood 5.2, psi	Stainless steel, psi	Aluminum alloy, psi	Glass 7.74, psi	Paper-phenolic laminate 9.14, psi	Stainless steel, psi	Aluminum alloy, psi	Average, psi
Natural rubber 3.10	190	270	250	160			43	130			170
Polyvinyl acetate 3.61	630	2960	3560	1990			2310	2480			2320
Cellulose nitrate 5.9	1000			1390	1580	1360	1680	1680			1450
Casein 7.18	150			1680	190	120	29	1030			530
Neoprene 10.42	230			180			160	230	90	130	180
Gum arabic 16.1	240			630			210	440	130	330	330
Resorcinol resin 450–480	590			1940			0	1370	0	0	650
Average	430			1140			620	1050	750[c]	820[c]	

[a] Values under materials are their dielectric constants.
[b] Because metals have mirror-image forces induced at their surfaces which are equal and opposite to the polar forces of the adhesives, stainless steel and aluminum alloy are distributed along the horizontal axis of the table in accordance with the dielectric constants of the adhesives used with them.
[c] Average shear-strength value for all adhesives with this metal.

TABLE 8 DOUBLE-LAP SHEAR-STRENGTH VALUES VERSUS MODULI OF ELASTICITY OF ADHESIVES AND ADHERENDS*

	Hard rubber 500,000 psi	Birch-wood 80,000 to 2,000,000 psi	Paper-phenolic laminate 2,100,000 psi	Glass 10,000,000 psi	Aluminum alloy 10,000,000 psi	Stainless steel 25,000,000 psi	Average, psi
Natural rubber 250	190	160	130	43	230	270	170
Neoprene 250	230	180	250	100	130	90	160
Cellulose nitrate 200,000–400,000	1000	1390	1680	1680	1360	1580	1450
Polyvinyl acetate 350,000–400,000	630	1980	2480	2310	3360	2960	2320
Gum arabic	240	630	440	210	330	130	330
Casein 540,000	150	1660	1030	29	120	190	530
Resorcinol resin 700,000–1,000,000	590	1940	1370	0	0	0	650
Average	430	1140	1050	620	820	750	

* Values underneath materials are their moduli of elasticity in pounds per square inch.

is modified by the addition of rubberlike materials. The combination gives a compound with desired properties such as proper modulus of elasticity and heat resistance, without affecting appreciably the attractive forces of the ingredients. The resulting adhesives are used to bond practically anything which can withstand the pressures and temperatures necessary for their application.

Strong bonds produced by adhesives at ordinary temperatures are not necessarily permanent under all conditions. Turner (16) has shown that when the temperatures are reduced large stresses are produced with rigid materials which have different coefficients of thermal expansion. These stresses serve to counteract the attractive forces producing the bond. Rigid adhesives may be either thermosetting types or thermoplastic types below their "second-order transition points." Thermoplastic types above this transition temperature flow sufficiently to reduce markedly the stresses induced by thermal-expansion action. Turner has also shown a method for formulation of plastic compositions to reduce the stresses for rigid materials by reducing the differences in coefficients of thermal expansion.

In this project the adhesive-adherend combinations were studied in the simplest possible form. The types of adhesives and adherends used covered a rather wide range. The attractive forces involved and the mechanical factors hindering adhesion also covered a wide range.

The problems involving a fundamental investigation of adhesion may be classified as follows: (*a*) Characteristics of the bond interfaces; (*b*) factors affecting contact such as cleanliness and wetting; (*c*) effect of physical properties of the materials themselves. Some specific problems indicated as a result of this work are as follows: (*a*) A more detailed study of the polarity theory; (*b*) the mechanism of bond rupture; (*c*) methods for producing clean surfaces; (*d*) wetting characteristics; (*e*) effect of modulus of elasticity on strength measurements; and (*f*) effect of flow characteristics.

Conclusions

From an investigation of the strength properties of various adhesive-adherend combinations to determine some aspects of the nature of adhesion, the following conclusions can be drawn:

1 The tensile-adhesion and shear strengths for a given adhesive-adherend combination did not differ greatly except for wood and paper-phenolic laminate, which are nonisotropic.

2 The highest values for tensile-adhesion and shear strengths were obtained with polyvinyl-acetate and cellulose-nitrate adhesives. These two adhesives caused failure in the adherends, except in the case of the two metals, stainless steel and aluminum alloy. The strength values varied from 1360 to 3600 psi with the metals, and from 400 to 2480 psi with the nonmetallic materials.

3 Resorcinol resin and casein gave strength values ranging from 590 to 1940 psi with hard rubber, paper-phenolic laminate, and birchwood, materials of low to medium modulus. They have very little or no adhesion for glass and the metals.

4 Natural rubber, neoprene, and gum arabic adhered to all the adherends, but the strength values were consistently low, ranging from 34 to 630 psi.

5 Comparative long-time load tests demonstrated the superiority of a thermosetting adhesive over a thermoplastic adhesive for supporting structural loads. The resorcinol resin showed no appreciable flow in supporting a load of 680 psi for 6 months without failure, whereas the polyvinyl acetate failed in 45 days under a load of 200 psi.

6 The rubber-type adhesives which were weak compared with the other adhesives in the static load tests were definitely superior in the impact tests.

7 Better correlation of shear strengths was found with the moduli of elasticity than with the dielectric constants of the materials used in the various adhesive-adherend combinations.

8 Further investigation of the surface chemistry involved is needed to obtain a better understanding of the nature of adhesion. Furthermore, physical factors, such as modulus properties, thermal expansion, and flow characteristics, may modify or completely nullify the effect of attractive forces between adhesives and adherends.

Acknowledgment

This investigation, performed at the National Bureau of Standards, was sponsored by and conducted with the financial assistance of the National Advisory Committee for Aeronautics.

The courtesy of the Allegheny Ludlum Steel Corporation, Arabol Manufacturing Company, Carbide and Carbon Chemicals Corporation, Casein Company of America, E. I. du Pont de Nemours and Company, Inc., Hercules Powder Company, and Pennsylvania Coal Products Company in furnishing materials for use in this investigation is gratefully acknowledged.

Bibliography

1 "List of Publications on Glue and Plywood," Anon, Mimeograph No. 513, Forest Products Laboratory, U. S. Department of Agriculture, August, 1944.

2 "Wood Aircraft Assembly Glues," by A. P. Dowling, *Modern Plastics*, vol. 23, September, 1945, pp. 156–158.

3 "Adhesives—New Materials and Practices," by B. P. Gray, *Plastics*, vol. 22, April, 1945, pp. 126, 200.

4 "Metlbond—A Metal Adhesive for Aircraft," by G. G. Havens, *Mechanical Engineering*, vol. 66, 1944, pp. 713–714 and 736.

5 "Use of Glue in Aircraft Construction," by J. T. Stephan, *Aviation*, vol. 42, March, 1943, pp. 132–133, 311, 313, 315–316 and 319–320.

6 "Reports of the Adhesives Research Committee 1, 2, and 3," by J. W. McBain, et al., H. M. Stationery Office, London, England, 1922, 1926, and 1932.

7 "Nature of Adhesion Between Glue and Wood," by F. L. Browne and D. Brouse, *Industrial and Engineering Chemistry*, vol. 21, 1929, p. 74.

8 "Survey of Adhesives and Adhesion," by R. C. Rinker and G. M. Kline, NACA TN No. 989, 1945.

9 "Gluing of Paper-Base Phenolic Plastic," Anon, Report No. WD-11101, Boeing Airplane Company, September, 1943.

10 "Specification for Gluing Paper-Base Phenolic Plastic," Anon, Report No. WD-11102, Boeing Airplane Company, October, 1943.

11 "The Gluing of Laminated Paper Plastic (Papreg)," Anon, Mimeograph No. 1348, Forest Products Laboratory, U. S. Department of Agriculture, January, 1944.

12 "Effect of Sanding Birch and Maple Surfaces Upon the Strength of the Glue Joint," Anon, Report No. W.E. 185-8-1, Curtiss Research Laboratory, August, 1943.

13 "Compounding and Processing of Neoprene Type GN," Anon, Report No. 42-2, E. I. du Pont de Nemours and Company, Inc., May, 1944.

14 "Tentative Method of Test for Tensile Properties of Adhesives," ASTM Committee D-14 on Adhesives, August 28, 1944.

15 "The Adsorption of Gases and Vapors," by S. Brunauer, vol. 1, Physical Adsorption, Princeton University, Princeton, N. J., 1943.

16 "The Problem of Thermal-Expansion Stresses in Reinforced Plastics," by P. S. Turner, NACA ARR, June, 1942.

17 "Fairing Compositions for Aircraft Surfaces," by P. S. Turner, Jewel Doran, and F. W. Reinhart, NACA TN No. 958, 1944.

Dynamic Shear Properties of Rubberlike Polymers

By I. L. HOPKINS,[1] NEW YORK, N. Y.

A simple apparatus for determining the dynamic properties of elastomers in shear at audio frequencies is appraised. Typical values of shear modulus and viscosity for several elastomers are given, both at room conditions and at 150 F. The frequencies of test range from 100 to 5250 cycles per second, the shear moduli from 0.5 × 10^6 to 480 × 10^6 dynes per sq cm and the viscosities from 20 to 75,000 poises.

Introduction

AMONG other means for measuring the dynamic elastic modulus and viscosity, or related properties, of elastomers, is the measurement of the effect of the elastomer on the resonant frequency and breadth of the resonant peak of some tuned mechanical system to which it is coupled. H. C. Rorden and A. Grieco[2] have described an apparatus according to this scheme, in which specimens of elastomers are coupled in shear to the prongs of tuning forks. The present paper describes this test in greater detail, presents typical data obtained with it, and discusses it analytically.

Test Apparatus and Materials

Apparatus. A diagrammatic sketch of the apparatus is given in Fig. 1, and the appearance of the equipment is shown in Figs. 2 and 3. The vernier condenser mounted on top of the oscillator is calibrated in terms of the change in frequency, at any given frequency, as a function of vernier dial change.

The apparatus used is given in Table 1.

TABLE 1 APPARATUS USED IN TESTS

Tuning fork	Mode	Frequency	Position	Effective mass, grams
		Hewlett-Packard oscillator—201B		
100~	1	99.1	S[a]	675
			L[b]	5140
	2	1238	S	114
			L	291
250~	1	249.1	S	914
			L	30500
	2	1584	S	93
			L	983
400~	1	398.2	S	334
			L	12100
	2	2420	S	50
			L	434
900~	1	897.3	S	215
			L	4170
?	2	5247	S	36
			L	438

[a] Position nearer free end of prongs.
[b] Position nearer base of prongs.

The difference between the nominal and actual frequencies at the first mode are due to the loading of the pads. These were of steel 0.25 in. × 0.30 in. × 1/16 in., and were fastened to the forks with Cycleweld. The faces of the pads were then ground coplanar. The effective masses of the forks are discussed in the Appendix. The following were also used:

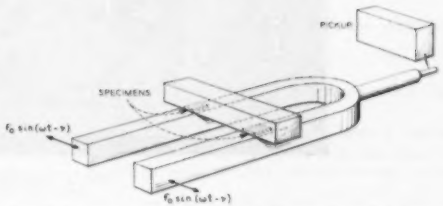

FIG. 1 DIAGRAM OF TUNING FORK WITH DRIVING FORCE, SPECIMENS AND PICKUP

Pickup—Rochelle salt crystal; ammonium dihydrogen phosphate crystal for 150-deg tests; moving coil.

Ballantine model 220 decade amplifier and model 300 a-c electronic voltmeter.

Cathode-ray oscilloscope.

One set earphones, with plug to match jack in voltmeter. These were invaluable in determining the sources of disturbance causing stray pickup.

The forks were held by their shanks, with short pieces of soft-gum-rubber tubing between the shanks and the clamps. These permitted free longitudinal motion of the shank, to the end of which the pickup was applied. Some care is necessary to insure that the whole fork in the rubber mounting does not have a resonance peak near the first or second-mode peak.

Specimens. The specimens were 0.20 in. × 0.25 in. in area and varied from 0.010 in. to 1/32 in. thick. It was necessary that the faces be flat and parallel within close limits in order that contact over the entire face be obtained, and in cases where the specimen had unsatisfactory faces or was too thick, one or both of the faces were ground. No adhesive was used between the specimens and the fork or the bridging bar, but by careful cleaning of the metal parts and the specimen with alcohol, or by water if alcohol was inadvisable, some of the specimens were made to stick lightly to the metal in the way that newly molded rubber sometimes will.

The following materials were tested:

1 Butyl rubber gum M169A, with 10 min cure at 60 psi steam.
2 Butyl rubber gum M169C, with 10 min cure at 60 psi steam.
3 Hevea rubber gum (formula unknown).
4 Silicone rubber gum.
5 Silicone rubber—filled.
6 Polypropylene sebacate
7 Plasticized cellulose nitrate.
8 Polyvinyl chloride acetate.
9 X6 polymerized tung oil.
10 X7 polymerized tung oil with dispersed polysiloxane liquid.

[1] Bell Telephone Laboratories, Inc.
[2] Memorandum, Bell Telephone Laboratories.

Contributed by the Rubber and Plastics Division and presented at the Fall Meeting, Worcester, Mass., September 19–21, 1950, of THE AMERICAN SOCIETY OF MECHANICAL ENGINEERS.

NOTE: Statements and opinions advanced in papers are to be understood as individual expressions of their authors and not those of the Society. Manuscript received at ASME Headquarters on July 21, 1950. Paper No. 50—F-24.

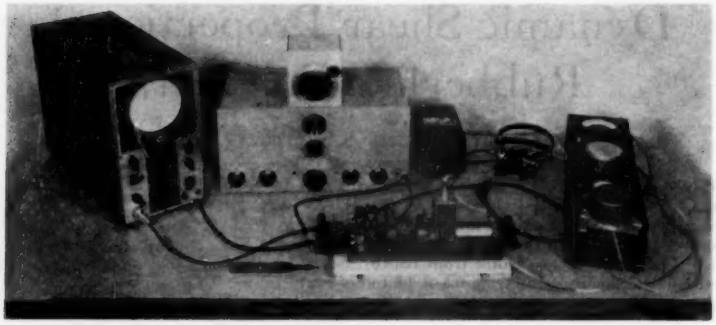

FIG. 2 GENERAL VIEW OF APPARATUS

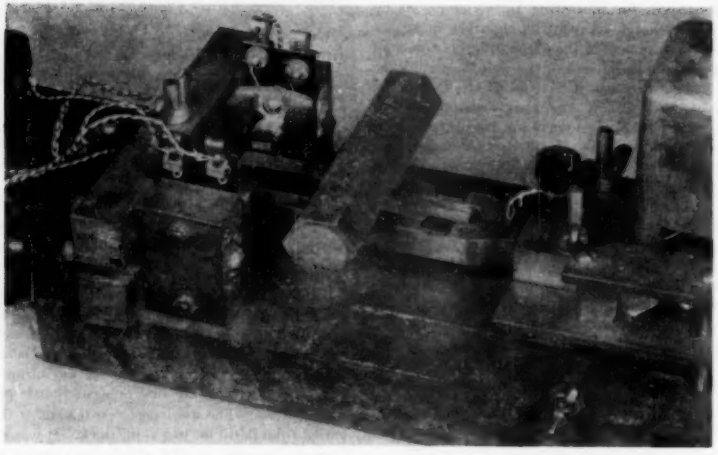

FIG. 3 CLOSE-UP VIEW OF TUNING FORK WITH ASSOCIATED EQUIPMENT

The compositions of these materials, in so far as we know them, are as follows:

Butyl rubber M169A	
GRI	100
Tuads	1.5
Captax	1
Agerite powder	0.5
Zinc oxide	5
Stearic acid	1
Sulphur	2.5
	111.5

Butyl rubber M169C—similar to M169A with 40 parts Kosmobile 77 black.

Paracon AP12. Probably propylene glycol sebacate, compounded with carbon black, and peroxide or sulphur-cured.

X6, crosslinked tung oil—a conjugated glyceride.

X7, ×6 with 30 per cent by weight of polydimethyl siloxane liquid dispersed in it.

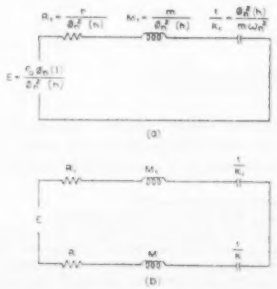

FIG. 4 ELECTRICAL CIRCUITS ANALOGOUS TO (*a*) UNLOADED AND (*b*) LOADED FORKS

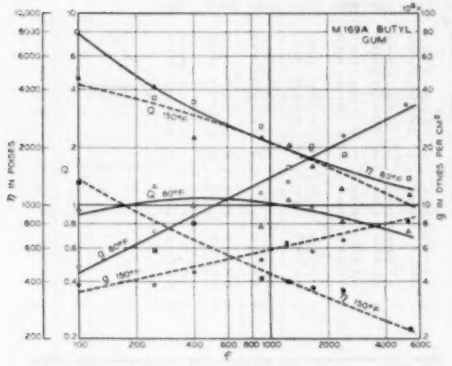

FIG. 5 DYNAMIC SHEAR PROPERTIES OF BUTYL RUBBER GUM M169A, AS A FUNCTION OF FREQUENCY

Method of Test. The oscillator was turned on about 1 hr before starting the tests to reach temperature equilibrium. The pads and bridging bar were cleaned with alcohol, and the specimens were dipped in alcohol or water and dried on filter paper. The oscillator was adjusted for resonance of the unloaded fork with the vernier dial near the low end of the scale. Vernier dial changes for 3-decibel (db) detuning each side of resonance were read. Then the specimens were put in place with the bridging bar and similar readings made. Usually the specimens were removed, replaced, and reread for a total of five readings. The choice of the *S* or *L* position in the fork was usually forced on the operator, the loading being too great for the *S* position, or the vernier-dial changes being too slight in the *L* position.

Tests were made at room conditions (70–80 F) and at 150 F.

RESULTS OF TESTS

The results of the tests are given in Tables 2 to 4, and in Figs. 5 to 14.

Discussion. If the shear modulus *g*, the viscosity η, and the phase constant *Q* are plotted against frequency, the scatter of points about smooth curves is manifest. Sources of error include the following:

1 Phase difference throughout the specimen.
2 Imperfect velocity response of pickup.
3 Uncertainty of exact size of specimen.
4 Imperfect adhesion to the fork or bridging bar.
5 Imperfect calibration of forks.
6 Errors in measurements of frequency changes.
7 Temperature variations.

TABLE 2 TEST RESULTS, MODULUS OF RIGIDITY *g*, DYNES PER CM²

(All values to be multiplied by 10^8)

Material	Frequency, cycles per sec: 100	250	400	900	1240	1580	2420	5250
AT 80 DEG F								
M169A butyl gum	4.8	7.3	8.8	11.6	13.1	19.7	23	33
M169C filled butyl	52	52	49	87	86	94	109	147
Hevea rubber gum	3.0	3.9	3.6	3.8	3.4	4.4	5.0	5.5
Silicone rubber gum	0.5	0.7	0.8	...	...	0.8	...	...
Filled silicone rubber	20	17	19	24	24	24	35	27
Polypropylene sebacate	10.4	10.3	11.8	12.0	17.5	13.0	15.6	18.0
Plasticized cellulose nitrate	65	66	61	106	115	134	124	254
Polyvinyl chloride acetate	12.6	17.2	21	...	38	30	...	94
X6 polymerized tung oil	..	59	60	50	...	169	142	379
X7 polymerized tung oil with dispersed polysiloxane liquid	..	83	87	67	...	234	227	477
AT 150 DEG F								
M169A butyl gum	3.9	3.9	4.5	5.1	6.4	5.7	6.6	8.2
M169C filled butyl	38	22	29	33	48	45	43	83
Hevea rubber gum	3.5	3.6	3.8	4.0	4.6	4.6	5.1	5.1
Silicone rubber gum	0.7	0.9	0.9	...	...	1.1	...	...
Filled silicone rubber	11.3	9.3	12.1	12.0	15.8	15.5	20	20
Polypropylene sebacate	4.5	5.3	5.6	6.2	9.2	7.3	10.8	7.9
Plasticized cellulose nitrate	6.0	8.0	9.7	10.6	17.3	12.1	14.5	38
Polyvinyl chloride acetate	6.8	7.3	6.4	7.4	8.3	9.7	10.6	10.6
X6 polymerized tung oil	12.6	16.3	16.2	40	42	29	46	81
X7 polymerized tung oil with dispersed polysiloxane liquid	10.5	17.5	18.2	29	45	41	51	163

TABLE 3 VISCOSITY, η, POISES

Material	Frequency, cycles per sec: 100	250	400	900	1240	1580	2420	5250
AT 80 DEG F								
M169A butyl gum	8000	3700	3500	2600	1550	2010	1840	1380
M169C filled butyl	34000	13100	10400	8300	4900	5500	4400	3000
Hevea rubber gum	350	240	177	116	55	68	60	43
Silicone rubber gum	300	126	106	...	...	53	...	...
Filled silicone rubber	4100	2300	1370	720	480	420	410	180
Polypropylene sebacate	5700	2600	1790	780	740	540	380	300
Plasticized cellulose nitrate	78000	28000	15200	10200	8700	7300	5500	5600
Polyvinyl chloride acetate	23000	6300	5500	...	3500	2400	...	3500
X6 polymerized tung oil	...	38000	23000	7600	..	11700	7500	8100
X7 polymerized tung oil with dispersed polysiloxane liquid	...	50000	32000	11000	..	10100	9700	9100
AT 150 DEG F								
M169A butyl gum	1320	590	810	420	400	270	380	220
M169C filled butyl	11400	3300	2900	2400	1980	1590	1060	1340
Hevea rubber gum	730	340	190	94	57	55	41	24
Silicone rubber gum	270	160	78	...	...	43	...	...
Filled silicone rubber	3100	1150	1050	420	330	290	220	100
Polypropylene sebacate	2600	1300	820	450	420	350	300	220
Plasticized cellulose nitrate	6400	2700	2200	2600	1920	1110	840	1130
Polyvinyl chloride acetate	2300	910	610	280	330	350	270	190
X6 polymerized tung oil	17300	8400	4400	3400	4000	3400	3300	2100
X7 polymerized tung oil with dispersed polysiloxane liquid	23000	10300	5900	4000	5300	4600	3500	3800

TABLE 4 MECHANICAL PHASE CONSTANT, Q

Material	Frequency, cycles per sec 100	250	400	900	1240	1580	2420	5250
At 80 Deg F								
M169A butyl gum	1.0	1.3	1.0	0.8	1.1	1.0	0.8	0.7
M169C filled butyl	2.5	2.5	1.9	1.9	2.3	1.7	1.6	1.5
Hevea rubber gum	13.6	10.4	8.2	5.8	7.9	6.5	5.5	3.9
Silicone rubber gum	2.7	3.5	3.0	...	...	1.5	...	...
Filled silicone rubber	7.8	4.7	5.5	5.9	6.4	5.8	5.6	4.5
Polypropylene sebacate	2.9	2.5	2.6	2.7	3.0	2.4	2.7	1.8
Plasticized cellulose nitrate	1.3	1.5	1.6	1.8	1.7	1.9	1.5	1.4
Polyvinyl chloride acetate	0.9	1.7	1.5	...	1.4	1.3	1.3	0.8
X6 polymerized tung oil	...	1.0	1.0	1.2	...	1.5	1.5	1.4
X7 polymerized tung oil with dispersed polysiloxane liquid	...	1.1	1.1	1.1	....	2.3	1.5	1.6
At 150 Deg F								
M169A butyl gum	4.7	4.2	2.2	2.2	2.1	1.6	1.2	1.1
M169C filled butyl	5.3	4.2	4.0	2.4	2.6	2.8	2.7	1.9
Hevea rubber gum	7.6	6.8	7.8	8.4	7.1	8.4	8.2	6.5
Silicone rubber gum	4.1	3.6	4.6	...	...	2.6	...	...
Filled silicone rubber	6.4	5.1	4.6	5.0	5.9	5.4	6.0	6.1
Polypropylene sebacate	2.8	2.6	2.7	2.4	2.8	2.1	2.4	1.1
Plasticized cellulose nitrate	1.5	1.4	1.8	0.7	1.2	1.1	1.1	1.0
Polyvinyl chloride acetate	4.3	5.1	4.2	4.7	3.2	2.8	2.6	1.7
X6 polymerized tung oil	1.2	1.2	1.5	2.1	1.6	0.9	0.9	1.2
X7 polymerized tung oil with dispersed polysiloxane liquid	0.7	1.1	1.2	1.3	1.4	0.9	1.0	1.3

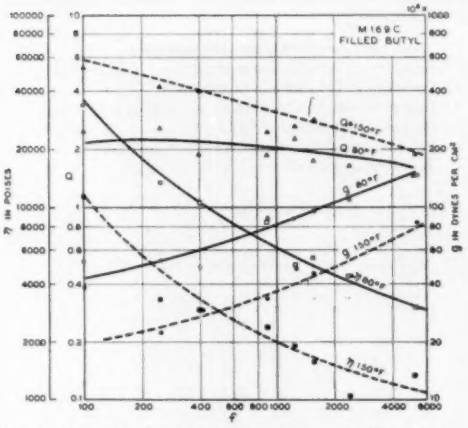

FIG. 6 DYNAMIC SHEAR PROPERTIES OF LOADED BUTYL RUBBER M169C, AS A FUNCTION OF FREQUENCY

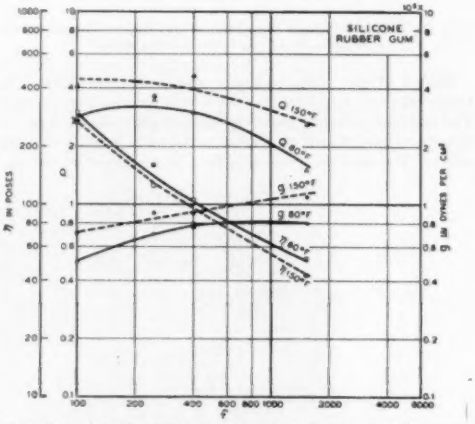

FIG. 8 DYNAMIC SHEAR PROPERTIES OF SILICONE RUBBER GUM AS A FUNCTION OF FREQUENCY

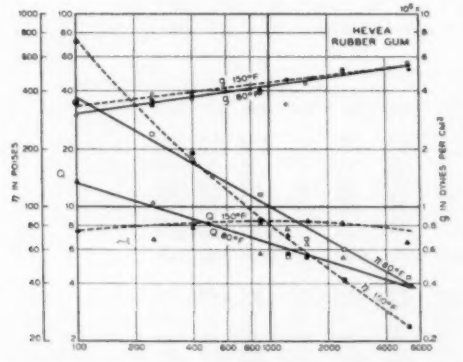

FIG. 7 DYNAMIC SHEAR PROPERTIES OF HEVEA RUBBER GUM AS A FUNCTION OF FREQUENCY

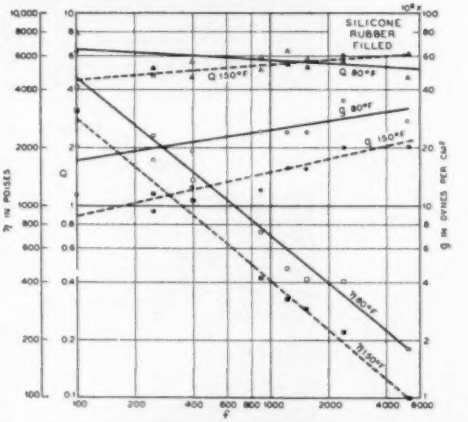

FIG. 9 DYNAMIC SHEAR PROPERTIES OF LOADED SILICONE RUBBER AS A FUNCTION OF FREQUENCY

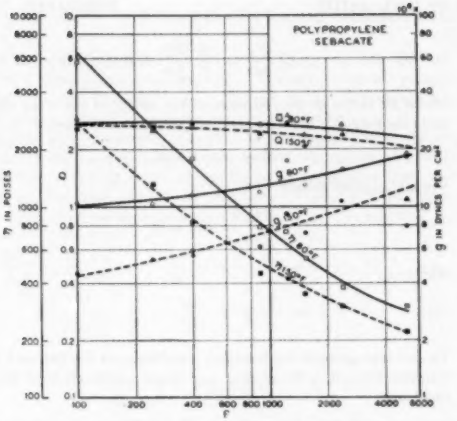

FIG. 10 DYNAMIC SHEAR PROPERTIES OF POLYPROPYLENE SEBACATE AS A FUNCTION OF FREQUENCY

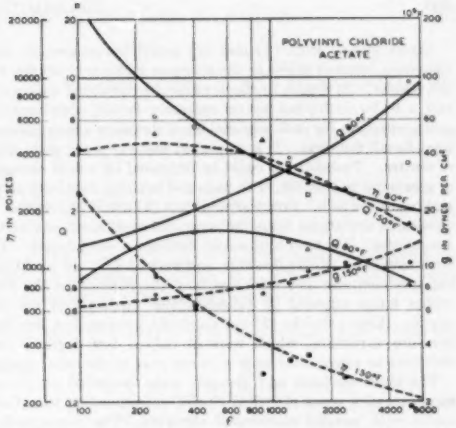

FIG. 12 DYNAMIC SHEAR PROPERTIES OF POLYVINYL CHLORIDE ACETATE AS A FUNCTION OF FREQUENCY

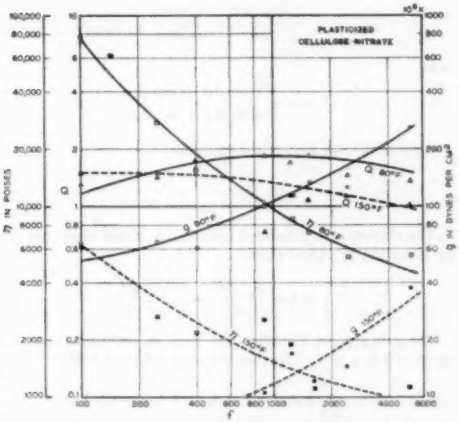

FIG. 11 DYNAMIC SHEAR PROPERTIES OF PLASTICIZED CELLULOSE NITRATE AS A FUNCTION OF FREQUENCY

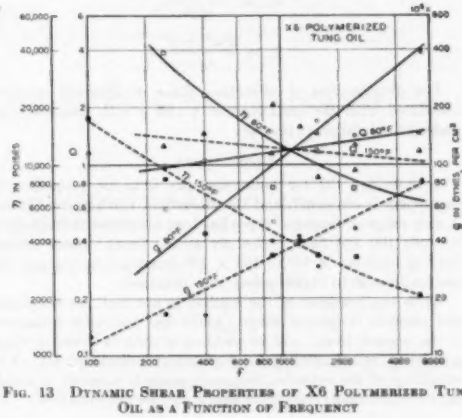

FIG. 13 DYNAMIC SHEAR PROPERTIES OF X6 POLYMERIZED TUNG OIL AS A FUNCTION OF FREQUENCY

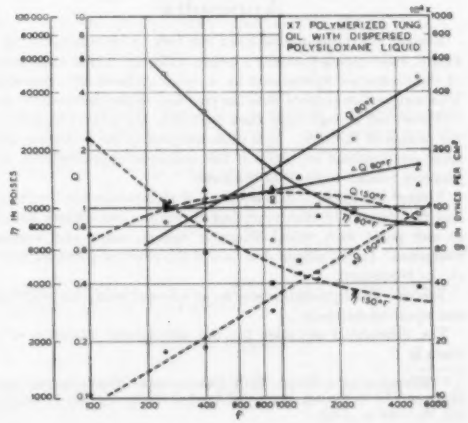

FIG. 14 (*right*) DYNAMIC SHEAR PROPERTIES OF X7 POLYMERIZED TUNG OIL WITH DISPERSED POLYSILOXANE LIQUID AS A FUNCTION OF FREQUENCY

Errors arising from (1) and (2) would be progressive with frequency, causing errors in the shape or location of curves, but not scatter; (3) would, in effect, cause the calculated values of η and g to be multiplied by an unknown factor, approximating unity, constant for each material since the same specimens were used for all the tests. It is suspected that (4) is the main cause of scatter. Probably (4) could be improved by actual clamping of specimens to the fork, with pads and bridging bars both above and below the fork. Errors arising from (5) would be revealed by consistent deviations from the mean curve at some one of the frequencies. No such systematic deviations were found. The error caused by (6) is calculable, and may be kept low by adjusting specimen size and thickness, and the position on the fork, within limits imposed by considerations discussed in the Appendix. Errors due to (7) are no doubt present, but the temperature variations, which were of only a few degrees, were sufficient to account for only a minor part of the total scatter.

The shear modulus and viscosity were computed on the assumption of a series electrical circuit, corresponding to a Voigt model with parallel mechanical elements. The corresponding Maxwell elements are given by

$$\eta_m = \frac{\eta^2\omega^2 + g^2}{\eta\omega^2}$$

$$g_m = \frac{\eta^2\omega^2 + g^2}{g}$$

The distributions of relaxation times of Maxwell elements associated with the variations of η and g with frequency are under consideration at present.

Conclusions

A technique (2) for measuring the dynamic properties of elastomers is discussed, and its theoretical validity established. A wide range of elastomer types has been measured at frequencies between 100 and 5250 cycles per second (cps). Shear moduli varying from 0.5×10^6 to 480×10^6 dynes per sq cm, and viscosities from 20 to 75,000 poises, were obtained.

While the precision of the method is not high, its simplicity and possible frequency range (which has not been exhausted in the present tests), and its yielding of data in terms of shear properties, recommend it for exploratory measurements. The advantage of the extended frequency range is manifest in avoiding the short-range conclusion that g and $\omega\eta$ are constants.

Appendix

Rorden and Grieco considered the fork to be equivalent to a simple mass-spring-viscosity system, with the added impedance of the elastomer represented by a series stiffness and viscosity. This assumption implied that the coupling of the elastomer to the fork does not change more than negligibly the forms assumed by the prongs of the fork. It is demonstrated in the following that these assumptions are valid if the specimen characteristics are properly related to those of the forks.

Young[3] has given a development of expressions for the forms and frequencies in free vibration of uniform cantilevers loaded at any point with combinations of spring, mass, and viscous resistance. It is a simple step to add the effect of a driving force at any frequency.

Young's development proceeds as follows, using his notation and equation numbers.

The differential equation for the free lateral vibration of a beam is

$$EI\frac{\partial^4 y}{\partial x^4} + \frac{m}{l}\frac{\partial^2 y}{\partial t^2} = 0 \quad \ldots\ldots [1]$$

where EI is the section stiffness of the beam, m the total mass, and l the length. We may assume a solution of the form

$$y = u(x)\sin\omega t$$

when $u(x)$ must satisfy

$$\frac{d^4u}{dx^4} - \beta^4 u = 0 \quad \ldots\ldots [2]$$

where

$$\beta^4 = \frac{m\omega^2}{lEI} \quad \ldots\ldots [3]$$

Taking into account the boundary conditions at the free and the clamped ends, it is found that any linear combination of the φ functions

$$\varphi_n(x) = \cosh\beta_n(x) - \cos\beta_n(x) - \alpha_n(\sinh\beta_n x - \sin\beta_n x) \quad [9]$$

will satisfy Equation [2], and hence

$$\frac{d^4\varphi_n(x)}{dx_4} = \beta^4\varphi_n(x) \quad \ldots\ldots [10]$$

also

$$\alpha_n = \frac{\cosh\beta_n l + \cos\beta_n l}{\sinh\beta_n l + \sin\beta_n l} \quad \ldots\ldots [8]$$

and $\beta_n l$ is the nth root of the equation

$$\cos\beta l = -\frac{1}{\cosh\beta l}$$

The corresponding natural frequencies of the beam are given by Equation [3], from which

$$\omega_n^2 = \frac{\beta_n^4 EIl}{m} = \frac{(\beta_n l)^4 EI}{ml^3} \quad \ldots\ldots [11]$$

The φ-functions, Equation [9], form an orthogonal set in the interval $0 \le x \le l$. The two following relations hold

$$\left.\begin{aligned} &\int_0^l \varphi_n(x)\,\varphi_m(x)\,dx = 0 \;(m \neq n) \\ &\int_0^l [\varphi_n(x)]^2\,dx = l \end{aligned}\right\} \quad \ldots\ldots [12]$$

and almost any function $f(x)$ in the interval 0 to l may be represented by a linear series of φ-functions, that is

$$f(x) = \sum_{n=1}^{\infty} a_n\,\varphi_n(x) \quad \ldots\ldots [13]$$

By virtue of Equations [12], the coefficients a_n are given by

$$a_n = \frac{1}{l}\int_0^l f(x)\,\varphi_n(x)\,dx \quad \ldots\ldots [14]$$

In particular, for a concentrated force F applied at $x = h$

$$a_n = \frac{1}{l}\int_0^l F\,\varphi_n(x)\,dx = \frac{F}{l}\,\varphi_n(h) \quad \ldots\ldots [17]$$

Then

$$F(x) = \frac{F}{l}\sum_1^{\infty}\varphi_n(h)\,\varphi_n(x) \quad \ldots\ldots [18]$$

[3] "Vibration of a Beam With Concentrated Mass, Spring, and Dashpot," by D. Young, *Journal of Applied Mechanics*, Trans. ASME, vol. 70, 1948, p. A-65.

With this development, as given by Young, we can now set up the equation for displacement of the beam, driven at any point at any frequency, and coupled to an impedance at any point. Equation numbers henceforth are our own.

Considering distributed damping of the beam due to air as $(r/l)\ (dy/dt)$ per unit length, that the beam is driven at $x = l$ by a force $f_0 \sin(\omega t - \gamma)$, is coupled to an impedance which results in a loading on the beam $f_1 \sin(\varphi t - \delta)$ at $x = h$, and that the beam vibrates in phase with $\sin \omega t$, we have the equation

$$EI\frac{\partial^4 y}{\partial x^4} + \frac{m}{l}\frac{\partial^2 y}{dt^2} + \frac{r}{l}\frac{\partial y}{\partial t} = -f_0 \sin(\omega t - \gamma) + f_1 \sin(\omega t - \delta) \quad [19]$$

Let

$$y = w(x) \sin \omega t$$

$$EI\frac{d^4 w}{dx^4}\sin \omega t - \frac{m\omega^2}{l} w \sin \omega t + \frac{r}{l}\omega w \cos \omega t = -\frac{f_0}{l}\sin(\omega t - \gamma)\sum_1^\infty \varphi_n(l)\varphi_n(x) + \frac{f_1}{l}\sin(\omega t - \delta)\sum_1^\infty \varphi_n(h)\varphi_n(x) \quad [20]$$

Letting $w(x) = \sum_1^\infty b_n \varphi_n(x)$, the left side of Equation [20] becomes

$$EI \sin \omega t \sum_1^\infty b_n \frac{d^4\varphi_n(x)}{dx^4} - \frac{m\omega^2}{l}\sin \omega t \sum_1^\infty b_n \varphi_n(x) + \frac{r}{l}\omega \cos \omega t \sum_1^\infty b_n \varphi_n(x)$$

By use of Equations [2] and [10] in the first term

$$m \sin \omega t \sum_1^\infty b_n \varphi_n(x)\omega_n^2 - m\omega^2 \sin \omega t \sum_1^\infty b_n \varphi_n(x) + r\omega \cos \omega t \sum_1^\infty b_n \varphi_n(x) = -f_0 \sin(\omega t - \gamma)\sum_1^\infty \varphi_n(l)\varphi_n(x) + f \sin(\omega t - \delta)\sum_1^\infty \varphi_n(h)\varphi_n(x) \quad [21]$$

Expanding the $\sin(\omega t - \gamma)$ and $\sin(\omega t - \delta)$ terms and equating coefficients of $\sin \omega t$ and $\cos \omega t$ terms, respectively, in the usual way

$$\left.\begin{aligned} b_n m(\omega_n^2 - \omega^2) &= -f_0 \varphi_n(l)\cos\gamma + f_1 \varphi_n(h)\cos\delta \\ b_n r\omega &= f_0 \varphi_n(l)\sin\gamma - f_1 \varphi_n(h)\sin\delta \end{aligned}\right\} \quad [22]$$

Now if the force $f \sin(\omega t - \delta)$ is the reaction to driving an impedance consisting of a mass M, a stiffness k, and a viscous component R with a displacement $y = w(h)\sin \omega t$

$$-f_1 \sin(\omega t - \delta) = w(h)(-M^2\omega \sin \omega t + R\omega \cos \omega t + k \sin \omega t)$$

whence

$$\left.\begin{aligned} f_1 \sin\delta &= R\omega w(h) \\ -f_1 \cos\delta &= (k - M\omega^2)\, w(h) \end{aligned}\right\} \quad [23]$$

Substituting Equations [23] in [22] and eliminating γ

$$f_0^2\varphi_n^2(l) = b_n^2[r^2\omega^2 + m^2(\omega_n^2 - \omega^2)^2] + 2b_n\varphi_n(h)\, w(h)[m(\omega_n^2 - \omega^2)(k - M\omega^2) + r\omega^2 R] + \varphi_n^2(h)w^2(h)[R^2\omega^2 + (k - M\omega^2)^2] \quad [24]$$

which is a quadratic in b_n. Solving for b_n and reducing somewhat gives

$$\left.\begin{aligned} b_n &= -\varphi_n(h)\, w(h)\,[m(\omega_n^2 - \omega^2)(k - M\omega^2) + r R\omega^2]/r^2\omega^2 + m^2(\omega_n^2 - \omega^2)^2 \\ &\pm \frac{\sqrt{f_0^2\varphi_n^2(l)\,[r^2\omega^2 + m^2(\omega_n^2 - \omega^2)^2] - \varphi_n^2(h)\, w^2(h)\,[r\omega(k - M\omega^2) - mR\omega(\omega_n^2 - \omega^2)]^2}}{r^2\omega^2 + m^2(\omega_n^2 - \omega^2)^2} \end{aligned}\right\} \quad [25]$$

Substituting this value of b_n in

$$w(h) = \sum_1^\infty b_n \varphi_n(h)$$

dividing both sides of the resulting equation by $w(h)$, and replacing $\varphi_n(l)$ by its value ± 2

$$\left.\begin{aligned} 1 = \sum_1^\infty \varphi(h) \sqrt{\frac{4 f_0^2}{w^2(h)}[r^2\omega^2 + m^2(\omega_n^2 - \omega^2)^2] - \varphi_n^2(h)\,[r\omega(k - M\omega^2) - mR\omega(\omega_n^2 - \omega^2)]^2} \\ - \varphi_n^2(h)\,[m(\omega_n^2 - \omega^2)(k - M\omega^2) + r R\omega^2] \\ \hline r^2\omega^2 + m^2(\omega_n^2 - \omega^2)^2 \end{aligned}\right\} \quad [26]$$

Equations [25] and [26], while containing the desired relations between applied force, frequency, and resulting motion, are too complicated to be useful. Simplifications may, however, be effected. In the first place, while

$$w(h) = \sum_1^\infty b_n \varphi_n(h)$$

in general, the total motion at and near any of the resonance frequencies ω_n, may be represented by

$$w(h) = b_n \varphi_n(h)$$

provided $\varphi_n(h)$ be not extremely small. Substituting this in Equation [25] we find

$$b_n = \frac{f_0 \varphi_n(l)}{\sqrt{[R\omega\varphi_n^2(h) + r\omega]^2 + [\varphi_n^2(h)(k - M\omega^2) + m(\omega_n^2 - \omega^2)]^2}} \quad [27]$$

for the displacement coefficient, and

$$b_n \omega = \frac{f_0 \varphi_n(l)}{\sqrt{[R\varphi_n^2(h) + r]^2 + \left[\varphi_n^2(h)\left(\frac{k}{\omega} - M\omega\right) + m\left(\frac{\omega_n^2}{\omega} - \omega\right)\right]^2}} \quad [28]$$

for the velocity coefficient. Differentiating Equation [28] with respect to ω, we find the velocity resonance to occur at

$$\omega_{res}^2 = \frac{\omega_n^2 + \frac{k\varphi_n^2(h)}{m}}{1 + \frac{M\varphi_n^2(h)}{m}} \quad [29]$$

With the unloaded fork, where $k = M = R = 0$

$$\omega_{res} = \omega_n$$

and

$$\omega b_n = \frac{f_0 \varphi_n(l)}{r}$$

If detuned to 3 db below the peak

$$\omega b_n = \frac{f_0 \varphi_n(l)}{\sqrt{2}\, r} = \frac{f_0 \varphi_n(l)}{\sqrt{r^2 + m^2\left(\frac{\omega_n^2}{\omega} - \omega\right)^2}}$$

which is satisfied by two values of ω, differing by

$$\Delta\omega_1 = \frac{r}{m} \quad [30]$$

With the coupled impedance, assuming that M is negligible, resonance occurs at

$$\omega_{res}^2 = \omega_n^2 + \frac{k\varphi_n^2(h)}{m}$$

which may be solved for

$$k = \frac{m(\omega_{res}^2 - \omega_n^2)}{\varphi_n^2(h)} \quad [31]$$

and we find that at 3 db below the peak, the values of ω are separated by

$$\Delta\omega = R\frac{\varphi_n^2(h)}{m} + \frac{r}{m} \quad [32]$$

From Equations [30] and [32]

$$R = \frac{m}{\varphi_n^2(h)}(\Delta\omega_2 - \Delta\omega_1) \quad [33]$$

It may be remarked that Equation [28] is the equation for current in a series circuit shown in Fig. 4. The equivalent mass and rigidity of the fork at any points (h) are given by

$$\frac{m}{\varphi_n^2(h)}, \text{ and } \frac{m\omega_n^2}{\varphi_n^2(h)}$$

respectively. While these may be computed, neglect of shear and rotation terms in the theory, and nonuniformity and end effects in the prongs of the forks make it preferable to measure $m/[\varphi_n^2 h]$ directly by adding small known weights to the prongs at $x = (h)$ and using Equation [29] with $k = 0$.

The use of Equation [28] instead of [26] involves neglect of all modes except the desired one. To form an estimate of the extent to which this is permissible, and assuming that it is the broadening of the resonance peak due to R rather than its shifting due to k, which may introduce appreciable error, we revert to Equation [26] with $r = k = M = 0$

$$1 = \Sigma \frac{\varphi_n(h)\sqrt{\frac{4f_0^2}{v^2(h)} - R^2\omega^2\varphi_n^2(h)}}{m(\omega_n^2 - \omega^2)}$$

$$= \frac{1}{m\omega_1}\Sigma \frac{\frac{\omega}{\omega_1}\varphi_n(h)\sqrt{\frac{4f_0^2}{V^2(h)} - R^2\varphi_n^2(h)}}{\left(\frac{\omega_n}{\omega_1}\right)^2 - \left(\frac{\omega}{\omega_1}\right)^2} \quad [34]$$

where $V(h) = \omega v(h)$ is the velocity. At resonance

$$\frac{4f_0^2}{V^2(h)} = R^2\varphi_n^2(h)$$

At 3 db below the peak

$$\frac{4f_0^2}{V^2(h)} = 2R^2\varphi_n^2 h$$

whence, by substitution in Equation [34]

$$\frac{\pm R}{m\omega_1} = \frac{1}{\left(\frac{\omega}{\omega_1}\right)\Sigma \frac{\varphi_n^2 h}{\left(\frac{\omega_n}{\omega_1}\right)^2 - \left(\frac{\omega}{\omega_1}\right)^2}} \quad [35]$$

from which $R/(m\omega_1)$ may be plotted as a function of ω in the vicinity of the resonance peaks under consideration. There will be two values of ω for each value of R, and their difference $\Delta\omega$ may be compared with that derived from Equation [33], for any given set of conditions.

It was found that while the error from this source was less than 1 per cent for any testable specimen, the choice of a location on the fork too near a node, possible for the sake of testing very stiff specimens, might lead to inaccuracy.

Correction for Finite Length of Specimen. The coupled impedance was presumed to act at the point $x = h$. Actually, it is distributed over a distance, over which $\varphi_n^2(x)$ may vary appreciably. If R, k, and M are distributed over the length from $h - \epsilon$ to $h + \epsilon$, spanning 2ϵ, instead of $\varphi_n^2(h)$ we should have

$$\psi_n^2(x) = \frac{1}{2\epsilon}\int_{h-\epsilon}^{h+\epsilon} \varphi_n^2(x)\, dx$$

In the development of the expressions for the forced vibrations of the beam and $\psi_n^2(h)$, the assumption is implicit that the motion of the face of the cantilever is in a straight line. At a node, however, a point on the neutral axis is stationary, and this point is a center of oscillation for neighboring points. Therefore

a test specimen at a node would be in torsion, and the development given here would be inapplicable. Actually, the specimens were relatively far from the nodes for both modes of vibration.

Effect of Specimen Shape on Relation Between Measured Over-All Stiffness and Viscous Resistance, and Computed Modulus of Rigidity and Viscosity. After the stiffness k and the viscous resistance R of a specimen have been calculated, the modulus of rigidity g and viscosity η may be found by the usual expressions

$$g = \frac{kt}{A} \text{ and } \eta = \frac{Rt}{A}$$

where

t = thickness of specimen
A = area of specimen

There will be a slight error arising from the free edges of the specimens. A correction, however, may be applied.[4] With a specimen 0.20 in. × 0.25 in. with the 0.20-in. dimension in the direction of shear, the true values for g and η will be greater than given by the foregoing expressions by the following factors:

Thickness, in.	Factor	Thickness, in.	Factor
0.005–0.012	1.01	0.047–0.055	1.06
0.013–0.021	1.02	0.056–0.063	1.07
0.022–0.030	1.03	0.064–0.070	1.08
0.031–0.038	1.04	0.071–0.078	1.09
0.039–0.046	1.05	0.079–0.085	1.10

Effect of Rotation and Lateral Contraction of Bar. Referring to Mason,[5] it appears that the error in frequency arising from neglect of rotation and lateral contraction is not greater than 1 per cent in a beam whose ratio of width to length is less than 0.1. Therefore this factor is not considered.

Discussion

W. J. Lyons.[6] In its simplicity from the experimental standpoint, the method described by the author, for the measurement of dynamic properties, is remarkably ingenious. The very small amount of sample required for the test recommends it as a means for the dynamic evaluation of unknown stocks in rubber products already fabricated, especially in cases where there is insufficient volume of continuous, unreinforced stock in any part of the product to fashion the larger test specimens used in other dynamic-property tests.

While a number of methods for the measurement of the longitudinal (Young's) dynamic modulus, and the corresponding frictional effects, by electrically driven mechanical systems have been developed,[7] and have been augmented by the acoustical methods of Meyer and Lotmar, Silverman and Ballou, Nolle and others, until recently the only method for dynamic shear measurements on high polymers has been that of Dillon, Prettyman, and Hall.[8] A refinement of this method has recently been announced in England,[9] and apparatus adaptable to shear measurements on elastomers has been developed at the Textile Research Institute, Princeton, N. J. As the former two methods, at least, are limited in frequency to the range below 1000 cps, Rorden, Grieco, and Hopkins[3] have made a substantial contribution in providing a method which reaches to above 5000 cps.

It is of interest to note that Hopkins' values for g for Hevea gum rubber at 80 and 150 F, at 100 cps, (3.0 and 3.5 × 10^8 dynes per cm²) are in good agreement with those of Dillon, Prettyman, and Hall[8] at 100 C and 60 cps (3.06 to 3.22 × 10^8 dynes per cm²). Hopkins' viscosity (internal friction) values for Hevea gum appear to be of the same order of magnitude as those of Dillon, et al.,[10] but whereas the latter found that internal friction decreases with increasing temperature, the author's values increase with temperature up to 400 cps. His data (Table 2) show this effect for silicone rubber also, at one frequency, 250 cps. From the fact of comparatively few cases in which this effect appears in his results, one is led to wonder whether it is not merely an experimental artifact. The magnitude of the differences in viscosity of the Hevea gum at the two temperatures, at the two lower frequencies, 100 and 250 cps, implies either that the observed temperature influence is real in the sample tested, or the technique is seriously faulty at these frequencies.

Most of the prior research on shear properties of polymers have been on Hevea and the conventional superelastic synthetic stocks, such as those of GR-S. The number of other materials on which the author has obtained dynamic data have considerably amplified our knowledge of shear properties. It is of interest to examine his graphs for the light they throw on the viscosity-frequency relationship. As is well known, it has been long recognized that for polymers of all kinds, over limited frequency ranges, the viscosity-frequency product is approximately constant. The author's curves indicate that for none of the materials evaluated by him does this relationship hold over the whole range 100–6000 cps. For Hevea gum at 150 F, the relationship apparently holds above about 400 cps. For Hevea gum at 80 F, silicone rubber filled, and M169A butyl gum at 150 F (approximately), linear relationships between log viscosity and log frequency are deduced, but the slopes of the graphs are such that the simple hyperbolic law for viscosity and frequency is not implied. The viscosity results for these materials support the modified law recently announced by Fletcher and Gent,[9] in which a fractional power of the frequency appears, replacing frequency to the power unity.

A. W. Nolle.[11] The method described in the paper appears to offer some special advantages, of which the compactness of the test unit, the utilization of small samples, and the provision for accommodating a wide range of stiffness, may be mentioned particularly. The results appear to be in general agreement with those which have been obtained by other methods.

As the author suggests, it would seem that the test instrument might be improved by modification of the arrangement for attachment of samples. An arrangement providing a larger clamping force might be advantageous, especially if provision were made for application of arbitrary static stress to the sample as an additional experimental variable.

An interesting adjunct to the paper is found in a recent Japan-

[4] "Effect of Stress-Free Edges in Plane Shear of a Flat Body," by W. T. Read, Paper No. 50—APM-6 presented at the National Conference of the Applied Mechanics Division, Purdue University, Lafayette, Ind., June 22–24, 1950, of The American Society of Mechanical Engineers.

[5] "The Motion of a Bar Vibrating in Flexure, Including the Effects of Rotary and Lateral Inertia," by W. P. Mason, *The Journal of the Acoustical Society of America*, vol. 6, 1935, pp. 426–429.

[6] Chemical and Physical Research Laboratories, Firestone Tire and Rubber Company, Akron, Ohio.

[7] "Hysteresis and Methods for Its Measurement in Rubberlike Materials. Part 1," by J. H. Dillon and S. D. Gehman, *India Rubber World*, vol. 115, October, 1946, pp. 61–68 and 76.

[8] "Hysteretic and Elastic Properties of Rubberlike Materials under Dynamic Shear Stresses," by J. H. Dillon, I. B. Prettyman, and G. L. Hall, *Journal of Applied Physics*, vol. 15, 1944, pp. 309–323.

[9] "Measurement of the Dynamic Properties of Rubber," by W. P. Fletcher and A. N. Gent, Trans. Institution of the Rubber Industry, vol. 26, 1950, pp. 45–63.

[10] Reference (7), fig. 24.

[11] Department of Physics, University of Texas, Austin, Texas.

ese publication.[12] That publication describes a similar experiment in which a single vibrating cantilever is used instead of a tuning fork, and in which by several trials the operator deduces the proper value of added mass to "tune out" the stiffness reactance of the sample. The band width of the resonance measures mechanical resistance, as in the present method. The sample is connected for deformation by elongation.

For frequencies greater than about 10,000 cps, the tuning-fork vibrator may prove inconvenient because of rapid phase variation with distance. A longitudinally vibrating bar would constitute a satisfactory resonator for the higher range of frequencies. The author of this comment has described an experimental technique,[13] comparable in principle to the present one, which makes use of longitudinally vibrating bars and which is readily adaptable to shear measurements. In combination, the two techniques would cover a frequency range from less than 100 cps to more than 25 000 cps.

Author's Closure

Since the preparation of the paper, some improvements have been made in experimental technique. A second relatively stable comparison oscillator permits small frequency changes in the driving oscillator to be measured accurately by timing the pattern on the oscilloscope screen. This use of only small frequency changes is a considerable theoretical advantage and results in data which are more accurate than previously obtained.

The manifestation of higher viscosity in silicone gum at 150 F than at 80 F at 250 cycles is probable due to scatter, as this material was so soft as to be at the lower limit of measureability. It is interesting to observe, however, that the shear modulus is higher at 150 F than at 80 F, as is required by the kinetic theory, although the ratio is somewhat in excess of the value 339/300, or 1.13, required by the theory.

Reconsideration of the Hevea rubber gum leads to the belief that there may have been slippage between the rubber and the fork or bridging bar, particularly at the lower frequencies where the amplitude of motion is the greatest. This condition would be aggravated by the fact that the specimens were not only thinner than any of the others and therefore subject to greater strains at a given displacement, but also had no surface tackiness. There is some indication of increased modulus at 150 F but not to the extent required by the kinetic theory. It is planned to retest Hevea gum using somewhat thicker specimens of a known compound. The new tests should provide clarification of all of the doubtful features of the data on Hevea given above.

[12] "The New Dynamical Method for Measuring Young's Modulus and Internal Friction of Fibers and Films," by H. Kawai and N. Tokita, *Journal of the Physical Society of Japan*, vol. 5, 1950, p. 17.

[13] "Methods for Measuring Dynamic Mechanical Properties of Rubber-Like Materials," by A. W. Nolle, *Journal of Applied Physics*, vol. 19, 1948, pp. 754–774.

Metals for High-Pressure Hydrogenation Plants

By G. A. NELSON,[1] SAN FRANCISCO, CALIF.

Many of the important chemicals of today's industrial economy require processing in the presence of hydrogen, at elevated temperatures and pressures, at some stage in their manufacture. The more familiar ones are ammonia, methanol, edible oils, and higher alcohols. In the petroleum-refining field, hydrogenation processes are becoming more and more important. In the future it can be anticipated that greater need for hydrogenation processes may arise, for example, hydrodesulphurization of crude oils or fractions therefrom, hydrogenation of carbon monoxide (Fischer-Tropsch), and destructive hydrogenation of oil residues or coal (Bergius process). These processes operate at high temperatures and pressures, where ordinary steels have their limits for safe operation. Although high-alloy steels can be used under these conditions, oftentimes more reasonably priced low-alloy steels are satisfactory. This paper summarizes the results of tests and data from operating plants, from which it is possible to establish practical operating limits for carbon and alloy steels for all degrees of severity of service. Additional corrosive effects by sulphur, nitrogen, and carbon monoxide are discussed.

WHEN processes are started involving high-pressure hydrogenation, the mechanical engineer will be faced with many problems including hydrogen attack, corrosion, erosion, and high-temperature stability of materials.

The purpose of this paper is to review what we know about metals as used by the Shell group of companies and others in lower-pressure plants, and, in view of these experiences, to offer ideas as to materials which may be required as high-pressure plants become of increasing importance.

The gases with which we have had some experience are hydrogen, nitrogen, ammonia, and hydrogen sulphide. These gases are inert to most metals at normal temperatures and pressures. At low pressures, the gases can be heated to moderately high temperatures without any damaging effect on metals. Conversely, at normal temperatures these gases can be handled safely in carbon steel at very high pressures, and we find this material to be specified by the Interstate Commerce Commission for transportation in high-pressure cylinders. However, when both heat and pressure are applied, these gases may become violently active in either creating internal damage to the steel or actually corroding steel at a very rapid rate. The effects of these gases on metals as the result of our experiences, when hydrogen gas mixtures are being processed, will be discussed.

Hydrogen

Early experiences in handling of hot hydrogen showed numerous failures, and many reports of these troubles are available in the literature. Zapffe[2] has compiled an imposing list of 427 references dealing with various phases of the effects of hydrogen on metals.

The damage produced by exposure of steels to high-pressure hydrogen may be described as decarburization and intergranular cracking. Even though these cracks are so tiny that they become visible only when viewed under a microscope, they are so numerous that their net effect produces a marked deterioration of physical properties, such as tensile strength, yield point, and ductility. A severely attacked piece of steel has a tensile strength in the order of 25,000 psi, as compared to a normal strength of about 60,000 psi; and the elongation on a test bar is reduced to zero from a normal elongation of about 30 per cent in 2 in. The strength is roughly comparable to that of a weak piece of cast iron.

There actually is no corrosion or wasting away of metal when it has become affected by hydrogen damage. In fact, a slight growth occurs. In one of our plants, tubing (22 ft long) operating in a noncritical-stress location and therefore made of carbon steel, becomes about 1 in. longer over an operating period of 5 years. The absence of any appreciable dimensional changes of an affected piece of steel requires inspection methods other than visual or by direct measurement. However, bending, hardness, and macroetch tests readily reveal the presence of any affected areas. The microscope is also used to define clearly the presence of microscopic cracks.

Figs. 1 and 2 show the appearance of carbon steel before and after exposure to hydrogen at high pressure and temperature. The damaged section shows not only a complete decarburization, but also that small inclusions such as oxides and sulphides have been reduced by this gas while diffusing through the steel.

Fig. 3 shows the appearance of a tensile bar taken from a section of low-alloy pipe which had been partially damaged by hydrogen attack. The side of the bar that is cracked and exhibiting no ductility represents the inner side of the pipe in contact with hydrogen. The outer section of the pipe represented by the ductile portion of the bar is still in sound condition. In practice, it is not unusual to find samples of this type. It occurs in borderline temperature-pressure conditions, where the alloying elements in the steel may not be sufficient to render the steel completely resistant to hydrogen. However, because of the temperature gradient across the wall as one proceeds from the hot side, a zone in the cross section is eventually reached where the temperature is such that the alloy is entirely adequate.

In borderline cases, a change of a few degrees in temperature represents the difference between satisfactory performances or gradual failure. In some cases, where hydrogen attack has been found partially extending through the walls of piping or pressure vessels and spare equipment is not immediately available, it has been found expedient to remove the insulation from the affected parts. This lowers the temperature in the wall to stop any further attack and permits the plant to operate until replacement parts can be obtained.

Hydrogen damage at high pressures is attributed to the ability

---

[1] Staff Metallurgist, Shell Development Company.

Contributed by the Petroleum Division and presented at the Semi-Annual Meeting, St. Louis, Mo., June 19–23, 1950, of The American Society of Mechanical Engineers.

Note: Statements and opinions advanced in papers are to be understood as individual expressions of their authors and not those of the Society. Manuscript received at ASME Headquarters, March 9, 1950. Paper No. 50—SA-3.

[2] "Boiler Embrittlement," by C. A. Zapffe, Trans. ASME, vol. 66, 1944, pp. 81–126.

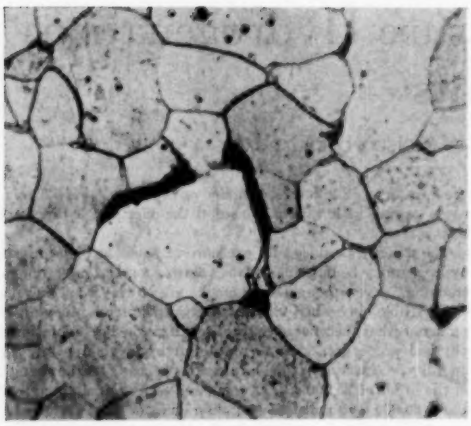

FIG. 1 LOW-CARBON STEEL BEFORE EXPOSURE

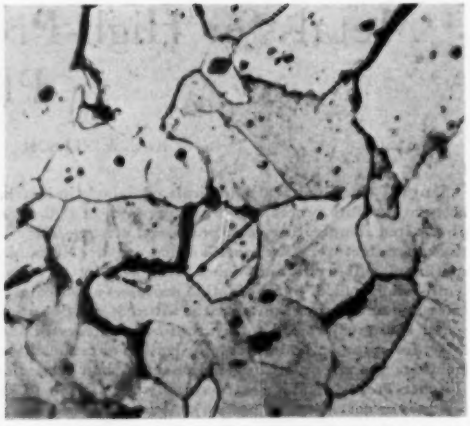

FIG. 2 LOW-CARBON STEEL AFTER EXPOSURE TO HYDROGEN

of the hydrogen to permeate the steel, resulting in the formation of methane by the reaction of hydrogen with the iron carbide. The methane which has been formed cannot diffuse out of the steel, and thereby gives rise to high stresses which lead ultimately to cracking at the grain boundaries. That methane is the ultimate reaction product has been demonstrated by F. K. Naumann[3] who showed that with a pure hydrogen gas entering a carbon-steel tube at high pressures and temperatures, appreciable amounts of methane were obtained at the exit end of the pipe.

The attack by hydrogen is prevented by adding to the steel any of the carbide-stabilizing elements. In ascending order of importance, they are manganese, molybdenum, chromium, tungsten, vanadium, titanium, and columbium. All of the austenitic steels are resistant because of their high chromium content. The noncarbide-forming elements, such as nickel and silicon, have no effect in preventing interior damage to the steel by hydrogen. The presence of impurities such as phosphides and sulphides has a tendency to increase attack; therefore the total amount of these elements should be kept below the minimum required by ASTM specifications.

As mentioned in the previous paragraph, carbide-stabilizing elements have the property of rendering a steel immune to hydrogen attack at high pressures and temperatures. However, plain carbon steel is also widely used and is perfectly safe as a constructional material, provided that the upper limit of temperature is known for a particular pressure condition. These limits have been determined by operators of hydrogenation plants, and as a result of a critical survey covering a wide range of pressures and temperatures, sufficient data have been accumulated to propose operating limits for carbon and alloy steels.[4]

The collected data from operating companies were assembled into chart form; and, by plotting borderline curves between satisfactory and unsatisfactory operating points, a clearer conception was obtained as to the suitability of carbon and alloy steels for a particular pressure-temperature condition. As the result of more experience, several adjustments to the curves were necessary, and a total of 22 revisions to the charts were made during a period of 7 years. The latest set of curves is illustrated

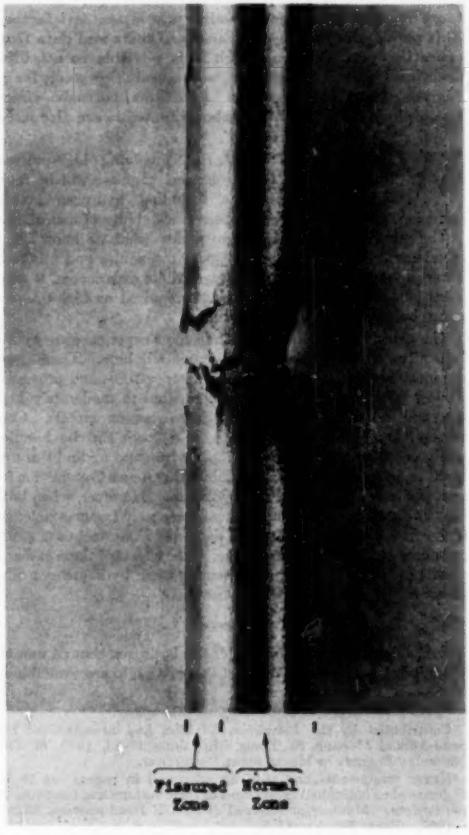

FIG. 3 APPEARANCE OF TENSILE-TEST BAR FROM HYDROGEN-AFFECTED LOW-ALLOY-STEEL TUBING

[3] "Steels for Fuel Plants," by F. K. Naumann, *Chemische Fabrik*, vol. 11, 1938, pp. 365–384.

[4] "Hydrogenation Plant Steels," by G. A. Nelson, American Petroleum Institute Procedings, Section 3, Division of Refining, 14th Mid-year Meeting, April 4–7, 1949, pp. 163–272.

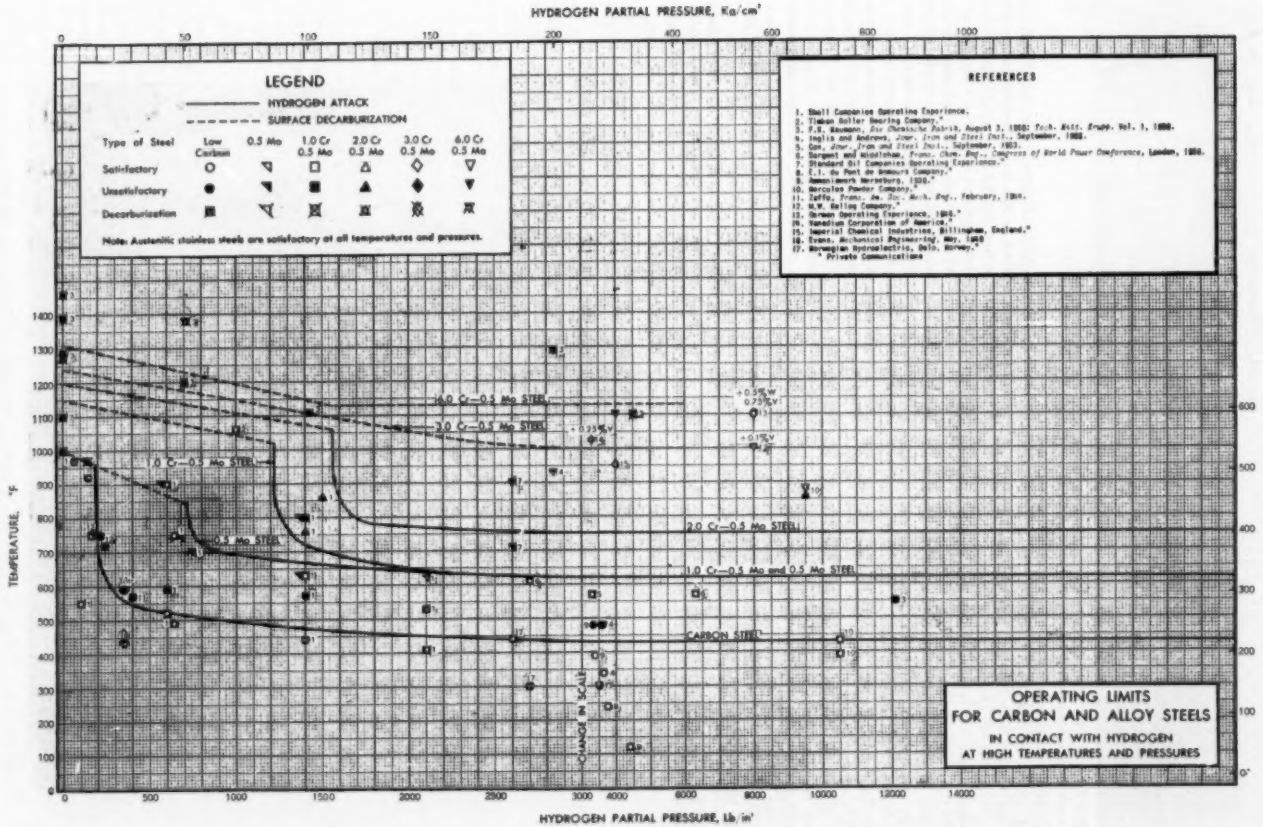

FIG. 4 OPERATING LIMITS FOR CARBON AND ALLOY STEELS IN CONTACT WITH HYDROGEN AT HIGH TEMPERATURES AND PRESSURES

in Fig. 4, and is presented with the expectation that further revisions will be required.

The curves in Fig. 4 have been plotted on the basis of hydrogen partial pressure. Some of the earlier charts had been prepared using references based upon the total plant-operating pressures. This led to some misunderstanding of the significance of the lines. As it was realized that hydrogen was the only component of a gas stream which could permeate the steel and create internal damage, all reference points were moved to correspond to the pressure exerted by the hydrogen alone. It is believed that the present form of presentation gives a much clearer idea of the materials to be used for a particular pressure-temperature condition.

The circumstances surrounding the locations of the curves shown in Fig. 4 might be described as follows: The high-pressure level for carbon steel (above 2600 psi) was located as a result of the advice of Standard Oil Development Company and Hercules Powder Company, which have used carbon steel in this temperature region for many years without failure; moreover, metallurgical examination of samples removed from the units showed no damage. The safe operating limits for carbon steel below 2600 psi were established from the experience of the Shell group, the revelations by Zapffe[2] and Evans,[3] M. W. Kellogg Company, and Standard Oil Company of California.

It may be of interest to note that, at 600 psi and 590 F, an unsatisfactory reference point for carbon steel is shown. The data surrounding this failure resulted from an inspection of a carbon-steel line which had been in operation in a Shell Oil Company plant for about 2 years. The particular line consisted of 6-in. schedule 160 carbon-steel piping, to which were attached by welding several smaller lines of 1 in., $1^1/_2$ in., and $2^1/_2$ in. schedule 160 carbon-steel pipe. Ring sections removed from the different sizes of pipe were hot-acid-etched, and Table 1 shows the damage to the walls from hydrogen.

TABLE 1 HYDROGEN DAMAGE TO CARBON-STEEL PIPING

Size of pipe	Wall thickness, in.	Per cent of wall affected
1-in. threaded nipple	0.280	0.0
$1^1/_2$-in. schedule 160	0.400	8.3
$2^1/_2$-in. schedule 160	0.555	50.0
6-in. schedule 160	0.848	35.0
6-in. schedule 160	0.873	80.0

These figures are cited to illustrate that variations in the practice of making steel may have a considerable effect on the ability of the particular steel to resist damage by hydrogen. It also indicates that, when plants are being inspected, a number of samples should be taken. In other words, using the foregoing example, if a sample had been taken only from the 1-in. nipple line, the entire line might have been passed as being satisfactory and would soon have failed. This conclusion was also reached by T. C. Evans,[3] who showed that, at 350 psi and 310 C, some samples of carbon steel were satisfactory, whereas others were severely damaged. In order to build plants to the upper limit of carbon steel, we must use steels from suppliers' stocks which may have a wide divergence of melting practice and, therefore, this material can be used only to the limit of the average quality of steels we can obtain. This has been the basis for the location of the carbon-steel curve.

Particular importance is being given to the upper limit of carbon steel. In hydrogenation plants, an example of which is shown in Fig. 5, all of the cold piping and equipment are made of

[3] "Hydrogen Attack on Carbon Steels," by T. C. Evans, *Mechanical Engineering*, vol. 70, 1948, pp. 414–416.

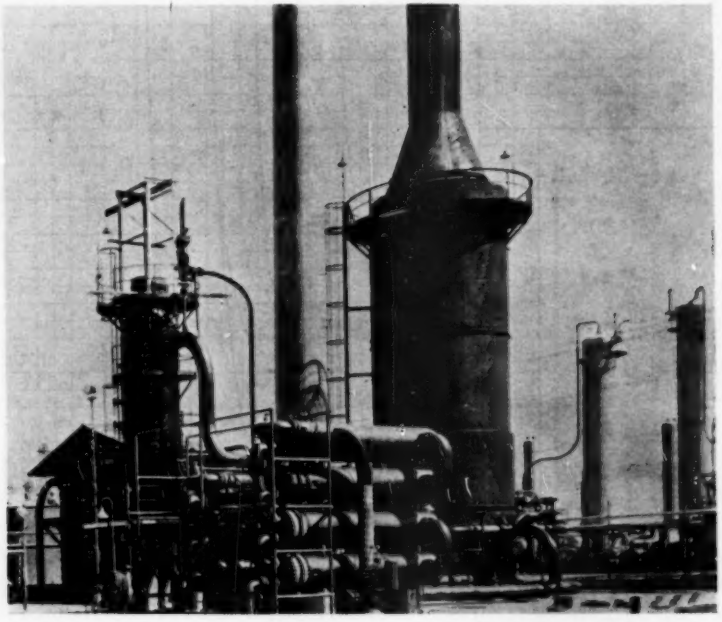

FIG. 5 VIEW OF HYDROGENATION PLANT SHOWING CARBON AND ALLOY-STEEL HEAT EXCHANGERS

FIG. 6 VIEW OF AMMONIA PLANT SHOWING USAGE OF CARBON STEEL

carbon steel. These include the compressor, purification, and some heat-exchange equipment. These pieces of equipment represent a considerable part of a hydrogenation plant, and it is necessary to protect by means of alloy steels only those parts of the plant where the limit for carbon steel is exceeded.

Another example of the wide usage of carbon steel is illustrated in Fig. 6. This is an ammonia plant operating at 2140 psi. Viewing the plant from right to left, all of the equipment (excluding low-temperature fractionating apparatus) in the background is constructed of carbon steel with the exception of equipment in the last building on the left. This building contains the catalyst chambers which are made of alloy steel, as are the accompanying exchangers and piping.

The carbon-molybdenum limiting curve has been established from samples taken from hydrogenation plants erected during the recent war. It is noted that no data are at present available for the extremely high-pressure region, and it is possible that the carbon-molybdenum curve may be somewhat altered in this area as the result of more experience.

The 1 per cent chrome-molybdenum curve is fairly well established with reference points. It might be stated that a number of chrome-vanadium steels (references 5 and 6 in Fig. 4), have been added at the high-pressure end of this curve. No data were available for the chrome-molybdenum steels at these pressures. However, from our experiences at one plant, which had operated at a pressure of 2140 psi, we found that, when the chromium was in the order of 1 per cent, chrome-vanadium and chrome-molybdenum steels had about the same resistance. Thus SAE 6120 and SAE 4120 were interchangeable for use as interior bolting materials. It seemed reasonable to insert these reference points to locate the chrome-molybdenum line.

In view of the equivalent resistance of vanadium and molybdenum when associated with chromium, it is felt that the entire set of curves could equally, or possibly better, apply to the chrome-vanadium steels. The reason for plotting the chart only as chrome-molybdenum steel is because we use large amounts of piping, and chrome-molybdenum analyses are available in many sizes of tube and pipe. It can be mentioned that many high-pressure vessels made of chrome-vanadium steel are giving satisfactory performance in hydrogenation plants.

The 2 per cent chrome-molybdenum line is not too well fortified by reference points.

The 3 per cent chrome-molybdenum, and the 6 per cent chrome-molybdenum lines have been extended only to 6000 psi. At pressures above 6000 psi and at high temperatures, information gleaned from reports of the technical oil missions covering wartime German experiences disclosed that both 3 per cent chrome-molybdenum, and 6 per cent chrome-molybdenum had to be fortified with other carbide formers, such as tungsten or vanadium, in order to make them hydrogen-resistant. The reference points for these steels are shown in the upper right-hand portion of the chart. Austenitic chrome-nickel steels could also have been used, but the tonnage required was too great for Germany's economy to take care of the high chromium and nickel contents.

The dashed lines at the tops of the hydrogen-attack curves indicate decarburization. This decarburization is not accompanied by intergranular fissuring, and the steels exhibit ductile properties with slightly lower than normal tensile strength—in this respect behaving much like steels which have been decarburized because of oxidation.

It was mentioned earlier in this paper that other elements than chromium and molybdenum also produced a sufficiently stable carbide which rendered a steel immune to hydrogen damage. During this investigation an attempt was made to evaluate the long-time performance of titanium, vanadium, and molybdenum steels when their alloy-to-carbon ratios were in proportion to the amount required to form a stable carbide. For these experiments, sets of small test bars were installed in reaction chambers of several companies. Unfortunately, the majority of operating conditions involved the complicating presence of ammonia, and the bars became nitrided. However, from microexaminations of the cores of these bars, it was indicated that steels would be free from hydrogen damage at extremely high pressures when the alloy-to-carbon contents were in the following proportions:

Titanium-to-carbon	= 4 to 1
Vanadium-to-carbon	= 5.7 to 1
Molybdenum-to-carbon	= between 30:1 and 60:1

HYDROGEN SULPHIDE AND SULPHUR

When other corrosives are in the process streams, the problem becomes more complicated, and additional measures may be required in order to fabricate apparatus which will be free from trouble. Our experience with sulphur is as follows: When sulphur is present, either as the element or as hydrogen sulphide, it has the ability to corrode either carbon steel or low-chromium steel when the temperature rises above 675 F. Sulphur corrosion is a scaling process and the ultimate reaction product is a layer of iron sulphide. If this layer becomes hard and clings tightly to the steel, it offers some resistance to further corrosion. This effect has been noted on transfer lines. However, in turbulent regions such as furnace piping and heat-exchanger tubes, the scale is jarred loose, with a consequent increase in corrosion.

The corrosion rate rises in relation to the amount of the sulphur in the stream, but a definite recommendation cannot be made as to the amount of alloy required to resist a given attack. As an example of the difference in metal composition required for varying sulphur contents, we might again refer to the heat exchangers shown in Fig. 5. Shell Oil Company had constructed two of these plants. In a plant on the West Coast which handles sweet crudes, the hot exchangers were made with 1 per cent chromium, 0.5 per cent molybdenum tubing. After 4 years the tubing in the hot exchangers had become affected by sulphur corrosion to the extent that they had to be replaced. The use of 5 per cent chromium, 0.5 per cent molybdenum tubing was considered adequate as a replacement material for a long life.

In a duplicate plant which had been erected in the Midwest and which was processing sour Texas crudes, it had been deemed advisable to construct the original tube bundles of 5 per cent chromium, 0.5 per cent molybdenum. These bundles failed after only 6 months in operation; and, for replacement tubing, 18 per cent chromium, 8 per cent nickel was required. The 18-8 tubing has now been in service for 4 years, and will probably be adequate. For complete resistance to sulphide attack, the high-alloyed steels, such as 12 per cent chromium or 18 per cent chromium, 8 per cent nickel, are required. These metals are frequently used as liner materials for reaction vessels and exchangers.

Nitrogen

Where nitrogen is also present with the hydrogen gas, it has been found that nitriding begins at temperatures above 850 F in a Shell ammonia plant operating at 2140 psi. This nitriding is typified by a thin, hard, brittle layer, and it occurs on steels containing more than 2 per cent chromium. Austenitic stainless steels are similarly affected. Its effect has not been of too great a consequence as it consists of a thin, hard, brittle case which usually extends to a depth no greater than $^1/_{32}$ in., even after prolonged exposure. Piping and heavy forgings have never failed as a result of nitriding.

However, a need exists for more information as to materials which will resist both hydrogen and nitrogen. Thin pieces of equipment such as expansion bellows, gaskets, heat-exchanger jackets, and the like, cannot operate with hard brittle layers present. Experiments are now in progress to determine the resistance to nitriding and hydrogen attack of high-nickel alloys such as Inconel, Hastelloys B and C, 15Cr-35Ni, and some of the special alloys developed during the war for high-temperature use in gas turbines.

For protection against nitriding, an alloy containing 16 per cent chromium, 15 per cent nickel, 3 per cent silicon, and 0.4 per cent carbon has been reported as satisfactory at 950 F and 12,000 psi. It is also understood that a high-nickel alloy containing 57 per cent nickel, 12 per cent chromium, and 1.7 per cent tungsten is used for converters in the Claude process of synthesizing ammonia. The life varies between 2000 and 20,000 hr, depending upon the quality of the casting.

Ihrig[6] recently reported the results of nitriding tests on chromium and austenitic stainless steels after being exposed to hydrogen-nitrogen mixtures at 13,000 to 15,000 psi, and at temperatures from 204 to 593 C. He concluded that although the austenitic chromium-nickel steels are the best for use at high pressures of hydrogen and nitrogen, care should be taken in the design of high-pressure vessels for such use, and advised that samples should be taken periodically to determine whether attack has been progressive.

[6] "Attack of Hydrogen-Nitrogen Mixtures on Steels," by H. K. Ihrig, *Industrial and Engineering Chemistry*, vol. 41, 1949, pp. 2516–2521.

Carbon Monoxide

Another element not ordinarily considered to have any effect at low pressures, but which develops into a severe corrosive at high pressures in the presence of hydrogen, is carbon monoxide. This gas at ordinary pressures is inert to most constructional materials even up to quite high temperatures. However, at high pressures, the corrosion is of such severity that special materials must be used, even though the temperature is quite low. While we have had no practical experience with carbon monoxide, the following relates the experiences in Germany. This summary was digested from several documents microfilmed by the Technical Oil Mission, describing pilot- and commercial-plant operations wherein carbon monoxide and hydrogen at high pressures were being handled.

Fig. 7 summarizes pilot-plant data from sheets obtained from the I. G. Farbenindustrie Ammonia Works (1943 I) Merseburg. The analyses of the metals tested are shown in Table 2. In an effort to evaluate possible metals of construction for high-pressure units containing mixtures of carbon monoxide and hydrogen, the chart shown in Fig. 8 has been prepared from the data in Fig. 7.

The tests were made in a 50/50 CO/H_2 mixture at pressures of 250 and 700 atm. An extremely severe corrosive condition was found to exist at both high and intermediate pressures at a temperature of 260 C (500 F). At this temperature mild steel corroded at rates up to 0.550 in. per year at 250 atm and 5.4 in.

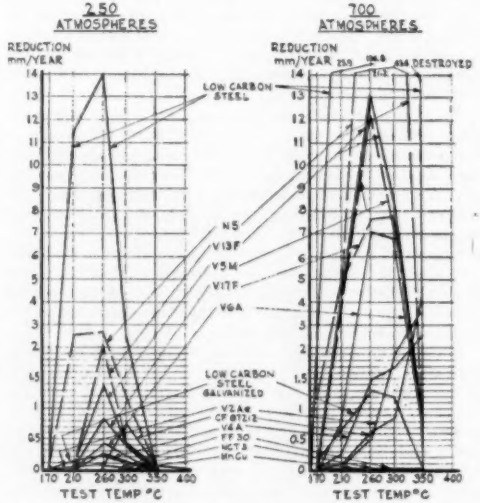

Fig. 7 Corrosion Rates by Carbon Monoxide at High Pressure in Presence of Hydrogen

TABLE 2 METALS USED IN CARBON MONOXIDE-HYDROGEN TESTS

Metal	Analysis C	Si	Mn	F	S	Cr	Ni	Mo	Ti	Cu	Fe	Sn
Mn bronze			5.1				0.3			94.1	0.2	0.1
FF30	0.35					30.25	0.20					
NOT3	0.09	2.4	0.7	0.023	Sp.	25.2	20.1					
V2A-extra	0.085					19.10	8.75		0.27			
V2A-extra	0.09					17.3	8.22		0.59			
V2A-normal	0.085					17.55	9.30					
V4A	0.106		0.40			17.5	9.20	2.30				
V6A	0.10	0.5	0.34			17.9	8.9			2.4		
Cf 87212	0.49	0.63	17.8			2.89	0.05					
V17F	0.08	0.60	0.58			16.2	0.20					
V13F	0.095	0.35	0.38	0.021	0.006	13.7	0.37	0.34				
V5M	0.17	0.46	0.52			13.9	0.57	0.24				
V5	0.12	0.25	0.75			3.36	0.08	0.30				
Low-carbon steel	0.09	Sp		0.016								

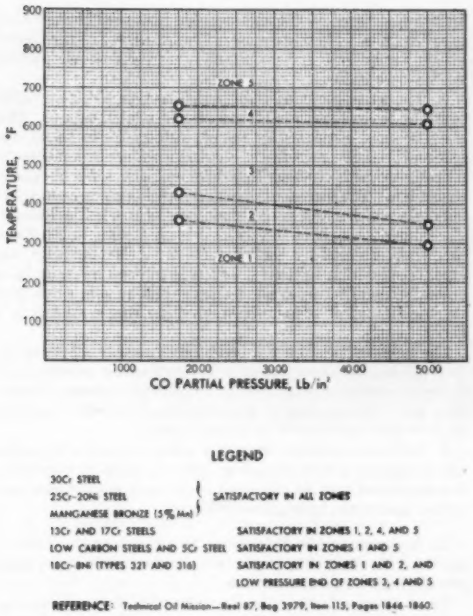

FIG. 8 CORROSION RESISTANCE OF METALS TO CARBON MONOXIDE

per year at 700 atm. Above and below 500 F, the corrosion rate dropped off rapidly. In preparing the chart shown in Fig. 8 it was considered that carbon monoxide was the only portion of the gas responsible for the corrosion, therefore the pressures are indicated as the partial pressure of carbon monoxide.

A summary report covering the experiences gained from the commercial-plant operations in Ludwigshafen shows among other data that diffusion-galvanized N5 steel (5 per cent chromium) has proved very satisfactory in reactors. No change was observed on the galvanized surface after 310 days of operation. The resistance to CO corrosion by galvanized steel, however, was evident only up to 250 atm pressure, as tests at higher pressures of 700 atm showed a high corrosion rate when temperatures rose above 180 C (356 F).

In their experimental work with high-chromium-steel samples, these pieces showed a chromium-rich surface layer of great hardness due to the "diversion of iron into the carbonyls." In case that this chromium-rich layer should prove to provide protection during the operations, it would be possible that V13F steel (13 per cent Cr), which showed great resistance to CO attack, could be utilized for the commercial operation.

As a result of their tests it was concluded that carbon monoxide is very corrosive to ordinary constructional materials at high pressures when the temperature is between 300 F and 650 F. In this range, special metals must be used.

HIGH-TEMPERATURE STABILITY

High-temperature stability will be required mainly to resist oxidation from furnace gases, hydrogen attack, and deformation from high stresses. It can be mentioned that from a survey of operating plants, most of the hydrogenation catalytic reactions occur at temperatures not over 600 C (1100 F). If such should be the final limit, many steels are now made which are entirely suitable for resisting oxidation. However, as the 1100 F temperature is approached, strengths rapidly drop and with the high stresses developed by the high pressures, many materials are unsuitable because of the necessity for providing an unreasonably thick wall. For present plants, the austenitic steels suffice. In the future it may be possible to use some of the highly alloyed gas-turbine materials if they become available in tubular form.

CONCLUSIONS

1 In order to produce damage to the structure of carbon steel by hydrogen, both high pressures and high temperatures are required.

2 Carbon steel varies in its resistance to attack with the manufacturing methods; and, in order to build commercial plants, limits for this material should be at a level where steel in its average condition will be adequate.

3 For protection against damage to steel by hydrogen, relatively small amounts of carbide-stabilizing elements are required.

4 When other corrosives are present in the process streams, measures for protection against these elements should be taken in addition to those required for resistance to hydrogen damage.

ACKNOWLEDGMENT

During the progress of this work, the metallurgical laboratories of a number of the co-operating companies performed many tests; and the author is grateful for their assistance. Thanks are expressed to the following individuals for their co-operation and advice, which were freely given; the companies they represent are also thanked for release of their data: H. D. Newell, Babcock and Wilcox Tube Company; J. E. Wilson, Climax Molybdenum Company; W. B. Kennedy, Columbia Steel Company; H. L. Maxwell, E. I. du Pont de Nemours and Company; C. E. Prechter, Hercules Powder Company; D. B. Rossheim, M. W. Kellogg Company; P. D. McElfish, Perry Kilsby, Incorporated; E. C. Wright, National Tube Company; M. Voogd and L. M. Roberts, Shell Chemical Corporation; A. J. Johnson, Shell Development Company; R. R. Bacon, A. E. Collins, and C. G. Brown, Shell Oil Company; M. A. Scheil, A. O. Smith Corporation; K. V. King, Standard Oil Company of California; M. S. Northrup, Standard Oil Development Company; A. G. Bagsar, Sun Oil Company; C. L. Clark, Timken Roller Bearing Company; G. F. Comstock, Titanium Alloy Manufacturing Company; D. L. Edlund, Vanadium Corporation of America.

Discussion

G. D. GARDNER.[7] Mr. Nelson is to be congratulated for this welcome extension of his fine work on the study of metals for high-pressure hydrogenation plants. The readily usable form in which he has presented the information he has gleaned from so many otherwise unavailable sources is a distinct service.

An earlier set of his curves showing practical limits for carbon and alloy steels in contact with hydrogen at high temperatures and pressures was used in selecting steels for the Coal Hydrogenation Demonstration Plant at Louisiana, Missouri. On the basis of his curves and available German reports, a limit of 375 F was set for the use of carbon steel. Also in agreement with his curves, steels for temperatures over 375 F were high-chromium and austenitic stainless steels.

As reported in papers presented at the Petroleum Mechanical Engineering Conference at Oklahoma City in 1949, high-pressure piping materials were divided into three temperature classifications. For use below the 375 F limit for carbon steels MT-1040

[7] Metallurgist, Coal to Oil Demonstration Branch, Office of Synthetic Liquid Fuels, Bureau of Mines, Louisiana, Mo.

which could be heat-treated to give desired mechanical properties, was first chosen. Later AISI 4130 with somewhat better weldability and better hydrogen resistance was used for some applications to permit comparison with the carbon steel.

For the intermediate temperature range, between 375 F and 850 F, a 9 per cent chromium, 1 per cent molybdenum steel was chosen. Although a lower chromium content would have been sufficient to prevent hydrogen attack the expected high hydrogen sulphide content and need for high mechanical properties dictated this higher alloy.

For temperatures over 850 F the austenitic stainless steel AISI type-316 was used because of its higher creep strength although the 9 per cent chromium steel would have been satisfactorily hydrogen-resistant.

The limited experience at the Hydrogenation Plant to date has substantiated the findings of Mr. Nelson. One section of carbon-steel piping has operated for several hundred hours near the top of the temperature range for carbon steels with at least 75 hr above the upper limit of 375 F. No hydrogen attack could be detected in a sample taken from this line. On the basis of the experience reported by Mr. Nelson, however, it may be that this single sample may not give sufficient information.

The reference to the complicating effects of hydrogen sulphide and sulphur is well worth noting. Because some of the coals to be treated in the demonstration plant will be high in sulphur, the danger of sulphide attack is ever present. It is felt that the 9 per cent chrome steel and the austenitic stainless steel used for temperatures over 375 F will adequately protect against such attack. It is hoped that information obtained from the further operation of the demonstration plant will furnish worth-while additions to the knowledge on metals for high-pressure hydrogenation service.

B. B. Morton.[8] The writer has read with interest the paper by Mr. Nelson and feels that the industry is fortunate in having the information he provides. There seems to be a trend in both the chemical industry and in the petroleum industry toward an extended use of hydrogen at elevated temperatures and pressures. The problem of selecting material for these units will be greatly facilitated by Mr. Nelson's contribution.

Some years ago the writer was concerned with the attack of hydrogen and also hydrogen sulphide upon metals exposed to a hydrogen pressure of about 200 atm at various temperature levels. Some observations made at that time have been confirmed by Mr. Nelson's findings. They are briefly outlined here for the purpose of emphasis.

1 Carbon steel was attacked progressively with increasing temperature. The attack began at about 700 F and increased in both rate and intensity at temperature levels above this.

2 Ni-Cr steel corresponding roughly to SAE 3320, was attacked at 900 F and above. Even when heavily decarburized, fissured, and sulphur-attacked, the steel retained a surprising amount of its original strength.

3 Resistance of steel to hydrogen attack increased with the complexity of the carbide. For example, a steel with 4–6 per cent Cr, 0.5 per cent Mo, and 0.10 Va, was quite resistant to hydrogen attack under 200 atm pressure at 1000 F and at 70 atm pressure at 1200 F. It was found more resistant than a steel of type 410 stainless to hydrogen attack but decidedly less resistant to sulphur attack. The resistance of type 410 to sulphur attack was not considered satisfactory under hydrogenation conditions.

4 A low-carbon Cr-V steel corresponding to about 6110 was particularly immune to hydrogen attack and performed excellent service as a "lens" in the high-pressure joint used in the hydrogenation units. These lenses operate at 800–1000 F. The sulphur attack was uniform and progressed at a very slow rate without marked penetration.

5 The austenitic, Cr-Ni alloys such as type 304, were highly resistant to hydrogen attack and also to sulphur attack. This alloy becomes mechanically loaded with hydrogen which was reflected in specimens pulled at room temperature by reduction in ultimate strength of about 10,000 psi and a considerable loss in elongation. The specimens were quite notch-sensitive and would fail in the punch marks even if these were located in the shoulder. The properties could be largely restored by heating to 600 F and completely restored by heating to 1200 F. No difficulty was experienced during service from this loading and the material is probably one of the most satisfactory for use in connection with the hydrogenation of petroleum products where sulphur is a factor.

The type 304 (18–8) which had been exposed in a hydrogenation unit became quite sensitive to intergranular corrosion and destruction could be brought about by moisture deposited from an inert gas. A treatment at the temperature of 1800 F restored the corrosion resistance of the exposed metal.

6 Rather surprisingly, brass was quite resistant to hydrogen and to sulphur attack though no use was made of this alloy. It is considered that the zinc acted as the catalyst to provide protection against the hydrogen sulphide.

M. A. Scheil.[9] Mr. Nelson is to be congratulated for his research on the effect of hydrogen and nitrogen on metals for high-pressure high-temperature service.

Fig. 4 shows valuable information for plate steel and forgings which have been in service for many years. We could add that our experience with weld metal used for carbon steel when subjected to hydrogenation has shown, in general, greater resistance to hydrogen embrittlement and decarburization than the carbon steel.

Weld metal containing carbon 0.08 – 0.11 per cent, manganese 0.35 – 0.45 per cent, silicon 0.15 – 0.25 per cent, sulphur and phosphorus 0.03 per cent max, molybdenum 0.10 per cent max. is used with carbon steel of the following composition: carbon 0.20 – 0.30 per cent, manganese 1.25 per cent max, silicon 0.30 per cent max., sulphur and phosphorus 0.05 per cent max. and has given satisfactory service. In fact, it has shown no tendency to embrittle where the parent-stock carbon steel has been severely attacked from hydrogen.

We were interested in Mr. Nelson's comments on nitrogen above 850 F at high pressures. In the catalyst basket of synthetic-ammonia converters it has been common practice to use the AISI 501 alloy (4–6 per cent Cr with $^1/_2$ Moly).

Recently we examined materials from a catalyst basket that had been in service about seven years. The highest temperature in the tubes was stated to be 1100 F. From our examination of several specimens obtained from this service we found the 5 per cent Cr alloy to be severely nitrided and embrittled. Fig. 9 of this discussion shows top, middle, and bottom cross sections of the inner and outer gas-cooling tubes. The mid-section of this tubing was most severely attacked and cracking generally started at the outside surface. Of interest are the stratified layers of nitrided material. It is evident that after the tube was nitrided to a certain depth the volume change separated the case from the core with attendant radial cracking thus allowing a new layer underneath to be nitrided. This process was repeated until several laminae formed.

[8] International Nickel Company, New York, N. Y. Mem. ASME.

[9] Director of Metallurgical Research, A. O. Smith Corporation, Milwaukee, Wis.

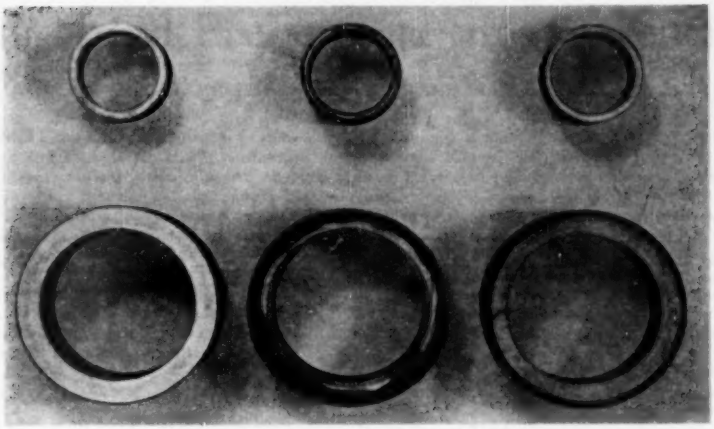

FIG. 9

AUTHOR'S CLOSURE

It is gratifying to have the excellent discussions by men familiar with the operation of high-pressure hydrogenation plants. The points that they bring out help not only to confirm the conclusions of this paper but also indicate directions in which further research must be pointed.

In regard to Mr. Gardener's comments, there is no doubt but that some heats of carbon steel might be adequate at temperatures over 375 F at the high pressure of 800 atm. However, in view of the erratic results which we have found at the high temperatures with steels obtained from different suppliers, we would not exceed the limit of 430 F at this pressure for a long and continued service. The use of carbon steel above this level would require constant inspection, and it would seem more advisable to rely on a small amount of alloy than to use carbon steel of questionable resistance.

The second point brought out by Mr. Gardener to the effect that at temperatures between 375 F and 850 F, a 9 per cent chrome, 1 per cent molybdenum steel is used, is a wise decision because it not only produces a resistance to both hydrogen and sulphur attack but also has the effect of simplifying the number of spare parts. In other words, if the exact limits for the 1 per cent chrome through 6 per cent chrome steels had been decided upon, a wide variety of parts of varying analysis would of necessity have had to be stocked.

Mr. Morton's comments are helpful and, although his operation of carbon steel at 700 F is somewhat higher than we have found in our experience, it may be that the samples were not exposed long enough to create hydrogen damage. In his point 5, the embrittling effect of hydrogen on an otherwise resistant stainless steel of the 18-8 variety brings up an interesting point. In discussions with operators of hydrogenation plants, they also pointed out that the 18-8 steels would lose some of their ductility after long exposure to hydrogen, but that this ductility was soon restored after the plant cooled off. They reported no breakages during cooling-down operations, and cooled their hydrogenation plants at the same rate at which they cooled their other plants where hydrogen was not present. In regard to point 6, we have also used brass bundles for condensing equipment without any damage from hydrogen.

Mr. Scheil's contribution, disclosing the superior resistance of a weld metal containing a small amount of molybdenum, is a further confirmation of the extremely beneficial effects which can be produced by the addition of tiny amounts of the carbide-stabilizing element, in this case being only 0.10 per cent molybdenum.

His revelations regarding the failure of AISI 501 alloy (4–6 per cent Cr with $\frac{1}{2}$ moly) in ammonia service presents an interesting problem. The temperature to which these tubes had been subjected was 1100 F, and, as evidenced by the photographs, they are severely embrittled and permanently damaged by the influence of the nitrided areas. The temperature of 1100 F is considerably above our operating temperature of 900 F, and it is quite possible that the difference of 200 F is sufficient to accentuate drastically the nitriding condition. In the body of the paper it was mentioned that several high-nickel alloys were being experimented with to determine those which would resist both nitrogen and hydrogen. Since the paper was written, we have now obtained information on test samples of the Hastelloys and, after an exposure for about a year to a temperature of 500 C and a pressure of 2840 psi in an ammonia catalyst chamber, the Hastelloys A, B, C, and D were found to be completely unaffected by either hydrogen or nitrogen.

A sample of nickel was also tested and, although it did not nitride, it was found completely cracked from hydrogen damage. Further checking of this sample revealed that it contained a small amount of carbon, and as such, probably reacted in a similar manner to low-carbon steel. Another sample of nickel is under test which is entirely free of carbon.

Cyclone-Fired Pressurized Steam Generator

By MERLE NEWKIRK,[1] MIDLAND, MICH.

The Dow Chemical Company has a number of plants in the United States and Canada for the manufacture of industrial and pharmaceutical chemicals and the production of magnesium metal. Their power plants supply process, high-pressure, low-pressure, and vacuum steam; electrical energy, compressed air, high and low-pressure water and stack gas. Several of the power plants are synchronized with public utilities. Power is purchased or sold depending upon the local conditions. This combination affords an opportunity to select and operate equipment beyond the scope of the average plant, and to put into use advanced ideas in power-plant design.

Desired Features Prior to Design

THE need for more steam and power in the Midland Plant of the author's company afforded the opportunity to install a new turbine and steam generator in what is known as the West Side Plant. In discussing this addition with management, several features were requested in its operation, as follows:

1 The elimination of objectionable fly ash.

2 Efficiencies as good or better than had been accomplished in the past.

3 Design the unit for absorption of heat and not for the convenience of cleaning. Utilize small tube sizes disregarding the necessity of mechanical internal cleaning.

4 Draining superheaters.

5 Highly preheated air temperatures with corrosive section made small for ease and speed in replacement.

6 Continuous operation on 100 per cent make-up feedwater with a minimum blowdown.

7 The maximum continuous rating possible to install in the existing building.

8 Substitution of blowers using clean atmospheric air, thereby eliminating the standard forced and induced-draft fans.

Description of Apparatus

The steam-generating unit, Figs. 1 and 2, has a rated capacity of 400,000 lb of steam per hr, generating steam at 1250 psig and 900 F, and fired with crushed, not pulverized, coal by two horizontal cyclone burners. The boiler unit has a total heating surface of 37,339 sq ft and a furnace volume of 24,900 cu ft.

All air and fuel is admitted to the cyclone primary furnace, and the flame and products of combustion discharge through a conical opening into the secondary furnace, where they are directed downward by water-cooled reflecting tubes so that they sweep the molten slag on the secondary-furnace floor. The flame and gases then turn through a slag screen and pass upward through the secondary furnace to the convection section. In the convection section are located a continuous-tube draining-type superheater, the secondary section of the continuous tube economizer, and the boiler generating tube section. The gases turn through the convection section and continue their flow downward through the first gas pass of the secondary-air heater, over the primary economizer, then turn upward and pass through the second gas pass of the secondary-air heater, on through a welded flue to the primary-air heater and finally to the stack.

The primary furnace is cylindrical, with its longitudinal axis set at a slight angle with the horizontal to facilitate gravity-draining of molten slag into the secondary furnace from which it is tapped through either of the two continuous slag taps, located one in each side wall of the secondary furnace, to an external slag chamber.

All furnace waterwall circuits discharge into and are fed from the 60-in. drum. To insure positive natural circulation in this unit, two 21-in. downcomers lead from each end of the main steam drum. These downcomers connect with the boiler circulation system.

The furnace of this unit is designed to operate under pressure, and since there are no induced-draft fans, all combustion air is supplied to the burners by the forced-draft blowers. Each of these blowers, supplied by the Joy Manufacturing Company, is designed to deliver 52,500 cfm of air at 77 in. water pressure. Two blowers have sufficient capacity to furnish the necessary air to the boiler at maximum rating, one blower serving as stand-by. Each unit is driven by an 800-hp Elliott Company direct-connected motor.

Removal of slag from the furnace is accomplished by an Allen-Sherman-Hoff Company "Hydrojet" slag-handling system. The two slag spouts, located on opposite sides of the furnace, are enclosed by slag chambers mounted above storage hoppers. A water-sealed expansion joint is provided between the slag chambers and hoppers. A constant water level is maintained in the hoppers at all times for the disintegration of the slag. Slag is removed periodically by means of high-pressure water nozzles arranged to sweep the floor of the hoppers. The slag is washed through the hopper outlets into a common watertight chamber, and passes through a metering grinder into a sump. The slag is transferred from the sump to the fill area by a Hydroseal pump.

Unique Features of These Installations Setting Them Apart From Others

Elimination of Objectionable Fly Ash. The fuel and ash are not ground to the fine particles that are necessary to get good combustion on a pulverized-coal installation. The coarse coal is brought into the feed section of the cyclone furnace in combination with heated air (approximately 250 F). This gives the larger particles of coal an opportunity to break up, and ignition takes place very close to the outlet of the coal-fed end. Here the coal meets the higher-temperature secondary combustion air of approximately 750 F. This induces very rapid combustion. As the products of combustion revolve around in the primary furnace, the heavier ash particles, such as clay, slate, and other elements that make up ash, are melted and adhere to the furnace walls in a manner similar to dust adhering to a surface coated with molasses. These screen tubes are studded and are covered with chrome ore, and when coated with molten slag act just like flypaper. The screens assist in catching the very small particles of ash that normally would be carried up into the unit. The molten ash in the cyclone furnace runs down the sides and out of

[1] Manager, Power Division, The Dow Chemical Company. Mem. ASME.

Contributed by the Power and Fuels Divisions and presented at the Semi-Annual Meeting, St. Louis, Mo., June 19–23, 1950, of The American Society of Mechanical Engineers.

Note: Statements and opinions advanced in papers are to be understood as individual expressions of their authors and not those of the Society. Manuscript received at ASME Headquarters on May 24, 1950. Paper No. 50—SA-38.

NO 13 BOILER
WEST SIDE POWER PLANT

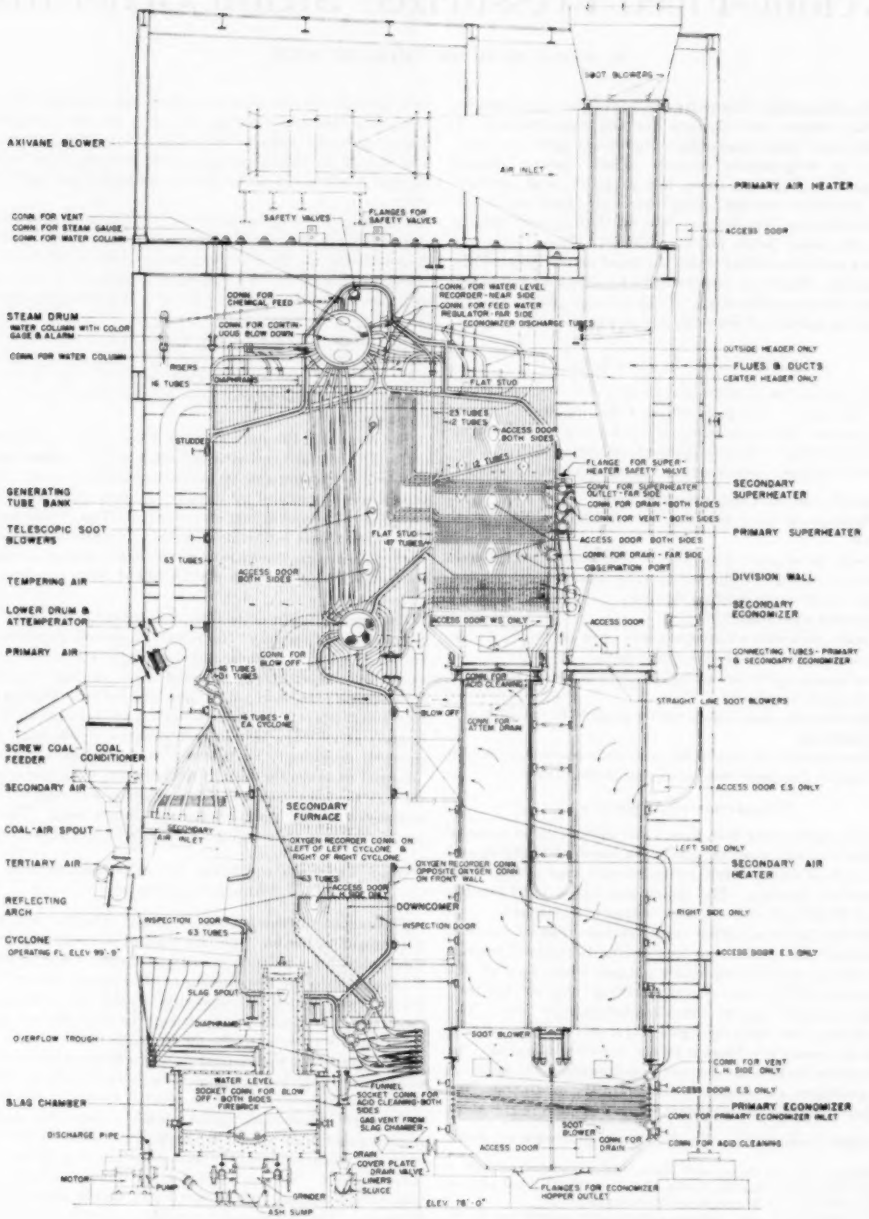

FIG. 1 NO. 13 BOILER WEST SIDE POWER PLANT

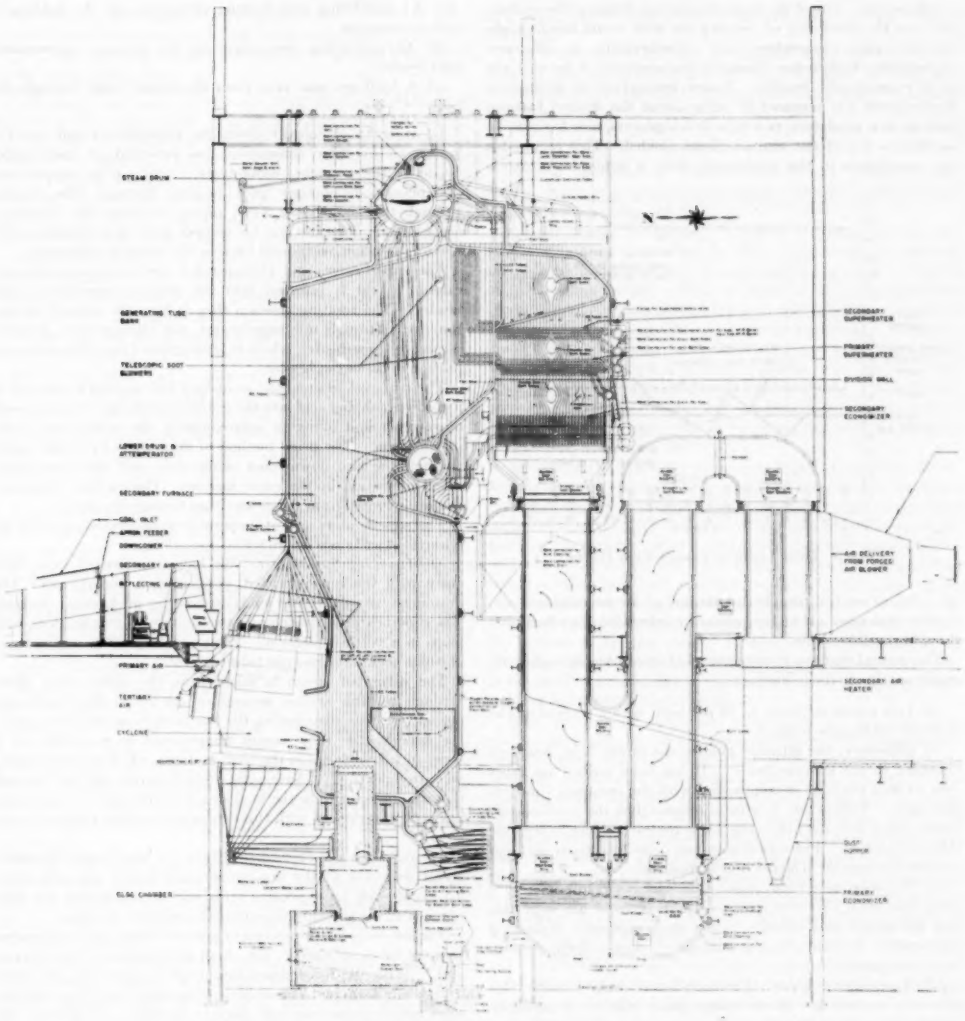

FIG. 2 SOUTH SIDE POWERHOUSE

a small opening under the throat leading into the secondary furnace. A pool of molten ash collects in the secondary furnace over which the gases from the primary furnace must pass. The slag is continually tapped and there is no appreciable accumulation. The tube screen through which the flame passes in the secondary furnace is at a location opposite the throat of the cyclone. Behind the slag screens the gases are very clear, indicating that the cyclone is doing a good ash-collecting job.

The air heaters were designed to assist in the dropping out of any dust, and provisions are made at the bottom of the second and third air heater to take out any deposits that may occur there.

To keep the unit free of any accumulation which might occur, the soot-blowing-system location has been carefully worked out. An "air puff" soot-blowing system, sequentially and automatically controlled, was chosen to accomplish this desired result. (It might be said here that soot as such has never been found.)

One of the reasons for using the pressure-type furnace, is the belief that better fly-ash recovery within the unit is possible as the gases are slowed down progressively as they pass through the unit. This is the reverse to the operation when induced-draft fans are used. How well the design is functioning is shown in Fig. 3.

Efficiencies. One of the basic ideas in the design of the cyclone unit was the possibility of creating one that would handle high-ash low-fusion-temperature coal. Furthermore, an efficiency approaching modern-day standards was necessary if the unit was to be economically feasible. A new conception in mechanical development was required to bring about the desired features such as, new insulators, new tube developments, new feeders—to mention a few of the characteristics needed. This required a new conception in the combustion field, a minimum of excess

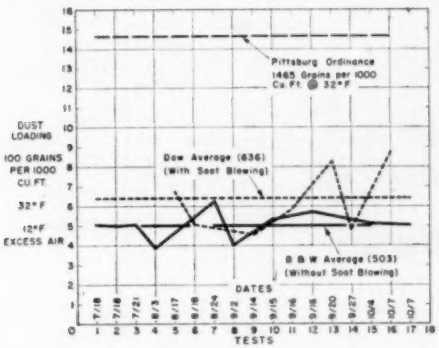

FIG. 3 DUST LOADING VERSUS TEST DATES

air, efficient control, simple distribution of air for combustion—a great deal more air at the point of combustion than had been thought possible before.

The several features in this unit that create higher boiler efficiency are due to the following:

(*a*) Low excess air, namely, 10 per cent, with a trace of smoke or CO at the furnace outlet.

(*b*) Efficiency, the ultimate goal in the power field, has been extended in the cyclone boiler. It has been pushed up 2 per cent to 90.5 per cent in comparison with the company's pulverized units. This is due to several reasons, but the predominant factor along with the low excess air is the carbon loss in the ash: this is 1 per cent Pulverized units run from 7 to 30 per cent and stokers run from 20 to 50 per cent carbon loss.

(*c*) The relatively clean absorption surfaces result in a very small loss from this standpoint. These surfaces are kept this way by simple soot blowers, rather than expensive deslagging equipment. Incidentally, the minimum in dust-collecting equipment is required.

(*d*) A secondary group of reasons which help to raise this efficiency are the low power consumption relative to auxiliary equipment, and the fact that no mechanical circulation of water is required.

Chemical Cleaning. Provision for mechanical cleaning complicates the design of a boiler, establishing limiting factors as to tube length, diameter, and shape. All tubes must be accessible for turbining, increasing the number of handhole plates in headers.

With the practicability of chemical cleaning definitely established, the design engineer is now free to concentrate on maximum heat absorption and efficiency instead of the provisions for mechanical cleaning.

The only provisions necessary for chemical cleaning of cyclone-furnace boilers are:

(*a*) An acid-filling and flushing connection on the bottom of each downcomer.

(*b*) An acid-filling connection on the primary economizer-inlet header.

(*c*) A hydrogen-gas vent from the steam drum through the roof.

In order to chemically clean the economizers and not the boiler, an overflow connection was provided on each outlet header of the secondary economizer. Acid can be pumped into the primary-economizer inlet header, through this section, through the main boiler water piping, and into the secondary economizer. The gas can be vented from this section or the treating solution overflowed back to the treating equipment.

The superheaters and attemperator also can be treated separately. Acid is pumped into the primary-superheater inlet header. The treating solution then follows the normal circulation path through this superheater, the attemperator, and the secondary superheater, where it is overflowed from the vent connection of the outlet header.

The two cyclones and the secondary furnace can be treated as a unit by pumping acid into the connections in the bottom of each downcomer and filling to approximately the center line of the steam drum. The usual method of cleaning is to fill the boiler through the two downcomer connections and the economizer-inlet connection in the same manner. During the treatment, the gas is vented from the steam drum through the roof.

The superheaters and attemperator were treated once for the removal of mill scale before initial operation.

Self-Draining Superheater. We have experienced some difficulty with the top-supported, pendant-type superheater. The draining-type superheater lends itself better to chemical cleaning. The superheater is divided into two units with four headers, with loops in a vertical position. There are no pockets in the tubes in which accumulations can lodge.

The saturated steam is taken from the main steam drum through multiple cyclone separators and led to the superheater header by tubes, distributing the flow both from the drum and to the superheater. The steam temperature is controlled by a series of tubes placed in the bottom drum, which is trade-named an "attemperator." Automatic controls govern the flow through the attemperator from the final steam temperature. No trouble has been experienced with this equipment and the control is very good.

Three-Section Air Preheater. There has been much discussion about corrosion at the low-temperature end of air preheaters. To avoid such an expensive replacement and reduce the time of renewal, the air heater was divided into three sections.

The low-temperature section or primary heater is so constructed that the tubes are short. The small sections can be renewed as a unit. With the low-temperature stack gas entering the tubes from the bottom and atmospheric-temperature air from the side, some condensation may take place in the tubes. If it does, with this type of arrangement, those sections or tubes can be replaced readily. Also, if trouble does develop, other metal can be used and the expense of a change will not be as great as if conventional designs were followed. Careful inspections have been made at each permissible opportunity and to date no excessive corrosion has been detected. In the two new boilers, aluminum tubes are used in the first rows to get additional information on corrosion.

The secondary heater is divided into two sections for the following reasons:

(*a*) Shorter tubes.
(*b*) Better heat recovery—economizer installation.
(*c*) To fit into space limitations.

(*d*) Provide a quiet gas turning chamber.

(*e*) On pressurized setting to keep the sections small.

(*f*) To get higher preheated air without subjecting the entire heater to high temperature.

Continuous Operation on 100 Per Cent Make-Up Feedwater With a Minimum Blowdown. One of the basic ideas in developing this type boiler was the saving of space. Therefore it was necessary to design a unit of intricately bent and assembled tubes, centered around a nucleus of one steam drum. Furthermore, the cyclone furnace itself, with its helical-wound tubes, created a geometrical complication of mechanical assembly. Therefore the idea of using mechanical cleaning was eliminated. A boiler with small tubes which could be cleaned by chemical methods permitted an arrangement suitable to the various heat-absorbing surfaces which were desired. This indicated that a nearly perfect water supply would be required.

One other factor was the requirement that these high-pressure boilers operate with 100 per cent make-up. Consequently, the water entering them had to be treated skillfully. The author's company solved the problem of silica removal and softening of the water by fluoride treatment and demineralization. Water treatment by this process has been very successful. Therefore it was decided that added capacity to supply the 100 per cent make-up for two similar units at the South Power Plant would be feasible.

Blowdown is about $1^1/_2$ per cent from the unit now operating. Since it goes to a 400-psi boiler, measuring the water discharge is not necessary. Also, the constituents of the feedwater are too low in concentration to analyze accurately enough for boiler-cycle concentration calculations. The water from this demineralization plant shows a consistent silica content of less than 0.5 ppm and the solids content of dissolved and suspended solids of 0.5 ppm.

Maximum Continuous Rating. The building in which this unit is installed was already constructed, and column spacings could not be changed. The original spacing was for a production of 150,000 lb of 400 psi 750 F steam. Coal bunkers and other coal-handling equipment were installed. There was need for all the steam that could be produced in this space at 1250 psi 900 F.

The cyclone-fired pressurized-furnace steam generator offered more than any other unit by approximately 25 per cent in floor area, 30 per cent in building volume, and 20 to 25 per cent in total weight.

The normal continuous rating of No. 13 is 400,000 lb per hr at 1250 psi, 900 F. This rating is easily maintained and, while its ultimate capacity has not been reached, it is expected to go to 500,000 lb per hr. This rating has to be maintained 24 hr per day, 7 days per week.

Elimination of Induced Draft. Induced-draft fans always have been a continual source of trouble. To eliminate this, pressure blowers are used, handling only clean, atmospheric-temperature air. It eliminates the fine balance necessary when forced and induced-draft fans are run in combination.

The efficiency of cold-air fans is a little better than when hot stack gases are handled. The erosion due to ash particles is eliminated.

Axial-flow blowers are used, three to a unit. Two carry the load. The third is a spare.

This combination has worked out very well. There has been no outage due to blowers. The only trouble has been with roller bearings and oil leakage, which, considering the newness of the design, is minor.

Constant-speed motors operating at 1725 rpm are used, and the air flow is controlled by dampers.

Some difficulty was expected in running high-pressure blowers, in parallel, but this has not been the case—they operate without hunting.

The noise level is too high for comfort and a method of suppressing the high-pitch squeal will have to be found. We now know how to do this and steps are now being taken to correct this nuisance.

Operating Characteristics

Cyclone operation is characterized by its simplicity and safety, which is generally unparalleled in other industrial applications to the burning of fuels.

In approaching the ignition of coal in a cyclone furnace, the following general procedure is used, considering the normal methods for caring for pressure parts and firing rates. A gas or oil torch is first ignited. Once the lighter is on, the coal is fed to the cyclone. Ignition is established almost immediately despite the lack of a fluid slag coating on the cyclone walls. Normally, about $^1/_4$ of full-rate air flow is the established rate for starting. However, no interruption in firing is necessary in the event that the air flow is too high or too low for the coal rate. Adjustments are simply made by the operator to obtain the balance desired. Ignition has never been lost in operating this unit to date, except through loss of coal feed.

In hundreds of losses of coal feed, only puffs of a minor nature have been experienced. These have been due either to malfunctioning of the automatic gas igniters in which the gas torches subsequently ignited after a series of unsuccessful attempts not followed by purging, or coal feed being suddenly re-established with the feeder set for maximum output. Actually, this puffing would not then have been readily recognized, had the observation port in the front of the cyclone been closed.

In the event of a coal-feed loss, it is possible to reignite a cyclone fire without an ignition torch. If the fires have been out up to 1 min, ignition is normally re-established easily from the hot slag. It is possible to exceed this time, especially if the air flow has been reduced shortly after loss of ignition.

With two-cyclone operation, balance of the cyclones with respect to excess air is probably the operating characteristic which requires the most skill. The instrument which permits the optimum balance of cyclones is the oxygen recorder. The best placement for these sampling probes in the unit has been found to be about 9 ft above the full stud area in the rear of the secondary furnace. After relocation of the sampling probe and modifying the deslagging spray at the inlet end of the probe, these instruments have still given intermittent and unsatisfactory operation. Up to the time that the oxygen recorders were made reasonably dependable, balance of the cyclones for various loads was accomplished chiefly as follows:

1 Adjusting total air flow to parallel steam flow.

2 Adjusting each cyclone feeder rpm to coincide with the proper total air-differential readings to each cyclone.

3 Observation of fluidity of the slag from the cyclone slag tap and the secondary-furnace slag tap.

Slag-fluidity overload ranges while firing coals having ash-softening temperatures (reducing atmosphere) of 2200 F are about as follows: With one cyclone in operation at 200,000 lb of steam per hr at 10 to 15 per cent excess air, slag fluidity from the secondary slag tap generally approximates the condition experienced with two cyclones operating at loads above 325,000 lb of steam per hr, that is, a minimum of attention is required at the taps. With two cyclones in operation at 300,000 lb per hr, slag does not flow quite as freely from one or both secondary slag taps as it does with one cyclone in operation at 200,000 lb per hr steam flow. However, with some attention, it is easy to maintain a steady slag flow from the secondary slag taps. By the

same token, with one cyclone operating, unit loads of 150,000 lb of steam per hr require some attention at the secondary slag taps. An absolute minimum load at which tapping from the secondary slag taps is impossible without constant attention has, to date, never been established.

For several months a relatively even mixture of Clearfield and Pocahontas coals has been fired. The ash-softening temperature of the Clearfield coal averages 2515 F, and the ash-softening temperature of the Pocahontas coal averages 2200 F. Slag is tapped continually from the secondary furnaces at loads of 340,000 lb per hr with a minimum of attention. Moderate attention was required for loads of 320,000 lb per hr with excess air of 15 per cent and lower. No continuous runs were made during this period with one-cyclone operation.

In order to maintain adequate cyclone air velocities, the following generalizations are made for this installation: At unit loads of 200,000 lb per hr with one cyclone in operation, optimum cyclone operational characteristics are had at 40 in. secondary-air pressure. At unit loads in the order of 350,000 lb per hr, with both cyclones in operation, optimum cyclone operational characteristics are obtained with around 43 in. of water pressure. Accountable for this difference is the variation in air temperatures to the cyclones with one and two-cyclone operation.

There have been times, during successive on and off operation of the cyclones, due to failure of the coal feed, when pile-ups of slag and unburned carbon have been caused in the cyclones, thereby choking the primary slag taps. Naturally, this condition impedes the best cyclone operation. On the other hand, it does not prevent successful unit operation. It has generally been true that tapping from the primary slag tap can be re-established in a period of about 1 hr. To accomplish this, the inboard secondary-air (velocity) damper is closed to increase the velocity in the rear of the cyclone and to limit locally the quantity of air. This will maintain better ash fluidity in the vicinity of the tap. In addition to this, it has been found expedient to increase the air pressures to the cyclone several inches, in order to better aid the movement of slag.

Within the secondary furnace the platen tubes have never been noted to have sufficient accumulations of molten slag to impede gas flow. Slag formation, instead, has been surprisingly uniform. The fluid-slag region extends generally to 10 ft above the full stud area in the secondary furnace. The transition is sharp, since above that elevation only a smattering of adhesive slag has been found. From the generating tubes on, no hard ash accumulations have been noted. All popcorn accumulations on the superheater tubes are easily removed by means of the telescopic blowers in that zone. Most of the accumulation beyond the molten-slag transition zone is fly ash of an extremely fine consistency with little or no tendency to form a hard mass.

Stack observations at extremely low excess-air conditions do not show the characteristic dense black emission. As the excess air is decreased, the dust emissions gradually assume a golden-brown hue, and with further decreases in excess air, they become a dark-brown emission.

Dust-Loading Tests

Dust-loading tests were taken both by the author's company and the Babcock & Wilcox Company. The sampling points for these tests were near the base of the 11-ft-diam stack about 15 ft above the primary-air-heater outlet. As a consequence of having to test out of doors, fly-ash tests were taken only at times during which weather conditions were acceptable for good testing. The author's company tests were made over approximately 5-hr periods at steady-load conditions with continuous soot-blowing. The Babcock & Wilcox tests were taken over approximately 2½-hr periods, during which no soot-blowing was done. In each case, 30 points across the stack were sampled. Sundry 60 and 30-point Pitot-tube probes for the unit loads tested indicated a relatively uniform velocity distribution across the stack. The velocity patterns for the 60 and 30-point probes were substantially the same.

Tests taken with coal-feed interruptions or unusual load changes were not considered representative of the tests taken for which the preceding conditions prevailed. A plot of the results is shown in Fig. 3. The average unit condition for the tests was 365,000 lb of steam per hr from the range of 345,000 to 400,000 lb steam flow.

For the Dow tests, several screenings and particle-size counts were made by the Dow laboratories. An example of a Dow test with a dust loading of 517 grains per 1000 cu ft of flue gas will be given later.

Coal-Feed Problems

Inability to get continuous feed of coal to this unit has been a factor which had caused rather intermittent operation. As has been explained previously, coal is fed from a parabolic bunker directly into coal scales which discharge into a 5-ft hopper. The coal is fed from here to the inlet end of the screw conveyers. The screw conveyers are 17¼ ft long with 9 in. pitch for one half of the screw length. The diameter of the screws is 9¾ in.

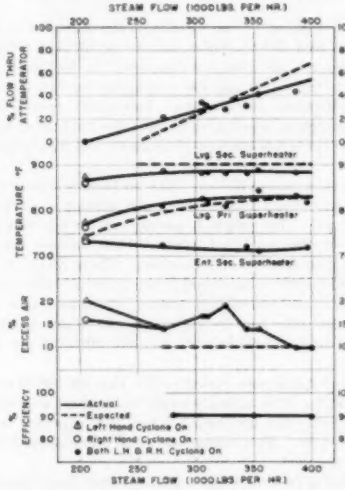

Fig. 4 Cyclone Burner Comparison Chart

Coal is conveyed up a 26-deg slope to the coal conditioner. Coal-feeding difficulties initially resulted from a combination of the following:

1 Sizing and moisture content of coal delivered to the screw.

2 Lack of coal-storage capacity between the screws and the coal scales.

3 Primary-air blowback through the screws with loss of coal feed.

During initial operation, Pocahontas coal was fired, the raw coal having relative sizing as given in Table 1.

This coal sizing, along with surface moisture content in the order of 7 per cent, consistently held up coal in the bunker, the scales, packed in the screw-inlet hopper, and on the screw flights.

TABLE 1 SIZING OF POCAHONTAS COAL

Screen size	Per cent through
4	76.5
6	66.7
8	57.2
14	42.0
28	27.5
48	16.6
100	9.4
200	5.0

The storage capacity in the screw-inlet hopper was then less than 1 min. The air pressure in the conditioner at the discharge end of the screws usually was about 44 in. of water. Hence coal hang-ups or failure of the screws to carry nearly full flights of coal resulted in blowback through the scales. This generally meant that primary-air pressures had to be reduced to the order of 20 to 30 in. until coal feed was re-established. During this time, that cyclone was out of operation.

Subsequent operation met with a greater degree of success, in that Piney Fork coal of different sizing (Table 2) was purchased for the unit.

TABLE 2 SIZING OF PINEY FORK COAL

Screen size	Per cent through
4	66.0
6	54.3
8	45.0
14	31.0
28	19.3
48	13.6
100	7.3
200	5.1

Hence the foregoing coal-feed problems were minimized. To improve further the coal-feed condition, the use of the scales was discontinued. The hopper above the screw inlet was redesigned. Adjustments were made at the inlet end of the screw conveyers and at the screw housings. Although continuity of feed has become a minor problem, chiefly due to firing coals of requisite sizing, the use of screw conveyers is not a final answer in feeding coal to pressurized cyclone furnaces. The fact remains that, once coal feed is lost, the screws offer no air-pressure seal against the primary air, with the consequent blowback of air through the screws. This condition ordinarily makes the re-establishment of coal feed a longer process than should be the case.

Cyclone-Tube Failures

The major cause of tube failure in the cyclone has been due to the up and down firing brought about by numerous interruptions of coal feed. This intermittent operation causes a wide variation in temperature which results in expansion and contraction of the cyclone. Consequently, the slag cracks and peels off leaving parts of the throat and the cyclone tubes bare. Since the heat release in the cyclone burner itself is very great (545,000 Btu per cu ft per hr) extreme-heat transfer is effected in this localized area. The high temperature damages the protective film of iron oxide which, under favorable conditions, covers the inside of the tube. Any condition which damages the protective film permits corrosion to continue. It is this repetitive process of forming an iron-oxide coating that robs the iron from the tubes. When this happens to a limited area, or areas, the attack will be localized and eventually will result in tube failure. Fig. 5 shows the location of leaks in the right-hand cyclone throat. Fig. 6 shows the area of tube failure in the left-hand cyclone. The area affected in the right-hand cyclone is in the same relative location.

Bailey Block Wear

The difficulty encountered in Bailey block wear on No. 13 boiler has resulted from numerous causes which can be, and are being, corrected. Since the blocks are subjected to a high temperature, the failure has been due to burning rather than erosion. In order to correct this burning, the blocks are now being made of a higher-temperature-resistant alloy. The blocks are being welded to the tubes, giving a better heat transfer between block and tube, thereby taking advantage of the cooling effect of the water. It also keeps fuel particles from getting under the block which add to the burning.

The bottom blocks in the outer row of the cyclone have experienced the greatest amount of burning. This, in a large part, is due to the high-temperature slag which drips adjacent to these blocks. This being the area traversed by the heavy stream of coal leaving the primary burner and entering the cyclone, there is an obvious indication of coke deposit which is being partially corrected with tertiary air. Again, the condition of the coal has some bearing on the amount of tertiary air used, Figs. 7 and 8.

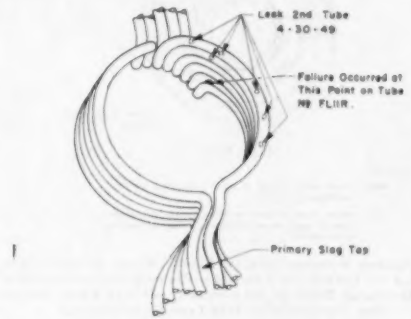

FIG. 5 ISOMETRIC-LOOKING INTO RIGHT-HAND CYCLONE THROAT

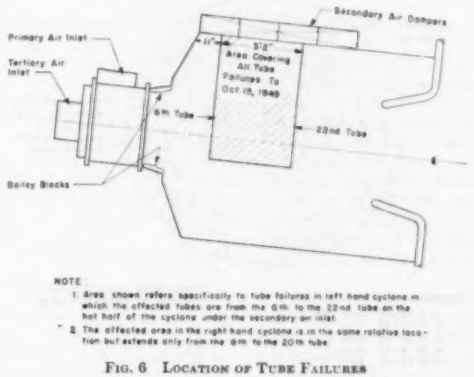

FIG. 6 LOCATION OF TUBE FAILURES

Slag Taps and Ash Pits

Maintenance of ash fluidity at the cyclone-burner tap is one of the most exacting of all operating considerations in the horizontal cyclone-firing method. Due to the relatively large amount of slag and the temperature at which it must be maintained in removal from the secondary furnace, the mechanical requirements necessary dictate a rather expensive installation, Fig. 9. The two systems, namely, the one on No. 13 boiler

and those on No. 14 and No. 15 boilers, are quite similar in operation, but the ash-ejection system has been improved greatly in the latter two units.

The slag is discharged from the secondary furnace to a slag chamber on each side of the furnace. Here it is swept by a stream of hot gases, maintaining a liquefied state, to the point where the

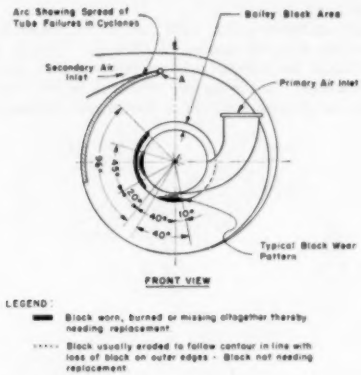

FIG. 7 SKETCH SHOWING BAILEY BLOCK WEAR, PARTICULARLY APPLICABLE TO LEFT-HAND CYCLONE—RIGHT-HAND CYCLONE HAS ALWAYS HAD SOME WEAR IN ARCS SHOWN, BUT FAR FROM MAGNITUDE EXPERIENCED WITH LEFT-HAND CYCLONE

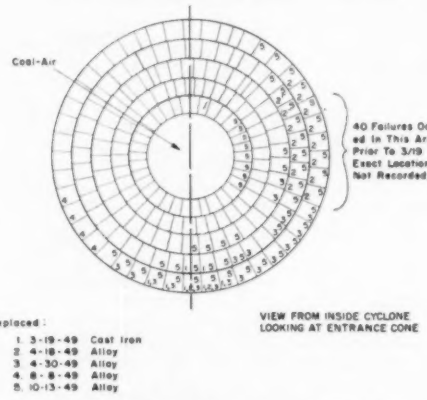

FIG. 8 LOCATIONS OF BAILEY BLOCK REPLACEMENT—CYCLONE 131

ash is deposited in circulated cool water through a water screen which expedites the diffraction. The slag is distributed by propeller agitation to three hopper bottoms. An improvement in the installation of No. 14 and No. 15 boilers in the distribution of the ash has been brought about by the addition of a distribution nozzle in the center hopper bottom. The ejection of the ash is by oscillating hydrojets with upstream hydrojets to help. The ash is ejected through a water-operated slide gate on No. 13 unit directly to grinder—to sump—to ash pump—to fill. In the new units it is deposited through a pressure door to a sluiceway—to an ash pit for deposition.

No. 13 boiler ash-handling system is a completely sealed unit from slag tap to ash pump. No. 14 and No. 15 units incorporate a small hopper bottom with a hydraulically operated "Ni-Resist" slide gate between the upper slag chamber and the hopper bottoms. It has been found necessary in the operation of No. 13 boiler to reduce the water level to a minimum or zero before the ash can be removed effectively. However, it was originally planned to hydrojet the ashes under a water seal. Due to the fact that the system is sealed and the hot gases are discharged at all times to the primary-economizer section of the boiler, and the fact that all parts of the system are insulated with monolithic refractory, no apparent damage has been caused by reducing the water to zero.

Make-up water in the quantity of 150 gpm is introduced into a vented pan on the slag-chamber roof and overflows over a serrated weir into the jacket surrounding the sides. Circulation is maintained by bleed-off nipples in the bottom. The overflow from the water jacket drains through a sealed expansion joint installed between the slag chamber and the hopper. The seal is designed for a positive pressure of 15 in. of water. It should be pointed out that the slag chambers are attached directly to the furnace walls and enclose the slag spouts, while the hoppers are mounted on the basement floor, thereby necessitating the seal. The make-up during operation is approximately 650 gpm, and during ash-ejection periods is 1800 gpm. Both systems are equipped with similar grinders and pumps along with alarms and electrical controls. However, the south installation is so designed that the water level rather than being maintained by float level is corrected by adjustment of a weir box. Other improvements such as observation-port enlargement, washing facilities for the observation ports, and interlocks relative to the water level, Ni-Resist gate, and the pressure-sealed doors have been incorporated to create the proper operation on the part of the personnel.

It has been found that the operation of all cyclone units, with high-volatile coal and low ash-fusion temperatures and moderately uniform sizing, has been accomplished with relative ease. Experience with other coals has indicated the necessity for rigid control, particularly when firing coals of higher ash-fusion temperatures. In the use of Pocahontas coal, an excess air of 8 per cent must be maintained or the tapping from the secondary chamber will be interrupted. Therefore the unit appears applicable to fuels of low ash fusion.

COALS, FIRED, NAMES AND LOCATIONS

In this unit it is possible to burn a wide variety of coals, which gives the advantage of shopping for coal on a cheaper cost per Btu basis. About 15 different kinds of coal have been used successfully. As long as it contains 30 per cent of $^3/_4$-in. down to 0 in. principally due to feeding, it is possible to handle it successfully.

Table 3 lists some of the coals which have been burned successfully

A BETTER STEAM GENERATOR

Experience with the cyclone-fired pressurized setting leads to the belief that radical improvements can be made on the present coal-fired steam generators:

1 Coal need not be pulverized, and those coals which have been uneconomical to prepare can now be handled successfully.

2 With clean combustion, the heat-absorbing surfaces can be arranged more effectively.

3 Superheaters can be placed among the generating tubes, making them smaller and more easily dedusted.

4 The entire structure of the unit can be arranged for bottom support, and not hung from the top to expand down.

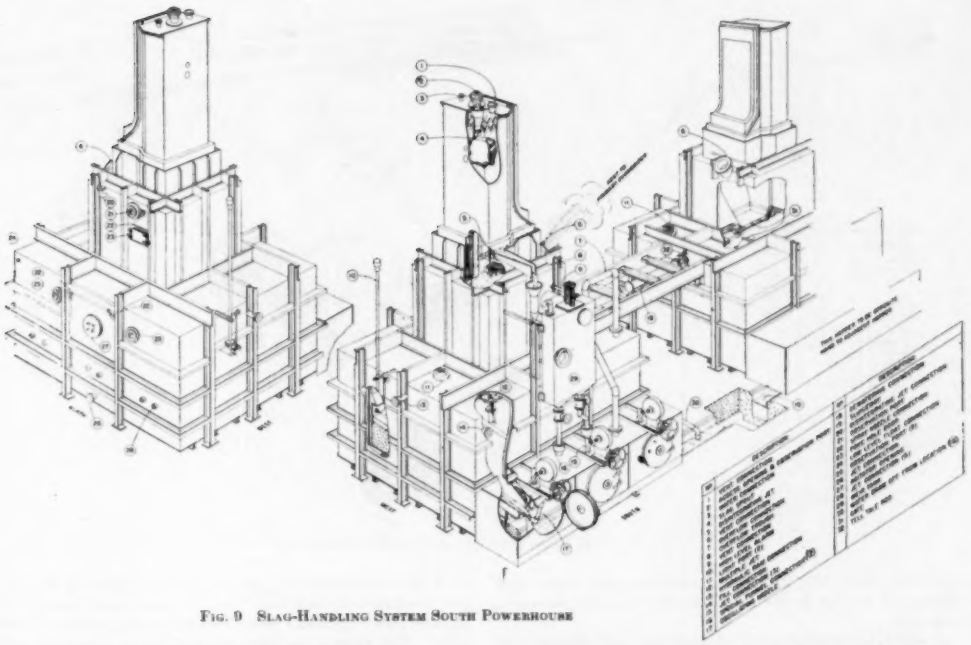

FIG. 9 SLAG-HANDLING SYSTEM SOUTH POWERHOUSE

TABLE 3 COALS USED SUCCESSFULLY

West Virginia	**Pennsylvania**
1 Pocahontas	1 C. L. Ames
2 Pursglove	2 Morgan (Snowshoe)
3 Jane Lew	3 DuBois & McHaffey
4 Birchard	4 Central West
5 Reppert Coal Company	
6 Tasa	
7 C. L. Ames	
Ohio	**Illinois**
1 Central West	1 Old Ben
2 Pittsburgh Consolidation	
3 Youghiogheny & Ohio	**Any state**
4 M. C. Hobart	1 Cleveland Cliffs

Coal Analysis

Fusion, deg F	2200 to 2700
Ash, per cent	2½ to 15
Moisture, per cent	3½ to 16
Volatile, per cent	20 to 39
Btu content	From 8000 to 13800 as received

5 Of most importance is the application of a hot-air turbine to supply air for combustion.

6 Circular form lends itself readily to ease of construction and semioutdoor installations.

7 Opposed firing will simplify the ash disposal.

COAL-PREPARATION PLANT AND WHY

One predominant and distinct advantage of the cyclone boiler is its ability to burn crushed or "conditioned" coal rather than pulverized fuel. This is true—it will use fuel of this nature. Not only that but several other advantages are apparent, namely, much less work is required on the coal before burning. The expensive pulverizer and its accompanying maintenance cost are no longer necessary. The work of the crusher used in the direct-fired method is nil, as the cyclone requires coal only sized to ¼ in., i.e., such that 90 per cent will pass through a No. 4 screen. Furthermore, it should be pointed out, experience indicates that coals of larger diameters may be burned successfully, resulting in a further reduction in work.

The coal-preparation plant is shown in Fig. 10. The coal for the power plant is moved by a fireless locomotive from a siding (after a track-weight station) to a gas-fired thawing pit. From the pit the coal moves to a track-hopper unloading station enclosed in a building. From the unloading station the coal is fed from the track hoppers by reciprocating feeders to a belt conveyer. This discharges the coal to a Bradford breaker for sizing, to a feeder, then to a belt conveyer which conveys the coal to a transfer tower, to an elevating belt conveyer, to twin silos. The coal is fed out of the silos through a roto-drier to a vibrating screen and crusher, and is then transported to the power-plant bunkers.

Hot air for the drying system is developed by a furnace equipped with a rotary stoker. Air is transported from the furnace through the drier by a Claridge fan and is discharged through an Aertec cleaner and an induced fan. The plant is equipped with a water curtain Roto Clone to collect coal dust at all apparatus and dispose of it. Arrangement is provided to transfer the coal from either silo to the other. Also, coal may be transported from the point of intereception by the Bradford breaker to an outside storage area and returned to the plant by bulldozer on a LeTourneau carrier to a receiving pit.

Discussion

W. H. ROWAND.[2] Sometime back it became apparent that fuel costs were on the rise along with other things and that the trend probably would continue for some time to come. To help

[2] Chief Engineer, The Babcock & Wilcox Company, New York, N. Y. Mem. ASME.

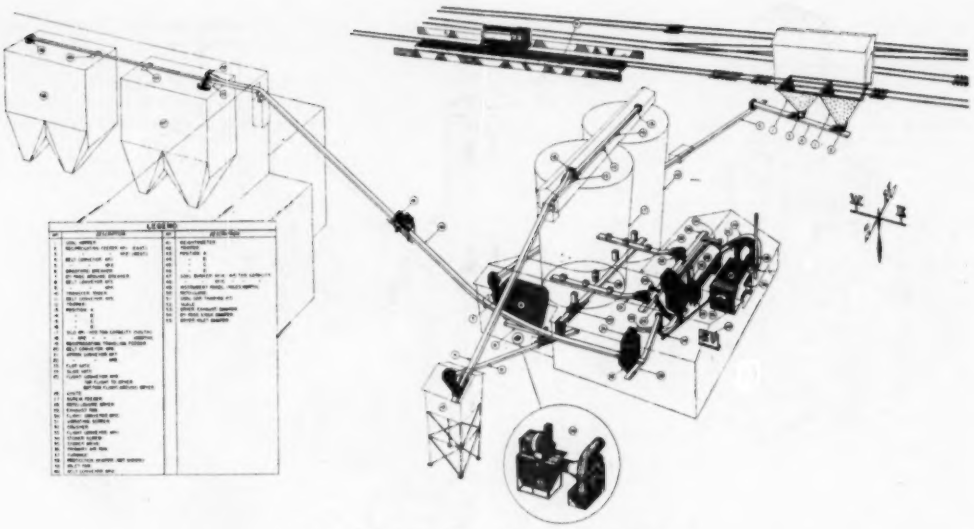

FIG. 10 COAL-PREPARATION PLANT SOUTH POWERHOUSE

offset this trend, higher steam temperatures and reheat were adopted by several in the power industry in their expansion programs.

In searching for other means of improving cycle efficiency, the author, his colleagues, and others in the power industry decided that the elimination of the induced-draft fan and operation of the boiler under pressure from the forced-draft fan also offered a substantial gain in efficiency in the order of 1 per cent. About $^1/_2$ per cent is due to the elimination of air leakage and another equivalent $^1/_2$ per cent is due to the power reduction in handling cold air only and a smaller quantity of it.

There was some risk involved, of course, from a reliability point of view in being able to build a casing which would be gastight over the large areas involved in a central-station boiler. The author and his colleagues deserve credit in being willing to take this risk and thus obtain the savings in first cost outlined.

The writer does not believe that reliability has been affected thus far by the omission of the induced-draft fan.

We all realized that the general type of casing and all of the details both in design and construction required careful attention for it to be satisfactory in service. After considerable study it was decided to use the "skin" type of casing right against the pressure parts which had proved satisfactory on earlier smaller units. This offered the following advantages compared with the conventional steel-cased construction:

Insurance against gas by-passing and hot spots.

Casing temperature above the dew point of the sulphur-bearing gases to prevent corrosion.

Insulation kept away from the sulphur-bearing gases to prevent deterioration.

Differential expansion between casing and pressure parts minimized, which simplified the sealing of terminals, and so forth.

In addition to the units described, there are three similarly designed central-station units in operation and nine others under construction. Undoubtedly there will be further refinements in design as additional experience is gained.

We agree that operating experience with the system justifies pressurized operation from the standpoint of reliability and cost saving, and are confident that it will find increasing use in the power field.

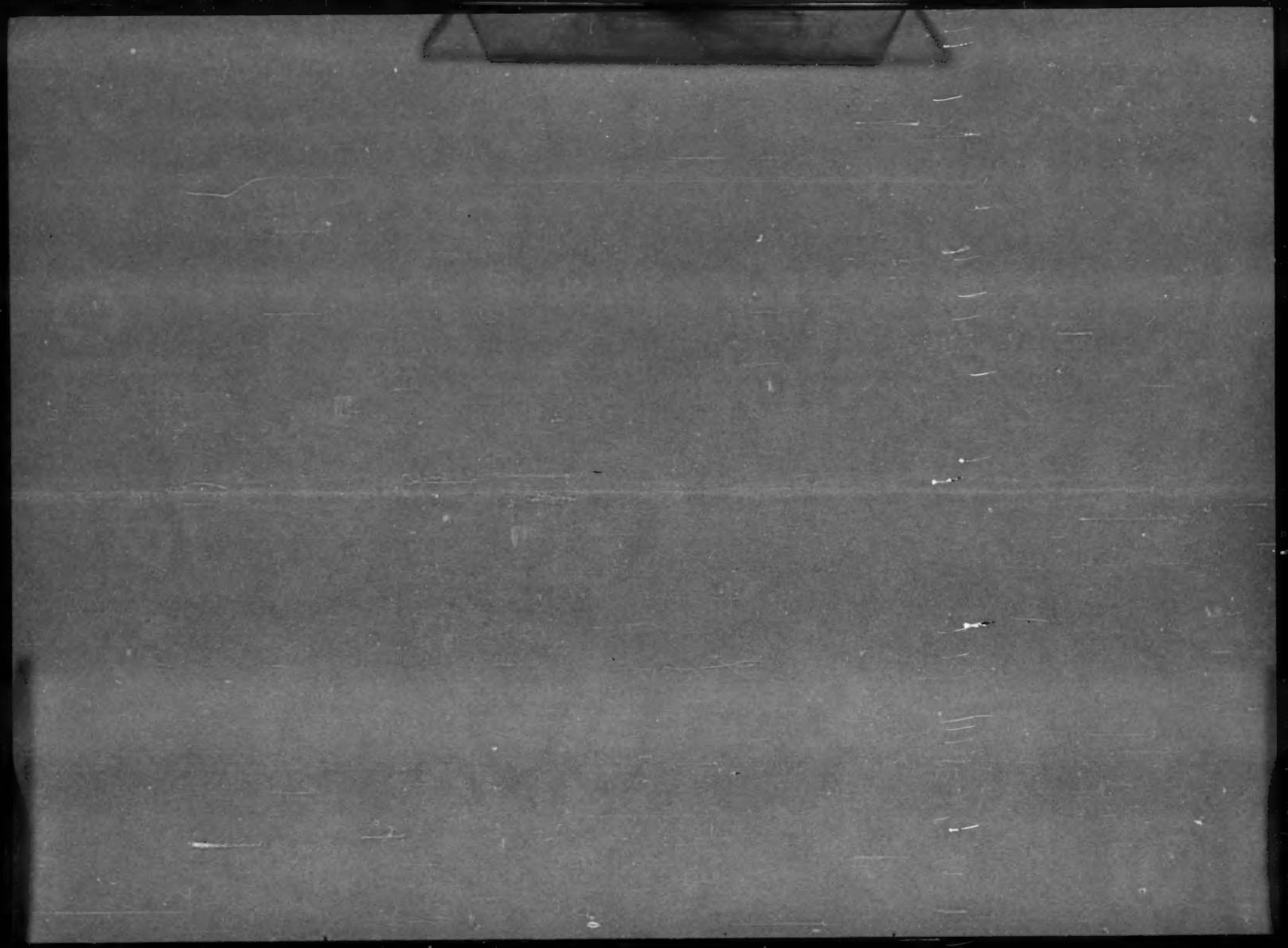

AN ASME PAPER

Its Preparation, Submission and Publication, and Presentation

To a large degree the papers prepared and presented under the ASME sponsorship are evidence by which its professional standing and leadership are judged. It follows, therefore, that to qualify for ASME sponsorship, a paper must not only present suitable subject matter, but it must be well written and conform to recognized standards of good English and literary style.

The pamphlet on "AN ASME PAPER" is designed to aid authors in meeting these requirements and to acquaint them with rules of the Society relating to the preparation and submission of manuscripts and accompanying illustrations. It also includes suggestions for the presentation of papers before Society meetings.

CONTENTS

PREPARATION OF A PAPER—

General Information—Style, Preferred Spelling, Length Limitation, Approvals and Clearances.

Contents of the Paper—Title, Author's Name, Abstract, Body of Paper, Appendixes, Acknowledgments, Bibliographies, Tables, Captions, Photographs, Other Illustrations.

Writing the Paper—Outline, Tabulations, Tables, Graphs, Charts for Computation, Drawings, Mathematics, Accuracy, Headings and Numbering, Lantern Slides, Motion Pictures, Typing, Number of Copies.

SUBMISSION AND PUBLICATION OF A PAPER—

Intention to Submit Paper Required in Advance, Meeting Dates, Due Dates for Manuscript, Discussers, Review and Acceptance, Proofs, Advance Copies and Reprints, Discussion and Closure, Publication by Others.

PRESENTATION OF A PAPER—

Time Limit, Addressing Your Audience, Public Address Systems, Use of Slides.

REFERENCES—

References on Writing and Speaking, Engineering Standards.

Price 35¢. No discount allowed. *A remittance must accompany all orders for $2.00 or less. U. S. Postage Stamps are acceptable.*

THE AMERICAN SOCIETY OF MECHANICAL ENGINEERS
29 West 39th Street, New York 18, N. Y.